REWORK OF GAP AND OVERLAP DEFECTS IN AUTOMATED FIBRE PLACEMENT MANUFACTURING

Stig McArthur

A Thesis submitted to the University of Strathclyde for the Degree of Doctor of Philosophy

Department of Design, Manufacturing and Engineering Management

University of Strathclyde

Glasgow, UK

April 2026

Signed: 

Date: 11/04/2026

Acknowledgements

This Thesis is the culmination of three and a half years of work, none of which would be possible without the network of support which I have been lucky enough to be surrounded by, who have all on numerous occasions and in different ways, helped in the production of this research, for which I would like to express my gratitude.

First and foremost, I would like to thank and acknowledge my supervisors, Jörn Mehnen, and Catherine Yokan, for their contributions to this Thesis. Both have provided invaluable guidance and support throughout this PhD. Secondly, to the wider research staff in both the NMIS composites team, particularly Alex Cochrane and Iain Bomphray for support in the early periods of the PhD and the NMIS-Composites technical staff, particularly Mate Csanyi and James Chilvers-Grierson who enabled many of the experimental works enclosed. Thanks also wider NMIS groups, in particular the Materials Testing team, and Dorothy Evans of the NMIS Doctoral Centre. Thank you also to the DMEM department research staff. Additionally, I have had the distinct pleasure of collaborating with a range of researchers during the PhD, and extend my thanks to them, namely Shaun McKnight, Carmelo Mineo, Rylan Gomes, Meirbek Mussatayev, and Alastair Poole.

During the course of the PhD, I have had the pleasure of being joined in the process by many fantastic friends both in the Strathclyde doctoral community, and in my personal life outside of university. Many of you are or have become life-long friends and your support and encouragement throughout has been a constant source of enjoyment and motivation.

I am grateful for all the support received from my family. Thank you to my parents Peter and Erica, and siblings Morven, Alasdair and Tove, who have always stepped in to help in difficult times and bolstered my belief and will.

Last but not least, my deepest thanks to my loving partner Sally, who has been at my side since this process began and whose support, encouragement and comfort through good and bad times has been unwavering.

List of Publications

Publication 1. S. McArthur, J. Mehnen, C. Yokan, and I. Bomphray, "*An overview of current research in automated fibre placement defect rework*," Procedia Comput Sci, vol. 232, pp. 2167–2180, 2024, doi: 10.1016/j.procs.2024.02.036.

Publication 2. S. McArthur, J. Mehnen, and I. Bomphray, "*Benchtop-AFP: an Exploration of Democratised Automated Fibre Placement*" in Proceedings of the 21st International Conference on Manufacturing Research, Glasgow, UK, Aug. 2024, pp. 1–6.

Publication 3. S. McArthur, C. Mineo, A. Poole, I. Bomphray, and J. Mehnen, "*Future-Proof Adaptive Path Correction in Automated Fibre Placement: A Concept Demonstration,*" in 2025 IEEE International Conference on Simulation, Modelling, and Programming for Autonomous Robots (SIMPAR), 2025, pp. 1–6. doi: 10.1109/SIMPAR62925.2025.10978996.

Publication 4. S. McArthur, S. McKnight, I. Bomphray, and J. Mehnen, "*Rework signature: assessing quality of reworked defects in automated fibre placement composites*," in Proceedings of the 21st European Conference on Composite Materials: Manufacturing, Nantes, France, Jul. 2024.

Publication 5. S. McArthur, S. McKnight, I. Bomphray, and J. Mehnen, "*Assessing the effectiveness of rework in automated fibre placement-produced composite laminates: A quantitative approach using out-of-plane waviness*," Compos Part A Appl Sci Manuf, p. 109081, Jun. 2025, doi: 10.1016/j.compositesa.2025.109081.

Publication 6. S. McArthur, C. Yokan, and J. Mehnen, "*Coupled deformation responses during thermoset AFP recompaction: Process parameter analysis and defect mitigation viability,*" Compos Part A Appl Sci Manuf, vol. 205, p. 109691, Jun. 2026, doi: 10.1016/j.compositesa.2026.109691.

Publication 7. S. McArthur, C. Yokan. J. Mehnen, "*Real-Time Adaptive Trajectory Control for Automated Fibre Placement Using ROS-Based Defect Mitigation*", in 7th International Symposium on Automated Composite Manufacturing, Delft, the Netherlands, 13 – 17 April 2026,

Thesis section	Linked Publication	Link
Chapter 4: Rework Process Analysis	Publication 1	Experimental study
Section 4.3.2: Experimental setup: Benchtop-AFP	Publication 1	Experimental setup
Section 4.3: Ultrasonic Testing	Publication 4 and Publication 5	Experimental study
Chapter 6: Recompaction-based automated rework	Publication 6	Experimental study
Chapter 7: Real-time trajectory control for defect mitigation	Publication 3 and Publication 7	Experimental study

Abstract

Automated Fibre Placement (AFP) manufacturing is the current state-of-the-art for high-rate manufacturing of high-performance composite parts. The method relies on the robustness and repeatability of robotic elements to enable rapid and reliable manufacturing of composite parts for a range of industries, including aerospace, automotive, renewables, space, defence and marine. While improvements in deposition rates are achieved through AFP compared to manual part manufacturing, the technique remains challenged by the presence of defects in manufactured parts, many of which rely on manually performed inspection and critically, rework. Importantly, the inspection and rework of these defects accounts for a disproportionately high amount of the cycle time. While the hallmark of AFP is its level of automation, surpassing most other composite manufacturing techniques, the process for inspecting and addressing these defects remains largely manually performed by skilled operators. This manual task necessarily requires the shutting down of automated production to ensure the safety of the operators, contributing to the reduction in manufacturing efficiency incurred by inspection and rework. Various research efforts have been performed for the development of automated defect inspection methods; little research, however, has been undertaken on the subsequent reworking step. Additionally, and critically, the effect of this reworking on part quality is not well understood and has not been rigorously studied prior to this Thesis. This Thesis addresses this gap, firstly through an analysis of the process and effect on part quality, both in structural and mechanical terms, of rework; and further to develop innovative automated methods for performing the reworking activity itself. Through this work, the fundamental research question of the effect of reworking defects under current best practices is answered, while paths towards automated reworking are developed and tested.

In current practice, manual rework is performed by skilled human operators through a variety of techniques. The techniques themselves are poorly understood in the literature and

instead exist as "crafts" of sorts; understood implicitly by the human practitioners themselves, but not documented, nor optimised. This research includes the first substantial body of research into this activity, to understand the key features and optimise the activity. This Thesis provides the first description of the existing knowledge both in the literature and through industry perspectives on the rework activity and provides a first-of-its-kind rework process analysis, resulting in a set of best practices for performing the activity while minimising the damage to the surrounding and removed material. Secondly, through various non-destructive and destructive testing procedures the effect of rework is examined. With the exploratory literature and experimental research on the manual reworking activity conducted, a series of test cases were developed in order to evaluate the effect of reworking on a composite part. These test cases were analysed through different quality analysis methods. Firstly, ultrasonic non-destructive testing (NDT) was used to demonstrate the variance in out-of-plane waviness amongst reworked specimens and also compared to pristine and defective specimens. The reworked specimens, while improved in terms of out-of-plane waviness from the defective benchmark, still fell below the quality of pristine specimens, highlighting that reworking is both variable and not necessarily a direct guarantee of pristine-like quality.

Further analysis through the ISO 14125 flexural tests revealed that reworking effectively restored much of the stiffness of the laminates to near-pristine levels, but a higher level of variance in results was seen, mirroring the non-destructive test results.

Further evaluation of the effectiveness of rework was performed by, firstly, analysing the microstructure of pristine, defective and reworked laminates through Scanning Electron Microscopy (SEM). The results showed that the reworked laminates displayed a higher degree of inter-ply disturbances centred around the rework sites, despite featuring reduced local variations in thickness compared to defective specimens. This was particularly the case where rework was performed on subsequent piles with identical fibre angles.

A novel Benchtop-AFP system was developed as a research platform to enable lab-scale laminate manufacture and was used for the Ultrasonic NDT test laminates. This collaborative robot-based system provided the flexibility and accessibility required for iterative experimentation, allowing for the codification and optimisation of rework strategies within a semi-automated environment. Beyond its application in this research, the Benchtop-AFP concept represents a contribution towards democratising AFP research, offering a scalable model for laboratory-scale studies of automated composite manufacturing.

Finally, from the literature review and expert outreach, evidence of significant space for the development of automated reworking methods exists. Two methods are investigated within this Thesis. Firstly, a recompaction based gap defect rework method is explored in terms of the effect of varying processing parameter levels through statistical analysis. The analysis showed an unintended coupling between the width change deformation and undesirable transverse displacement of the tow, while the overall magnitude of width change was insufficient for effective gap defect mitigation. Secondly, a real-time trajectory control method was developed making use of an expanded motion control toolkit and a ROS-hosted end-to-end defect detection to correction system. Using this method, effective mitigation of the extent of gap defects was achieved during the initial deposition step, within the constraints of the system design.

Within the scope of this thesis is the analysis of the rework activity specifically for defects occurring during automated fibre placement. These are limited to placement and process induced defects and excludes material-based defects.

This Thesis demonstrates that while manual rework offers partial remediation of AFP-induced defects, the results of the process are highly variable. By codifying manual rework practices and systematically evaluating their impact on part quality, this work provides a foundation for standardised study and optimisation. Furthermore, it pioneers automated rework methods, including tow reconsolidation techniques and a real-time trajectory correction framework based on sensor-informed control, marking a significant step toward fully autonomous AFP. These contributions collectively address a critical gap in AFP manufacturing and advance its readiness for industrial deployment in high-performance composite applications.

Table of Contents

List of Figures

List of Tables

List of Abbreviations

AFP - Automated Fibre Placement
ANOVA - Analysis of Variance
ATL - Automated Tape Laying
CFRP - Carbon Fibre Reinforced Composites
CMC - Ceramic Matrix Composites
CNC - Computer Numerical Control
CTE - Coefficient of Thermal Expansion
CTS - Continuous Tow Shearing
DOE - Design of Experiments
EC - Eddy Current
FW - Filament Winding
GFRP - Glass Fibre Reinforced Composites
GUI - Graphical User Interface
HGT - Hot Gas Torches
HMI - Human-Machine Interface
IQR - Interquartile Range
IR - Infra-Red
ITRA - Interfacing Toolkit for Robotic Arms
KRL - Kuka Robot Language
LLS - Laser Line Scanner
LP - Laser Profilometry
LPS - Laser Profile Scanner
MMC - Metal Matrix Composites
NDT - Non-Destructive Testing
OFB - Optical Fibre-Bragg
PLC - Programmable Logic Controller
PMC - Polymer Matrix Composites
PTFE - Polytetrafluoroethylene
RM - Reworking Methods
RMSTD - Root Mean Squared Transverse Displacment
ROS - Robotic Operating System
RSI - Robot Sensor Interface
RTM - Resin Transfer Moulding
SEM -Scanning Electron Microscopy
T_g - Glass transition temperature
TCP - Tool Centre Point
TCP/IP - Transmission Control Protocol/Internet Protocol
UDP - User Datagram Protocol
UT - Ultrasonic Testing

Glossary of Terms

Automated Fibre Placement (AFP) – A robotic manufacturing process that precisely lays narrow strips (tows) of pre-impregnated composite material onto complex moulds, layer by layer, to create lightweight, high-strength parts. The process involves heating, cutting and compacting these fibre tows onto a surface, building complex 3D structures with tailored material properties.

Compaction – The act of applying pressure on the composite material in the mould through the thickness direction which helps the placed tow adhere to the substrate and drives matrix flow under pressure

Composite – Three-dimensional combination of at least two materials differing in form or composition, with a distinct interface separating the components. Composite materials are usually manmade and created to obtain properties that cannot be achieved by any of the components acting alone.

Consolidation – A processing step in which a fibre and matrix are compressed to reduce voids and achieve a particular density.

Course – A set of tows deposited on to the mould by the AFP End-effector in a single pass. A course may contain as many tows as the End-effector may deposit in a single pass, i.e., a single tow in a single tow End-effector, or multiple in an End-effector supporting multi-tow deposition.

Coupon – A small-scale, representative specimen used in mechanical and material testing to evaluate the properties of fiber-reinforced plastics and laminates.

Defect – Imperfections in the in the layup which may cause the part to fail cosmetically, or, more critically, mechanically

Detection – The process of identifying, locating and characterising defects in the layup, typically occurs in-process, rather then post-process.

Deposition – The process of laying up material in the mould.

End-effector – The device or tool mounted on the end of the robotic arm, responsible for interacting with the environment or workpiece.

Fibre – One or more filaments in an ordered assemblage.

Gap – An unfilled space between two adjacent tows.

In-plane waviness – Fibre deviations that manifest side-to-side remaining within the flat plane of the ply.

In-process – Processes or actions occurring during the deposition process, rather than between the deposition of sperate plies.
Inspection – The process of identifying, locating and characterising the quality of the layup. Typically occurs between the deposition of plies, rather than in-process.
Lamina – Subunit of a laminate consisting of one or more adjacent plies of the same material with identical orientation.
Laminate – Any fibre- or fabric-reinforced composite consisting of laminae with one or more orientations with respect to some reference direction.
Layup – To place or the process of placing layers of reinforcing material into position in or on a mould; also used to refer to the reinforcing materials as placed in the mould ("the layup").
Matrix – Material in which reinforcing fibre of a composite is embedded. Matrix materials include thermosetting and thermoplastic polymers, metals and ceramic compounds.
Mandrel – A form, fixture or male mould used as the base for production of a part in processes such as layup or filament winding.
Nip-point – The physical intersection between the incoming composite material (tape) and the substrate.
On-the-fly – Processes which can be stopped, started, altered in real-time during deposition without stopping the machines movement across the mould.
Out-of-plane waviness – Fibre undulations that manifest in the through-thickness direction of the laminate.
Overlap – Defects where adjacent tows are improperly aligned, causing them to partially cover or stack on top of each other.
Ply – A single layer (or lamina) used to fabricate a laminate. Also, the number of single yarns twisted together to form a plied yarn.
Prepreg- Fibrous reinforcement (sheet, tape, tow, fabric or mat) pre-impregnated with resin and capable of storage for later use. For thermosetting matrices, the resin is usually partially cured or otherwise brought to a controlled viscosity, called B-stage. Additives (e.g., catalysts, inhibitors and flame retardants) are used to obtain specific end-use properties and/or improve processing, storage and handling characteristics.
Recompaction – A secondary pass with the compaction roller over material which has already been deposited on the mould.
Repair – The act of restoring structures to their original structural integrity from damage incurred in use.

Resin – A solid or pseudo-solid polymeric material, often of high molecular weight, which exhibits a tendency to flow when subjected to stress, usually has a softening or melting range, and usually fractures conchoidally. As composite matrices, resins bind together reinforcement fibres and work with them to produce specified performance properties.

Rework – The modification of defective plies or tows during the manufacturing process, to mitigate or eliminate the defects.

Steering – The bending of composite tows along a curved path.

Substrate – Material that provides the surface on which an adhesive-containing substance is applied for any purpose, such as bonding or coating.

Stacking sequence - Arrangement of ply orientations and material components in a laminate specified with respect to some reference direction.

Tack – Stickiness of an uncured prepreg.

Tape – Thin, unidirectional prepreg, available in up to 12-inch width in carbon fibre

Thermoplastic – A class of plastics that can be repeatedly softened by heating and hardened by cooling through a temperature range characteristics of the plastic, and that in the softened state can be reshaped by means of moulding or extrusion.

Thermoset – A class of plastics that, when cured by thermal and/or chemical or by other means, become substantially infusible and insoluble. Once cured, a thermoset cannot be returned to the uncured state.

Tooling - The mould, either one- or two-sided and either open or closed, in or upon which composite material is placed in order to make a part.

Tow – continuous, ordered assembly of essentially parallel, collimated filaments, normally continuous filaments without twist. Same as strand but used when the reference is specific to carbon fibre.

Trajectory - The exact path, schedule, and orientation required for the robot to lay fibres accurately across a contoured mould.

Unidirectional – General term denoting orientation of fibres in one direction.

Viscosity – Describes the tendency of a material to resist flow. The higher the number, the greater the resistance to flow.

Void – Any pocket of enclosed gas or air within a composite.

Warpage – Dimensional distortion in a composite.

Chapter 1. Introduction

1.1 Preamble

Composite materials are a unique class of materials which combine the properties of constituent materials to result in a material with improved mechanical properties compared to either of the constituents alone. These materials have been used in human industrial society for thousands of years; in its earlier forms as the combination of fibrous plant or animal fibres with natural glue-like materials [1]. Composite materials are made of a combination of a stiff component, often elongated, embedded in a softer more compliant constituent forming the matrix [2]. The role of the matrix is to hold the reinforcement in place and transfer mechanical loads to the reinforcement. The role of the reinforcement is to provide stiffness and strength to the material [3], [4].

Composite materials are anisotropic, meaning their mechanical properties vary depending on the direction of mechanical loading. This is caused because the stiffer reinforcement constituent is often in fibrous form, and the fibres are aligned in a certain direction [2]. This property allows for the generation of parts with controlled anisotropy by carefully aligning fibres in a desired direction to support stresses from specific loading conditions [5].

Modern composite materials come in a range of formats, characterised by their matrix material, and their reinforcement material. Matrices come in the form of polymer matrices, ceramic matrices, and metal matrices [1]. Polymer matrix composites are the most widely used in industrial applications predominantly in the form of thermoset polymer matrices [2]. Thermoplastic polymer matrices are gaining in usage across several industrial applications due to their increased recyclability [6]. The enhancements to material properties through the combination of reinforcement with the matrix is often much less pronounced in metallic or ceramic matric composites than in polymer matrix composites, as the goal of reinforcements

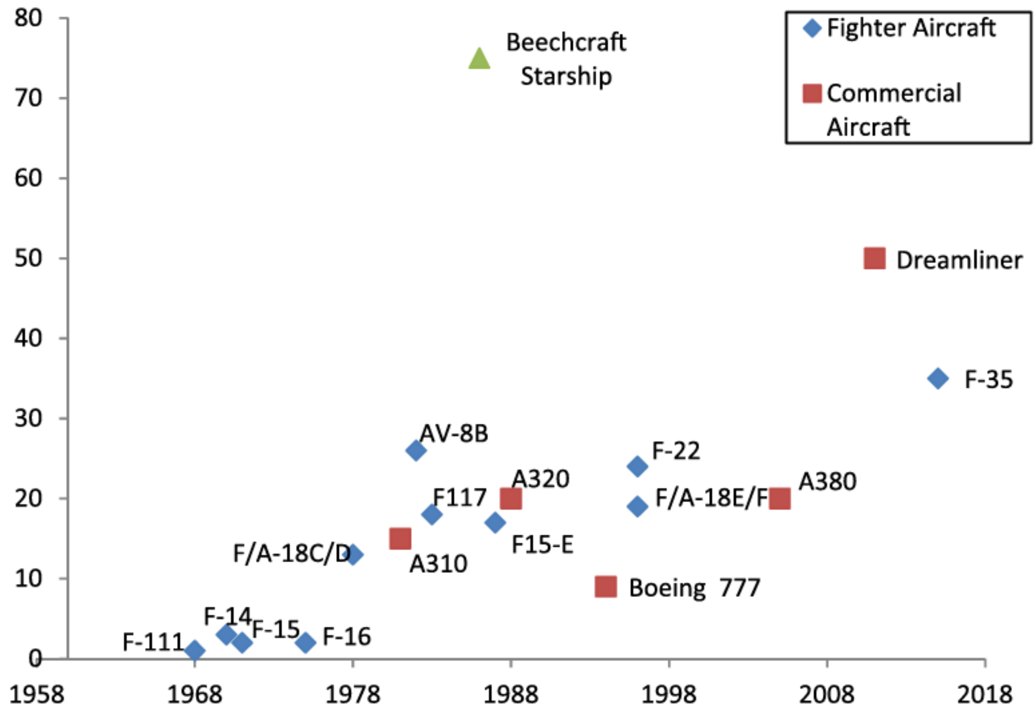

Figure 1.1. Composite component weight percentage of aircraft mass by year, from [7]

is typically to increase the toughness of the matrix, though the potential for improvement in properties through combinations is still present above and beyond what is possible with the base matrix material alone [2]. Fibre reinforcement materials can be natural fibres such as flax, carbon fibres and glass fibres. Reinforcements may also come in particulate form, short loose fibres, or in monofilament form [2], however fibres are the overwhelmingly dominant option demanded by the market [8]. Advanced composite materials are composed of high strength fibres embedded in moderately high temperature resins, with a fibre volume fraction of 0.5 – 0.7. Typically, in aerospace applications the target volume fraction is 0.62 [9]

The main attractiveness of composites lies in their exceptional strength-to-weight ratio, along with the capability for controlled anisotropy [4], [6]. They are used in various industries including aerospace, marine, automotive, sports goods, wind energy, construction, fluid storage and transmission [2]. In aerospace and automotive, the combination of light weight, and high stiffness and strength are very attractive. Usage examples include airframes, fuselage panels, rotor blades, and car body panels. Figure 1.1 shows the increasing use of composite materials in aircraft as a percentage of total aircraft mass over the last 6 decades, adapted from [7]. The use of composites for aircraft components has demonstrated weight savings of the order of 25% compared to aluminium, however the weight savings come with a cost increase in the order of 50-100% [9]. Other applications include yacht hulls, wind turbine aerofoils [10], surfboards [11] and vaulting poles [12].

1.1.1 Automated Fibre Placement (AFP)

Automated Fibre Placement (AFP) is at the forefront of automated composites manufacturing and is the result of developments of the established Filament Winding (FW) and Automated Tape Laying (ATL) methods. FW involves the wrapping of wetted fibre bundles around a rotating mandrel [9]. Since the fibre bundle is held in tension when wrapped, it must follow a geodesic path, meaning there is no in-plane curvature in the bundle, as such, the fibre angles available for deposition are limited. This limitation in fibre angle limits the possible tool geometries that FW may be used for [9]. FW has been used extensively for rocket motor cases, pressure vessels and other tubes [13]. It has the highest rate of production of any of the composites manufacturing techniques at approximately 50kg/hr, but can results in poor surface finish, and high void content by comparison to hand layup (3 % compared to < 1 %) [9].

ATL involves the placement of composite tapes onto a tooling, often using gantry systems or robotic end-effectors. Early ATL machines placed large 50-300 mm tapes on flat surfaces. ATL is very suitable for the manufacture of large components with low surface curvature [13]. Specific use cases include the vertical and horizontal tailplanes, and centre wing box of the A380 airplane [14] and the Airbus A350 upper shell fuselage skin section [15]. The technique can perform poorly over more complex surfaces because of the width of the tape used [16], often generating gaps, wrinkles, folds and other defects caused by tow buckling during steering, leading to improper tessellation of the material across the mould surface [17].

Whereas ATL uses large tapes, AFP utilises much smaller width (3.7 - 6.35 mm) tapes, referred to as tows [6]. These smaller width tapes allow for more complex curvatures and features of laminates to be deposited by the tape delivery system. The earliest account of using tows instead of larger ATL tapes was patented by Goldsworth et al. in 1974 [18]. In this patent, larger ATL tapes were split into smaller tows by a mechanism inside the placement head. The first dedicated AFP machines began to be developed by Hercules Aerospace in 1980, and within the decade were made commercially available and used by The Boeing Company, Lockheed Martin Corporation, and Northrop Grumman [19]. AFP machines were conceived of and are still functionally a combination of the differential payout capability of FW and the compaction and cut-restart capabilities of ATL [6]. Throughout the 1990s developments of the system continued, notably the development of a system capable of delivering 24 tows at once, enabling a layup rate of 30 m/min with a corresponding productivity of 1.9 kg/h [20]. Further developments focused on reliability over complex geometry including the delivery of tows on a curvilinear path, known as tow steering. Applications of tow steering showed a 450 % increase in productivity, reduced material wastage from 62 % down to only 6 % and cost reductions of 43 % compared to FW and hand layup [21], [22]. Tow steering allows for the manufacture of parts with further tailored mechanical properties, allowing, for instance, for the generation of variable stiffness panels, used in aerospace applications.

Both ATL and AFP machines typically feature degree-of-freedom systems, with mounted custom end-effectors responsible for the delivery of tapes onto the tooling surface [6]. This allows for tapes to be deposited at varying fibre angles, allowing for the manufacturing of laminates with controlled anisotropy. As a developed technology at the cross section of FW and ATL, many of the design features of both systems are incorporated into the standard design principles of AFP systems. The operation and overall design are very closely aligned with that of an ATL machine [6].

1.1.2 AFP Defects

Despite its many advantages, AFP suffers from a high defect rate as a result primarily of head movement, improperly steered fibres, and variations in material [14], [23]. The inspection, detection, removal, and rework of these defects present a significant challenge. Defects are imperfections in the layup that cause the final part to fail structurally or mechanically. In the literature, defects are broadly categorised into those induced through improper management of process parameters, and those induced through improper placement of material [13].

Process-induced defects are caused by improper management of the key parameters of layup speed, temperature, compaction force, tension, and environmental conditions. Incorrect management and programming of these parameters lead to defects such as poor tow adhesion, wrinkles, gaps and overlaps, and increased presence of voids [13]. The presence of defects in a laminate lead to improperly managed stresses within the final part [24] and therefore parts with lower load capacity [25] and fundamental frequency [26]. A full description of the defects, their cause and their effects is given in the literature review section of this Thesis.

The identification of defects has garnered a lot of interest in research, particularly in terms of automated inspection and identification methods. These include laser profilometry, thermography, visual inspection, eddy current inspection. In general, these methods identify defects after a ply has been deposited, allowing technicians to locate and identify sites for rework.

The focus of this Thesis is on the procedure of reworking, performed after the inspection and identification of defects within a ply. Reworking is defined by Hughes et al. [27] as:

"The finishing step that can mitigate the source of scrap waste. Rework refers to the manual inspection and modification of defect plies or tows."

In current AFP manufacturing practices, reworking of defects is performed manually by technicians, sometimes using intelligent detection and identification methods to aid in the location and characterisation of the defects. Methods for automated defect rework or mitigation at the time of writing do not exist. Analysis of the typical cycle times for AFP by Electroimpact [28] and Boeing [29] found that inspection and rework accounted for 63 % and 32 % respectively. Further analysis by Rudberg et. al, [30], found that AFP cells are typically only used to layup material 42 % of the cycle time, with the rest of the cycle divided between inspection (28 %), tool moves (11 %), reliability recovery (10 %), and operator breaks (9 %). The extent to which rework is successful in practice is, prior to the publication of this Thesis, unexamined. The limited discussion of the practice that exists in the literature highlighting the generation of secondary defects through the reworking procedure [31].

The motivation for this Thesis this lies in generating new understanding of the role reworking plays in part quality as it is currently practiced, to improve the process, with the aim of moving towards more automated methods of mitigation and rework, to improve the efficiency and machine utilisation of AFP cells.

1.2 Aim and Objectives

The aim of this thesis is the generation of new knowledge that will aid in the further understanding and ultimately automation of the reworking of placement induced defects in AFP. In the context of AFP, there has been limited research focused specifically on reworking activities, despite extensive work on defect detection and inspection. Currently, in commercial AFP, reworking is typically performed manually by expert practitioners using an array of hand tools [31]. The effectiveness of these activities is not well-studied in the literature and is usually assessed by subsequent visual inspection of the defect site. As such, the primary evaluation metric of the reworking procedure remains cosmetic, and it is unclear to what extent defect reworking restores or preserves the underlying mechanical performance of the affected part.

Additionally, progress of the AFP manufacturing technique towards smarter, more effectively automated manufacturing is reliant on more advanced levels of defect control, inspection, and reworking. If, through further research, automated methods of performing the reworking activity are to be developed, an understanding of the reworking method from first principles must be generated. It is the generation of these principles, and the knowledge of the impact of rework as a distinct step in the manufacturing process that are the primary contributions of this Thesis, as well as the development of smart automated methods for defect mitigation.

Motivating and structuring the Thesis are two central research questions:

(Q1) What is the impact of reworking defects on part quality?

The impact in question is cosmetic, mechanical, and in terms of impact of reworking for machine time and operator labour. By determining the impact of rework as a practice, the case for process improvements, innovations or optimisation is made evident.

(Q2) How can reworking be improved?

Given the assessment from question (Q1), the reworking process may be improved to yield minimal negative impact to the laminate, or to the cycle time of typical AFP production, or improvements may made to efficiency approaching fully autonomous AFP.

This Thesis addresses both research questions through experimental work and through improvement of the AFP process itself. In achieving this, novel automated processes are developed and evaluated, reducing the effect of lost cycle time for manual inspection and reworking of defects, removing the possibility of human error, and improving the overall quality of the final composite products.

Objectives were defined within each of the research questions as QX.O(n). They are as follows:

(Q1.O1) Examine the manual reworking process in line with the current state of the art practices.

(Q1.O2) Suggest guidelines for manual reworking, to inform further study of the activity with reduced variability.

(Q1.O3) Examine the effect of reworking in terms of geometric consistency in the laminate and part performance and determine the effective reduction in the mechanical performance knockdown induced by defects.

(Q2.O1) Investigate viable methods for increasing the effectiveness of reworking and reducing the process efficiency reductions incurred by manual rework.

(Q2.O2) Develop automated methods of reworking that do not incur the process efficiency reductions associated with manual reworking, while maintaining the defect mitigation and quality control in the parts.

(Q2.O3) Validate the developed methods of automated reworking for their effectiveness in addressing defects.

1.3 Methodology

This Thesis encompasses three distinct phases of research.

Phase 1 involved an exploration stage to contextualise reworking within AFP. An extensive literature review was conducted to summarise the state-of-the-art in reworking, AFP defects, their causes and effects, and the methodologies for defect inspection and detection. This was complemented by interviews and questionnaires with AFP experts (presented in Chapter 3), which established a baseline understanding of current practices, challenges, and research opportunities.

Phase 2 followed this exploration stage, informed by the lack of evidence within literature and expert knowledge of a codified body of research in either the reworking procedure itself, or the effect of said procedure on the mechanical performance of the part. As such, experimental studies were undertaken to overcome these knowledge gaps. Firstly, the reworking procedure was examined, exposing the constraints of efficiently reworking parts whilst maintaining the quality of materials in the composite layup. To examine the results of the reworking procedure, both destructive and non-destructive methods were used. A novel benchtop-scale AFP system was developed and used for the initial reworking studies, to facilitate small-scale, low-cost research into sub-processes within the AFP manufacturing technique. Through Non-Destructive Testing (NDT) the internal structure of laminates following defect reworking were examined, and fundamental differences in structure and variability across samples were uncovered. Secondly, destructive tests were performed to examine the effect of these sub-laminate level structural differences, which delivered a comprehensive and measurable metric of the knockdown effect of defects, and the subsequent effect on quality in reworked samples.

Phase 3 focused on the development, testing, and validation of automated reworking techniques. Building on knowledge from the previous stages, this phase introduced novel, non-invasive, and automated reworking methods, moving beyond the state-of-the-art manual procedures. The first of these methods relied on a recompaction based width change in order to bridge the gap between gap defects and fully tesselate tows across the tooling surface. This was studied parametrically and within the context of first ply thermoset AFP. Alongside this, a method of real-time adaption of deposition paths using live profilometry data was developed to allow for more adaptive material deposition for the limitation and mitigation of placement induced defects. This aligns with the broader trend in the literature toward automation of inspection and detection, with the aim of achieving a more fully automated, end-to-end AFP process.

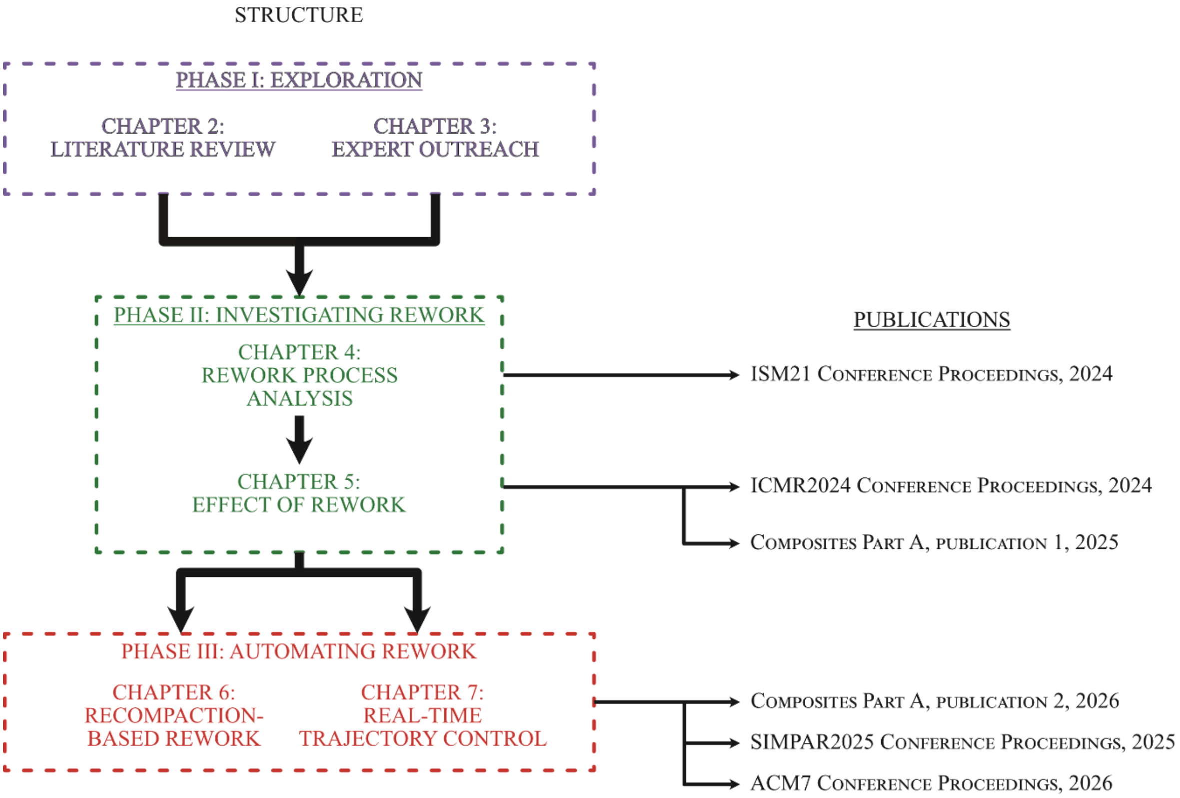

Figure 1.2. Thesis Reading Guide by paper

The layout of the chapters of this Thesis reflects the structure of the three phases above.

Chapter 2 reviews notable literature in AFP research, examining defect studies with a focus on cause, effect, inspection, mitigation and rework. Chapter 3 reflects on learning from interviews conducted with industry experts and how these agree or contrast with academic literature highlighted in Chapter 2. Chapter 4 details a rework process analysis examining the effect of varying the reworking method on damage to the surrounding material. Additionally, ultrasonic NDT was used on representative panels to quantify the effect of reworking following the method defined through the process analysis. Together, these results in a set of best practices for effective reworking of gap and overlap defects. Chapter 5 examines the effect of reworking in terms of mechanical performance under ISO 14125 flexural strength testing and in terms of the laminate microstructure. Chapter 6 introduces the recompaction based automated defect rework method. The method is examined parametrically in terms of the effect of various process parameter tunings on the resultant deformation modes. Chapter 7 details the development and testing of a real-time trajectory control architecture using the Robotic

Operating System (ROS) middleware, aimed at mitigating the extent of detected gaps and overlaps in a robotically controlled AFP system.

1.3.1 Research Philosophy

Following the Saunders research onion framework [32], the methodology of this Thesis is described in terms of research philosophy, approach, strategy, time horizon, and associated methods.

At the highest level, philosophy, Saunders, [32], defines several paradigms:

- Positivism, the belief in objective reality, measurable facts, and reliance on scientific methods.
- Interpretivism, which focuses on subjective meanings and understanding phenomena from the perspectives of those involved.
- Realism, which recognises a reality independent of human thoughts and beliefs, though such reality may be interpreted in various ways.

In this research, a positivist position was adopted, emphasising objective measurement and empirical evidence to inform the knowledge outcomes. This stance was deemed most appropriate, given the relatively practical domain and applied implications of the research, where subjectivity was minimised. Furthermore, the methods employed were necessarily reliant on direct measurement of empirical data for both investigation and validation.

For the research approach, Saunders, [32], outlines three main approaches:

- Deductive (moving from theory to observation)
- Inductive (moving from observation to theory)
- Abductive (iteratively moving between data and theory)

Initially, in phases I and II, deductive reasoning was used to structure the investigation of the reworking method, resulting in a new body of knowledge. Subsequently, inductive reasoning was employed to develop, test, and validate novel techniques based on the findings from the deductive phase.

Regarding research strategy, Saunders lists several options, including experiment, survey, case study, action research, grounded theory, ethnography, and archival research. An experimental approach, defined by Saunders et al., [32], as a controlled investigation involving the manipulation of variables, was predominantly used throughout this work. Additionally, some mixed methods, particularly semi-structured expert interviews, were employed during early fact-finding stages. The experimental strategy best aligned with the practical aims and discipline-specific contributions of this research.

1.4 Contributions to Knowledge

This Thesis contributes new knowledge to the field of automated composite manufacturing by delivering the first systematic analysis of rework efficacy in AFP, encompassing both manual and automated methods for the reworking of gap and overlap type defects. It codifies previously undocumented, craft-based manual rework practices into standardised methodologies for experimental evaluation and quantifies the mechanical and cosmetic impacts of rework on composite part quality, revealing both its potential and inherent variability.

The thesis advances AFP automation by developing and validating real-time, in-process rework and defect rework and mitigation strategies, including recompaction methods and closed-loop trajectory correction via sensor-informed control architectures.

A further contribution of this Thesis is the development and application of a novel Benchtop-AFP platform for systematic, laboratory-scale study of rework processes. This platform served as a research-enabling tool, facilitating controlled experimentation on manual, collaborative, and automated defect rework within a cost-effective and accessible environment. By lowering the barrier to experimental AFP research, it contributes to the field both through its use in this study and as a scalable model for future exploration of AFP process development, human–robot collaboration, and defect mitigation strategies.

Collectively, this work progresses AFP towards a fully autonomous manufacturing system, reducing reliance on manual intervention and increasing process robustness.

Chapter 2. Literature Review

This chapter establishes the technical and industrial context within which the research presented in this Thesis is situated. It proceeds from first principles to the specific challenges that motivate the work, building a progressive case for why the rework of defects in AFP presents an open and consequential problem.

The chapter begins with the fundamentals of composite materials, including their constituent principles, mechanical behaviour, and industrial sectors which drive their adoption. After this a brief survey of the composite manufacturing landscape from which AFP emerged is presented. Manual layup, FW, and ATL are each considered in terms of their capabilities and limitations, establishing the context for AFP one of the leading advanced composites manufacturing techniques.

Section 2.3 examines AFP in detail, including the operating concepts, industrial history, and hardware variations. Current developmental trends in AFP research are introduced as well as a performance comparison against alternative advanced composites manufacturing techniques.

Section 2.4 introduces and discusses one of the main challenges facing AFP directly, focusing on defects, with particular emphasis on gap and overlap defects as these are widely reported as the most commonly occurring defects type. The causes and structural consequences of the defects are examined first, followed by a review of the detection and inspection systems that have been developed to identify them within the manufacturing cycle. Defect management strategies are then considered, including process design interventions, remediation approaches during curing, and the emerging capability of Continuous Tow Shearing (CTS) to address defect formation at its source.

The chapter concludes with a review of defect rework, where the literature reveals a consistent and significant absence of documentation of procedures, decision-making criteria, evaluation methods, or characterisation of the effect of rework. It is this gap that the present Thesis seeks to address.

2.1 Composite Materials: Fundamentals and Applications

2.1.1 Composite Material Principles

Composite materials are a class of material defined by the combination of two or more constituent materials to create a results material with enhanced material properties than either of the two constituent materials possess alone [9]. Composites appear in the natural world including wood, where the lignin matrix is reinforced with cellulose fibres, and in human and animal bones, where the collagen fibres reinforce the mineral matrix [1]. Composites generally consist of two constituent component materials which play different but interconnected roles in the resultant material, these are (1) the matrix, and (2) the reinforcement [2], [9]. The matrix is typically the phase of the composite material whose role is to transfer the load to the reinforcement and hold the reinforcement in place [3], [33]. The role of the reinforcement is to improve the mechanical properties of the matrix materials as the principal load carrying medium [3], [4]. Typical reinforcement forms are flakes, fibres, or particles [1], however, fibres are the overwhelmingly dominant option demanded by the market [8]. Composites can be broadly categorised by the geometry of their reinforcement, or by their matrix material type, typically Polymer Matrix Composites (PMCs), Metal Matrix Composites (MMCs) and Ceramic Matrix Composites (CMCs) [1]. PMCs are the most common choice among advanced composite materials [1]. Matrix materials in PMCs are typically categorised as either thermoset or thermoplastics polymers [3]. Thermoset polymers are insoluble and infusible after cure, while thermosets are formable at high temperatures and pressures [1]. Table 2.1 gives an overview of the key differences between thermoset and thermoplastic polymers.

Table 2.1. Key differences between thermoplastic and thermoset polymers

Thermoplastics	**Thermosets**
Soften upon heating and pressure	Decompose upon heating
High strains to failure	Low strains to failure
Indefinite shelf life	Definite shelf life
Can be reprocessed	Cannot be reprocessed
Non-tacky and easy to handle	Tacky
Short cure cycles	Long cure cycles
Higher fabrication temperatures and viscosities make processing difficult	Low processing temperatures
Excellent solvent resistance	Fair solvent resistance

Thermoset polymer matrices are the most commonly used in industry today, however issues around the difficulty in recycling thermoset polymer composites systems have led to increasing interest in utilising thermoplastic polymer composites [6].

The combining of the matrix and the reinforcing fibres is referred to as 'impregnation' [34]. This can be performed prior to the composite being formed to the shape of a part, that is, composites can be 'pre-impregnated' to form flat sheets referred to as 'prepregs'. These prepregs can then be used to form a part shape without the need for subsequent impregnation to occur.

Most engineering materials are both homogeneous, meaning the material has uniform properties throughout, and isotropic, meaning that the material properties are the same in every direction [1]. Composite materials by contrast are often inhomogeneous, meaning that the material has non-uniform properties over the body, and is non-isotopic [1], [5]. Non-isotropic materials can be defined as either orthotropic, meaning that the material properties in three mutually perpendicular directions at any point in the body are identical, or anisotropic, meaning that the material has material properties that differ in all directions at any point in the body [5]

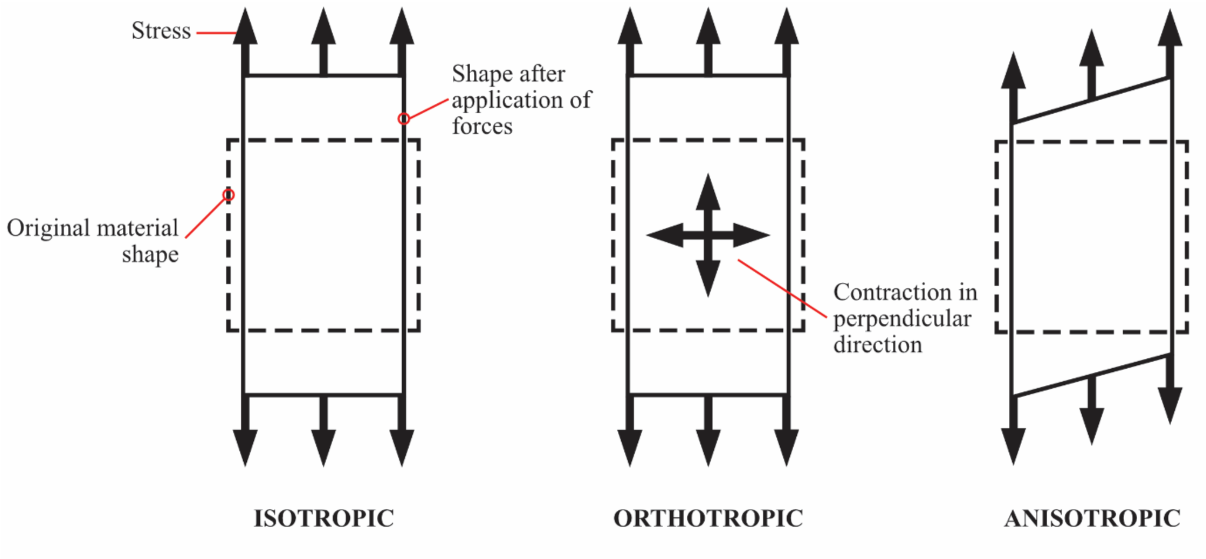

Figure 2.1. Mechanical behaviour of material types under normal stresses, from [5]

In isotropic materials, the application of normal stresses causes extension in the direction of the stress and contraction in perpendicular direction, but no shear deformation. In orthotropic materials, the application of normal stress in one of the principal directions results in extension in the direction of the stress and contraction in the perpendicular direction to the stress. The magnitude of extension in one principal direction under a given normal stress is different to the magnitude of extension of the same stress applied to a different principal direction. In anisotropic materials, the application of normal stresses results in not only extension in the direction of the stress and contraction in the perpendicular directions, but also to shear deformation. This same behaviour can be seen in orthotropic materials subject to normal stress in a non-principal direction [5]. Figure 2.1 shows a representation of the behaviour of isotropic, orthotropic, and anisotropic materials under normal stresses.

The non-isotropic nature of composite materials can be used to create structures tailored to complex loading requirements [1]. A fundamental concept in understanding composite structures is the laminate concept. The fundamental principle here is that the properties of the laminate are determined by the properties of the individual layers, or plies, which form the laminate [35]. Since the material offers different mechanical properties depending on the fibre direction, the sequencing of the plies determines the non-isotropic qualities of the resultant component. The sequencing of stacking of these plies and their respective ply angle is of great importance to the final mechanical properties of the composite part and is a key stage in the design of composite products [36]. This can be done to produce parts with tailored anisotropic qualities, such as being stiffer in expected loading conditions or allowing maximum flexural strength in directions likely to experience bending loads [4], [6]. Alternatively, the stacking sequences of plies can be designed in such a way as to result on components with quasi-isotropic qualities, meaning that the combination of the fibre directions through the layers results in comparably similar mechanical properties in all directions. Plies are typically defined in reference to their fibre angle with respect to a reference 0° coordinate system, and usually are deposited at 0, 90 and +/- 45 degrees fibre angles [6]. Composite design guidelines suggest that designing components with balanced and symmetrical stacking sequences is essential to ensuring stable laminates, particularly as the laminates as subject to curing, during which unbalanced or unsymmetrical laminates may experience warpage as the material deforms during the curing process, where the applied heating leads to differences in thermal expansion, as the expansion coefficients are different parallel or normal to the fibre axis, or as a result of uniaxial loading [9]. Figure 2.2 shows examples of stacking sequences illustrating laminate classifications which are balanced, symmetric, neither or both.

Unbalanced and asymmetric	Unbalanced symmetric	Balanced asymmetric	Balanced symmetric
0°	0°	0°	0°
90°	90°	60°	60°
	90°	120°	120°
-30°	0°		120°
+30°		0°	60°
-30°	-30°	60°	0°
+30	+30°	120°	
	+30°	0°	0°
	-30°	60°	135°
		120°	90°
			45°
			45°
			90°
			135°
			0°

Figure 2.2. Examples of stacking sequences

2.1.2 Industrial Applications and Market Context

Analysis of the size of the global composites market reports total sizes of USD 93.69 [37] or USD 108.8 [38] billion in 2023, USD 125.60 billion in 2025 [39], with compound annual growth rates reported as 6.9 % [37] and 10.8 % [38] or 5.97 % [39] raising the market size projections to USD 181.7 billion by 2028 [38] or USD 224.28 billion by 2035 [39]. The most favoured materials for reinforcement are glass and carbon, with glass being the industry favourite in 2024 accounting for 61 % of all revenue share [39].

The use of composite materials has seen a significant uptake across various industries due to their unique advantages, including high strength-to-weight ratio, corrosion resistance, and tailorable properties [9]. The aerospace and aviation industries have been pioneering the adoption of composites, leveraging their lightweight yet robust nature to improve fuel efficiency, reduce emissions, and enhance overall performance [40]. The widespread use of carbon fibre reinforced polymer (CFRP) composites in modern aircraft structures, such as the

Boeing 787 (2011) and the Airbus A350 (2015), which are composed of 50 and 52 % composites, respectively, exemplifies this trend [15].

The automotive industry has also embraced composites to reduce vehicle weight, improve fuel economy, and meet stricter emission regulations. CFRP and glass fibre reinforced polymer (GFRP) composites are increasingly used in vehicle body structures, chassis components, and interior applications [41]. Additionally, the growing demand for electric vehicles has further accelerated the adoption of composites, as their lightweight nature can contribute to extended driving ranges.

The renewable energy sector, particularly wind turbine manufacturing, has seen a significant uptake of composite materials. GFRP and CFRP composites are widely used in wind turbine blades due to their high strength-to-weight ratio, fatigue resistance, and ability to withstand harsh environmental conditions [42].

Other industries, such as construction, marine, sports equipment, and consumer goods, have also recognized the benefits of composites and are increasingly incorporating them into their products and structures [34].

As composite materials continue to evolve and their manufacturing processes become more automated and cost-effective, their adoption is expected to further accelerate, enabling the development of lighter, stronger, and more sustainable products across a wide range of industries.

2.2 Composites Manufacturing Context

Traditional, composite manufacturing has been a predominantly manually performed process, through the ancient forms of composite materials through to modern advanced composite materials. In recent years, especially in high-performance applications, automation of the manufacturing process has advanced into maturity and is beginning to see use across many advanced sectors. The manual layup method of composite manufacturing is briefly introduced, as many of the fundamental aspects of automated composite manufacturing have their origin in this manual manufacturing methods. Following this, a more detailed discussion of the introduction and development of automated composite manufacturing methods is given, leading to an introduction to AFP, including the history, development and current direction of the technique. To give context to this discussion, a brief discussion of automation and Industry 4.0 is given.

2.2.1 Manual Layup Techniques

There are various techniques for manufacturing composite materials, traditionally these involve a substantial amount of manual labour throughout the process [34]. The simplest and oldest of these methods is hand layup [4]. Gutowski [9], reported that despite the advancements in automated techniques in 1997 over half of all advanced aerospace composites structures were manufactured using hand layup. In 2025, Harik and Brasington [6], still report hand layup as “the most common and widespread technique for composites at present”.

Hand layup consists of the manual placement of fibres or prepregs inside a female mould and the working of the material into the shape of the preform using operator’s hands or hand tools [4], [43]. The use of hand rollers can ensure equal repartition of the resin [6] and ensure good contact and the removal of trapped air between plies [44]. The manufacture of the preform shape within the mould is then followed by the curing of the material [6], [8]. Hand layup is also heavily used when manufacturing composite parts using prepregs, where a prepreg is draped over a mould, after which operators manipulate its form with their hands until the sheet takes the form of the mould upon which it is draped. [43]. When performing manual layup using prepreg, the prepreg ply in its initial planar form will often have a total area which is greater or lesser than the total surface area of the face of the mould onto which it is to be applied. In these cases, the sheet must be manipulated by hand using rollers and hand-shearing to cover the full surface area required [43].

Hand layup has been found to be best suited to manufacturing smaller parts with complex geometries [8]. Crowley et al. [45] reports features that typically enable a part to be defined as complex include double-curvature, intersecting planes and sharp corners, and that the magnitude of this complexity can be roughly approximated by the severity of the geometry involved in these features. As part size increases, the time taken for manual layup increases and the cost-effectiveness versus automated methods of composite manufacture decreases [34]. Modelling of costs for five aerospace companies based in China by Weitao Ma [46], found that labour costs accounted for 42 % of total manufacturing costs.

Beyond hand layup, additional conventional composite manufacturing techniques such include Resin Transfer Moulding (RTM) and Pultrusion. RTM refers to a range of techniques sharing the feature of the injection of resin into a fibre preform inside of a closed tool [8], [9]. The potential for high productions rates has made RTM an attractive manufacturing method for the automotive industry. The use of a closed die is unique in composites manufacturing and can lead to parts with excellent dimensional stability and surface finish [44], however, this comes with an increased tooling cost. RTM allows for the manufacturing of very complex parts with a reduction or elimination of the need for assembly, and is best suited, according to Gutowski [9], for medium volume, small- to medium-sized complex parts.

Pultrusion involves the pulling of fibres through a wetting station filled with uncured resin and into a heated die, where the resin is cured. Similar in method to extrusion methods used in non-composite manufacturing, the method is best suited for the manufacture of parts with a constant cross-section [9]. As a result of the wetting process, fibre volume fractions can be as high as 75 %. This can result in parts with extremely high strengths comparable with steel and aluminium with a reduction in density of 20 % and 60 % respectively [44].

2.2.2 Manufacturing Automation

Innovation in manufacturing and heavy industry in recent decades has become synonymous with increases in manufacturing automation. In fact, the strongest movement for change in manufacturing is through Industry 4.0 [47] which seeks to blend the physical and biological spheres with the digital and bring automation to the forefront of modern factories of the future. Robotics will, of course, play a very large role in this change [48]. An industrial robot can be defined as:

> *"Automatically controlled, re-programmable, multipurpose manipulator, programable in three or more axes, which can be either fixed in place or mobile for use in industrial automation applications."[49]*

The authors of the robotic review this definition is taken from also argue that a robot should be implemented in an industrial scenario for four main reasons:

1. Reduced cost.
2. Improved Productivity due to higher output at lower cost than human labour.
3. Better quality due to ability to perform tasks with a high degree of consistency.
4. Elimination of hazardous tasks.

The robots of today can be classified generally by the work envelope they can operate within. This work envelope is a 3D space which can be reached by the robot given the number, type, and configuration of its joints. Robots are classified as one of 6 general types, based on their 1) the joint types, 2) number of degrees of freedom, 3) arrangement or orientation of the axes, 4) overall workspace geometry. The 6 general robot types are: cartesian, cylindrical, spherical, selective compliance articulated robot arms (SCARA), articulated, and parallel [50].

An area that is receiving considerable attention in contemporary research and development is robots capable of safely collaborating with humans, called "Cobots" [51]. Utilising the strength and power of robots and robotic systems alongside the critical judgement and awareness of human operators is an attractive proposal which can help to bridge the gap between wholly human operated manufacturing environments and wholly robotic systems [52].

Despite tremendous incentivisation and positive uptake, manufacturing automation does not come without significant disadvantages to manufacturing companies. Particularly the capital investment required for the initial stages of developing an automated system which can act as an exclusionary factor for many small and medium manufacturing companies [53].

2.2.3 Filament Winding (FW)

Filament Winding (FW) is the process of winding fibres around a mandrel-mounted mould [9]. The fibres pass through a bath of the matrix resin before being wound around the mould. A carriage containing the fibres and matrix bath is typically used and translates along an axis parallel to the main axis of the mandrel. The speed of translation of this carriage controls the fibre angle of the deposited material. Typically, FW is used for cylindrical parts such as storage tanks, for which it is highly repeatable and cost-effective [13]. A limitation of FW is its inability to produce parts where material follows a non-geodesic path [9]. It is also difficult to obtain uniform fibre and resin distribution throughout a part using FW [54], [55]. FW manufactured parts typically have a resin void content of 3% per part, compared to 1% per part for hand layup [9]. The process of FW can be highly cost-effective and is highly repeatable [13], and boasts one of the highest production rates of any composites manufacturing process at approximately 50kg/hr [9].

2.2.4 Automated Tape Laying (ATL)

ATL involved the layup of prepreg tapes, typically 50-300 mm in width over large, flat or slightly curved tools [6]. The tape laying process involves the tape being unwound and laid down in the desired shape with the desired fibre orientation of each ply [5]. ATL systems typically utilise a computer-controlled gantry system to precisely control the deposition paths of the tape onto the tooling, as well as controlled tension in both the tape and backing paper unwinding mechanisms, and automated cutting of the tape at the end of the deposition path [16]. ATL is very suitable for the manufacture of large components with low surface curvature [13]. Specific use cases include the vertical and horizontal tailplanes, and centre wing box of the A380 airplane [14] and the Airbus A350 upper shell fuselage skin section [15]. The technique can perform poorly over more complex surfaces because of the width of the tape used [16], often generating gaps, wrinkles, folds and other defects caused by tow buckling during steering, leading to improper tessellation of the material across the mould surface [17].

The starting up and slowing down of the placement head can be slow, hence ATL machines, like AFP machines are best suited for manufacturing large shell structures, such as fuselage and wing skins, or batch layup of large panels from which smaller structures can be cut out [9].

2.3 Automated Fibre Placement

2.3.1 AFP Concept and History

Automated Fibre Placement (AFP) is an advanced composites manufacturing technique that combines the advantages of ATL and FW [9]. Specifically, AFP was developed to overcome the limitations and constraints of FW [56]. In AFP, long, thin tapes of composite materials, typically 3.175 mm, 6.35 mm or 12.7 mm wide and referred to as tows, are laid sequentially onto a mould at pre-determined deposition paths [57]. The earliest account of using tows instead of larger ATL tapes was patented by Goldsworth et al. [18] in 1974. In this case larger ATL tapes were split into smaller tow by a mechanism inside of the placement head. Dedicated AFP machines began to be developed by Hercules Aerospace in 1980, and within the decade were made commercially available and used by The Boeing Company, Lockheed Martin Corporation, and Northrop Grumman [19]. Throughout the 1990s developments of the system continued, notably the development of a system capable of delivering 24 tows at once, enabling a layup rate of 30m/min with a corresponding productivity of 1.9 kg/h [20].

More recent developments in AFP manufacturing focused on tow steering, i.e., the delivery of tows over a curvilinear path [6], with of tow steering shown to increase productivity by 540 %, reduced material wastage from 62 % to only 6 % and reduce costs by 43 % compared to FW and Hand Layup [21], [22].

The unique advantage of AFP over FW is the ability to steer tows through non-geodesic curved paths, allowing for more reliable deposition of material over more complex geometry [58]. The use of thinner tapes in AFP allows for more successful tessellation of tapes over complex surfaces than ATL, making use of more complex and tighter steering radii without tow-buckling [13], [59]. In contrast to FW, in AFP tows are deposited directly onto the tool surface with minimal tension and controlled compaction pressure [60]. The largest AFP machines can deposit up to 32 tapes at once from the same end-effector and can independently stop and start each tow to tailor the width of the material being deposited with each pass [61]. This manufacturing technique is well-suited for the manufacturing of very large parts with low geometrical complexity [59], such as blades for wind turbines, composite pressure vessels, and aircraft wing components [62], [63].

The main disadvantage of AFP is its high cost for tooling and operating costs, and relatively high cycle time [64]. These methods do not see extensively widespread use in composite manufacturing due to the high capital investments associated with the required equipment [65]. Additionally, in a review of automated prepreg layup [14], researchers found that these techniques lacked in productivity and frequently produced parts containing defects. Other researchers [66] have noted that the use of AFP and ATL is currently constrained to only very large parts of simple geometries, compared to hand layup.

Table 2.2. Overview of AFP applications in Aircraft within the 2000s, adapted from [67]

Aircraft Model	Component made by AFP
Boeing F/A-18E/F	Air intake passage, rear flank coverings, stabilator covering
	Boeing C-17 Globemaster engine fan covering, landing gear housing
Leonardo AW609	fuselage panels
Boeing V-22	Osprey aft fuselage, flank layers, drag angle, stabilising protrusions, holding point
Raytheon Premier I	Body sections
Hawker 4000	Body sections
Lockheed F22 Raptor	Tailplane rotation axis
Sea Launch	Cargo shield

2.3.2 Industrial Applications and Case Studies

AFP has been utilised extensively in the aerospace industry for the manufacturing of wing spars and sections of fuselage [63], [68]. The ability of AFP to manufacture bespoke, variable stiffness composite components has led to an increase in the adoption of composite materials in new markets, such as energy, where wind-turbine blades have been manufactured using the technique [62], [69]. Table 2.2 describes some of the applications of AFP within aircraft manufacturing within 2000-2010, from [67].

2.3.3 System Hardware Variations

AFP systems come with a range of different hardware configurations all of which are subject to ongoing research and development. In the following section the main hardware variances shall be discussed along with the current research challenges and breakthroughs for each type of hardware.

2.3.3.1 Platforms

AFP machines come in three main types, characterised by the platform the AFP head is mounted on, and that which provides the motion of the head across the geometry of the part. These are (1) horizontal gantry, (2) vertical gantry, and (3) robotic arm. Figure 2.3, Figure **2.4**, and Figure 2.5 shows diagrams of each of the three types. Vertical Gantry systems use a large gantry which can move in three directions, with the end-effector able to deposit material vertically onto to the tooling plate.

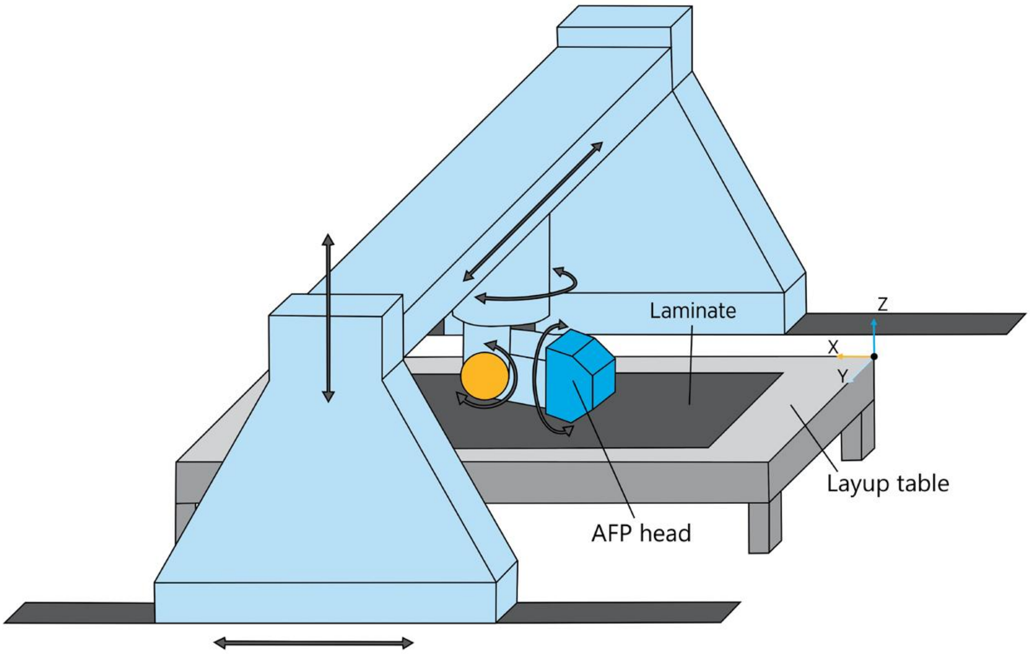

Figure 2.3. Vertical Gantry AFP system, adapted from [6]

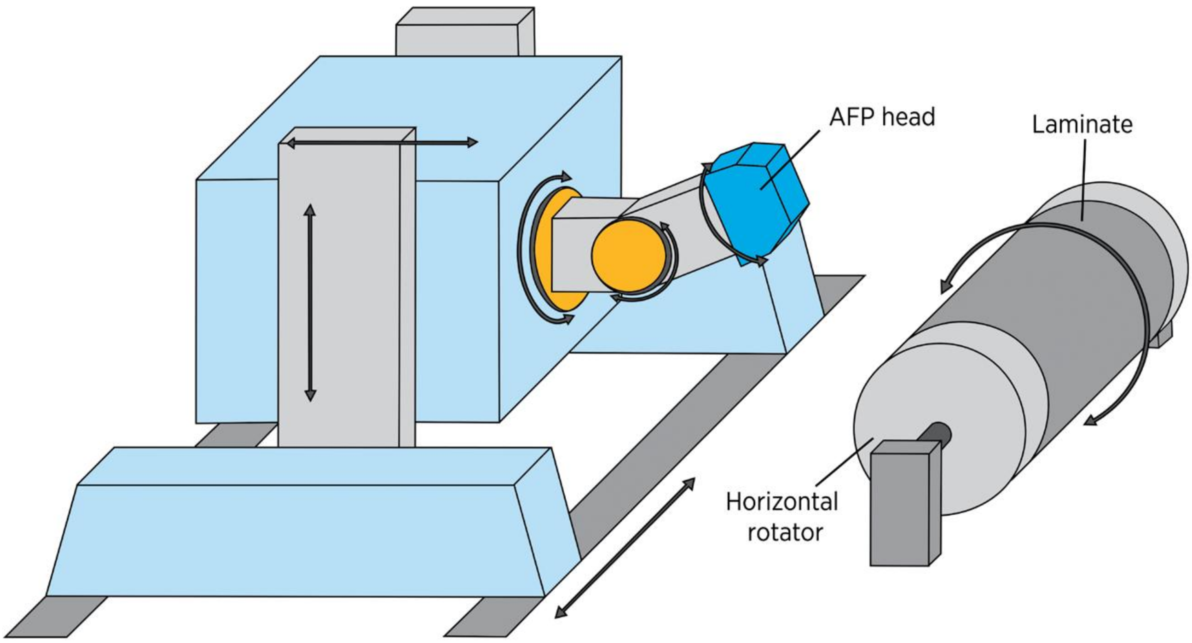

Figure 2.4. Horizontal Gantry AFP system, adapted from [6]

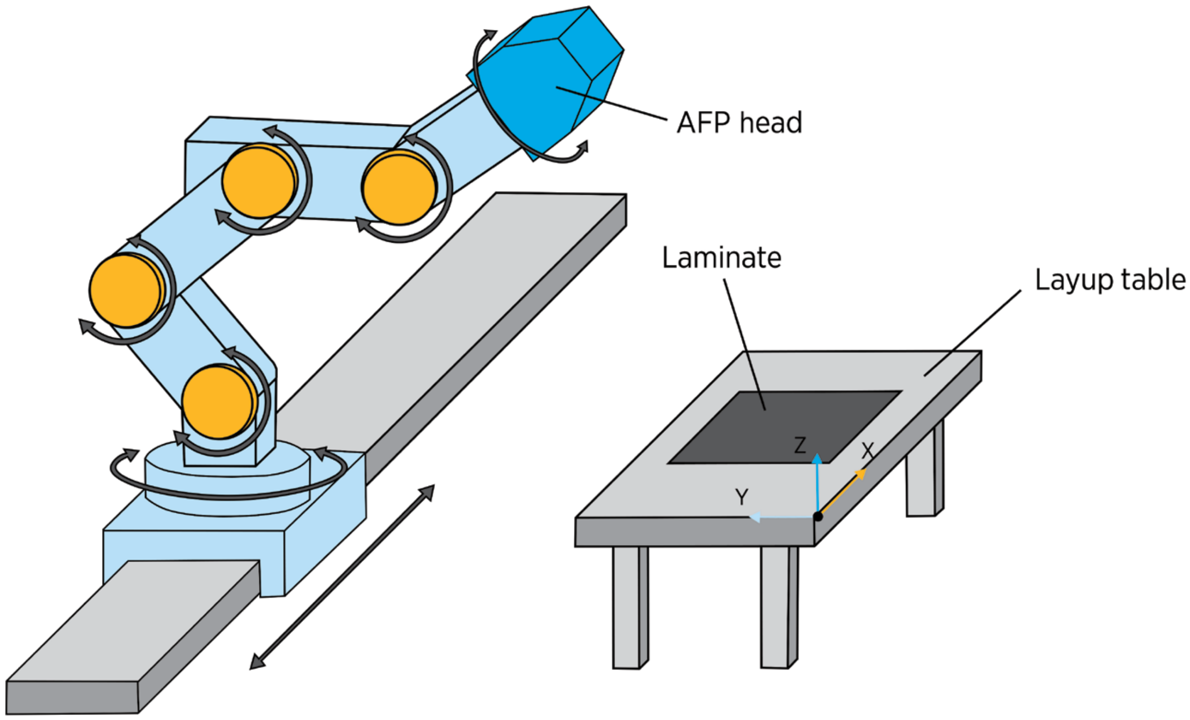

Figure 2.5. Robotic AFP system, adapted from [6]

Vertical Gantry systems are the most common and are particularly suited to long parts which are not mounted on a rotator [6]. Horizontal gantry systems have an end-effector which can travel in three directions on a gantry, but deposits tows horizontally onto the tooling [6]. Horizontal gantries are more suitable for parts with large height or those which require rotation, as in some cases a vertical gantry would impede the required motion. Robotic AFP cells make use of the degrees of freedom of the robotic arm for flexible deposition of material onto both rotational and stationary tooling. The key difference between robotic AFP and vertical and horizontal gantry systems is that in robotic AFP the material is located in the end-effector itself, rather than in external material storage [6]. Robotic arm type AFP machines are most suitable for parts with complex shapes with more extreme curvatures, as it has a far wider range of possible movements [68]. Recent advances in tooling configurations in robotic AFP have seen the tooling mounted on the robot, while the end-effector remains stationary or rotates around one axis [6], or dual robot toolless AFP where tow robots deposit material synchronistical without an intermediate tooling surface [70].

2.3.3.2 End-Effectors

A schematic diagram of a typical AFP system is shown in Figure 2.6. Typical features include several rollers, for ensuring tension in the incoming tow, unwinding backing paper, depositing the tow at a controlled rate through the add roller, and at a controlled compaction force through the compaction roller. A single tow Accudyne 1000+ end-effector, [71], is shown in Figure 2.7.

A key benefit of AFP is that the usually separate phases in composite manufacture including layup, heating of the tooling to increase tackiness, and consolidation are merged within the layup head [6]. This greatly increases productivity [72].

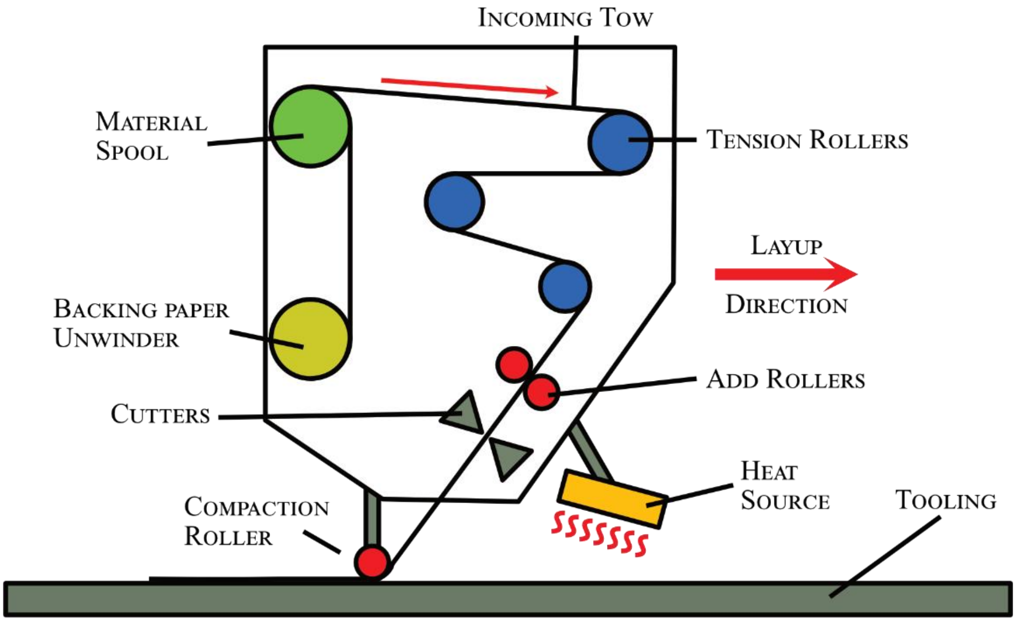

Figure 2.6. Schematic Diagram of AFP end-effector

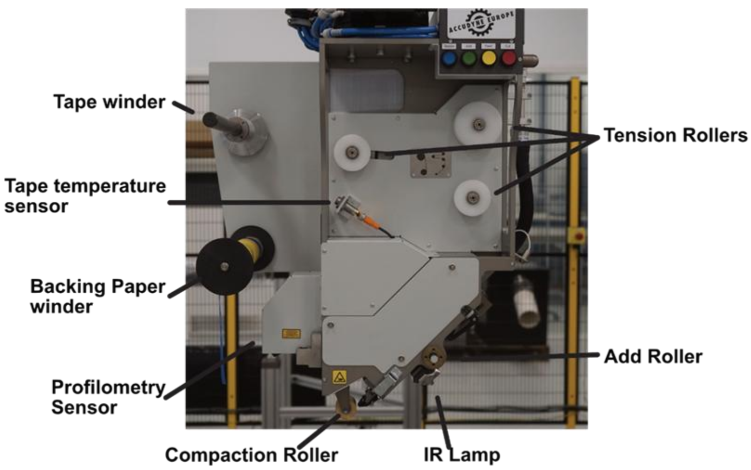

Figure 2.7. Single tow Accudyne 1000+ end-effector [71].

2.3.4 Critical Process Parameters

The process of manufacturing parts through AFP involves a number of critical, controllable but interdependent process parameters. Control of these parameters is essential for the manufacturing of parts with minimal defects. The key processing parameters are introduced below.

2.3.4.1 Layup Speed

Layup speed (mm/s) is the velocity at which the end-effector moves across the layup surface. Layup speed is in essence an indirect parameter, as it does not directly influence the quality of the layup, but its effects on other parameters can cause quality variations [6]. Higher speeds reduce the dwell time for external heating sources over the material, reducing the temperature input and potentially increasing resin viscosity [73] but also resulting in less time where the material is subject to compaction force and heating, leading to weaker cohesion [74]. Conversely, lower speeds lead to longer thermal exposure which leads to improved polymer healing up until the applied temperature leads to thermal degradation of the material [75]. An overarching aim of research and development in AFP manufacturing is in the minimising of layup time, while maximising layup accuracy [58]. Various experiments examining different layup velocities have shown alterations in layup quality and the required processing parameters, such as [76], [77]. Joining the control of heating levels to the tool speed is important in ensuring uniform-like heating across the spread of the substrate. For instance, in curvilinear paths that include steering, the speed will often be reduced during steering elements of the path. Without coupled control of the heating level during these slower sections, they will be subjected to higher heating levels and can burn, which will negatively affect the overall quality of the final part [6].

2.3.4.2 Compaction Force

Compaction force (N) is the normal force delivered through the compaction roller in the AFP end-effector which helps the placed tow adhere to the substrate and drives matrix flow under pressure.

Compaction rollers are an essential part of the AFP head. Their main functions are to 1) place the tows, 2) facilitate the required levels of tack, and 3) reduce voids between the tows [60]. These functions are achieved by the application of pressure by the compaction roller to both the tow and the substrate directly after the application of heat by the heat source [6]. Compaction pressure is critical in developing intimate contact between plies, however excessive compaction levels can lead to material degradation [78]. Brasington et al., [68], present the different types of rollers as follows.

Generally, smaller scale AFP production, makes use of solid or perforate compaction rollers [68]. The deciding factor in which roller to use is the hardness of the roller, measured through the durometer scale, the international standard in material hardness. The higher the value on the durometer scale for a given material, the harder said material is. Studies have been performed by Bakhshi and Hojjati [60] examining rollers with different durometer values, specifically 35, 60, 85 durometer, and one stainless steel roller. The study presents that the stiffness of the roller determines the mode of application of the compaction force, as well as the area over which this compaction force is spread. Generally, softer roller materials apply lower pressure over a larger area. Conversely, harder roller materials apply a higher pressure

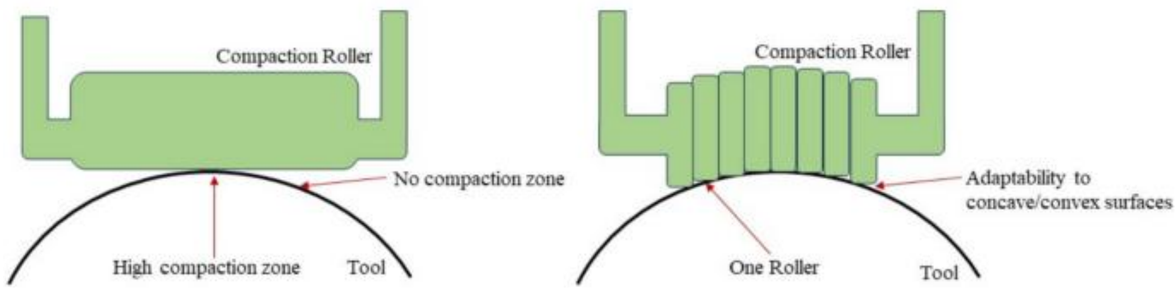

Figure 2.8. Conventional solid (left) and segmented (right) compaction roller, adapted from [58]

over a more concentrated area. Bakhshi and Hojjati determined that that the optimal configuration was a soft-material roller capable of applying the required compaction force, as the wider area over which the pressure is spread ensures a more fully compacted part.

Segmented rollers feature multiple small roller sections that can move separately on the same shaft. These are used to ensure more evenly spread compaction force across the length of the roller. This is particularly an issue for curved parts being consolidated with a non-segmented roller [78]. Some segmented compaction rollers are designed to more intelligently adapt to more complex tool surface geometries by utilising internal bladders controlled pneumatically or hydraulically [79]. Figure 2.8 shows examples of a conventional solid and segmented compaction roller, adapted from [58].

One issue with the compaction of thermoplastic composites is the requirement for extreme heating and cooling to ensure their proper processing. Historically this has been very difficult to achieve with a standard AFP setup and the types of compaction rollers mentioned above. Research by Lamontia et al., [80], investigated the issue and proposed a system including three separate rollers. The first roller is heated and provides the initial compaction force and initiates the healing process of the polymer chains in the composites in a thin line. The second roller is also heated but has an area geometry and is used to complete the healing process. The third roller chills the material and compresses any remaining voids in the material. Research from Bakhshi et al., [60], highlights that steel is the favourite material for thermoplastic compaction rollers as it can most effectively sustain the high temperatures used in the process.

2.3.4.3 Temperature

Heat is typically delivered via Infra-Red (IR) lamps, lasers, or hot gas torches (HGTs). These heat the tow or the tooling surface ahead of the nip point to ensure proper adhesion [6]. Several types of heat source hardware are found in literature. The following section explores these types and the relevant literature discussing their application. The application of heating systems varies depending on the material used, since thermoset and thermoplastic materials have vastly different thermal properties and responses. Thermoset materials do not have a melting point, they are instead characterised by their sub-ambient glass transition temperature (T_g) before curing occurs (usually on or around 0°C) and the dry or wet T_g after curing (~120-200°C) [6]. Thermosets typically require lower temperatures for placement, hence allow for the use of AFP systems with heating components with lower outputted heating levels [6]. Thermoplastics require significantly processing at temperature above their melting temperature, (T_{melt}) [9], which can be approximated, from [81], as:

$$T_{melt}(°K) \approx (1.5 - 2) \cdot T_g(°K) \tag{2.1}$$

Thermoset systems, by comparison have a cure onset temperature approximately defined as:

$$T_{cure} \approx T_g \tag{2.2}$$

The result is that for systems with approximately equal T_g much higher processing temperatures are required for processing. In typical aerospace grade materials, thermoset composites are cured at around 170°C, whereas near-equivalent thermoplastic materials would require processing temperatures of 350° or higher [9].

Usually, this means the IR heaters are not appropriate for use with thermoplastic material systems [6].

HGTs were the initial heat source used at the inception of the design and use of both AFP and ATL machines [82]. They are comparatively inexpensive, but the temperature is difficult to control relative to other heat sources [83]. Typically, a HGT uses hot gas which by controlling the flow rate can control the temperature applied [84]. HGTs are capable of producing high enough temperatures needed for the consolidation of thermoplastic layups [85]. Compared with laser heaters, HGTs have the following advantages, as noted by [86], [87]: lower safety concerns, provides more distributed heating, ability to heat both the polymers and fibres.

IR heaters are the most common form of heaters found in AFP systems [6], [68]. IR heaters function by passing heat onto the substrate through radiation. In radiation, when the heat energy hits an object, some of this energy is absorbed, while some is reflected away, and some is transmitted through. For this reason, most IR heaters include a reflector mirror to ensure most of the energy is emitted in the correct direction [88], [89]. IR heat sources often take the form of bulbs which can be individually controlled as well as being operated at a percentage of their capacity. This is typically synchronised with the layup speed [6]. Recent research was conducted to develop a closed loop system where the control of the power supplied to bulbs, which is performed informed by sensors measuring the heat on the surface [90]. The main disadvantage of IR heaters is the inefficiency of their heat transfer and non-uniform heat dispersal [88]. IR heaters are also not capable of producing high enough heats for the consolidation of thermoplastic composites [68].

The first concept of laser heaters was developed in the 1980s by Beyeler et al., [91]. In the ensuing time since their inception, laser heaters have become lower cost and more robust [6]. The main advantages of laser heat sources are the high energy density, more focused heating, the enabling of faster processing rates, and resultant laminates with better surface quality. The main disadvantages are the necessary safety precautions required for laser-assisted AFP systems, including laser shielding and additional PPE, as well as the fact that laser heating is not compatible with glass fibre materials and other materials which do not absorb the laser's energy [6]. Experimental work by Stokes-Griffin and Compston has shown that laser-assisted AFP has comparatively better interlaminar strength versus placement rate [92]. Table 2.3 Shows a summary of the heating technologies, from [6].

Table 2.3. Summary of the characteristics of common AFP heating systems, from [6]

Heating System	**Material**	**Controllability**	**Temperature**
Hot Gas Torch (HGT)	Thermoset/Thermoplastic	Low	Medium
Infrared (IR)	Thermoset	Medium	Low
Laser	Thermoplastic	High	High
Pulsed Light	Thermoset/Thermoplastic	High	Medium/High

2.3.4.4 Tension

Tension in the tow as it is passed through the end-effector and deposited onto the mould is essential in ensuring the shape and disposition of the tow is correct as it is placed on the tooling surface [6]. The rollers in the end-effector are individually actuated to ensure proper management of tow tension during placement. When the tow tension is excessively high, tow slippage can occur, as the tensioning force overcomes the adhering force between the tow and substrate [93]. When tows are deposited over concave curvatures, high tow tension can lead to bridging [6]. In low areal weight composite materials, excessive tow tension in extreme cases can lead to roping of tows [6].

2.3.5 Technology Development Trends

A major constraint for the adoption of AFP to more complex parts is the design of the AFP head. In order to manufacture larger parts more effectively, larger heads have been developed, the size of which is a direct barrier to the navigation of the head over complex curvatures without contacting any other section of the part surface [94] [95]. Current research in the direction of deploying AFP on more complex curvatures has focused on modular AFP heads [79].

Several companies are using industry 4.0 enabled systems for advanced AFP manufacturing. Systems like MTorres's kinematic digital twins [96] enable sequence optimisation and collision detection, while Broetje-Automation's SOUL RMOS Digital Twin [97] supports online path creation and integration with Siemens Virtual NC-Kernel for accurate virtual machine simulations. MTorres's Edge Data Analytics platform features self-diagnosis routines and predictive alarms [98], complemented by Coriolis Composites' CoDa platform for high-frequency data collection and traceability [99]. Tools like Coriolis's CADFiber and CATFiber enable early incorporation of manufacturing constraints in path planning [100], [101], while Addcomposites' AddPath software integrates FEA for fiber placement

Table 2.4. Summary of Material Deposition rates for several advanced composites manufacturing methods, from [107]

Fabrication Method	**Rate (lb/hr)**
Hand Layup	1.5
Preplied Broadgoods	3
Tape Laying Machine	10
Filament Winding	100

optimization and stress analysis [102]. Coriolis's HMI system provides comprehensive control and traceability [103], while MTorres employs Augmented Reality for immersive visualization of assembly instructions [96]. Electroimpact's RIPITx system conducts in-process defect inspections [104], Ingersoll's ACSIS detects defects with over 99% accuracy [105], and Fives' COAST system uses Optical Coherence Tomography for real-time inspection [106].

2.3.6 Performance comparison and limitations

Each of the several methods for fabrication of advanced composite structures occupies a distinct niche defined by geometry, production volume, labour demand, and cost profile.

Early analysis helps contextualise the scale of difference between the approaches. Freeman and Stein, [107], reported deposition states panning nearly two orders of magnitude, with hand layup achieving 1.5 lb/hr, while FW reached 100 lb/hr, with tape laying machines occupying a middle ground at 10 lb/hr (Table 2.4). A cost and cycle time analysis by Krolewski and Gutowski, [108], of a 4-ft^2 24-ply part produced at an annual volume of 2,000 units further illustrates this variance (Table 2.5).

Table 2.5. Cost and cycle time for a 4-ft^2, 24-ply part for annual production of 2000 parts, from [108]

Fabrication Method	**Cost ($)**	**Cycle time (hr)**
Manual	353.4	3.911
Automated Cutting	502.4	3.291
Robotic Transfer	529.1	1.526
Tape Layup	471.0	1.772
Robotic Layup	518.3	3.075
Pultrusion	93.5	0.145
Filament Winding	226.4	2.459

Table 2.6. Performance comparison for ATL, AFP, and Conventional Composites Manufacturing techniques, from [13]

Specification	ATL Method	AFP Method	Conventional Methods
Material Scrap	Low	Low	High
Labour Costs	Low	Low	High
Repeatability	High	High	Low
Accuracy	High	High	Low
Productivity	High	High	Low
Cost effective	Yes	Yes	No
Material Types	Wide Tapes	Narrow tows	Wide Tapes
Layup speed	Very high	Relatively high	Very high
Components' geometry	Large components	Curved & contoured surfaces	Large components

Pultrusion offered the lowest cost ($93.2) and shortest cycle time (0.145 hr), while manual layup, robotic transfer, and robotic layup all clustered between $350-5530 and 1.5 – 4 hr cycle times. These figures reflect the fundamental trade-off between capital investment and per-part economics that underpins the choice of manufacturing method.

A comparison of automated placement techniques, summarised by Oromiehie et al., [13], positions ATL and AFP as comparable in key respects (Table 2.6). Both techniques achieve low material scrap, low labour costs, high repeatability, and high accuracy relative to conventional hand layup-based methods. The primary distinction lies in geometric capability and material format: ATL is best suited to large, relatively flat or gently curved components using wide tapes, while AFP using narrow tows, is designed for complex contoured surfaces. Conventional manual methods, though capable of handling wide tape formats similarly to ATL, are characterised by poor repeatability, high labour demand, and low productivity.

A broader process comparison including FW, vacuum infusion, RTM, compression moulding, and pultrusion provides (Table 2.7), from [109], shows AFP at the higher end of both capital equipment cost and tooling cost, with a mid-to-high finished part cost. This pattern is consistent with its positions as a high-capability, high-investment technology.

AFP's primary advantage over manual layup is throughput. The process has been demonstrated to achieve deposition rates of approximately 8.6 kg/hr [14], compared to roughly

Table 2.7. Overview of composite manufacturing techniques, from [109]

Moulding method	Production rate	Capital equipment cost	Tooling cost	Labor cost	Finished part cost
Filament winding	Mid	Mid-high	Mid	Low	Low
Vacuum infusion processing	Low	Low	Low	High	Mid
Resin transfer moulding	Mid	Mid	Mid	Mid	Mid
Compression moulding	High	High	High	Low	Low
Pultrusion	High	High	High	Low	Low
Automated fiber/tape placement	Mid-high	High	High	High	Mid-high

1 kg/hr for hand layup [110], a nearly ninefold increase. In terms of labour, analysis of early automated composites manufacturing methods including both ATL and AFP showed reductions in person-hours of 70-85 % relative to manual layup [111]. A review commissioned by the United States Department of Defence, [112], found that AFP could deliver manual labour savings of up to 50 % for complex contoured parts, with savings of greater than 10 % for simpler, flatter parts. The latter reflecting cases where AFP's geometric capability offers less marginal benefit over simpler automated or manual methods. Despite these productivity advantages, AFP faces significant economic and operational challenges. Capital acquisition costs for AFP systems range from approximately £1.0-1.2 million [113], [114], [115], representing a major barrier to adoption, particularly for smaller institutions, and educational facilities [112].

When compared directly with FW for the manufacture of composite pressure vessels, AFP has been found to be 1.77 times more expensive [116], highlighting that FW remains the more economical choice where part geometry permits its use.

Analysis of the typical cycle times for AFP by Electroimpact [28] and Boeing [29] found that inspection and rework accounted for 63% and 32% respectively. Further analysis by Rudberg et al. [30] found that AFP cells are typically only used to layup material 42% of the cycle time, with the rest of the cycle divided between inspection (28%), tool moves (11%), reliability recovery (10%), and operator breaks (9%). These figures underline the degree to which defect occurrence and its downstream consequences, rather than raw deposition speed, govern overall throughput in practice.

AFP systems face challenges including lack of standardization, difficulty with complex geometries, reliance on operator feedback, early-stage Augmented Reality (AR) and Artificial Intelligence (AI) integration, and inability to dynamically adjust layup strategies in real-time without pre-programmed parameters [6].

2.4 Defects in AFP

Defects are irregularities and imperfections in the layup which may cause the part to fail cosmetically, or, more critically, mechanically. Since AFP is often used for the manufacturing of high-performance composites parts, for instance for the aerospace sector, the quality of the components must be very tightly controlled. It is for this reason that the study of the cause, effect, mitigation. and critically in this Thesis, the rework of defects has warranted attention in literature and in industry. In this section the relevant literature on defects in AFP is discussed beginning with definitions of common defects, followed by discussions on the cause and effect of these defects. Finally, a discussion on the existing literature on the reworking of defects is be introduced. This area of defect management has remained critically understudied in the literature and forms the basis of the central gap that this thesis addresses.

Extensive reviews [13], [117] exist covering the range of defects occurring in AFP manufacturing. Defects are imperfections in the layup that cause the final part to fail structurally or cosmetically through improper management of applied stresses [24]. In the literature, defects are broadly categorised into those induced through improper management of process parameters, and those induced through improper placement of material [13]. Harik et al., [117], provide identity cards and descriptions of the key placement-induced defects.

Table 2.8. AFP Defects and Descriptions

Defect	Description
Gap	Where the space between tows is larger than a specified maximum allowable value.
Overlap	Where the edge of a tow is placed over the top of an adjacent tow. Typically overlaps occur where gaps do.
Twist	Where the face of the tow facing away from the mould surface changes along a length of the tow. This is typically caused by slippage and twisting inside the AFP head.
Wrinkle	Where a fold is formed across the width of a tow and excess material is consolidated on top of the same tow. This is typically caused by the wrong settings of the feed rate of the tow causing bunching of material before the point of consolidation.
Fold	Where material becomes caught and is consolidated folded over along the length of the tow.
Pucker	Where a section of the tow does not adhere to the layup surface despite the lengths before and after adhering properly.
Bridging	Where a tow is stretched across a radius in the mould surface and lifts off the mould surface. This is typically caused by improper feeding of material during the laying up around the radius.

Table 2.8 describes these identified defects and their descriptions. This work focuses specifically on gap and overlap defects, which are cited as the most common types of defects [117].

2.4.1 Cause

Oromiehie et al., [13], state that gaps and overlaps are primarily resultant from discrepancies between the designed and actual laid paths. Guin et al., [118], note that tow-to-tow gaps do not appear in a predictable basis over typical AFP processes, rather, they maintain that gaps are seen to be randomly occurring and isolated in nature. Brasington et al., [117], find the most common cause of gaps and overlaps is as an effect of steering during layup of a complex part. They further note that most gaps arise from (1) variability in tow width, (2) demanding tow-steering induced by a complex mould shape, or (3) sub-par AFP system setup and performance.

Gaps may also arise from the placement strategy. For instance, in the layup of a ply with a constant fibre angle, gaps are inevitable when tows are deposited on any part of the tooling surface which is not parallel to plane on which the layup of that ply began [119]. Additionally, where two regions of the part at different fibre orientations meet, gaps and overlaps are inevitable [120]. Gap and overlap defects often manifest with triangular geometry at tow boundaries or with rectangular geometry when they occur in a sequence of tows aligned in the same fibre direction [121].

2.4.2 Effect

Due to the non-isotropic nature of composite materials, analysis of the effect of defects depends on a range of factors, including the loading conditions and direction, the type of defect, and the configuration of the defect within the test specimen. As such, in the section below a range experimental works analysing the effect of gap and overlap defects are discussed in detail.

Sawicki and Minguet [122], presented research testing the effect of the presence of gap and overlap defects in laminates tested under compressive loading with the defects in each 90° ply of three different laminate stacking sequences. Their results showed reductions in compressive strength of 5 - 27 % in laminates containing at least one gap or overlap of 0.76 mm in width. Further, the authors showed that, for gaps larger than 0.76 mm, the rate of reduction in strength remains constant, while for gaps smaller than this threshold the stated rate decreases. Croft et al., [24], presented a comprehensive review of the effects of gaps and overlaps on the ultimate tensile strength of composite parts at a lamina level using fibre tension, fibre compression, and in plane-shear tests. Additionally, the authors conducted tests to determine the effects of the defects at a laminate level, using open-hole compression tests and open-hole tension tests. The authors concluded that, compared to a pristine baseline, the ultimate tensile strength varies by less than 5 % at a lamina level, and up to 13 % at a laminate level. Comparing the behaviours under tension and compression, gaps result in a similar change of ± 3 %, deemed as negligible by the authors. Overlaps on the other hand do not significantly change the results of tensions tests, but under compression change the results from 3 % to 12 %.

Lan et al. investigated the impact of isolated gaps and overlaps on the tensile, [123], and compressive, [124], loading conditions, and the influence of curing the laminates with or without a caul plate. For compressive loading, gaps resulted in a 12 % reduction in compressive strength after curing with a caul plate, and 20 % reduction without. Overlaps, however, resulted in a 12 % reduction with a caul plate, and 55 % reduction without. Under tensile loading conditions minimal reduction was seen through the introduction of the defects, with overlap defects aligned with the loading condition increasing the tensile strength of the coupons. Significantly, Lan et al. [124], showed that plies aligned in the same direction can partially heal gaps and overlaps during the curing process, and that the degree of healing is enhanced using a caul plate.

Elsherbini et al., [125], investigated the effect of 3.125 mm width gaps running across the width of $[0]_9$ laminates. on the tensile fatigue behaviour of the laminates. They concluded that the influence of the gaps reduced the fatigue life of the laminate, but that this effect was magnified at higher maximum stress levels and diminished at lower maximum stress levels.

Guin et al., [118], investigated the effect of 1.27 mm gaps under tensile and compressive loading. They tested $[+45/-45/90/0]_{2S}$ laminates with gaps either in all of the plies, or in only the 90° plies. Their results showed reductions in performance across all tests for coupons with defects in all the plies, but limited reductions in those with defects only in the 90° plies. The authors correlate the extent of the knockdown in mechanical performance to the degree of out-of-plane waviness in the laminate as caused by the defects. In those coupons with defects only in the 90° plies, the presence of the defect free plies confines the waviness locally to the defect regions.

Woigk et al., [126], examined the effect of 2 mm wide gaps and overlaps in the ±45° and 90° plies of a $[+45_2/90_2/-45_2/0_2]_{3S}$ test laminate under tensile and compressive loading. Their investigation showed that isolated gaps both aligned and staggered in the thickness direction showed limited reductions in tensile strength of 1.3 % and 0.2 %, respectively. Meanwhile, overlaps caused a 3 % increase in the tensile strength of the coupons. Combined gap/overlaps however caused a larger 7.4 % decrease in the tensile strength. Under compressive loading, aligned gaps and overlaps caused a 7.6 % and 9.5 % increase in compressive strength respectively, while staggered gaps showed a smaller 1.3 % increase. Again, combined gap/overlap defects showed a large 14.7 % reduction in compressive strength. The authors concluded that the number of defects has less of an effect on the mechanical performance of the test coupons that than degree of fibre misalignment.

Ngyuen et al., [127], [128]., studied the influence of gaps and overlaps on tensile and compressive properties of laminate across a range of defect configurations. In [127], Nguyen et al., inserted gaps and overlaps ranging in size from 0.8 mm to 12.7 mm in a quasi-isotropic $[+45/0/-45/90]_{2S}$ laminate with a stagger between defects ranging from 0.0 mm to 25.4 mm. Under tensile loading the effect of gaps showed up to a 60 % reduction in tensile stiffness and 55 % reduction in strength. Staggering the gaps reduced the knockdown in properties. Overlaps, conversely, increased stiffness and strength by up to 20 %. This effect was diminished by staggering the overlaps defects. Under compression loading, gaps produced up to a 45 % reduction in stiffness and strength, and when staggered this effect was reduced to only a 30 - 35 % reduction. Overlaps had a minimal effect on compressive strength, the highest being a 20 % reduction when defects were fully aligned through the thickness direction of the coupons. The authors concluded that the degree of waviness was more significant than the size or distribution of the defects on the reduction of mechanical properties.

In a further experimental work, [128], Nguyen et al., manufactured quasi-isotropic $[45/0/-45/90]_{2S}$ laminates with gap and overlap defects aligned in the thickness direction of sizes 1.5875, 3.175, 6.35, and 12.7 mm in all four of the 90° plies. The coupons were tested under tensile loading conditions. The knockdown in tensile strength varied from 5 % for the 3.175

mm overlaps, to 26 % for the 12.7 mm gaps. Gaps sizes of 1.5875 mm to 6.35 mm exhibited similar strength knockdowns, whereas 12.7 mm gaps showed a more significant knockdown. Specimens with overlaps exhibited limited knockdown in tensile strength and this effect was not seen to be modulated by overlap size.

Nartey et al., [129], investigated the effects of gaps and overlaps by the degree of out-of-plane waviness they produced in the resultant laminate under tensile and compressive loading. The authors examined micrographs of the laminates and found waviness deviations in the angle of the ply of up to 12.4°. They found a strong correlation between the knockdown in mechanical performance with the out-of-plane wrinkle angle. A wrinkle angle of 7.8° produced a 21 % reduction in tensile strength, while a maximum compressive strength knockdown of 37 % was observed for a wrinkle angle of 12.4°.

Ghayour et al, [130], examined the flexural response of laminates containing gaps. 2 mm gaps were introduced into a quasi-isotropic $[0_2/45_2/90_2/-45_2]_{2s}$ laminate. A reduction in flexural strength and flexural stiffness of 32 % and 35 % were observed for gaps. Short beam shear tests showed a reduction in the interlaminar shear strength (ILSS) of 13 %.

Ghayour at el. [131], also investigated effect of gaps on the impact strength of laminates. They found that gaps reduced the maximum sustainable impact force by 17 % and increased the delamination area during impact by 50 %.

Böckle et al., [132], introduced 3.175 mm defects into $[45_2/-45_2/0_2/90_2]_s$ laminates and tested the response under tensile and in-plane shear loading. Test sets of either two gaps, two overlaps, four gaps, or four overlaps, in the 90° plies at the centre of the laminate. Their results showed minimal impact on tensile strength for two defects, a 20 % strength reduction for four gaps, 12 % reduction for four overlaps. In terms of in-plane shear gaps showed a 5 % reduction in strength while overlaps resulted in a 6 % increase in strength.

Del Rossi et al,, [133], introduced half-gap, half-overlap defects with a length of 63.5 mm and width varying between 1.27 mm and 2.45 mm in a $[45F/(-45\ T/\ 0T/\ 45\ T/\ 90T)_2]_s$ laminate, where ‘F’ are woven fabric plies deposited by hand-layup, and ‘T’ are unidirectional tape plies deposited by AFP. The tests varied 1) number of defects, 2) width of defects, and 3) orientation of defects, and tested coupons under tensile and compressive loading. The results showed that under tensile loading in the 0° direction, minimal impact of the embedded defects was seen. Small strength reductions seen for 45° and 90° defects. 0° defects show negligible effect. Configurations that induced greater waviness out-of-plane exhibited more pronounced strength reductions. Increases in defect width led to decreases in tensile strength. Under compressive loading, greater numbers of defects led to greater reductions in strength. The largest reductions in compressive strength were observed for laminates exhibiting the greatest ply waviness.

Nimbal et al., [134], examined increasing quantity of triangular gaps with a max width of 5 mm spanning the width of the specimen in [45/-45/0/90]2s laminates under compressive loading conditions. They found that 2, 4, and 6 embedded gaps reduced compressive strength by 29.1 %, 24.2 %, and 31.3 %, respectively. Further a correlation between the degree of waviness and compressive strength loss was seen.

Suemasu et al., [135], performed tensile and compressive tests on quasi-isotropic [45/0/-45/90]2s, laminates with embedded 3.175 mm gaps or overlaps between each course of 16 tows. For gapped specimens a reduction of 18.1 % and increase of 1.7 % was seen for tensile and compressive strength respectively. For overlaps specimens a reduction of 18.3 % and increase of 4.9 % in tensile and compressive strength respectively was seen.

In a further work, [136], Suemasu et al., examined the effect of 3.125 mm gaps in the 7th and 10th -45° plies of one $[45/0/-45/90]_{2s}$ laminate and in the 12th (45°) and 10th (-45°) plies of another laminate of the same stacking sequence. Three specimens were cut from each of the laminates so that the gaps were configured in different ways through the gauge section. Some specimens featured gaps entirely enclosed with the gauge section, while others featured only the gap ends of one more gap. The results indicated that the presence of gaps led to a significant reduction in compressive strength. Specimens with gaps showed a marked decrease in strength compared to those without. The maximum strength reduction was observed in specimens where gaps overlapped at the gage section, highlighting the interaction effects of multiple gaps. The failure modes were similar across different specimen groups, with damage concentrated around the gapped areas.

In another work, [137], Suemasu et al., examined the effect of 3.175 mm gaps in the 45° top ply, -45° third ply, and the 90° fourth layer respectively of a $[45/0/-45/90]_{2s}$ quasi-isotropic laminate during open-hole tension testing where the defects intersected with the hole. The effect of the defects on the open hole tension strength was minimal, with increases of 1.7 % and 2.1 % for the specimens with the 45° and -45° defects respectively, and a slight reduction of 2.2 % for the specimen featuring a 90° defect.

Cartié et al., [138], examined the effect of gap defects of sizes 0.5, 3.175, and 6.35 mm and overlaps of 3.175 mm in the central 90° plies of a $[90/0_7/90_2/0_7/90]$ laminates. Their results showed that the gaps and overlaps at this scale did not significantly affect the interlaminar shear strength under short beam shear testing conditions.

Quiang et al., [139], examined the effect of defects on the response of L-shaped specimens under 4-point bending testing. The authors examined the effect of 2 mm gaps, overlaps, and gap/overlaps in the 90° plies of a $[45/90/-45/0]_{2s}$ laminate at the inflection point of the L-shapes specimen. The results showed a 31.2 % decrease in the interlaminar tensile strength for the specimens containing gaps, a 12.3 % increase for specimens containing overlaps, and a slight reduction of 2.1 % for specimens containing gaps and overlaps.

Overall, extensive research has established that gap and overlap defects cause varying levels of mechanical performance knockdown, across a range of different loading conditions.

Despite this, no study has evaluated the performance of laminates containing reworked gap and overlap defects.

2.4.3 Detection/Inspection Systems

Currently, inspection of parts for quality control in AFP is either done manually through vision by a skilled operator [140] or, in more modern systems, aided by or solely performed using one of the following described automated methods [6], [68].

A major issue with the visual inspection method is the low contrast between the substrate and tows, making defects difficult to see with the naked eye. Additionally, the process of manual inspection is very time intensive and relies on expert-level knowledge [68]. The time-delay caused by manual inspection is very costly the manufacturers using AFP where manufacturing process efficiency is a key factor. Inspection and rework, as previously covered account for a disproportionately high amount of cycle time in AFP and relegate material deposition time to as low as 24 % of the total cycle [28], [29], [30]. An important definition to note is of *in-process* inspection and ply-by-ply inspection. In ply-by-ply inspection, the inspection system is dormant until all or part of the layup process is completed, whereupon the AFP deposition is halted while the whole part is inspected for defects. *In-process* inspection methods, by contrast, are capable of inspecting the surface of the substrate as tows are deposited on top. This maximises machine usage during the entire process, hence improving process throughput [68].

Thermography, laser profilometry (LP), and eddy current inspection have all be developed to enable robust automated inspection systems. Brasington et al., [68], provide the summary Table 2.9 showing different types of defects and the ability of commonly used inspection techniques to identify them.

Table 2.9. Detection capabilities of different techniques for various defect types, from [68]

Technique	Profilometry	Thermography	Eddy Current
Gap	✓	✓	-
Overlap	✓	✓	-
Wrinkle	✓	✓	*
Twist	✓	✓	✓
Missing Tow	✓	✓	✓
Pucker	✓	✓	*
Fold	✓	✓	*
Bridging	*	✓	*
Splice	✓	✓	✓

✓ = Can detect well
* = Can detect but not distinguish from other defects
- = can detect depending on size

2.4.3.1 Thermography

Thermographic inspection refers to the use of thermal imaging cameras, usually combined with an imaging processing software. The thermal camera is used to analyse the difference in temperature between tow and substrate. The difference in temperatures recorded are caused by differences between the heat transferred through the laminate and hence are indicative of differences in the tows. Through this data, information on tow position and the existence of defects can be derived.

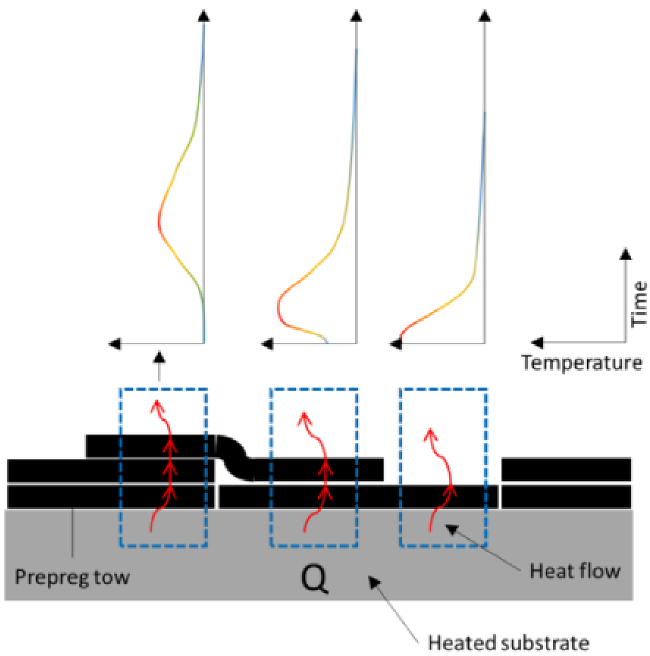

Figure 2.9. Thermography working principle, adapted from [141]

Research by Gregory and Juarez [141] described the process of detecting gaps and overlaps through thermography, Figure 2.9, adapted from [141], graphically describes the process of detecting gaps and overlaps through analysis of the thermal signal. In cases of a gap, the decrease in substrate thickness causes less heat to be absorbed, thus a higher temperature is read. Conversely, in cases of an overlap, more heat is absorbed by a thicker substrate, hence a lower temperature is recorded [142]. Experimental research by Juarez et al., [143], demonstrated the ability of thermography to successfully inspect for and identify all defect types. Other researchers such as Schmidt et al., [144], used thermography and an edge detection algorithm to localise tows and detect temperature discrepancies in them.

Experimental research by Juarez at al. [143], demonstrated the ability of thermography to successfully identify all defect types. Denkena et al., [142], used thermography and an edge detection algorithm to localise tows and detect temperature discrepancies. In [145], Schmidt et al. combined thermographic detection methods with a Convolutional Neural Network (CNN) to detect material-based defects rather than placement-induced defects including changes in tow width, thickness and fibre-matrix-ratio in-process. Their results showed effective classification of material defects in the prepreg material tested on a limited dataset.

2.4.3.2 Laser Profilometry

LP functions using a laser which is projected onto the surface of the layup. The reflected patterns can be used to infer the surface geometry of the layup and hence, any deviations in the pattern are indicative of defects and other layup discrepancies [68], [146]. A benefit of this method is that it can overcome the colour contrast issues cited for the inspection of AFP-produced parts [147]. Brasington et al. [68], in a review of defect detection methods, notes that LP requires the use of complex data processing algorithms to produce the detection results from the raw data collected. This entails a high demand for processing power, especially where high feed-rate AFP processes are considered. The authors also note that with proper optimisation of data processing, LP offers superior surface detail and, thus, eases analysis and identification of defects compared to other inspection methods currently in use.

Experiments were performed by Cemenska et al., [148], and found that LP was successful in detecting gaps and overlaps with sizes between 0.004” (0.1016mm) and 0.200” (5.0800mm). Foreign object debris (FOD), bridging, puckering, delamination, and tow twist were also successfully identified, providing these defects were large enough in their deviation from the expected surface topology than the minimum resolution of the profilometer used. Koptelov et al., [149], used an LP sensor combined with autoencoders, Long-Short-Term Memory (LSTM) networks, and a Convolutional Neural Network (CNN) to predict twist and pucker defects 5 mm and 2 mm respectively before they develop. Burke et al., [150], used an LP sensor combined with a CNN to detect and classify placement induced defects in real-time. Tang et al., [151], [152], developed AFP-seg, a LP based semantic segmentation network capable of detecting positioning defects with high precision at a rate of up 200 profiles per second. Yadav et al [153], used a LP sensor to constantly monitor the width of incoming tapes, and adjust the compaction force delivered on deposition in real time in order to modify the tape width. Krobholz et al., [154], used a LP sensor mounted 1100 mm ahead of the nip-point to detect the edge of the previously laid tow, and adapt the deposition path of the current tow to reduce any misalignment between them. Sacco et al., [155], utilise four LP sensors and a Fully Convolutional Network to perform semantic segmentation and rapidly detect and classify defects in the layup with a high accuracy rate for gap and overlap defects.

Current industrial technologies making use of LP include profilometry systems mounted directly on the AFP end-effector, such as those from *InFactory Solutions GmbH*, [156], [157], *Electroimpact, Inc.* [30], [148] and *Edixia Automation* [158]. Online profilometry assessment systems have been developed by *Danobat Group* [159], [160] and *Flightware, Inc* [161]. *Loop Technology, Ltd,* [162] present a system where an external robot from the ply depositing system carries the LP sensor over the laminate to perform the inspection. This system necessitates a subsequent inspection step and thus makes in-process inspection impossible.

2.4.3.3 Eddy Current Inspection

Eddy Current (EC) Inspection relies on the anisotropic electrical conductivity featured in composite parts, governed by the fibre orientation [163]. EC sensors function on the principle that the measured electrical impedance of an electromagnetic coil when excited by a sinusoidal signal depends on the induced current density within the material being scanned [164]. EC is capable of detecting fibre orientation and misorientation [164], as well as sub-surface defects that may not present the topography of the laminate, such as in-plane waviness [165] or wrinkles [163].

The combination of the morphologies of defects necessitates that one method is not sufficient for the detection of all defect types. For instance, robust methods for detection of out-of-plane defects, such as LP, may fail to capture in-plane defects. As such, fusion of sensor modalities remains a pressing area of interest in AFP research [68].

Despite the disproportionately high cycle time associated with inspection and rework [28], [29], [30], and the considerable research effort devoted to developing effective detection systems across a range of sensor modalities introduced above, none of the literature reviewed above addresses the rework step that follows defect detection. The section below discusses the approaches to defect management that do exist.

2.4.4 Defect Management and Aviodance

Managing defects in AFP manufacturing is an active area of research, broadly pursued through three strategies: modifying the process or material system to prevent defect formation; using path-planning and stacking sequence approaches to limit their structural impact; and applying remediation techniques during the curing process to reduce their effect on the consolidated laminate. Each process contains distinct trade-offs, and none guarantee fully defect free solutions for complex composite structures at industrial scale. The following sections examine each strategy in turn, before considering recent innovations in AFP head design that address defect formation at its source.

2.4.4.1 Prevention through Process Design

These methods primarily concern process- and path-planning methods. They accept that AFP will generate some defects aim to work around them structurally or geometrically, rather than mitigating or eliminating the defect formation at the source. Matveev et al., [166], propose a method of AFP using dry fibre composite tows, as opposed to the prepreg material used in typical AFP methods. The layup of these dry fibre tows is followed by RTM using vacuum bag technology. Gaps of 1 mm were left between the tows in order to act as channels for the resin to flow down. The authors note in their results that the resultant gaps remaining after the RTM process were narrower than the programmed gap width between the tows as a result of this resin infusion process. Other authors have proposed the strategic placement of plies of specific fibre direction on the two outer plies in a layup, thus ensuring that gaps and overlaps that form are not present on the exterior of the laminate [167], [168]. These methods do not, however, solve the problem of gaps and overlaps in the internal layers.

2.4.4.2 Remediation during Curing

Gap/overlap defects cause irregularities in the structure of cured laminates, typically manifesting as changes in the cured ply thickness (CPT) [118]. During curing, the resin softens and its viscosity decreases, allowing it to flow into the void regions created by tow misalignments under the pressure of the vacuum [169]. The characteristics of this flow depend on the type of resin and the stage of curing. It can involve percolation flow, where the resin moves along the fibre direction, or squeeze flow, where the resin flows transverse to the fibre direction [170]. While resin redistributes freely into these voids, fibres cannot follow, resulting in ply surface undulation that propagates through the laminate thickness and produces out-of-plane waviness in the consolidated part.

The use of a caul plate during curing can partially mitigate these effects by constraining the laminate surface and encouraging more uniform resin distribution, reducing void content and thickness variation [123]. However, the constraint that limits thickness variation also restricts fibre movement, which can prevent full consolidation of overlap regions and leave resin-rich zones with lower fibre volume fraction, and consequently reduced load-bearing capacity, compared to the surrounding laminate [123], [124]

2.4.4.3 Continuous Tow shearing

An important innovation in the AFP manufacturing technique is the development of Continuous Tow Shearing (CTS). This method, developed out of the University of Bristol, utilises a gripping shoe set in the AFP head before the compaction roller to apply an in-plane shear to the tow as it is delivered to the tooling surface [171]. Figure 2.10 and Figure 2.11 show a diagram of the concept of the CTS prototype head and the resultant path achieved through CTS compared with conventional AFP tow steering.

CTS has demonstrated the ability to steer tows at 10 times the curvature of those in conventional AFP without the accompanied process- and placement-induced defects [172]. More recent advances in the method have demonstrated effective placement of tows over complex 3-dimensional surfaces with high levels of tow steering with minimal defects when compared to conventional AFP material deposition over the same surface (Figure 2.12, after [173]). While the CTS method shows exceptional promise in ensuring defect free AFP deposition for increasingly complex use cases, the bespoke end-effector is not at this stage industry standard.

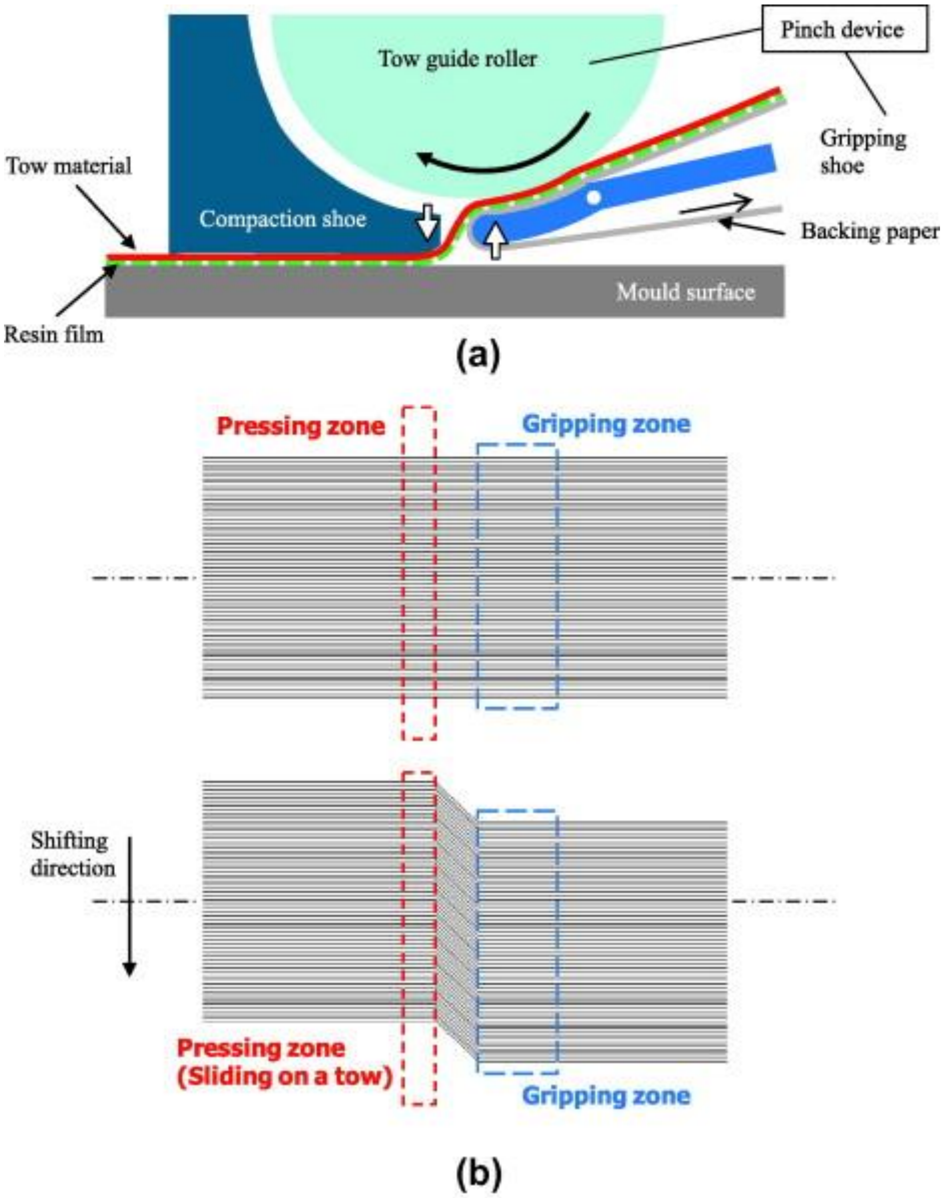

Figure 2.10. Diagram of CTS head (a) and of function of CTS (b), from [171]

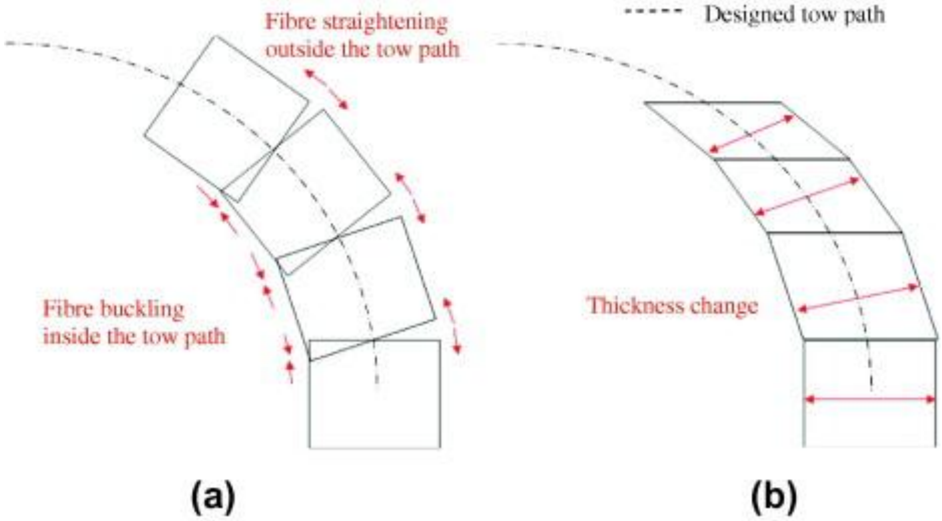

Figure 2.11. Comparison of theoretical tow behaviour under tow steering conditions in conventional AFP (a) and CTS (b), from [171]

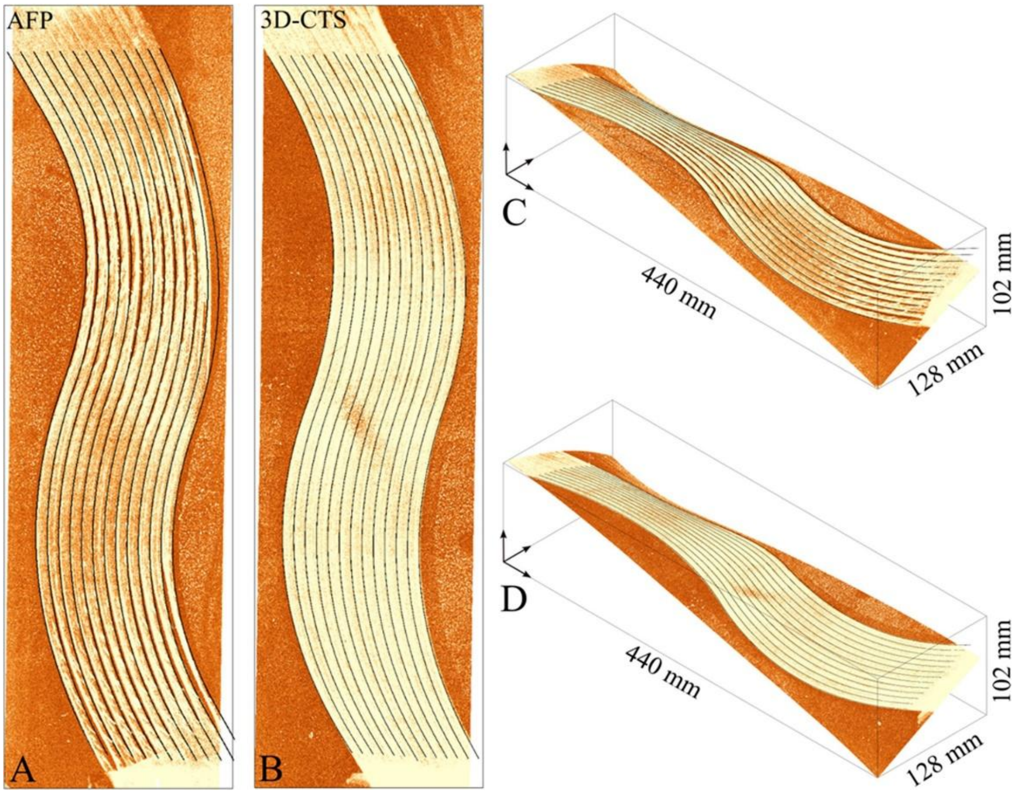

Figure 2.12. Side-by-side comparison of laser line scan of conventional AFP (A) and 3D-CTS (B) after complex 3-dimensional tow steering, with tow boundaries overlaid (black); and 3D view of AFP scan (C) and CTS scan (D), from [173]

There are critical shortcomings to the above-described methods for defect management. Firstly, design-stage methods such as the work of Matveev et al., [166], and the suggestion of intelligent ply ordering both cannot guarantee defect free layups and instead attempt to mitigate their impact. Furthermore, curing based mitigation is passive and limited by the physical limits of cure kinetics. While process-level interventions such as caul plate consolidation can attenuate the structural consequences of gap and overlap defects, they neither eliminate the defects nor restore the laminate to its nominal near-pristine condition.

CTS, while demonstrating excellent results in depositing defect-free courses across complex steered paths, is a planning-level tool, and as such cannot react to un-forecasted defects. Further the method is not industry standard. Where defect severity exceeds acceptable tolerances, a more direct intervention is required.

2.4.5 Rework of Defects

Reworking defects after layup offers a route to recovering structural performance without condemning the part to scrap, an important consideration given the material and labour costs associated with AFP manufacturing [27]. Currently, the state-of-the-art practice is manual rework, performed by skilled practitioners [31], [174]. This is not widely reported in the literature and hence remains as a craft known within industry but lacking any scientific study or standardisation across industry. Typically, remedial rework is employed, where for gaps and overlaps, the defective tow is first removed, taking care not to damage the underlying or surrounding plies, followed by the re-laying of a new tow in place where the misaligned tow was. Several tools are used by practitioners in order to perform this including tweezers, picks, and flat panel tools. See Figure 2.13 (left) for a range of these tools. Care should be taken to control the peel angle when removing the misaligned tow both in terms of the in-plane and out-of-plane angle both of which should be kept as close as possible to 0° with respect to the fibre direction and surface normal, respectively. This practice shall be examined in greater detail in Chapter 4 of this Thesis.

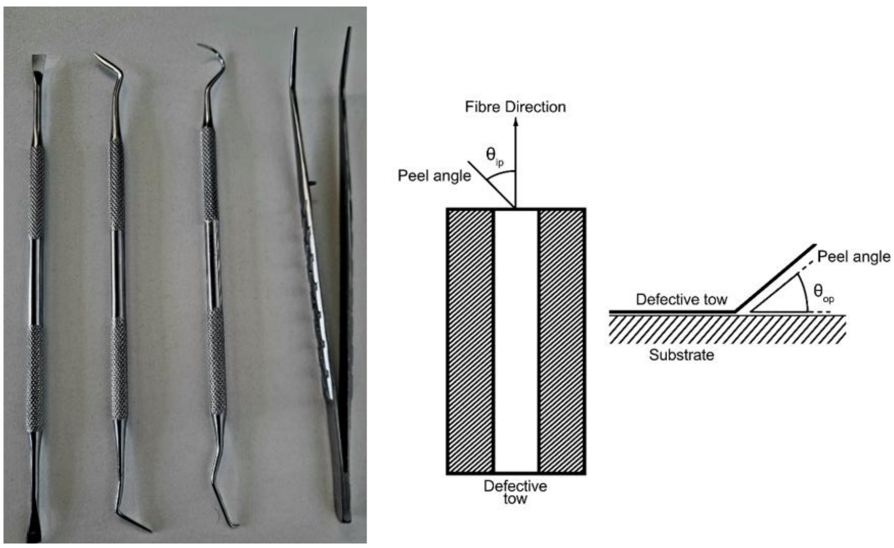

Figure 2.13. Reworking hand tools (right); in-plane (middle) and out-of-plane (right) peel angles (adapted from [174])

While currently a best practice can be determined based on a cosmetic approval/disapproval basis, the implications of rework on the quality of a part has not been studied yet. In this Thesis, this effect of defect rework is examined in more robust detail. The primary goal of reworking is to achieve near-pristine quality by modifying defective plies or tows to mitigate scrap waste [27]. Hence, if measurable differences in quality are observed between reworked specimens and pristine ones, the effectiveness of reworking techniques must be drawn into question.

2.5 Chapter Summary

AFP manufacturing sits at the forefront of automated manufacturing of advanced composite structures and features exceptional capabilities for high-rate, high-complexity manufacturing with the labour-economic benefits inherent to automation. Despite these benefits, significant drawbacks remain. Defects, particularly gap and overlap defects which are the most prevalent, occur routinely during the normal course of AFP manufacturing and with greater frequency in edge cases where extreme tow geometries are required. The high capital costs associated with AFP equipment further concentrates the development of the technique to well-resourced institutions, slowing the pace at which these limitations are systematically addressed.

Gap and overlap defects produced measurable knockdowns in mechanical performance for finished structures, a consequence that has been extensively documented in the reviewed literature. Rigorous inspection and quality control within the manufacturing cycle is of utmost importance in aerospace, renewables and automotive industries, and therefore in the application of AFP. Disproportionately large amounts of the cycle time are spent on the inspection and rework activities to the detriment of actual material deposition time. Considerable research effort has been directed at resolving the inspection problem, with innovative inline systems and automated detection methods enabling reduced time and operator dependency for part assessment. Despite this, rework remains poorly characterised at every level, despite being the downstream consequence of inspection. The process itself lacks standardised procedures, as noted by Sacco et al., [31], relying instead on the tacit knowledge of skilled practitioners with little formal documentation of technique, tooling, or decision criteria. Sacco's work is instructive in analysing the process for the reworking of wrinkle defects but does not address the reworking of the more commonly occurring gap and overlap defects. The structural consequences of rework are similarly under-documented, with acceptance criteria in current practice based largely on surface appearance rather than quantified structural recovery. This absence of rigorous characterisation represents a significant gap. Rework is already performed routinely in AFP manufacturing, yet the conditions under which it can be trusted to return a part to specification are not formally established. Addressing this gap through systematic evaluation of rework outcomes and the development of reworking solutions which ensure repetitive outcomes forms a central motivation for the work presented in this Thesis.

Chapter 3. Expert Outreach: unveiling rework practice across industry and academia

Chapter 2 established a knowledge gap relating to the practice, evaluation, standardisation and basis for improvement of defect rework in AFP. Despite this gap in the knowledge, the process remains well-practiced within AFP manufacturing. As such the critical perspective of practitioners is necessary in order to examine the full picture of the practice. This chapter addresses this through semi-structured interviews with three AFP experts from industry and research institutions. A framework and thematic analysis of the interviews capture the perspectives of practitioners on current challenges, practices and future directions for AFP, defects in AFP, and the reworking of defects. These insights informed the experimental design of the subsequent experimental methodology and validated the research priorities established through the literature review.

The interviews were conducted with three objectives in mind. Firstly, to understand current industrial practices for defect detection and rework. Description and discussion of these practices and the implications on the quality of AFP manufactured components are not discussed in detail in the literature and thus require further examination. The second objective was to identify pain points and unmet needs in AFP manufacturing. The final objective of the interviews was to validate the research priorities of this Thesis against industrial requirements.

The research followed an exploratory, qualitative design appropriate for investigating under-researched phenomena [175]. The full survey and answers are included in Appendix 3A: full Questionnaire Transcript and Appendix 3D: Coded responses by question and expert.

Table 3.1 Expert Profiles for interview

ID	Role	Organisation type	Experience	Geographic Focus
Expert 1	Senior Research Lead	UK Research Institute	9+ years leading AFP projects	Europe
Expert 2	R+D Engineer	US Manufacturing Company	40+ years organisational AFP experience	Global (100+ sites)
Expert 3	Research Lead	UK Aerospace Consultancy	Extensive OEM collaboration	UK/Europe

3.1 Methodology

3.1.1 Expert Selection and Rationale

Purposive sampling, [176], was employed to ensure representation across key dimensions of AFP expertise and application contexts. The selection criteria were deliberately designed to address the research gaps identified in Chapter 2. Specifically, a minimum 5-years direct experience with AFP technology was required and ensured a depth of knowledge about defect management practices rarely documented in the literature. Geographic and contextual diversity was desired to capture variations in practices in different regions and under different conditions of AFP use.

Three experts participated in the study, selected for their complementary perspectives on AFP implementation and defect management. Table 3.1 summarises their profiles.

The three-expert sample size aligns with recommendations for qualitative research where depth of expertise and diversity of perspectives are prioritised over sample size [177]. Additionally, since AFP is a relatively niche field of research, outreach to vast numbers of participants is not practical. The selected experts provide complementary viewpoints spanning the AFP value chain from research through manufacturing to application consulting.

3.1.2 Interview Design and Structure

A semi-structured interview approach was selected to balance consistency across participants with flexibility to explore emergent themes [178]. A standardised questionnaire was developed containing 20 open-ended questions organised into three predetermined thematic areas:

1. AFP Technology and Implementation (7 Questions)

This more generalised set of introduction questions enabled the experts to report on their experience and understanding of AFP from the perspective of their experience and industrial context. This information provides critical information in explaining variances between experts' perspectives on later questions. Additionally, through questions relating to the current state-of-the-art, advantages/disadvantages, recent and future advances of AFP a broad picture of the landscape of AFP perspectives within industry is developed allowing for contextual framing of the research questions and methodology through the remainder of this Thesis.

2. Defect Characteristics and Detection (8 Questions)

The experts were then asked target questions relating to their experience of defects within AFP, covering the common types of defects, the impacts of those defects on the components, inspection and detection techniques, and evaluation of the defects and their impact. Through this theme an impression is built of the needs of industry when compared to the research properties from the literature, as well as the technological gaps and opportunities that exist.

3. Defect Management and Quality Assurance (5 Questions)

Finally, as the core theme of this Thesis, the experts were asked questions relating to the rework of defects. This was done to address the gap in information within the literature on this key area. Questions ranged from descriptions of the methods and tools used for rework, evaluation methods for the effectiveness of reworking, the standardisation of the practice and opportunities for its improvement. The variation of perspectives allowed for a variety of information to be obtained to build a clearer picture of the priorities of the experts as they relate to rework. Since such little information exists in the literature covering this step in the AFP manufacturing process, this information was vital in informing the priorities and experimental design of the remainder of the Thesis.

Interviews were conducted between January 2023 and April 2023 using commercial video conferencing software. Participants received the questionnaire in advance, allowing time for reflection and, if desired, consultation with colleagues. Written responses were received from all three experts. Follow-up interviews were conducted via video conference software where responses required additional context or explanation. Informed consent was obtained from all participants for the reporting of these responses, and all participants were offered anonymity and are identified only as Experts 1, 2 and 3, respectively. Company and organisational identities are not disclosed.

3.1.3 Analysis Approach

Framework analysis [179] was employed as the primary analytical method. This approach is particularly well-suited to semi-structured interviews with small sample sizes and combines both deductive and inductive analytical strategies. Framework analysis consists of five interconnected stages:

Stage 1: Familiarisation. Here all interview responses were read multiple times to gain overall understanding of content, tone, and emphasis patterns.

Stage 2: Identify a thematic framework. A hybrid coding framework was developed combining the deductive themes based on the questionnaire structure (three predetermined themes) and the inductive themes which emerged through patterns identified during the familiarisation stage. Table 3.2 presents the complete coding framework.

Stage 3: Indexing. Here each expert response was systematically coded using the framework. Responses often received multiple codes where they addressed multiple themes. A coding matrix was developed to track which experts addressed which themes and to identify patterns.

Stage 4: Charting: coded chats were organised into thematic charts enabling systematic comparison across experts. Each chart is focused on a specific theme and displayed all expert responses in a comparable format. This visual organisation facilitated pattern identifications including:

- Consensus items (C), where all the experts agreed.
- Majority patterns (M), where 2/3 experts aligned.
- Divergent views (D), where experts disagreed or emphasised different aspects.

Stage 5: Mapping and interpretation. Here patterns identified in stage 4 were interpreted using a context-dependant perspectives framework. This analytical step allows for examination of how the organisational context, production volumes, and material system experience influence expert priorities and perspectives.

Table 3.2. Coding Framework from Expert interview analysis

Code	Theme	Sub-theme	Type
TECH-CHAL	AFP Technology	Implementation challenges	Deductive
TECH-REC	AFP Technology	Recent advancements	Deductive
TECH-FUT	AFP Technology	Future directions	Deductive
DEF-TYPE	Defects	Defect types encountered	Deductive
DEF-IMP	Defects	Impact and severity	Deductive
DEF-INSP	Defects	Inspection methods	Deductive
DEF-DET	Defects	Detection-rework relationship	Deductive
RW-PROC	Rework	Rework process description	Deductive
RW-TOOL	Rework	Tools and techniques	Deductive
RW-EVAL	Rework	Effectiveness evaluation	Deductive
RW-STD	Rework	Standards and guidelines	Deductive
RW-IMP	Rework	Improvement opportunities	Deductive
PREV	Defects	Prevention of Defects	Inductive
TIME-CRIT	Process	Time criticality in rework	Inductive
INTEGR	Technology	Automation integration	Inductive
COST	Economics	Cost considerations	Inductive

3.1.4 Limitations

Several limitations should be acknowledged. Firstly, with three participants, findings reflect expert perspectives but may not represent the full diversity of views across global AFP industry. However, the expert sampling ensures that viewpoints from key contexts are represented. Secondly, responses given by the experts are self-reported and based on the experts' perceptions and recollections which may differ from observed practices or documented procedures. Thirdly, AFP technology develops rapidly. The experts' views reflect the state of the field at the time of the interviews (2023) and may not capture subsequent developments. Despite these limitations, the expert interviews provide valuable practitioner perspectives that complement the academic literature and inform the experimental design of subsequent chapters.

3.2 Thematic Analysis

Following indexing and charting, the framework matrix (Appendix 3D: Coded responses by question and expert) was used as an analytical tool to map patterns across experts and themes rather than report findings question-by-question. Results are therefore presented thematically, aggregating coded responses across multiple interview questions in line with the 'mapping and interpretation' stage of framework analysis [179].

3.2.1 AFP technology and implementation

Across a range of questions, the experts were asked about their understanding of the current context of AFP research, development and use in industry.

3.2.1.1 Advantages of AFP

A summary of the main findings relating to the advantages of AFP is shown in Table 3.3, overpage.

Table 3.3. Expert Perspectives on main advantages of AFP

Expert	Consensus/Majority perspectives	Divergent Perspectives
Expert 1	Extensive lightweighting, leading to reduction in fuel consumption and emissions in aircraft (M1) High accuracy and repeatability (M2)	Minimal material wastage
Expert 2	Extensive lightweighting with superior strength-to-weight ratio (M1) Flexibility in component design (M3)	Minimal or no post-processing
Expert 3	High repeatability (M2) Flexible design space (M3)	Improved operator health and safety at scale. Reduction in labour and recurring costs

There was majority (M) agreement among the experts on both the potential in AFP to produce very lightweight components with excellent strength-to-weight ratio (M1), and on the flexibility provided by the technique in the designing of components allowed by the deposition of tows at specific fibre angles through the end-effector (M3). Majority views were also expressed on the advantage of the high repeatability of the method (M2).

The experts expressed some divergent views on the advantages of AFP. Expert 1 highlighted the minimal material wastage incurred through AFP manufacturing. Expert 2 highlighted the lack of post-processing. It should be noted that this was reported in relation to the specific manufacturing setup at their company, and this is not universal to AFP manufacturing. Expert 3 highlighted the human centric secondary benefits of the reduction in labour costs and increases to operator health and safety because of this repeatability. These divergent viewpoints represent differences in emphasis, rather than contradicting perspectives.

3.2.1.2 Challenges in Implementation

Regarding the main challenges in development and implementation of AFP in industry, all three experts independently cited the high cost for both the AFP equipment itself, and Expert 1 additionally cited the cost for the material slitting into tows suitable for use with AFP machines. A further consensus view was expressed in the relatively slow deposition rate of AFP compared with other methods. Expert 2 related this to the need in advanced composites market sectors for high production rates as a barrier to more widespread adoption of AFP. Both Experts 1 and

Table 3.4. Implementation challenges by expert

Challenge Category	Categorisation	Expert 1	Expert 2	Expert 3
High costs	C1	"High costs for accurately slitting material" "High costs of equipment."	"The cost of these work cells can be expensive"	"[High] capital costs"
Inspection	M1	"Time consuming and labour-intensive inspection requirements" "Due to large data processing requirements, some automated inspection systems struggle to flag defects in real-time"		"Defect inspection and rework … are harder/longer to resolve vs manual [layup]" "Inspection – each ply requires 100% inspection with aero[space] industry"
Software limitations	D1	"Current composites design software isn't yet mature enough to automatically design composite structures that fully exploit the physical abilities of AFP machines"		
Slower depositions	C2	"Relatively slow"	"Need to increase manufacturing processes to achieve market acceptance"	"Typically, slower depo[sition] rates vs P&P or manual on smaller-medium components"

3 cite the difficulty in inspection and rework as well as the time and labour costs associated with these activities. These reports of the time and cost of inspection and rework are congruent with the findings from the literature. In a divergent viewpoint not expressed by the other experts, Expert 1 cites the immaturity of composites design software in utilising the ability of AFP systems to deposit tows on optimised curvilinear paths for variable stiffness laminates.

3.2.1.3 Recent advances in AFP

The experts were asked to provide their impressions of recent advancements in AFP technology, and particular areas of interest for research and development. Here a range of

Table 3.5. Expert perspectives on the most important recent advances in AFP technology

Expert	Recent advance	Quote
1	Numerical Design tool	"[Organisation] have been working on a numerical design tool for automatically designing optimised curvilinear variable stiffness laminates"
2	Dual laser AFP	"We have just built the first dual laser AFP machine… …This creates more efficient heating and can result in faster production"
3	Continuous Tow-Shearing (CTS)	"Tow shearing looks to show promise"
	Defect Inspection	"Substantial improvements in in-process inspection"
	Multi-Material Formats	"Multiple material formats (tow widths) in development or use"
	End-effector design	"Low-cost/ Single tow end-effectors for R&D and other bespoke applications"

divergent viewpoints were reported. Expert 1 cited research within their organisation focused on design software that could utilise the curvilinear path deposition possible through AFP and use this for the manufacturing of variable stiffness laminates. Expert 2 cites the development of laser assisted AFP, in particular a dual laser system capable of controlling the heat of both the substrate and the incoming material, allowing for more efficient heating and therefor of faster deposition rates. Expert 3 referenced advances in CTS. improvements in in-process inspection systems, multi-material format AFP heads, and low-cost AFP systems for R&D applications. The divergence of views across the experts highlights the divergence of developmental trends seen across AFP research and development.

3.2.1.4 Future research and development

Table 3.6 displays the viewpoints of the experts in relation to the future research trends and development of AFP manufacturing.

There was a majority view (Experts 2 and 3) that inspection related future directions presented a high-level of promise within AFP research and development, particularly on the fly/in-process defects inspection. Other divergent views expressed include independent control of lasers for in-situ consolidation of thermoplastic AFP, improved software integration between the robot and end-effector, increased speed of manufacturing, and advances in CTS. Similarly

Table 3.6. Expert perspectives on future directions of AFP research and development.

Response Category	Categorisation	Expert 1	Expert 2	Expert 3
Inspection	M1		"Flaw detection capabilities" "On the fly flaw detection"	"In-process inspection"
Independent laser control	D1	"For high quality in-situ consolidation of thermoplastic composites, having independently controlled lasers for heating substrate and incoming tape looks like a good idea"		
Software integration	D2		"Better software integrations between robot and processing head"	
Speed	D3		"Speed of manufacturing"	
Continuous tow-shearing	D4			"Tow-shearing"

to the previous sub-theme, the divergence of views indicates the divergence of research and development aims within AFP currently.

3.2.2 Defects Characteristics and Detection

The next theme of questioning was centred around the existence and impact of defects in AFP. The purpose of this questioning was to gauge the opinions and experience of the experts as it relates to this core area of research intensity in AFP.

3.2.2.1 Defect types

In terms of the common defects seen by the experts in their experience of AFP, Expert 1 cites Gaps, overlaps, inaccuracies in adds or cuts, folds, and waviness on the edges of steered tows. Expert 3, similarly, to Expert 1 cites gaps, overlaps and missing tows. They also reference

Table 3.7. Expert perspectives on common defect types

Defect type	Categorisation	Expert 1	Expert 2	Expert 3
Placement-induced defects	M1	"Gaps, overlaps, inaccurate ads or cuts, tape folding, fibre waviness on the inside of steered tapes"		"Gaps, overlaps, missing tows"
Bond quality defects	D1		"If any of [the] process parameters are not accurate, or the incoming pre-preg material does not meet out quality standards, you could end up with inconsistent bond quality and ultimately a failed part."	

fuzzballs, classified in the literature as Foreign Objects. Expert 2 primarily cites inconsistencies with bond quality caused by improper management of processing parameters.

The discrepancy between the responses from Experts 1 & 2 and Expert 3 may be attributed to the differing context of these experts, where Experts 1 and 2 are from an academic/consultancy context, whereas Expert 2 is reporting from the context of a manufacturer.

3.2.2.2 Defect impact

A strong consensus view exists on the effect of defects among all three experts, all of whom independently cited knockdowns in mechanical performance and the related component failure as an effect of defects. This is in direct agreement with the literature reported in the previous chapter.

Table 3.8. Expert perspectives on defect impacts

Impact reported	Categorisation	Expert 1	Expert 2	Expert 3
Stress management	C1	"If not detected and reworked, they [defects] contribute to stress concentrations and performance reductions, e.g., strength"	"[bong quality defects] … could end up with … ultimately a failed part"	"If not detected can affect component performance or scrappage."

3.2.2.3 Evaluation of defects

Table 3.9 shows the perspectives of the experts on the evaluation of the effect of defects. Some specific information has been redacted from Expert 2's response to maintain anonymity. There is a divergence in approaches between the three experts on the evaluation of defects. Expert 1 cites several industry standards for testing composite structures. Expert 2, by contrast, cites material testing prior to manufacture (testing process redacted to maintain anonymity). Expert 3 reports the primary method of evaluation as a numerical approach using Finite Element (FE) analysis. This divergence of approach has its roots in the industrial context of each of the experts, and in the differing emphasis on defects occurring in the manufacturing process (Experts 1 and 3), and fundamental defects in the material (Expert 2).

Table 3.9. Expert perspectives on specific evaluation methods for the effect of defects

Expert	Evaluation methods
Expert 1	"ASTM D2344M ASTM D3518 ASTM D3039M ASTM D6641M"
Expert 2	"Every batch of material we receive is NOL processed. Once passed we know the materials have made our specifications for manufacturing"
Expert 3	"Effect of defect assessed through FE analysis"

3.2.2.4 Defect inspection methods

Table 3.10 contains the experts' perspectives on the defect inspection process in AFP, separated into three categories and drawn from the responses to several questions. Three key categories of responses were drawn out of the responses as they related to defect inspection. All three of these categories were consensus among the experts. Category 1 was that inspection is a time-consuming task. Experts 1 and 2 cite this explicitly, whereas Expert 3 cites the need to inspect 100% of every ply, which implies this is time-consuming nature. All three experts explicitly or implicitly link this to the performance requirements of advanced composites in the industries making use the advantages of AFP manufactured parts, such as aerospace.

The second category is automation, where all three experts pointed to advantages or opportunities in automating the inspections task. Expert 1 describes existing work on automated inspection within their organisation and discusses the benefits of this in terms of time and effort reduction for inspection and rework. Experts 2 references on-the-fly defects detecting in the context of promising developments for AFP. Expert 3 references some automated inspection methods in use currently and cites improvements in in-process inspection as a particularly important recent development in AFP.

Thirdly, all three experts indicated explicitly or implicitly that visual inspection was a core component of defect inspection in AFP. Experts 1 and 3 cite this explicitly, whereas Expert 2 cites automated inspection under the category of promising developments or future directions, implying that the standard is still visual inspection methods.

Table 3.10. Expert perspectives on defect inspection

Inspection categorisation	Categorisation	Expert 1	Expert 2	Expert 3
Time consuming	C1	"Time consuming and labour-intensive inspection requirements" "Due to large data processing requirements, some automated inspection systems struggle to flag defects in real-time" "AFP is often used for critical and very lightweight structures, where costs to closely inspect each ply can be justified"	"Tow defect inspection and rework … are harder/longer to resolve vs manual [layup]"	"Each ply requires 100% inspection within Aerospace industry"
Automation	C2	"Automated defect detection can point to areas of interest and reduce efforts to locate defects and remove and readd material as necessary" "[organisation] has collaborated on some means for automated defect detection, through processing of laser line scanning and imagery"	"[automated] flaw detection capabilities"	"Defects are detected … or through use of laser/optical systems (in-process) or by using NDT post-cure" "Substantial improvements in in-process inspection"
Visual Inspection	C3	"This is commonly done with visual inspection"	Implied	"Defects are detected either visually…"

3.2.2.5 Detection – Rework relationship

Table 3.11 shows the experts perspectives on the relationship between the inspection task and rework task. As highlighted in the previous chapter, these processes are often grouped into a single process when considering their impact on processing time. The aim of these questions was to ascertain the experts' viewpoints on the relationship between the two processes as they currently exist, and the impact of advancements of one or both processes on the other. The experts were asked about the influence inspection methods has on the reworking step. Experts 1 and 3 were in explicit agreement that intelligent detection can lead to faster reworking through more rapid location of defects for reworking. Expert 3 further suggests that *"rework at the time of detection"* could produce large benefits through reduced downstream processing. Expert 2 does not state this explicitly but suggests that "early detection would be useful" when asked about improvements to reworking methods.

Experts 1 and 2 agree about the role that automated detection systems can play in the reworking process itself, though their impression of the way in which automation can improve rework differs. Expert 2 reported that "[defect detection] *…will affect processing conditions – i.e. raise/lower temperature, increase or decrease compaction.*". Whereas Expert 1 cited automating the process of relaying tows after defect tow removal as the key benefit. The discrepancy in response here can be attributed to differing interpretations of the reworking methods. Expert 2, as shall be reported below, reports reworking methods differing in terms of machine processing parameters, while Expert 1 describes rework methods centred around the removal and redeposition of defective material. Expert 3 contrasts both experts by stating that "rework methods are consistent regardless of detection methods".

Table 3.11. Expert perspectives on the relationship between detection and reworking

Relationship categorisation	Categorisation	Expert 1	Expert 2	Expert 3
Reduction in time/effort	C1	"Automated defect detection can point to areas of interest and reduce effort to locate defects and remove and readd material as necessary"	"Early detection would be most useful"	"Digital data stream-lines defect recording, offering improvements in location and severity" "If defect detection can be translated to rework at time of identification, reduces down-stream inspection, rework, concessions"
Automation of rework	M1	"Automating the process for instructing the AFP machine to relaying only the tapes that were removed"	"Defect will affect processing conditions – i.e., raise/lower temperature, increase or decrease compaction"	
No relationship	D1			"Rework methods are consistent regardless of detection methods"

3.2.3 Defect Management and Quality Assurance

The third major theme of questions centred around defect management and quality assurance. This includes most of the discussion around reworking and mitigation of defects. Expert 3 declined to report back on some questions in this section, however, some responses from the previous questions fit into this theme and are included.

3.2.3.1 Rework Process

Table 3.12 details the description and characterisation of the reworking process from the perspectives of the experts.

Table 3.12. Expert perspectives on the defect reworking process

Expert	Response
	Divergence 1: Rework Method
Expert 1	"Use hook and pick style tools to remove tapes as necessary. Then use the machine to relay tapes where they've been removed" "It is necessary to heat tapes, e.g., with a heat gun, to remove them, though it can still be challenging to do this nearly without breaking fibres and leaving some behind. Pulling tapes straight, i.e., not bending them back on themselves, helps remove tapes neatly, though this is often only practical if there is a tab (free end) to start with" "Remove and readd material as necessary"
Expert 2	"Hot irons and other method to batch gaps. Compaction afterwards to ensure consolidation"
	Divergence 2: Reworking Tools
Expert 1	"Generally, use hook and pick set style tools" "Pulling tapes straight…" "Often only practical when there is a tab (free end) to start with"
Expert 2	"Hot irons and other method to batch gaps. Compaction afterwards to ensure consolidation"
	Majority Agreement 1: Use of heat
Expert 1	"It is necessary to heat tapes"
Expert 2	"Hot irons and other method to batch gaps. Compaction afterwards to ensure consolidation"
	Majority Agreement 2: Time consuming process characterisation
Expert 1	"… reduce effort to locate defects and remove and readd material as necessary"
Expert 3	"Tow defects … rework … are harder/longer to resolve vs manual [layup]" "Detected defects incur costs to rework"
	Majority Agreement 3: Lack of standard reworking procedures
Expert 1	"Please share any you know of"
Expert 2	"None"

A divergence in approaches was seen between Experts 1 and 2 when asked about their reworking approach. Expert 1 described a method involving the use of hook and pick tools to pull away defective tows, followed by the replacement of the removed tows. Expert 2 described the use of hot irons combined with compaction to consolidate gaps. Both experts agreed that the use of heat was necessary to manipulate the material. This divergence in method may relate to the divergence in defect types reported by the two experts, where Expert 2 was more focused on bond-quality related defects, and Expert 1 reported placement-induced defects such as gaps and overlaps. In characterising the reworking process, both Expert 1 and 3 reported that the reworking process was time and effort intensive.

Table 3.13. Expert perspectives on evaluation methods for rework

Expert	Evaluation Method
Expert 1	"Inspect the rework"
Expert 2	"Peel test to ensure bonding"
	"Compaction afterwards to ensure bonding"

Importantly, majority agreement was found between Experts 1 and 3 in describing the time-consuming nature of the reworking process, this agrees with the findings from the literature and serves to justify the research focus in improving the process. Finally, there is further agreement in the lack of standards for the reworking process between Experts 1 and 2. This, again, is supported by the evidence from the literature and supports the research emphasis placed on this area.

3.2.3.2 Evaluating Rework

In terms of evaluating rework after the process was completed, divergent methods were discussed by Experts 1 and 2. Expert 1 referenced inspection of the rework as the method for determining success, in light of their earlier answer on defect inspection techniques, it is inferred that this referred to visual inspection primarily.

Expert 2 referred to peel-tests being performed after rework, to determine in the proper adhesion had been obtained between the reworked tow and the substrate. They also report that compaction should be used afterwards to ensure bonding.

As in previous sections, the divergence in evaluation methods relates to the divergence in defect types that the experts are referring to.

Table 3.14. Expert perspectives on directions to improve reworking

Expert	Improvement opportunity
Expert 1	"Automated inspection to point to defect areas and reduce efforts to locate defects and automating the process of instructing the AFP machine to relaying onto the tapes that were removed."
Expert 2	"Can always be improved. Early detection would be most helpful" "On the fly flaw detection"

3.2.3.3 Improvements to reworking

Lastly, both experts were asked to identify areas of promise in industry or research for the improvement of the reworking process. Both Experts 1 and 2 highlighted furthering the level of automation in their answers, with Expert 1 referring to automated detection systems which inform the machine programming to relay tapes to the appropriate area, and Expert 2 referring to ever-earlier detection systems and on-the-fly detection systems.

3.2.4 Emergent themes

3.2.4.1 Prevention

With regards to the prevention of defects, Expert 1 referred to machine maintenance, especially keeping the end-effector components cool, to reduce the chance of material sticking to components and causing defects. Expert 2 referred to material testing prior to manufacturing, to reduce material-induced defects.

Table 3.15. Defect prevention methods

Expert	Prevention Method
Expert 1	"For thermoset materials, keeping head components, such as feed rollers and cutters, cool, to reduce how tacky the material is will reduce fibres sticking to these components and contributing to defects and downtime."
Expert 2	"Material testing (NOL's) prior to product manufacturing."

Table 3.16. Expert responses relating to time requirements in AFP

Time context	Characterisation	Expert 1	Expert 2	Expert 3
Defect related time cost	M1	"Time consuming… inspection requirements" "Some automated inspection systems struggle to flag defects in real-time"		"If defect detection can be translated to rework at time of identification, reduces down-stream inspection, rework, concessions"
Wider implications of time requirements	C1	"Challenges for quality in-situ consolidation (ISC) of thermoplastic composites at economically viable deposition rates"	"Automotive and aerospace markets can have demanding production timelines. Need to increase manufacturing processes to achieve further market acceptance for advanced composites."	Implied

3.2.4.2 Time criticality

A further inductive sub-theme arising from the analysis was the criticality of time with the reworking process and in AFP more broadly. Table 3.16 summarises the key findings for this emergent sub-theme.

A majority view exists between Experts 1 and 3 relating to the time requirements associated with inspecting and reworking defects. A consensus view exists across the three experts on the time demands placed on AFP manufacturing as a result of the advanced composites market sectors typically engaged in AFP manufacturing.

3.2.4.3 Automation integration

Another emergent theme was the integration of further automation into the AFP process. Table 3.17 describes these automation opportunities referenced by the experts. All three experts

Table 3.17. Expert perspectives on automation integration opportunities in AFP

Automation opportunities	Expert 1	Expert 2	Expert 3
Inspection to rework	"Automated detection can point to areas of interest and reduce efforts to locate defects…" "Automated inspection to point to defect areas and reduce efforts to locate defects and automating the process for instructing the AFP machine to relaying only the tapes that were removed."	"Substantial improvements in in-process inspection with numerous systems now being deployed" "Flaw detection capabilities" "Can always be improved. Early Detection would be most helpful." "On the fly flaw detection."	"Digital data stream-lines defect recording, offering improvements in defect location & severity (less effort in concessions). Obviously if defect detection can be translated to rework at time of identification, reduces down-stream inspection, rework, concessions."
Robot to End-effector coordination		"Better software integration between robot and processing head"	

indicated that automation of the inspection-to-rework process would bring substantial improvements to the process in terms of reduced effort and time, and reductions in the associated costs of inspection and rework delays to production. Expert 2 references improvements to the software integration between robot and end-effector.

3.2.4.4 Cost

Lastly, an emergent theme across many of the categories was cost. This was seen in both positive cost implications of AFP in its current state and in recent developments, and negative cost implication. Experts 1 and 3 cite the positive costs associated with AFP in both direct terms through reduced material wastage, and reductions in labour/recurring costs, and in indirect costs in the case of Expert 1 through reduced aircraft fuel consumption through lightweighting. Expert 2 cites a direct cost reduction within their AFP system through the elimination of post-processing. In terms of developments, Expert 3 reports the positive development of low-cost

Table 3.18. Expert perspectives on cost related concerns in AFP

Cost context	Expert 1	Expert 2	Expert 3
Positive cost implications	"AFP Contributes to reduced aircraft fuel consumption" "AFP processes also waste very little material"	"By eliminating the post process, we save time and money"	"labour/recurring cost reductions" "Low cost/single tow end effectors"
Negative cost implications	"High costs for accurately slitting material" "High cost of equipment" "Expensive"	"The cost of these work cells can be expensive" "This equipment is often beyond the budget of most academic institutions" "The raw materials used in [AFP] manufacturing can be expensive as well"	"Capital costs"

single tow end-effectors as a positive for enhance R+D opportunities without the high capital costs associated with most AFP cells.

These high capital costs were reported by all three experts as a direct negative cost implication for AFP manufacturing cells. Experts 1 and 2 also cite the cost of the materials used in AFP as a barrier to entry.

3.3 Key Findings and Research Gaps

From the above analysis some key findings can be drawn out through the consensus, majority agreement, and divergence among the experts. These findings have implications for the research gaps identified from the literature, and the experimental design for the remainder of the Thesis. Table 3.19 shows the key consensus items.

The high capital costs reported as a consensus across the experts validates the novel benchtop-AFP approach, used for part of the analysis of the effect of rework in chapter 5 which shall be introduced in due course. This low-cost approach enabled critical R+D on sub-processes such as reworking without the capital costs associated with large scale AFP manufacturing cells.

Table 3.19. Strong consensus items

Topic	Finding	Evidence	Implications for Thesis
Capital Costs	Equipment cost is primary adoption barrier	All three experts independently cite costs	Validates low-cost Benchtop-AFP approach (Section 4.3.2)
Rework Standards	No industry standards exist	E1: "Please share any you know of?"; E2: "None"	Validates need for systematic study (Chapter 4)
Future direction	Automated detection required	All three experts cite in various forms	Supports integration with detection systems (Chapter 6 and Chapter 7)

The lack of reworking standards matches the findings in the literature and is a cornerstone of this Thesis. The lack of any standards introduces high levels of variability within the reworking process, as such subsequent chapters introducing best practices and studying the effect of reworking aim to address this gap.

Finally, the consensus on the benefit of automated detection, and the direct linking of this to increases in efficiency in reworking supports the direction taken in the automation focused chapters (Chapter 6 and 7) of this Thesis, where automated methods of reworking are explored.

Table 3.20 shows the majority agreement items identified through the thematic analysis. These were, firstly, that gap and overlap defects were the most common type of defects. This was explicitly states by Experts 1 and 3 and is supported by the literature in [117]. Expert 2 contrasted this by focusing on bond-quality defects. The implication of this finding is the support of the focus through this Thesis on gap and overlap defects.

Secondly, there is majority consensus between Experts 1 and 3 that inspection and rework are major bottlenecks. While this is not stated explicitly by Expert 2, they did not provide

Table 3.20. Majority agreement items

Topic	Finding	Evidence	Implications for Thesis
Primary defects	Gaps and overlaps most common	Experts 1 and 3 cite explicitly	Validates focus on gap/overlap defects
Key challenges	Inspection and rework are major bottlenecks	Experts 1 and 3 cite	Validates research motivation
Inspection methods	Visual inspection is primary	Experts 1 and 3 cite	Establishes baseline practice

Table 3.21. Key divergence items

Topic	Divergent views	Possible explanation
Defect emphasis	Geometric defects (E1 and E3) vs bond-quality defects (E2)	Industrial vs research context
Rework tools	Picking tools (E1) vs Hot irons (E2)	Primary focus of E2 on gap rework, rather than other defects

responses to the contrary. This validates the motivation of this Thesis to develop and improve the reworking process and is supported by the findings of Rudberg et al., [28], [30] and Halbritter et al., [29], reporting on the cycle time lost to inspection and reworking.

Lastly, Experts 1 and 3 explicitly state that visual inspection is the primary method of inspecting laminates for defects, and Expert 1 reports this as the primary method for evaluating rework. Expert 2 does not explicitly state visual inspection as the primary inspection method but implies this through their responses relating to automated inspection methods. This finding supports the focus of the Thesis as it finds visual inspection to be the baseline method for both inspection of defects and rework. Through the work contained in this Thesis a more robust method of rework evaluation is proposed.

Key divergences are shown in Table 3.21. Experts 1 and 3 diverge from Expert 2 on the primary defects seen in AFP manufacturing. An explanation of this is the industrial context of the experts, where 1 and 3 are situated in academia and consultancy, whereas Expert 2 is situated in a manufacturing company.

A second divergence is seen between Experts 1 and 2 on the primary tools and method for reworking. Expert 1 reports hand picking tools, whereas Expert 2 report the use of hot irons. This divergence can be explained by the divergence primary defects identified by the experts and as such differing methods for reworking are used.

Table 3.22. Implications and validation status of research gaps based on experts' perspectives

Research gap (from Literature Review)	Expert Validation	Expert Evidence	Status
Lack of rework process understanding	Validated	Diverse processes (E1, E2); varied tools (E1 vs E2)	Strong need for further process understanding.
Need for systematic rework guidelines	Validated	E1 asks for standards; E2 says "None" exist.	Need for standardisation of the reworking process.
Effect of rework on part quality	Validated	E3 mentions "concessions" process. E1 cites simply inspecting the rework, implied that this is visual only. E2 mentions peel tests for bond-quality related defects	Requirement first study on the effect of defects.
Integration of detection and rework	Validated	Experts independently cite on the fly detection and the link between detection and rework as positive.	Integration of inspection and rework desirable for future development.

3.3.1 Validated Research Priorities

The implications for the research priorities in this Thesis are reported in Table 3.22. The expert interviews provided strong validation for the research gaps identified in the literature review.

Regarding the lack of rework process understanding, experts confirmed that current practices are non-standardised and vary significantly between organisations. Both Expert 1 and Expert 2 described different approaches and tools, highlighting a strong need for further process understanding and documentation of best practices.

The need for systematic rework guidelines was particularly evident when Expert 1 explicitly requested information about existing standards, while Expert 2 stated that none exist. This absence of industry-wide standards confirms the necessity for developing standardised reworking processes that can be adopted across the AFP community.

The effect of rework on part quality also emerged as a validated concern through the experts' responses. Expert 3 mentioned the "concessions" process, suggesting that reworked defects often require special acceptance procedures. Expert 1's reliance on visual inspection of rework implies limited quantitative assessment, while Expert 2's use of peel tests for bond-quality defects indicates that current evaluation methods are defect-specific, and lack a unified approach. This evidence underscores the requirement for systematic studies examining how rework impacts final part performance.

Finally, the integration of detection and rework systems was validated as a critical development area. Multiple experts independently identified on-the-fly detection and the linkage between detection and rework as highly desirable advancements. Expert 1 emphasised automated inspection to reduce defect location efforts and enable automated relay instructions, while Expert 2 highlighted early detection and on-the-fly flaw detection as key improvement opportunities. This convergence of expert opinion confirms that integration of inspection and rework represents a valuable direction for future technological development.

Chapter 4. Rework Process Analysis

The previous chapters have established that reworking of gap and overlap defects remains outside of the formal characterisation within literature, whilst being a process that demands disproportionately large amounts of the cycle time of a typical AFP manufacturing cycle. The extent to which the reworking method is understood by experts in the field remains similarly underdefined, with variances in methods and loose characterisation of processes being emergent themes from the previous chapter. Further no standards exist for ensuring repeatable results from the reworking process. In this chapter, the first discussion in the literature of the reworking process is presented, specifically with respect to gap and overlap defects in laminates. These defects are the most commonly seen in industry and hence present the most pressing case for an improvement of understanding and thereafter an improvement or innovation of the processes.

The first step to investigating the effects of reworking and outlining improvements to the process is to analyse the manual process and record it in literature. Following the limited information gathered from the literature and from expert interviews, reworking methods were evaluated for gap and overlap defects. A study on best practice was conducted, testing various mechanistically determined reworking methods, and best practices for reworking were developed in terms of limiting the damage to neighbouring tows both within and around the defect. The outcomes of this study serve as a foundation for studying the effect of reworking, by standardising the process which shall be used in the subsequent study of reworked samples and allows for the proposing of improved methods and introducing automation to the defect reworking process.

4.1 Rework state-of-the-art

Much of the discussion of the reworking process in the literature is included in the literature review (Section 2.4.5). A reminder of the key points is included here.

A definition of rework in the context of composite manufacturing is given by D. Hughes [27]:

> *"Rework is the finishing step that can mitigate the source of scrap waste. Rework refers to the manual inspection and modification of defect plies or tows."*

It is the contention of the author of this Thesis, that this definition need not be restrictive to manual inspection and modification, and research in future should expand this to include automation. Rework is a necessary step in mitigating the effects of defects on the mechanical performance of composite structures, and in reducing the waste generated through scrapping [27]. Analysis of the typical cycle times for AFP by Electroimpact [28] and Boeing [29] found that inspection and rework combined accounted for 63 % and 32 % respectively. While further analysis by Rudberg et al., [30], reported 28 % of cycle time for inspection, 10 % for reliability recovery, and only 42 % for material deposition, respectively.

The process of reworking has not been extensively reported in the literature. Table 4.1, repeated from Chapter 3, describes the experts' knowledge on the process of reworking defects, the characteristics of the process, and a description of the tools used during the process. Crucially, experts gave different accounts of the reworking process, and none had any knowledge of standards relating to the rework process.

In, [31], Sacco et al. examined the effect of manually reworking defects on a composite part containing two curves. Technicians performed rework manually using a range of tools, like those used in manual layup. Figure 4.1 displays some of the typical tools used by technicians for the rework activity. The techniques used by the technicians to rework defects include shifting tows, reapplications of tows, and replacing tows.

Table 4.1. Experts' perspectives on the defect reworking process

Expert	Response
	Divergence 1: Rework Method
Expert 1	"Use "hook and pick" style tools to remove tapes as necessary. Then use the machine to relay tapes where they've been removed" "It is necessary to heat tapes, e.g., with a heat gun, to remove them, though it can still be challenging to do this nearly without breaking fibres and leaving some behind. Pulling tapes straight, i.e., not bending them back on themselves, helps remove tapes neatly, though this is often only practical if there is a tab (free end) to start with" "Remove and readd material as necessary"
Expert 2	"Hot irons and other method to batch gaps. Compaction afterwards to ensure consolidation"
	Divergence 2: Reworking Tools
Expert 1	"generally, use "hook and pick set" style tools" "Pulling tapes straight…" "Often only practical when there is a tab (free end) to start with"
Expert 2	"Hot irons and other method to batch gaps. Compaction afterwards to ensure consolidation"
	Majority Agreement 1: Use of heat
Expert 1	"It is necessary to heat tapes"
Expert 2	"Hot irons and other method to batch gaps. Compaction afterwards to ensure consolidation"
	Majority Agreement 2: Time consuming process characterisation
Expert 1	"… reduce effort to locate defects and remove and readd material as necessary"
Expert 3	"Tow defects … rework … are harder/longer to resolve vs manual [layup]" "Detected defects incur costs to rework"
	Majority Agreement 3: Lack of standard reworking procedures
Expert 1	"Please share any you know of"
Expert 2	"None"

While some techniques are discussed in literature, no standards exist on either processes or tolerances involved in defect reworking. This view was supported by interviews conducted by the author of this Thesis with experts, discussed in Chapter 3.

In their conclusion to the paper, Sacco et al. [31] propose a set of best practices recommendation for rework of defects for a part of this type. These include:

- In areas of large curvature or where high degrees of steering are used, only those defects resulting from improper adhesion between the tow and substrate should be repaired. Other defects are likely design-driven.

- Replacement of tows for wrinkles is proposed over reconsolidation to avoid the creation of transverse wrinkles.
- Only large wrinkles should be repaired through reconsolidation together with the application of additional heat.

Since the process of manually reworking defects is similar in nature to the manual laying up of composite parts, the examination of this method is prudent. Elkington et al., [43], examined and categorised the different techniques used by technicians in performing this task. They defined eight techniques used by technicians and characterised these different techniques by the operation required to perform them. Table 4.2 outlines these methods. The characterisation in Table 4.2 from Elkington et al., [43], is supplemented by the author of this Thesis to include the requirement for two hands or only one hand, and the use of motion of the operator's hand across the material. Elkington et al. characterise the manual layup operation as combinations of (1) *Grasping*: where a section of the material is held in place by the hand of a technician, (2) *Pulling*: where a section of the material is held by the technician and pulled in a direction, and (3) *Pressing*: where the technician pushes their hand across the surface of the material, typically against the surface of the mould.

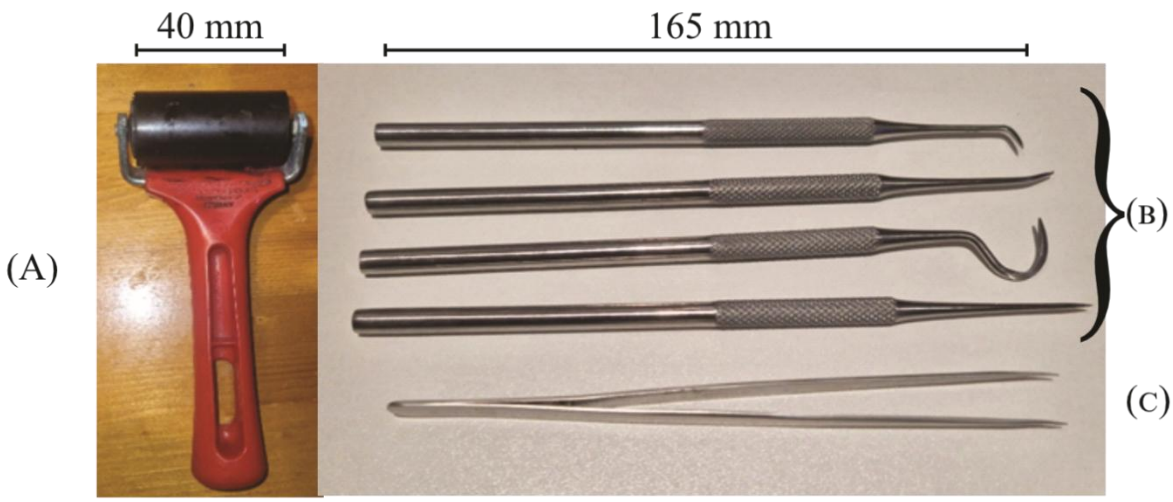

Figure 4.1. hand tools used in reworking; (A) roller, (B) hook and pick tool set, (C) tweezers

Table 4.2. Characterizations of hand layup techniques (after [43])

Technique	Grasping	Pulling	Pressing	Both hands necessary	Motion Necessary
One-handed guiding	✓	×	✓	✓	×
Two-handed guiding	✓	×	✓	✓	×
Manual folding	✓	✓	×	✓	×
Hoop shearing	×	×	✓	✓	✓
Double-tension shear	✓	✓	×	✓	×
Tension and sticking	✓	✓	✓	✓	✓
Mould interaction shearing	×	×	✓	×	×

✓= is required, × = is not required

With the above literature in mind, an investigation into the effectiveness of reworking gap and overlap defects using a variety of reworking methods was undertaken and is described below. The primary method of evaluation was a qualitative evaluation of the extent of damage to surrounding areas in the laminate, and to the rework site itself. A controlled full factorial experiment was developed evaluating the reworking methods, the influence of external heating to soften the resin at the rework site, and the influence of various gap defect sizes on the reworking outcomes.

4.2 Study on best practice

A study was developed to evaluate several reworking methods for their success in reworking defects with minimal damage to the surrounding material. The section below describes this study.

4.2.1 Experimental Setup

From the literature and interview findings on rework, the following aspects were identified as key in the process: 1) size of the overlap defects, 2) peel angle, and 3) use of external heat. As such a controlled experiment was designed to determine the effect of these on ease and success of rework.

Reworking methods (RMs) were defined based on the peel angle conditions as discrete separation methods reflecting the relative dominance of tool-applied separation forces and tow tension. Five methods were defined; these were:

- Tool-dominated: where both peel angles were minimised, and the main separation force is provided by the pushing of the tool against the exposed underside of the tow being removed at the interface between it and the substrate.
- Mixed-mode: where the in-plane angle was maintained at 45° while the out-of-plane angle was minimised, and the tool provides a supporting force at the interface between the tow being removed and the substrate. The peel front at the interface is simultaneously subject the shear force by the tension from the in-plane peel angle, and opening assistance by the pushing force from the tool.
- Opening-assisted: where the in-plane angle was perpendicular to the tow direction, and the out-of-plane angle was still minimised. In this method, the force at the tow-substrate interface is more dominated by the angled tension force, and the tool guides the peel front along the length of the tow, rather than providing substantial force to remove the tow.
- Bending-assisted: where the in-plane angle was perpendicular to the direction of the tow, and the out-of-plane angle was held at 45°. Here the tool is similarly sublimated by the tension force, with an additional bending component through the increased out-of-plane angle.
- Reverse peel: where the in-plane angle was maximised to 180° and the out-of-plane wangle was minimised, meaning the tow was entirely bent back upon itself. Here the tool plays little to no role in either providing force to remove the tow, or in guiding the peel front.

Figure 4.2 shows a description of the out-of-plane and in-plane peel angles for removal of an overlapped tow.

Table 4.3 summarises different rework methods in terms of peel angles and tool dominance. The reworking was performed by the same expert each time in order to minimise the variation in technique.

The success of the reworking is measured by the extent of damage to 1) the tow being removed, 2) the overlapped tow, 3) the underlying tows. This is captured in images of the reworking and through a damage analysis matrix shown in the Results section (Section 4.2.2).

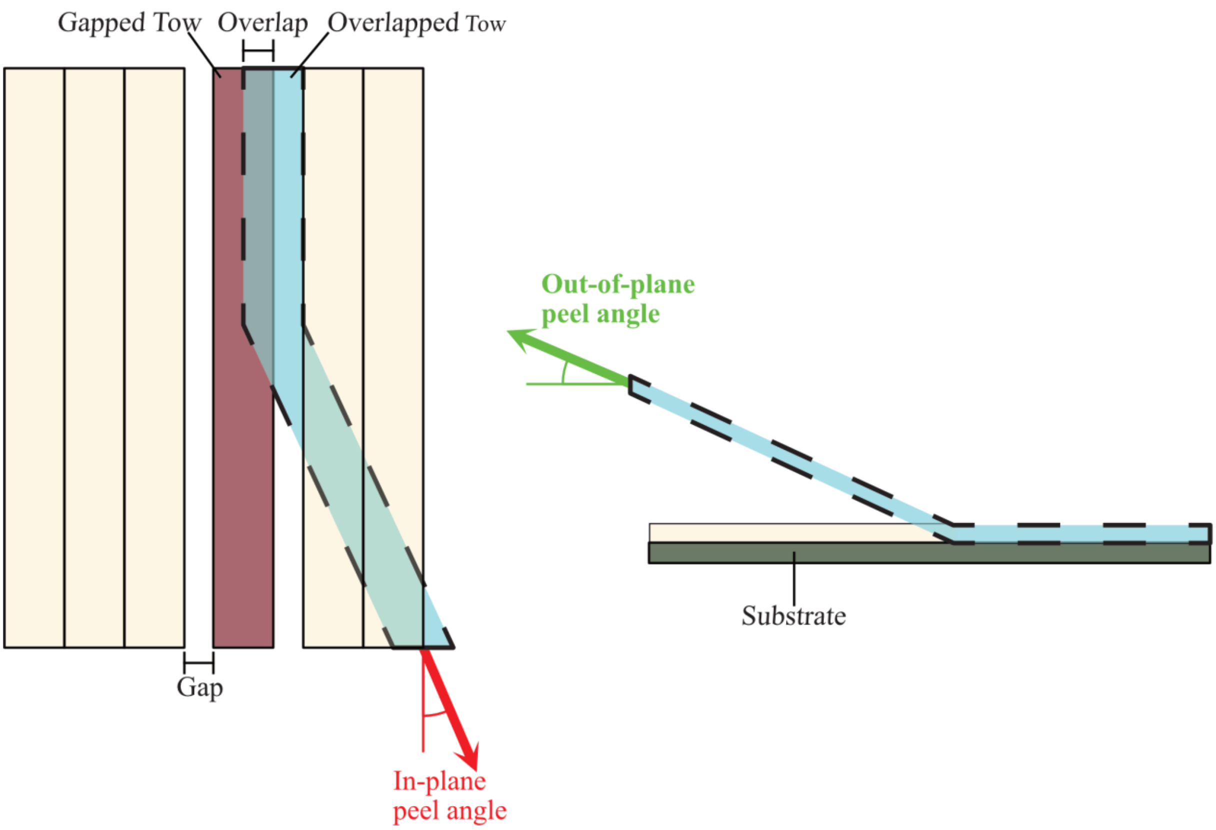

Figure 4.2. In-plane (red) and out-of-plane (green) peel angles for reworking an overlapped defect (blue)

Table 4.3. Reworking methods and corresponding peel angles

Peel angle method	Abbreviation	In-plane peel angle	Out-of-plane peel angle
Tool-dominated shear separation	RM1	0°	0°
Mixed-mode (shear + opening), tool-dominated	RM2	45°	0°
Opening assisted, tool guided	RM3	90°	0°
Opening and bending assisted	RM4	90°	45°
Reverse peel (tow dominated)	RM5	180°	0°

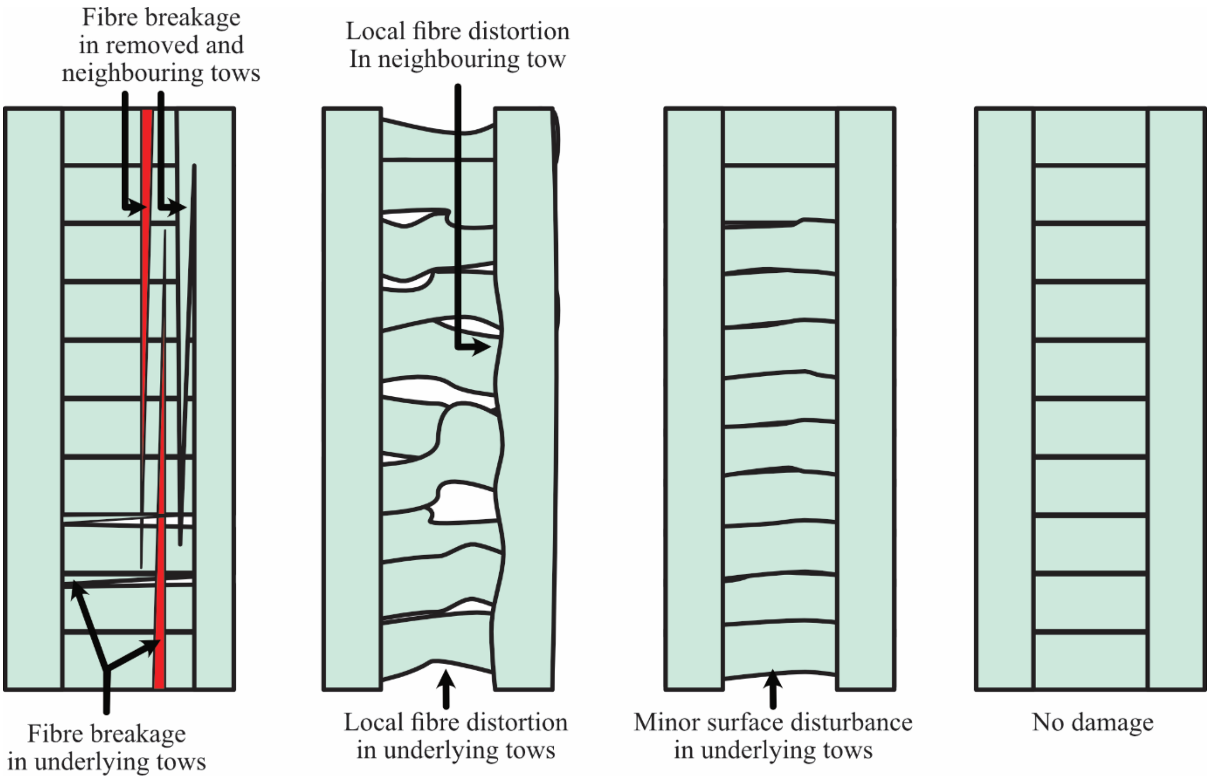

Figure 4.3. Diagram of damage levels post-reworking

This analysis allows for a set of best practices to be developed for gap and overlap rework which have not previously been discussed in the literature and can serve to inform subsequent studies of effect of the reworking process.

The damage analysis matrix is measured for the four distinct regions which are part of or neighbouring the rework site. The damage was classified under a scoring rubric ranging from 1-4 corresponding to: 1: fibre breakage/tow disruption, 2: local fibre distortion and/or resin smearing, 3: minor surface disturbance (no fibre breakage), and 4: no-visible-damage. **Figure 4.3** displays a diagram of the damage types.

To conduct the experiment, a 650 x 475 mm panel was manufactured with a $[90/0]_3$ structure using Hexcel® M91/34%/UD194/T700GC 6.35 mm width prepreg tows. The AFP system used comprised of a KUKA KR120 R3100 6-axis industrial robot, a bespoke single tow Accudyne AccuFP 1000+ fibre placement head [71], and a heated tooling plate upon which the tows were deposited, set to 55°C. The first layer was deposited with no defects. The second layer was deposited with 10 gap/overlap defects manufactured through shifting every 5th tow in the lateral direction by the defect size amount. The subsequent tow was deposited as programmed and hence would overlap the gapped tow by the set defect amount. 10 defect instances per 0° ply allowed for the testing of each of the rework methods (RM1 to 5) with and without external heating. Following the removal of the defective tows, new tows were deposited without the lateral shift in the gapped tow, resulting in a ply without any defects. The size of the defect was increased through 2.5, 4.0 and 6.0 mm in the 2nd, 4th and 6th plies, respectively. This allowed for the evaluation of rework for defect sizes ranging from small but still consistent with the threshold for reworking (2.5 mm) to larger gap/overlap defects (4.0 mm) up to the largest defects (6.0 mm) where the gap size nearly covers an entire tow width (6.35 mm) an extreme case where removing the overlapping tow from directly on top of another tow become exceedingly difficult. Formally, this follows a $5 \times 2 \times 3$ full factorial design with three factors: rework method (5 levels), heat augmentation (2 levels), defect size (3 levels).

4.2.2 Results

The damage matrices for the different defect sizes and rework methods are shown in Table 4.4 - Table 4.6 In the following, the performance of each of the rework method is discussed along with comparisons between the method. For each of the rework methods, a table is provided showing description and analysis of the effect of the tension and tool component of the method, and the effect of the geometry of the peel front. For all three the effect of introducing heat is included in the table.

Table 4.4. Damage matrix for 2.5 mm defect

	Heated (Y/N)	Removed tow	Gapped tow	Neighbouring tows	Underlying tows
RM1	Y	4	1	1	2
	N	4	4	4	3
RM2	Y	1	2	4	4
	N	1	2	2	4
RM3	Y	4	2	4	2
	N	2	2	4	2
RM4	Y	1	2	4	3
	N	1	2	1	3
RM5	Y	1	1	3	3
	N	1	1	1	3

Table 4.5. Damage matrix for 4.0 mm defect

	Heated (Y/N)	Removed tow	Gapped tow	Neighbouring tows	Underlying tows
RM1	Y	4	1	2	2
	N	4	4	4	3
RM2	Y	1	2	4	4
	N	1	2	1	4
RM3	Y	1	2	4	1
	N	1	1	1	2
RM4	Y	4	1	4	2
	N	1	1	4	3
RM5	Y	1	1	1	1
	N	1	1	1	2

Table 4.6. Damage matrix for 6.0 mm defect

	Heated (Y/N)	Removed tow	Gapped tow	Neighbouring tows	Underlying tows
RM1	Y	4	4	4	3
	N	4	4	3	3
RM2	Y	1	4	1	4
	N	3	3	4	3
RM3	Y	4	1	4	2
	N	4	1	4	2
RM4	Y	4	4	4	3
	N	4	4	4	2
RM5	Y	1	1	4	2
	N	1	1	4	2

4.2.2.1 RM1: Tool-dominated shear separation

Figure 4.4 shows radar charts showing the performance of RM1 across the different defect sizes and showing the influence of heated versus unheated reworking. Increasing effectiveness of the RM for each of the regions is indicated by larger spread of the radar chart into that area, representing more effective damage limitation across the four material areas examined. The blue shaded area indicates the effect of the RM without the additional heat input, whereas the red shaded area indicates the effect of the RM with additional heat input. Both areas are opaque so that the full extent of each of the shaded areas can be seen, hence some area appears purple where the red area is overlayed over the blue and vice versa.

Compared with the other method evaluated, RM1 saw the least damage across all defect sizes, in particular when heat was included. Table 4.7 describes the tension and tool components of the method, and the peel front geometry as well as their effects on reworking and the effect of heating. For the 2.5 and 4.0 mm defects there was a marked increase in the performance of the method when heat was introduced. The input of the heat softens the resin across the gapped tow, overlapped tow and underlying tows, and allows for a cleaner separation, primarily by the force exerted through the tool and assisted by the tension force. For the largest defect size, where the overlapped tow almost fully covers the gapped tow, minimal difference in performance was seen with the introduction of additional

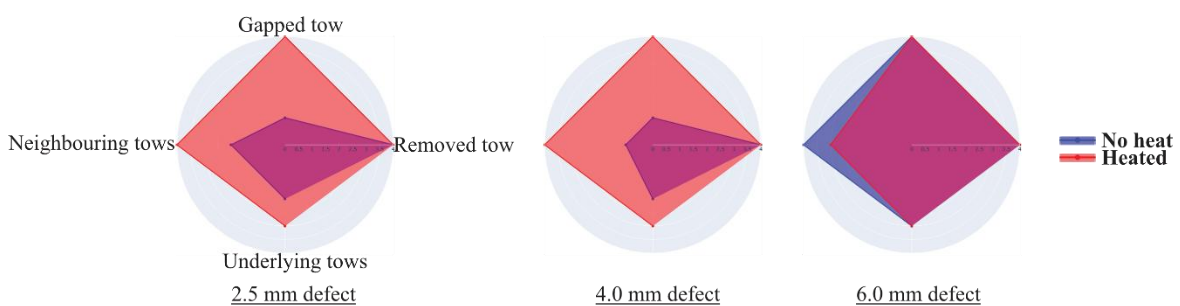

Figure 4.4. RM1 radar charts showing influence of heat for various defect sizes

heat. Since in the reworking of these large defects both gapped and overlapped tows were removed at once, and the dominant component was tool assisted separation, minimal damage to neighbouring or underlying tows was seen. The greatest degree of damage across all defect sizes was to the underlying tows, where some disturbance to the surfaces was seen, through the sliding contact of the tool. Figure 4.5 shows RM1 and examples of low- and high-level disturbance to the underlying surface.

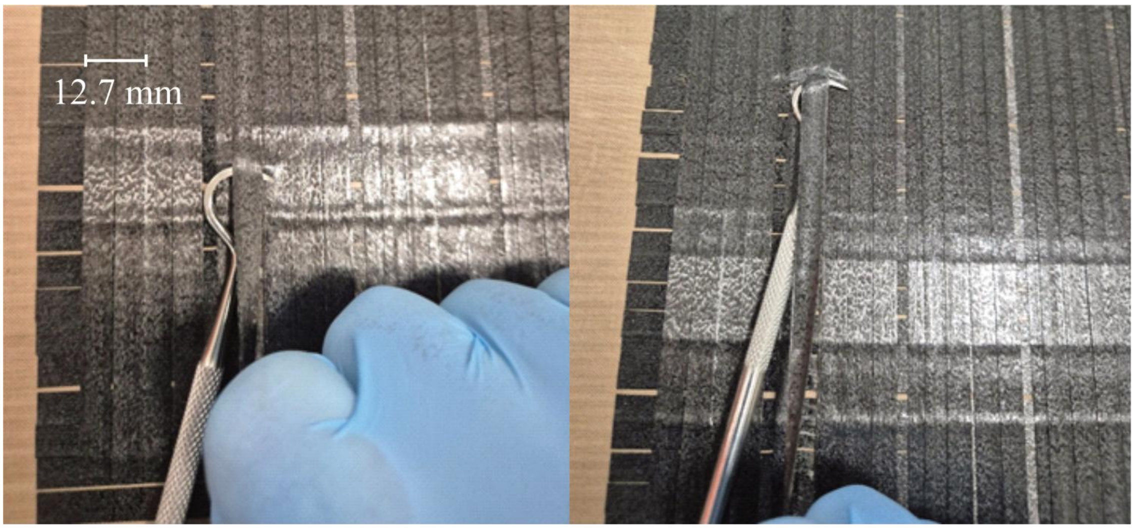

Figure 4.5. RM1 progression, showing low (left) and higher (right) level delaiminations to underlying surface

Table 4.7. Analysis of RM1 components and effects on reworking

	Description	Effect on reworking	Effect of heating
Tension component	Tension supplied through tow length, aligned with fibre direction and parallel to the tooling surface.	Minimal tension component, plays more of an assistive role to the tool dominated procedure.	Resin softening may allow for more elastic deformation, i.e., stretching, of the tow being removed, rather than a more brittle response resulting in tow/fibre breakage
Tool component	Separation force applied through sliding the tool along the length of tow at the peel front.	Primary mechanism for breaking adhesion between tow to be removed and underlying material.	Resin softening allows for easier overcoming of the adhesive forces, though can lead to increased damage in underlying layer through compressive forces imparted by tool.
Peel front geometry	Square peel front matched to the width of the tow being removed	Concentration of disruptive forces along peel front within the width of the tow.	Heating allows for the overcoming of adhesion forces with less forces, lessening the concentration of forces at the peel front,

4.2.2.2 RM2: Mixed Mode

RM2 performed poorly in both heated and unheated trials for damage to the removed and gapped tows. Notably, the heated trial performed worse in terms of damage to the neighbouring tows than the unheated trial. In both heated and unheated trials there was limited damage to the underlying tows. A reasoning for this is the distribution of the tension force across an extended peel front in RM2 compared to RM1 due to the increased in-plane peel angle. In contrast with RM1, the tool component of RM2 plays a minimal role in the reworking process. Rather than directly engaging in breaking the adhesion between the removed tow and the underlying surface, in RM2 the tool advances the peel front along the surface of the removed tow.

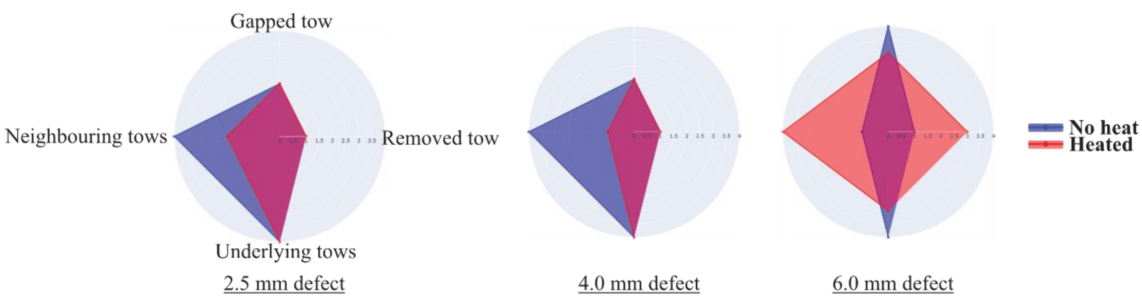

Figure 4.6. RM2 radar charts showing influence of heat for various defect sizes

Table 4.8. Analysis of RM2 components and effects on reworking

	Description	Effect on reworking	Effect of heating
Tension component	Tension applied through length of tow at 45° in-plane an 0° out-of-plane.	45° in-plane angle adds a bending component to the applied tension force	Softening of resin allows adhesion to be more easily overcome, leading to a "rolling" peel front.
Tool component	Tool assists in advancing peel front but is secondary to tension component.	Minimal effect on reworking.	Minimal effect of heating on tool component.
Peel front geometry	Angled peel front because of 45°in-plane peel angle.	Distribution of stress concentration across a larger peel front reduces damage at interface between removed to and other regions	Softened resin further reduces the stress concentration at peel front and lessens damage extent.

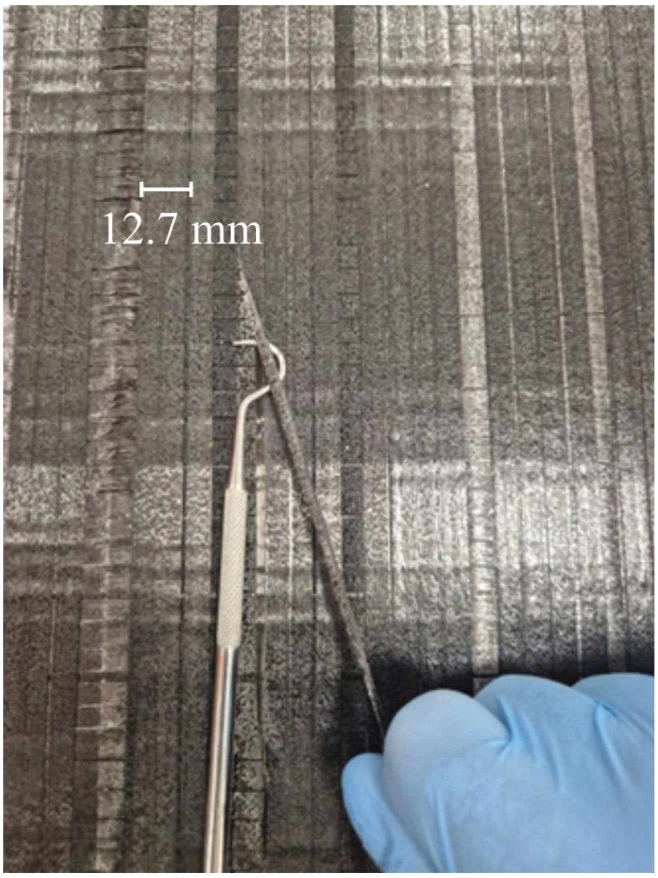

Figure 4.7. Peel front in RM2

4.2.2.3 RM3: Opening assisted

RM3 both achieved less damage than RM2 when directly comparing the heated and unheated trials, but more damage in both types than RM1 heated. Notably larger disturbances to the underlying tows were seen for this method in both trials. As with RM1, the peel front is aligned directly with the underlying tows, but in contrast to RM1 the tension force is applied perpendicular to the surface of the tapes. There was minimal damage to neighbouring tows in both heated and unheated trials of RM3, due to the absence of lateral forces through the peel front. RM3 has very minimal impact from the tool component. Similarly to RM2, the tool assists in advancing the peel front along the length of the tow, however this extent of the force was limited as pushing the tool beyond the peel front would alter the rework method from opening assisted peel to reverse peel.

Figure 4.8. Fibre breakage during RM3

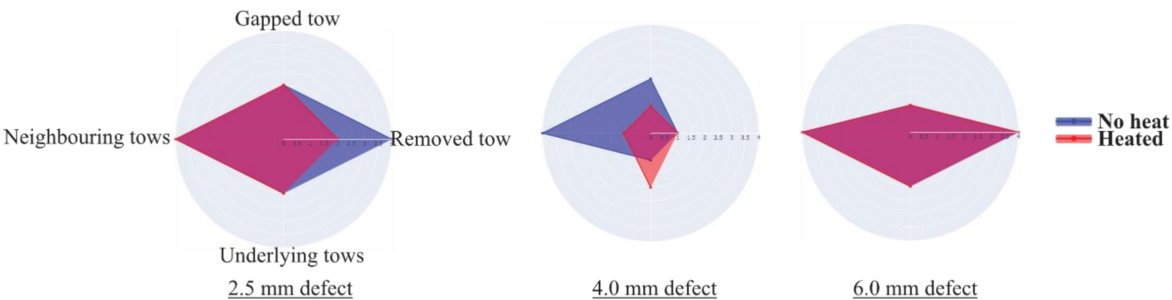

Figure 4.9. RM3 radar charts showing influence of heat for various defect sizes

Table 4.9. Analysis of RM3 components and effects on reworking

	Description	Effect on reworking	Effect of heating
Tension component	Tension applied through length of the tow at 0° in-plane and 90° out-of-plane	Extreme stress concentrations from perpendicular force application	Resin softening slightly mitigates stress concentration
Tool component	Tool follows tool front but cannot apply force without changing peel angles	Tool component overshadowed by tension component	Minimal effect of heating on tool component
Peel front geometry	Square peel front matched to the width of the tow being removed	Concentration of disruptive forces along peel front within the width of the tow	Heating allows for the overcoming of adhesion forces with less forces, lessening the concentration of forces at the peel front

4.2.2.4 RM4: opening and bending assisted

RM4 combines the in-plane angle of RM2 with the out-of-plane angle of RM3, the result is a higher tension component that RM1 or RM2, but lesser than RM3 as it is mitigated by the in-plane angle. The peel front is wider and more angled than in RM3, mitigating the damage to underlying tows marginally. The introduction of the in-plane angle also introduces a bending force to the removed tow; this led to increased damage in the tow as it was removed. The effect of increased heat was limited in this RM with slightly improved response in terms of damage to underlying tows. An explanation of this is the resin softening allowing for a steadier "rolling" of the peel front along the underlying tows surface, especially in the wider and angled fronts seen in this RM, this rolling of the front induces less disruptive fore on the underlying material layer. Similarly to RM2 and RM3, the influence of the tool component was minimal in this reworking method, merely aiding in advancing the peel front rather than providing substantial force to break the adhesion between the tapes. This is similar especially to RM3 where imparting force through the tool in the tow would change the reworking method from opening and bending assisted peel to reverse peel.

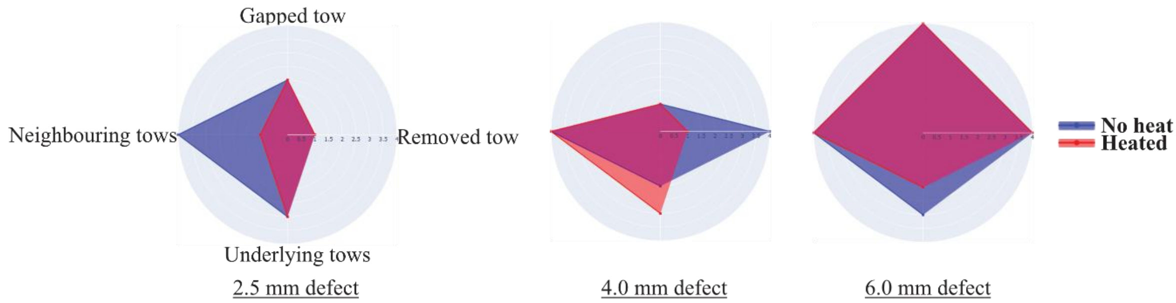

Figure 4.10. RM4 radar charts showing influence of heat for various defect sizes

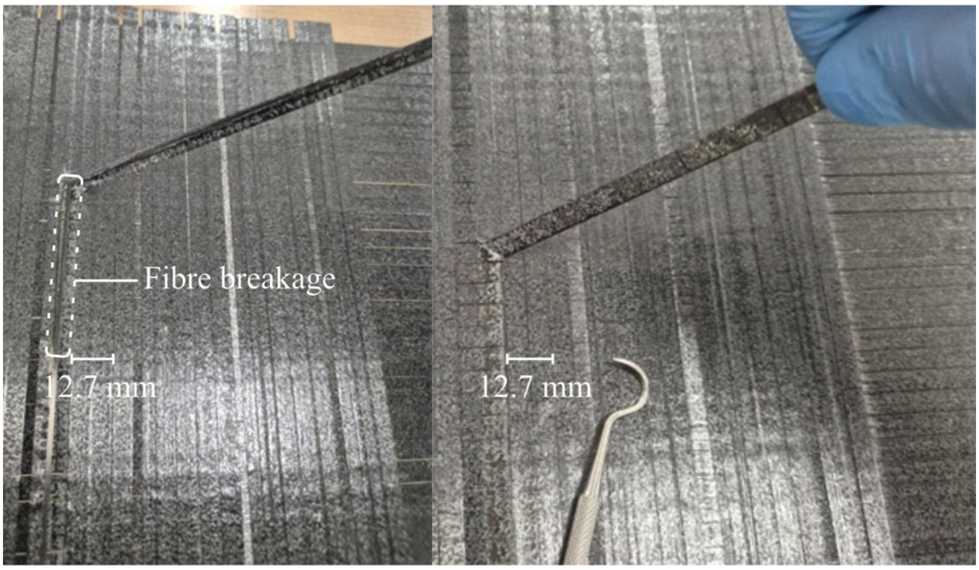

Figure 4.11. Fibre breakage (left) and peel front (right) during RM4

Table 4.10. Analysis of RM4 components and effects on reworking

	Description	Effect on reworking	Effect of heating
Tension component	Tension applied through length of tow at 45° in-plane and 90° out-of-plane	Large stress concentrations at peel front, but mitigated by bending force through 45° in-plane peel angle	Softened resin lessens force required to overcome adhesion and thus stress concentrations
Tool component	Tool follows tool front but cannot apply force without changing peel angles	Tool component overshadowed by tension component	Minimal effect of heating on tool component
Peel front geometry	Angled peel front because of 45°in-plane peel angle	Distribution of stress concentration across a larger peel front reduces damage at interface between removed to and other regions	Softened resin further reduces the stress concentration at peel front and lessens damage extent

4.2.2.5 RM5: Reverse peel

RM5 performed the worst on all measures for all defect sizes. This method tended to induce immediate tow breakage in both the tow being removed and the neighbouring and gapped tows. The exception was in the 6.0 mm defect where there was limited damage to the

Table 4.11. Analysis of RM5 components and effects on reworking

	Description	Effect on reworking	Effect of heating
Tension component	Tension applied through length of tow at 0° in-plane and 180° out-of-plane	Reverse peel force leads to uncontrolled stress concentration and resolution at peel front, often leading to fibre breakage in tow being removed	Minimal effect of heating on tow breakage
Tool component	Tool follows exposed tool front	Tool component introduced unstable forces along tool front	Minimal effect of heating on tool component
Peel front geometry	Square peel front matched to the width of the tow being removed	Concentration of disruptive forces along peel front within the width of the tow	Heating allows for the overcoming of adhesion forces with less forces, lessening the concentration of forces at the peel front

neighbouring tows as the entire defect was contained within the width of the gapped tow, and the absence of any in-plane angle meant that there was limited interaction between the tows being removed and the neighbouring tows. The tool played a role in aiding in the breaking of the adhesion between the tapes, however due to the reverse peel, the tool tended to introduce unstable forces along the exposed peel front, leading to more frequent and severe breakages in the tow being removed.

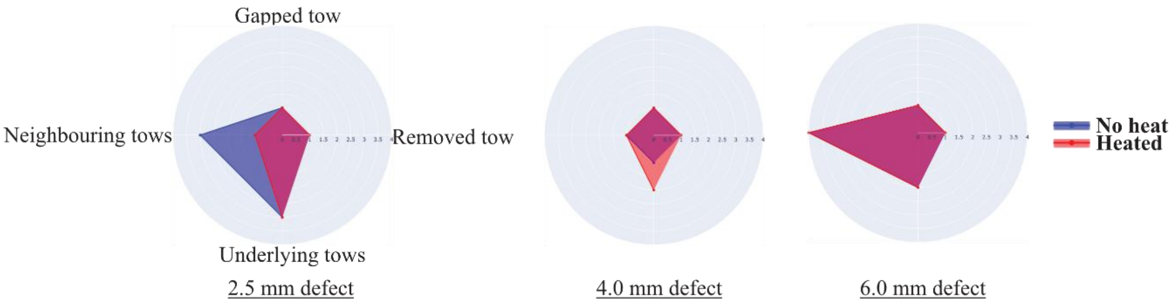

Figure 4.12. RM5 radar charts showing influence of heat for various defect sizes

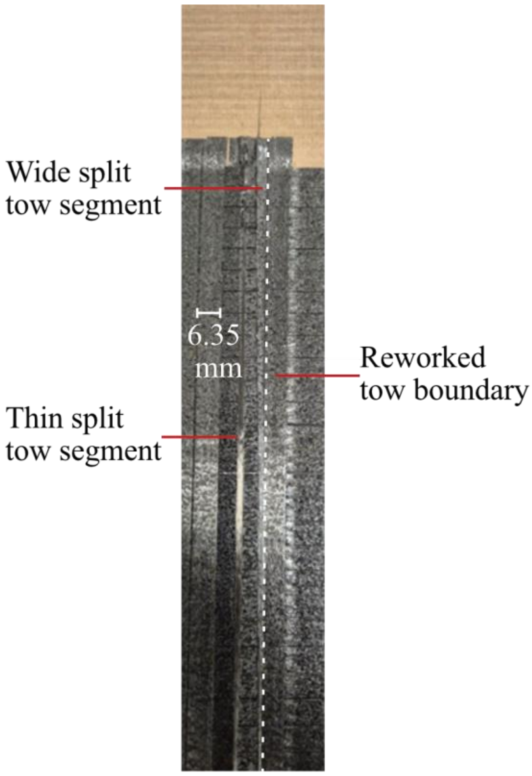

Figure 4.13. Fibre breakage after RM5

Figure 4.13 shows the aftermath of RM5, where the tow has split along its length on both sides, leading to further removal of these fibre bundles.

4.2.2.6 Comparison between rework methods

Figure 4.14, Figure 4.15, and Figure 4.16 show a comparison of the cumulative scores for each of the reworking methods across the different defect sizes and as a cumulative score across all the defect sizes combined. In Figure 4.14, for the 2.5 mm defect, we see RM1-heated as the least damaging reworking method. RM2-RM4 all showed mixed damage extents and a negative influence of introducing heat, this pattern is consistent for the 4.0 mm defect but breaks for the 6.0 mm defect. The size of this defect being the entire width of the gapped tow means that the reworking methods were fundamentally different than in the other two defects where in the largest defect both tows were removed simultaneously, as such the negative scores relating to damage to the gapped tow are not present. Across all the defect sizes, RM5 resulted in the most damage to all the investigated regions.

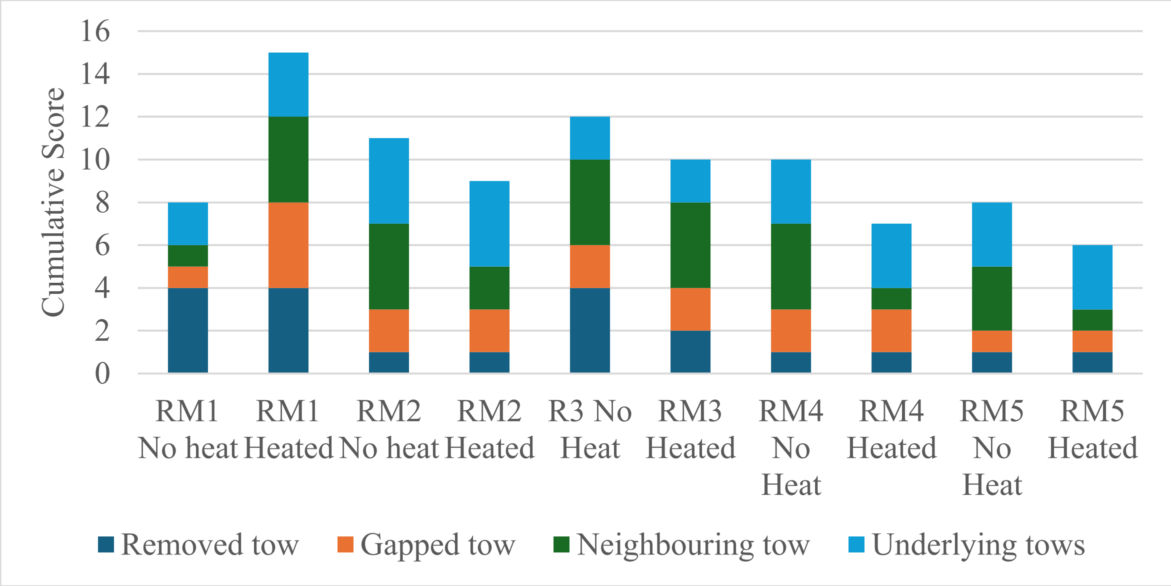

Figure 4.14. Cumulative Scores for each rework method for defect size 2.5 mm

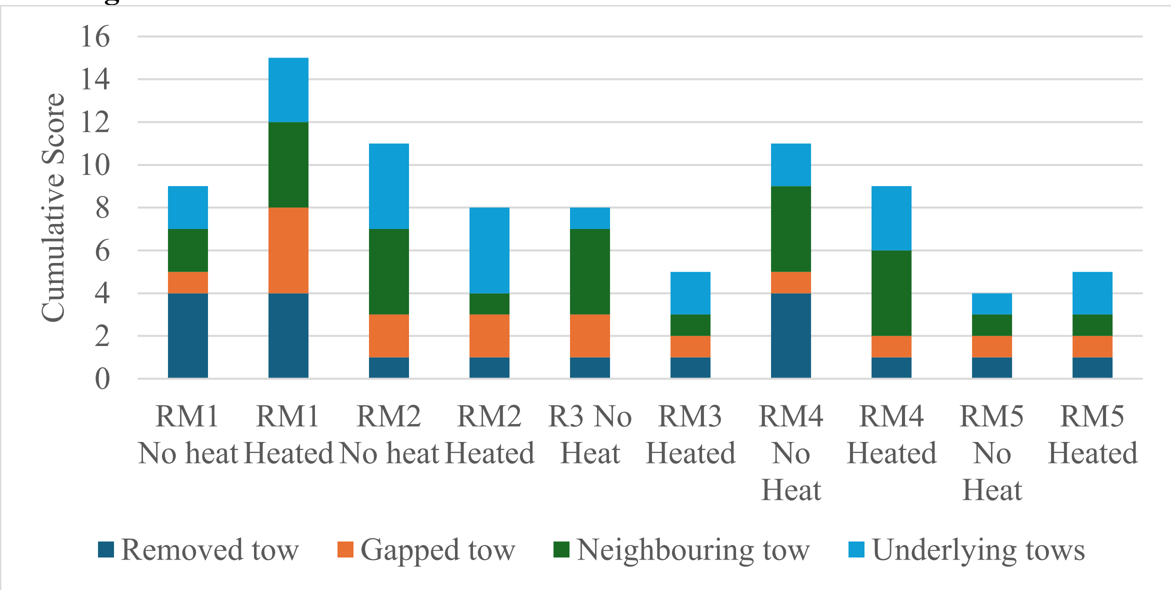

Figure 4.15. Cumulative Scores for each rework method for defect size 4.0 mm

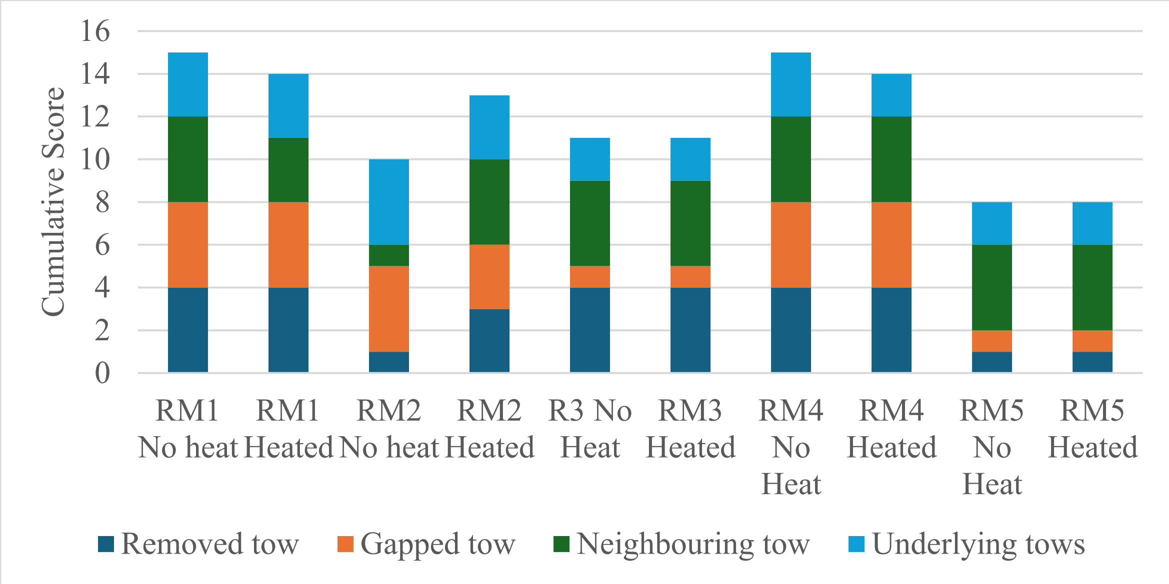

Figure 4.16. Cumulative Scores for each rework method for defect size 6.0 mm

Figure 4.17 compares cumulative scores for all defect sizes for unheated RMs, and Figure 4.18 for heated RMs. The results for unheated RMs show more mixed results, where no single reworking method outperforms any others. RM1-heated displays the most consistency in results, and results in the least damage across any of the defect sizes.

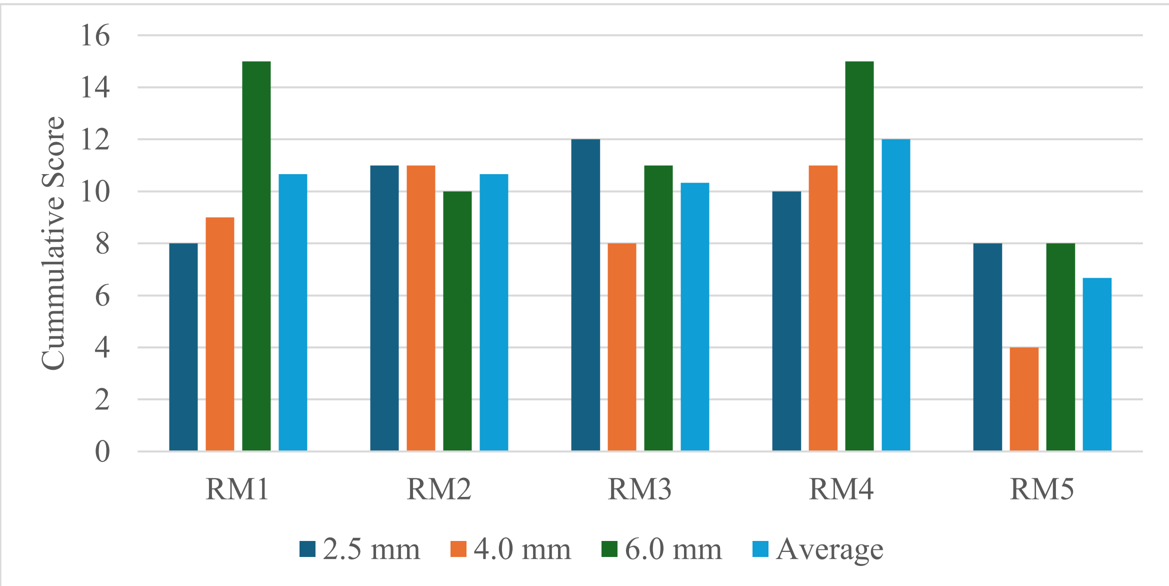

Figure 4.17. Cumulative scores for unheated rework methods by defect size and average across all defect sizes

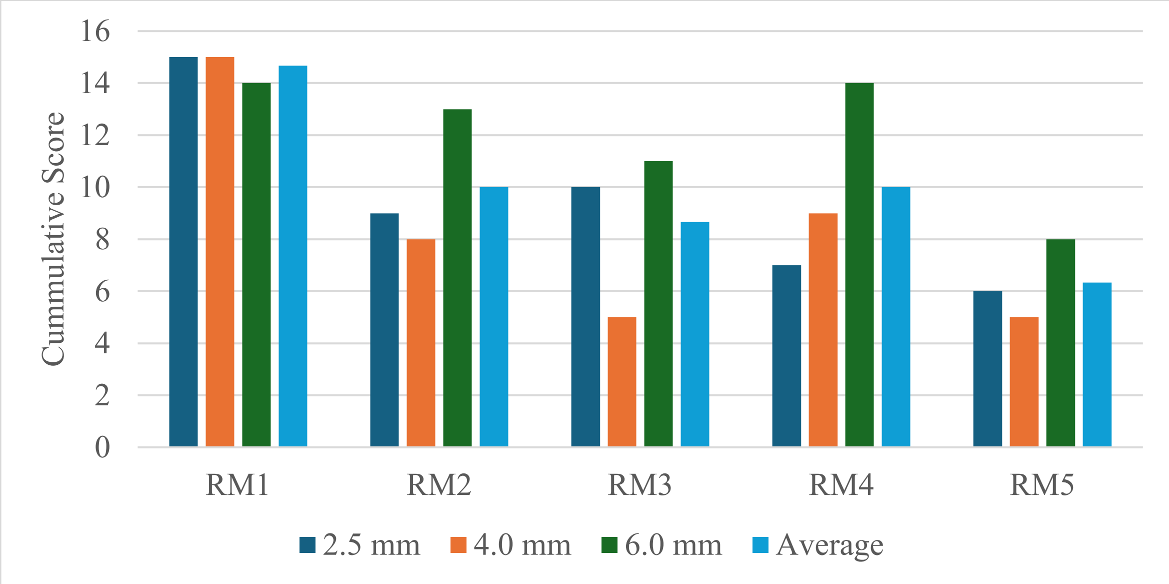

Figure 4.18. Cumulative scores for heated rework methods by defect size and average across all defect sizes

From this experimental study, RM1 was used to evaluate the effect of the reworking procedure and to suggest best-practices for remedial reworking of gap and overlap defects. The following sections details and Ultrasonic NDT method used to evaluate the effect of the reworking method. Following this, the best practices are presented and critically examined against existing literature.

4.3 Ultrasonic Testing

With the reworking method evaluated in terms of visual damage to the surrounding material in the section above. Further tested was performed to validate the effect of the method on the internal structure of test laminates after curing. In order to perform this testing, an Ultrasonic NDT method was used, using laminates manufactured through a novel Benchtop-AFP manufacturing cell, with pristine, defective and reworked laminates manufactured. In the case of the reworked laminates, the best practices and rework method defined in the section above were followed strictly to ensure objectivity in the results.

4.3.1 Introduction

Several studies from the literature point to out-of-plane waviness as a result of placement defects as the key driver of reductions in mechanical performance of composite parts manufactured through AFP. Nimbal et al., [134], found wave severity directly correlated to compressive strength loss, with increases from 3° to 7° leading to larger strength reductions. Lan et al., [123], [124], in several studies found the influence of a caul plate, which limits the extent of out-of-plane waviness, to partially mitigate the detrimental impact of placement-induced defects. Del Rossi et al., [133], found that configurations of embedded defects that induced the greatest out-of-plane waviness led to the greatest decrease in compressive strength. Woigk et al., [126], in a study of gaps and overlaps in both tensile and compressive loading, found that the severity of the knockdown in performance was correlated most closely with the degree of out-of-plane waviness induced by the defects. Ngyuen et al., [127], similarly found through study of differently staggered gaps and overlaps of varying sizes across tensile and compressive loading, that the degree of out-of-plane waviness was more critical than defect type or size for predicting strength knockdowns. Guin et al., [118], found that 1.27 mm gaps led to increased rate of failure under compressive loading due to buckling or interlaminar shear failure, and that the increased waviness was responsible for the failure initiation.

It can thus be said that out-of-plane waviness is a critical metric in evaluating and predicting the decreased performance of composite structures featuring placement induced defects. Equipped with this understanding, it remains to be uncovered the extent to which reworking mitigates this out-of-plane waviness, compared with un-reworked defects, and to what extent this waviness is mitigated or propagated through the laminate in subsequent layers. Evaluation of laminates can be performed to examine 1) the extent of waviness in defective laminates against pristine laminates, and 2) the extent of waviness of reworked laminates against the opposing benchmarks of pristine and defective laminates.

4.3.2 Experimental setup: Benchtop-AFP

In order to perform experiments investigating the reworking process without incurring the high capital costs, and machine utilisation costs of using a conventional AFP machine, a low-cost benchtop setup was developed. This allowed for the later testing and recording of reworking techniques in a small-scale, low-cost, research friendly environment. The following section describes the conceptualisation, rationale and configuration of the setup.

The high capital cost associated with traditional AFP systems remains one of the primary barriers to their widespread adoption, especially for smaller organisations, research institutions, and educational facilities with limited budgets [112]. Stated costs for acquisition of AFP machinery from literature range from £1.0-1.2M [113], [114], [115]. This view was expressed by all of the expert interviews and detailed in Chapter 3.

This financial barrier, along with machine availability, motivated the exploration of alternative approaches, such as the Benchtop-AFP technique proposed in this chapter, which aims to provide a more cost-effective solution for research and development in automated fibre placement sub-processes. Although this setup is not intended to replace conventional

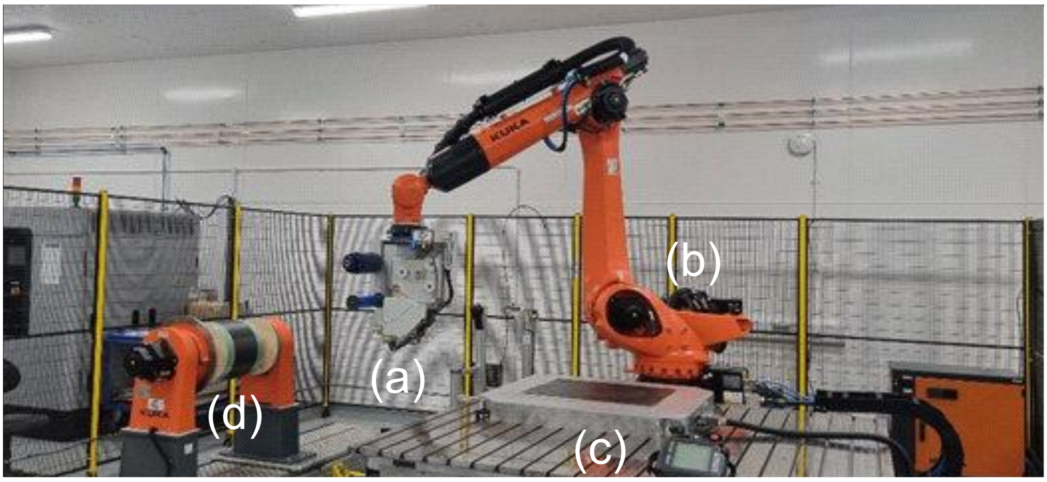

Figure 4.19. Conventional AFP system featuring (a) AFP end-effector, (b) 6-axis industrial robot, (c) heated tooling place, and (d) rotating mandrel

AFP systems in a manufacturing environment and does not replicate the full capabilities of an industrial AFP head, it retains some of the key components of the manufacturing technique. As a result, it supports the study of sub-processes within the conventional AFP manufacturing cycle. The low cost and footprint enable smaller-scale and more flexible research environment that is accessible to a wider range of users.

4.3.2.1 Concept Design and evaluation

To viably generate comparable samples to conventional AFP, the core features of an AFP system were mimicked through readily available technology. Figure 4.20 shows a non-scaled diagram of Benchtop-AFP. Tows are placed on the Polytetrafluoroethylene (PTFE) film covered 3D-print bed by the human operator, considering alignment and ply orientation, and controlling the tow tension through tactile response. The collaborative robot (cobot) is then programmed to pass a compaction roller over the tow and apply the desired consolidation force along the length of the newly placed tow.

Using a 3D-print bed, the tool temperature parameter from conventional AFP can be mimicked to a repeatable and accurate level. The temperature of the print bed was tested with a heat sensor gun and found to agree with the stated temperature in the control hardware. The chosen print bed was a disassembled Creality Ender-3 Pro 3D-printer, capable of rapidly heating between 0-110°C. A new printer can be purchased directly from the manufacturer for £236.

The use of a collaborative robot for the application of consolidation force was used as the deployed force could be controlled with similar repeatability as in the heated tooling aspect. In the developed Benchtop-AFP system, a Universal Robots UR10e robot was used. The UR10e can deploy a consistent normal force along a tool path of up to 100N. The UR10e is available in the range of £30,000 from retailers or direct from the manufacturer. Even cheaper models of

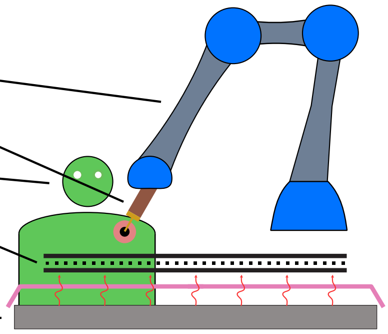

Figure 4.20. Diagram of Benchtop-AFP

collaborative robots are widely available on the market. In recent years, cobots have become increasingly ubiquitous in many manufacturing research settings.

Benchtop-AFP occupies a new space between traditional AFP and hand layup. This is illustrated in Table 4.12 and Figure 4.21 with reference to key process descriptors.

Benchtop-AFP, as a proof of concept, retains the core features from typical AFP systems of controllable compaction pressure, and a heated tooling bed for a far reduced price than that of the typical AFP systems. While it does not include an AFP end-effector as in typical AFP systems, the positional accuracy of layup, and the application of tension through the tow is human led, hence derived from operator proficiency. Moreover, with the human "in-the-loop" with the Benchtop-AFP system, novel methods in human-robot collaborative composites layup could be developed.

Table 4.12. Comparison between manufacturing techniques

	AFP	**Benchtop-AFP**	**Manual Layup**
Scale	High	Low	Low
Cost	High	Medium	Low
Flexibility	Low	High	High
Collaboration	Low	High	Medium
Throughput/Efficiency	High	Low	Medium
Variability	Low	Medium	High

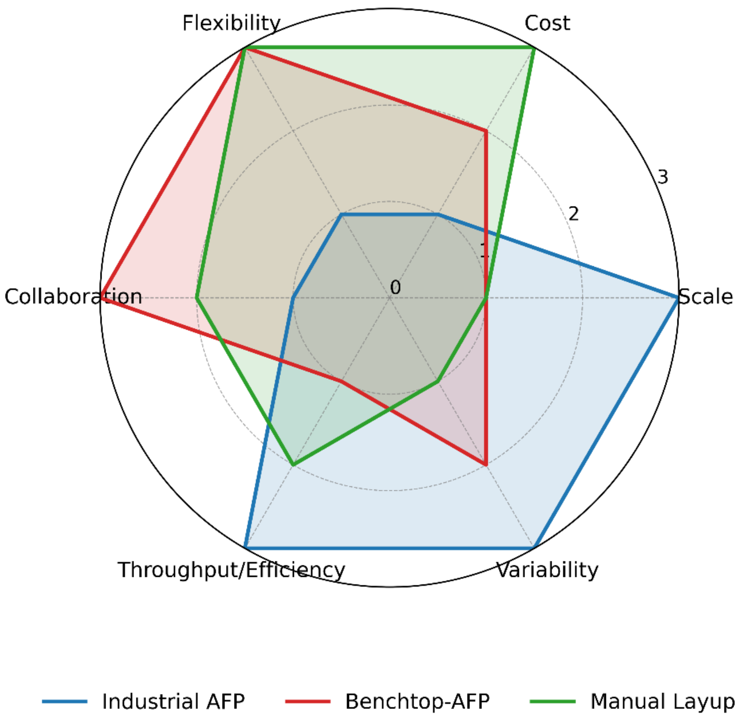

Figure 4.21. Comparison of Benchtop-AFP against conventional AFP and manual layup

The lowered system price when compared to typical AFP is the cornerstone of the benefits of this system. Here, smaller institutions or researchers can feasibly acquire or use existing technology to perform research on aspects of AFP at a small scale. It is important to note here, that in the current configuration of Benchtop-AFP, there is a large constraint on the scale of the parts which may be produced, governed in the first instance by the size of the 3D-print bed used, and secondarily by the reach of the collaborative robot used.

Given the manual nature of reworking as the current state-of-the-art [174], Benchtop-AFP is uniquely placed as a collaborative technique for producing small scale laminates with defects upon which rework research may be performed.

While Benchtop-AFP may have limitations in terms of part size, layup rate, and overall complexity compared to industrial AFP systems, it could provide a valuable platform for researchers, educators, and small-scale manufacturers to explore and develop AFP techniques, optimise fibre placement strategies, and test new materials or configurations without the need for multi-million-dollar investments.

The use of a collaborative robot opens the space for a human-centred approach to AFP research and development. Benchtop-AFP sits in a unique space between typical AFP and hand-layup or other traditional composites manufacturing methods. It benefits from the reduced variability of an automated method, while not suffering from the prohibitive costs associated with typical AFP configurations. This comes with a reduction in scale when compared to AFP and to a certain extent efficiency, where traditional measures such as part throughput are concerned, however, the removing the industrial robots or gantries from the configuration leaves a more flexible and collaborative workspace. Here the benefits of automation can be married with the intuition and skill of human operators.

Benchtop-AFP will not replace conventional AFP, but it does provide an alternative working space within which to examine sub-processes. In the following section the laminates generated through the approach are tested using Ultrasonic NDT. The primary aim of this is to examine the effect of reworking, however, by comparing those results with results from laminate manufactured using conventional AFP, as shall be discussed in Chapter 5, a demonstration of the viability of the Benchtop-AFP method is shown.

4.3.3 Experimental Procedure

Using the Benchtop-AFP setup, Hexcel® M91/34%/UD194/T700GC 6.35 mm width prepreg tows were used to layup 120 x 120 mm laminates with a [90, 0, 0, 0, 90] structure, deposited on a 150 x 150 x 2 mm aluminium tooling plate, heated from below. Artificial 2.5 mm gap and overlap defect were inserted at 3 places within the defective laminates to allow for three different data sources per laminate. The defects were inserted artificially by deliberately misaligning a tow, in sequence, leading to a gap between the misaligned tow and the previous tow, and an overlap of the following tow on top of the misaligned tow. Figure 4.22 illustrates the laminate structure and defect configurations through multiple cross-sectional views. The figure presents both the overall laminate geometry and coordinate system, along with detailed views of the defect locations, particularly focusing on ply 3 where the defects are embedded.

The specimens were manufactured with a tooling temperature of 60°C and using a consolidation force of 100N using a hard silicon roller. Following the completion of layup these were cured as per manufacturer's instructions.

Three classes of specimens were manufactured. These were: pristine, where all tows were placed in alignment and the resulting laminate was therefore free of defects; defective, where on the innermost 0° ply (ply 3) a 2.5mm misalignment was artificially induced in specific tows, as described in Figure 4.22. The subsequent tow was placed in the original alignment, such that a dual gap/overlap defect was created.

Finally, reworked specimens, where the same process was followed as for the defective specimens, however these defects were manually reworked in-line with the reworking method RM1 as described in more detail in Section 4.2. Following reworking, the subsequent plies were laid up in the correct alignment. Thus, reworked specimens should cosmetically appear similarly to the pristine specimens. Curing was performed as per the material manufacturer's instructions, described in [180].

Two specimens were generated for each of the specimen classes, each containing three distinct defect instances in the case of the defective and reworked specimens. In the subsequent NDT scans, each of these defects were scanned individually, or, in the case of the pristine specimens, three distinct regions were scanned corresponding to the locations of the defects in the other defect classes.

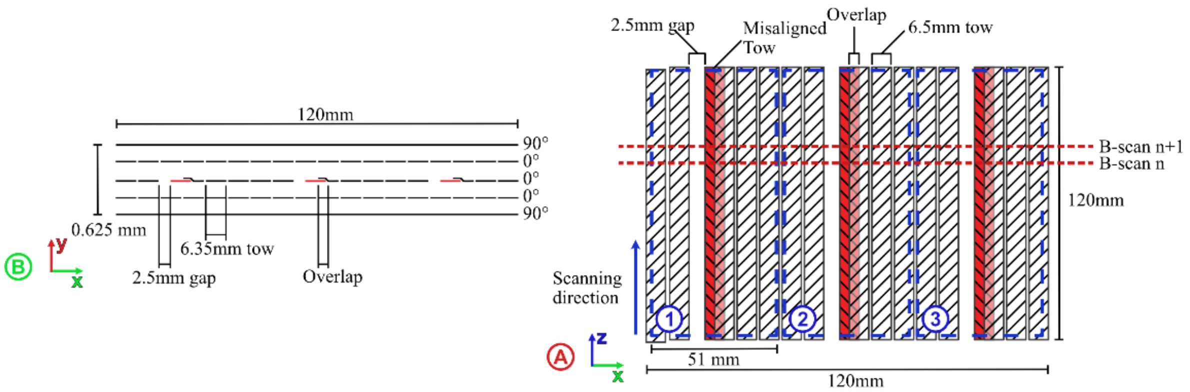

Figure 4.22. Multi-view representation of laminate structure and defect configurations: (B) B-plane cross-section showing 0° and 90° ply orientations with defect locations and parameters; (A) A-plane cross-section of the 0° ply (ply 3) illustrating scanning regions 1-3 and consecutive B-scan positions, repurposed from [181]

Henceforth, the following nomenclature is used to discuss the scans. *Xn_N*, where *X* refers to the specimen class (P, D, or R), *n* refers to the specimen number (1 or 2), and *N* refers to the scan area within a specimen - where each area in a given specimen is numbered from 1 to 3 corresponding to the areas from left to right with respect to Figure 4.22 lower-right, numbered 1 to 3. For example, P2_2 is the scan of region 2 of pristine specimen number 2.

An ultrasonic-NDT method was employed to investigate the laminates post-cure. Ultrasonic Testing (UT) is widely adopted for volumetric inspections of composite components. Unfocused, bulk wave inspection was used to inspect the specimens. In this inspection method, sound waves are excited on the surface of a component, and the reflected/scattered wave from internal scatterers provides valuable information about the volumetric discontinuities of the component. UT allows for the detection of a diverse range of defects or discontinuities. A manually deployed 64-element, 5 MHz Olympus RollerFORM [182] was used to collect the ultrasonic data. The use of a linear phased array probe, allowed for the capture of through-thickness, depth-wise images (known as B-scans). The component was scanned parallel to the orientation of the top ply surface. Water was used as an acoustic couplant to ensure effective acoustic transmission between the roller probe and the specimen. For more in-depth discussion on the method, readers are directed to [183]. Within each of these

B-scans the internal 0-degree layers could be seen running horizontally through the scan, at a specific step (henceforth referred to as 'Slice') along the y-axis (Figure 4.22).

From this perspective, out-of-plane waviness in the plies can be seen. Out-of-plane ply waviness propagates through the layers of the laminate, due to the sequential, additive nature of AFP as new plies are lied directly on top of existing plies. In the case where there are undulations in the underlying ply, the surface of the subsequent ply will follow the contours of the underlying ply during compaction. Further, during curing, as noted by Simacek et al., [184], both shear and bleeding resin flow will occur from the edge of gaps inward in the transverse direction allowing resin to fill voids. In a perfectly pristine specimen, minimal internal out-of-plane waviness is expected, as there is no negative space for the plies to lie in when compacted and then subsequently during curing. Conversely, in a defective specimen, maximum out-of-plane ply waviness is expected. The outcomes of this study are on the level of out-of-plane waviness seen in reworked specimens.

Figure 4.23, Figure 4.24, and Figure 4.25 show the samples after curing. A warping is exhibited in all samples, with the corners of the aluminium plate bending inward on the non-composite side. The thickness of the aluminium plate (2 mm) contributes significantly to this curvature. Initially in the curing process, both the aluminium and uncured composite expand freely as temperature increases. Since aluminium typically has a Coefficient of Thermal Expansion (CTE) of approximately 23.1×10^{-6} K^{-1} [185], and uncured M91 resin has a reported CTE of 5.2×10^{-5} K^{-1} [186], the composite component expands more than the aluminium. However, once curing is complete and rigidification occurs through cure-induced vitrification, the composite's effective CTE is greatly reduced. During the subsequent temperature ramp-down, the aluminium component now contracts more than the composite component as aluminium now has the higher effective CTE of the two bonded materials.

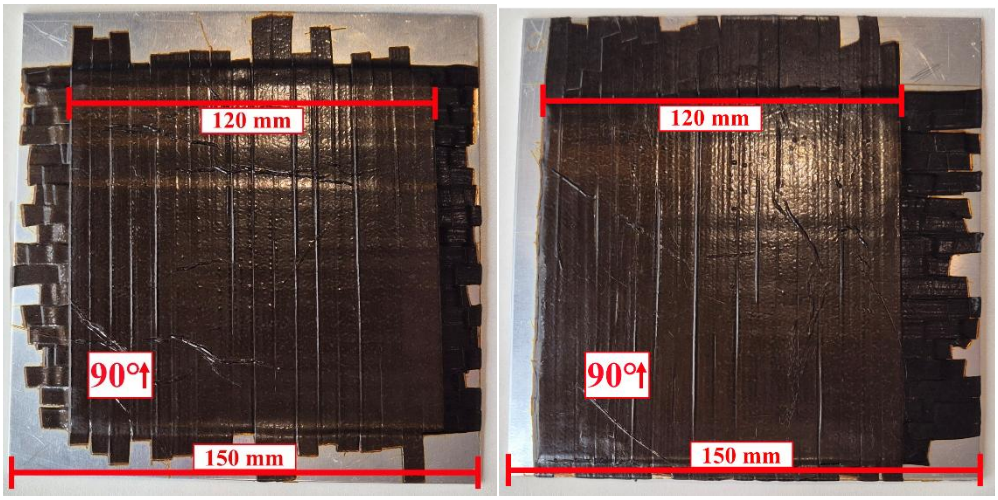

Figure 4.23. Pristine Samples 1 and 2 (left and right)

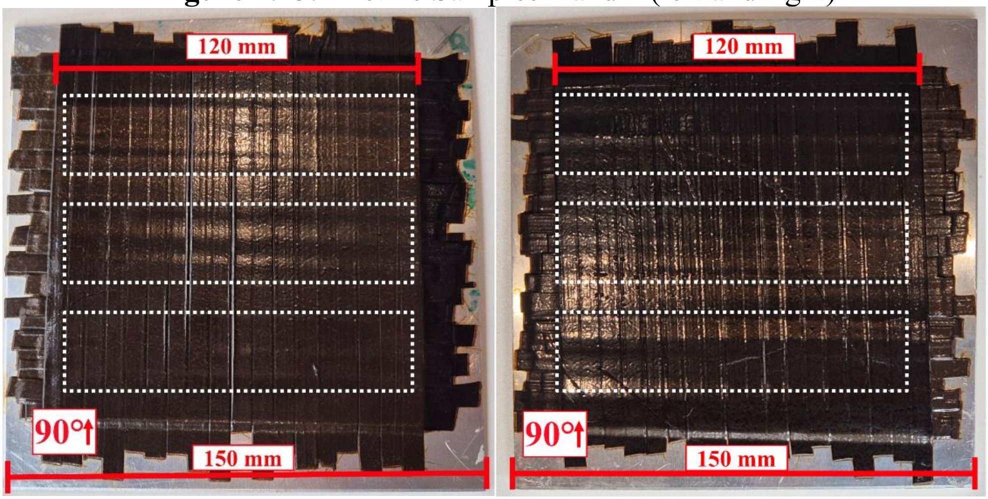

Figure 4.24. Defective Samples 1 and 2 (left and right), showing defect locations (white-dashed)

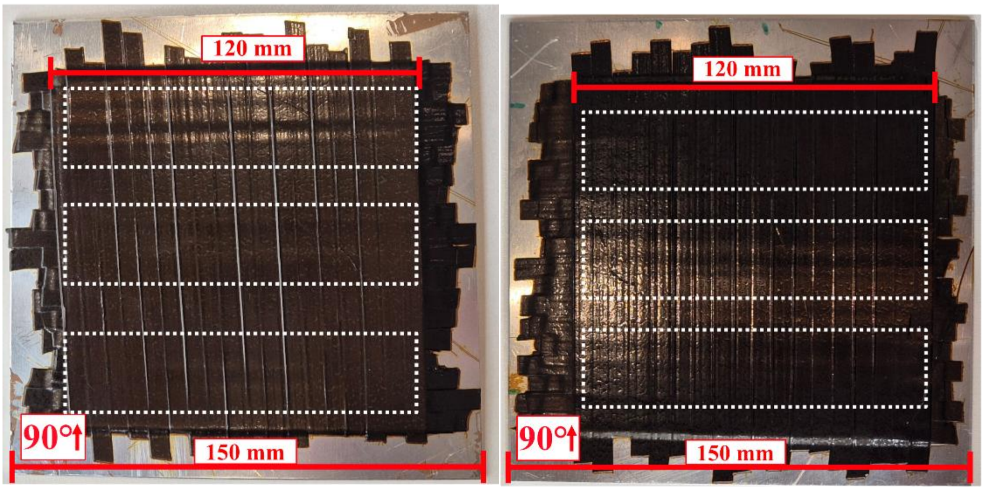

Figure 4.25. Reworked Samples 1 and 2 (left and right), showing rework locations (white-dashed)

The differential contraction creates internal stresses that generate a bending moment rather than simple tension. This causes the composite side to become convex and the non-composite

Table 4.13. Warpage of specimens as measured using 3D scanner.

Sample	Metric	Bottom Left	Bottom Right	Top Right	Top Left
Defective 1	Height (mm)	5.75	7.37	5.46	7.89
	Relative deviation from average (%)	-13.05	11.32	-17.48	19.22
Defective 2	Height (mm)	6.96	4.78	7.31	4.99
	Relative deviation from average (%)	15.76	-20.43	21.65	-16.99
Pristine 1	Height (mm)	7.16	6.27	6.18	6.12
	Relative deviation from average (%)	16.25	-4.19	-5.53	-6.53
Pristine 2	Height (mm)	5.34	6.2	7.72	5.33
	Relative deviation from average (%)	-13.06	0.79	25.55	-13.28
Rework 1	Height (mm)	4.91	7.12	4.02	7.21
	Relative deviation from average (%)	-15.54	22.50	-30.95	23.99
Rework 2	Height (mm)	6.67	5.91	6.24	6.16
	Relative deviation from average (%)	6.77	-5.34	-0.06	-1.38

aluminium side to become concave. The differential contraction induces residual stresses throughout the bonded assembly, with the result being warpage in both the x and y directions, producing the observed doubly curved shape with corners bent inward on the non-composite side of the aluminium plate. This mismatch in thermal expansion behaviour during the cooling cycle, driven by cure induced rigidification, is the primary mechanism behind the deformation, as both materials experienced identical thermal conditions within the autoclave during processing.

Table 4.13 presents the maximum height measurements at the corners of each sample, captured from the underside to record the degree of warpage. All locations referenced in the table correspond to the top side orientation shown in Figure 4.23 - Figure 4.25.

For accurate measurement, an EinScan HX [187] handheld 3D scanner was used to create volumetric scans of the samples. These scans were subsequently aligned and converted into height maps from which the maximum deviations were determined. In all samples, these maximum deviations consistently occurred at the four corners.

Distinct warpage patterns emerged across the sample categories. Both defective samples exhibited pronounced diagonal warpage patterns, with opposite corners showing similar elevation characteristics. The pristine samples displayed warpage dominated by a single corner, which differs from the more symmetrical pattern observed in the defective samples. Given the nominally balanced composition of these laminates, this asymmetric warpage in pristine samples may be attributed to the positioning of material relative to the centre of the aluminium plate. Specifically, in pristine sample 2, the most severe warpage appeared at the upper right corner where there is least material present.

The reworked samples showed remarkably different behaviour from each other. reworked 1 exhibited diagonal warping similar to the defective samples, while reworked sample 2 demonstrated the least warpage among all samples examined. This considerable variation between reworked samples shows a pattern that persists throughout subsequent analyses in this work.

4.3.4 Results

As the roller probe was scanned across the component, B-scans were concatenated to produce three-dimensional datasets containing through-thickness and spatial information. This data underwent processing to extract the internal ply topography using the following method:

Firstly, a two-dimensional data slice was obtained from the three-dimensional array where the signal was most pronounced, facilitating data processing and minimising the impact of noise on the signal. Next, to enhance the signal-to-noise ratio, a thresholding approach was employed. The mean and standard deviation of the data slice were calculated, excluding values below a predefined static threshold. A thresholding operation was then applied, setting values below (mean - standard deviation) to zero, thereby reducing noise. The noise-reduced data slice was then smoothed using a Gaussian filter with a sigma value of 1 [188]. This value enabled smoothing of measurement noise while preserving the edges of signals needed for subsequent thresholding steps. A local adaptive thresholding technique (Sauvola's method, [189]) was applied to binarise the smoothed data, creating a binary image representation where pixels containing ply material were assigned a value of 1, and pixel containing no material were given a value of 0. Through this approach, regions containing continuous material were mapped. The binary image underwent further processing using morphological operations, such as closing and opening, to remove small discontinuities and smooth the boundaries of the detected material regions. Connected regions in the binary image were labelled with ply number based on their position in the specimen. Unconnected regions within the same ply could then be processed together to extract the topography of the entire ply rather than in sections. For each ply region, the middle line was extracted by finding the mean y-coordinate for each x-coordinate within the region. Linear interpolation was applied to fill any gaps in the middle line resulting from discontinuities in the ply region. Figure 4.26 shows the process for a data slice. Note that in Figure 4.26 (F) each distinct region is represented with a distinct colour for visualisation purposes only.

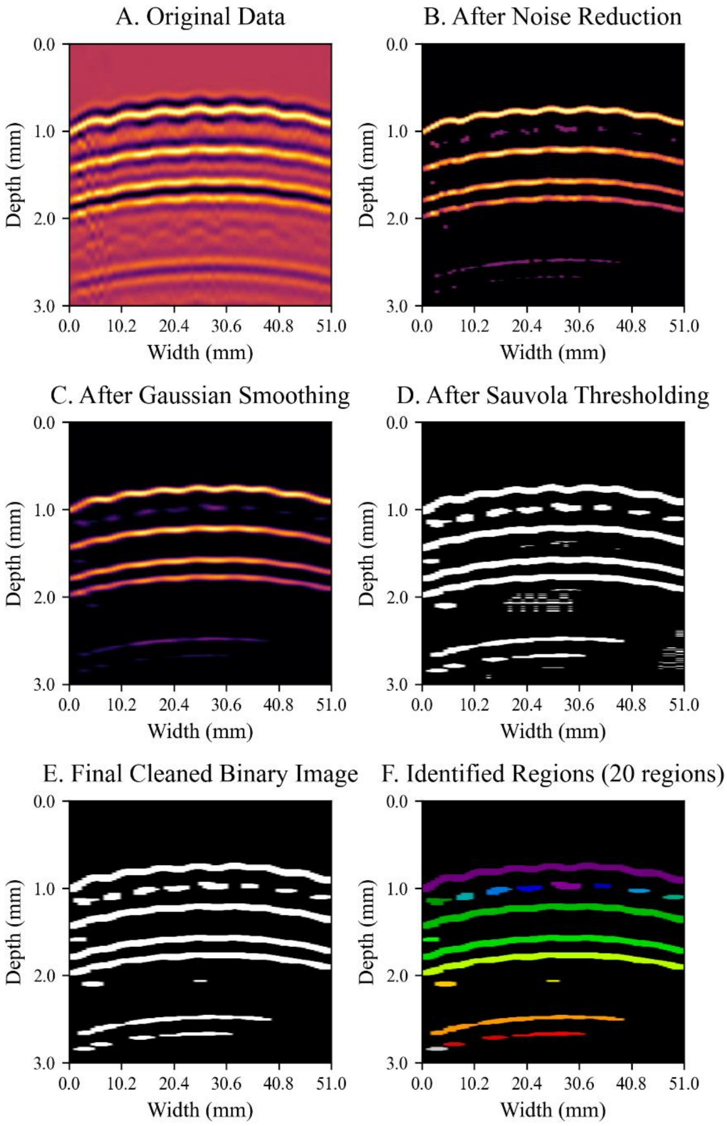

Figure 4.26. Ultrasonic signal processing pipeline for composite material characterisation. The six-stage process illustrates: (A) original B-scan data showing reflected ultrasonic signals; (B) noise reduction using adaptive statistical thresholding; (C) Gaussian smoothing to enhance signal continuity; (D) Sauvola local thresholding for binary classification of material boundaries; (E) morphological operations to refine and connect material regions; and (F) region identification and labelling for subsequent ply tracking and waviness analysis. Each distinct region is color-coded to demonstrate the algorithm's capability to isolate individual plies for topographical extraction and quantitative assessment of structural integrity.

To quantify the waviness of the plies, a three-step process was employed: fitting a quadratic polynomial to the identified middle lines of each ply, normalising the data to this quadratic line, and finally calculating key waviness metrics based on the deviation from this fitted curve. Normalising the signals using the best-fit quadratic curve allowed for a comparative analysis of the results, ensuring that the waviness metrics were not influenced by variations in curvature caused by warping during the curing process, which could otherwise affect the outcomes between different specimens and regions.

For each identified ply, the quadratic polynomial was fit to the middle line coordinates using a least squares method. The general form of the quadratic equation used is:

$$y = ax^2 + bx + c \tag{4.1}$$

Where y represents the vertical position of the ply, x is the horizontal position, and a, b, and c are coefficients to be determined.

The fitting process utilised the curve_fit function from SciPy's [188] optimise module, which implements a non-linear least squares algorithm to fit the function to the data points. This method minimises the sum of the squared residuals, defined as:

$$S = \sum_{i=1}^{n} \left(y_i - f(x_i)\right)^2 \tag{4.2}$$

Where y_i are the observed y-coordinates, $f(x_i)$ are the predicted y-coordinates from the quadratic function, and n is the number of data points.

The following assumptions were made for this fitting process:

1. The relationship between x and y can be adequately approximated by a quadratic function.
2. The errors in the y-values are normally distributed.
3. The x-values are known without error.
4. The data points are independent of each other.

With a quadratic polynomial y_{fit} in the general form of Eq. 4.1, the y coordinates for a ply middle line were flattened by:

$$y_{flat} = y - y_{fit} \tag{4.3}$$

With a set of normalised ply topologies, the waviness metrics were calculated. Firstly, the RMS waviness quantifies the average magnitude of deviations from the normalised middle line for a given ply. The RMS waviness, W_q, was calculated in derived form, from ISO 4287:1997, [190], as:

$$W_q = \sqrt{\frac{1}{n}\sum_{i=1}^{n} y_{flat,i}^2} \tag{4.4}$$

The units of the RMS waviness are the same as the units of the y-coordinates. In this analysis, these units are millimetres, derived from pixels as in the image space. The y-axis scale in millimetres is calculated based on the response time of the ultrasonic signal, and the speed of sound through the composite material. For the sake of the comparative analysis performed in this Thesis, the effect of the aluminium backing plate on the response time of the ultrasonic signal is not considered. Hence the physical distances in y shown, and the derived waviness metrics (measured in mm) are approximation based on these assumptions. While there can therefore be said to be some error in this scaling, it nevertheless allows for comparative study between the specimen types in this study, reinforcing the conclusions of this study.

The process for scaling the y-axis was as follows.

Key parameters:

1. Speed of Sound (c): The speed at which the ultrasonic wave propagates through the medium. In this study, the ultrasonic signal travels through the thickness of the laminate, transverse to the fiber direction. Based on similar composite materials studied in [191], $c \approx 3000\, ms^{-1}$. While the exact speed of sound for our specific material has not been experimentally determined, this value was adopted due to the comparable material properties between our composite and the referenced study.
2. Sampling Rate (fs): The rate at which the signal is sampled in the time domain, given as $fs = 100\, MHz = 100 \times 10^6 Hz.$
3. Depth Per Pixel (d_{pixel}): The physical distance represented by each pixel along the y-axis.

The one-way travel distance refers to the depth calculation being based on the signal propagating from the transducer to the reflecting boundary and back. Since the total round-trip distance is measured, the depth per pixel (d_{pixel}) is calculated using half that distance to represent the one-way travel distance. This accounts for the fact that the signal must travel to and from the reflecting surface.

The time interval between consecutive samples (Δt) is the inverse of the sampling rate:

$$\Delta t = {}^{1}\!/_{fs} = {}^{1}\!/_{100 \times 10^6} \text{ seconds} \tag{4.5}$$

Each pixel corresponds to a signal travel distance of:

$$d_{pixel} = c \cdot \Delta t \tag{4.6}$$

However, since the ultrasonic wave must travel to the reflecting boundary and back, the one-way travel distance is:

$$d_{pixel} = c \cdot \frac{\Delta t}{2} \tag{4.7}$$

Substituting Eq. 4.6, gives:

$$d_{pixel} = \frac{\mathrm{c}}{2fs} \tag{4.8}$$

Given, $c = 3000\, ms^{-1} = 3000 \cdot 1000\, mms^{-1}$ and $fs = 100 \times 10^6\, Hz$:

$$d_{pixel} = \frac{\mathrm{c}}{2fs} = \frac{3000 \cdot 1000}{2 \cdot 100 \times 10^6} = 0.015\, mm \tag{4.9}$$

The y-axis values are finally scaled by multiplying each pixel index y_i by d_{pixel}:

$$y_{scaled} = \mathrm{y} \cdot d_{pixel} \tag{4.10}$$

The x-axis scaling is calculated as

$$x_{mm} = {}^{w}\!/_{x_{max}} \tag{4.11}$$

Where w is the probe width of 51 mm.

The scaled values x_{scaled} for each value of x_i were calculated as:

$$x_{scaled} = x_i \cdot x_{mm} \tag{4.12}$$

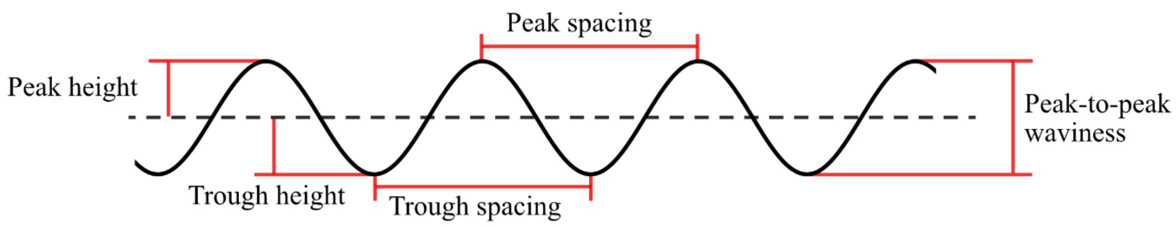

Figure 4.27. Graphical description of waviness metrics.

To evaluate the out-of-plane waviness of each ply, several waviness metrics were used. Firstly, a waviness value for each of the plies was calculated using Eq. 4.4.

Further waviness metrics calculated were the Peak-to-peak Waviness, W_z:

$$W_z = \max(y_{flat}) - \min(y_{flat}) \tag{4.13}$$

The average wave height, $\overline{W_h}$, was calculated as:

$$\overline{W_h} = \frac{1}{K}\sum_{k=1}^{K}\left|\frac{y_{P,k} + y_{T,k}}{2}\right| \tag{4.14}$$

Where K is the number of peak-trough pairs, $y_{P,k}$ are peak heights, and $y_{T,k}$ are trough depths.

The average wave, λ_w, spacing was calculated through:

$$\lambda_w = \frac{1}{M-1}\sum_{m=1}^{M-1}(x_{P,m+1} - x_{P,m}) \tag{4.15}$$

Table 4.14 shows the definitions of the waviness metrics recorded as well as interpretations for higher and lower values for each. Figure 4.27 shows a graphical description of the metrics peak height, trough height, peak spacing, trough spacing, and peak-to-peak waviness on an idealised sine wave curve.

The section below displays and discusses the data recorded through the ultrasonic scanning method detailed above. The numerical results below are median values for the waviness metrics across a selection of 10 random B-scans with valid and interpretable signals for each of the individual scans Xn_n. This gives an impression of the waviness across the length of each

Table 4.14. Waviness metrics descriptions and interpretations

Metric	Definition	High Value Interpretation	Low Value Interpretation
RMS Waviness	The root mean square of deviations from the best-fit line, measuring overall roughness	Strong variations, significant roughness	Smooth signal, minimal fluctuations
Peak-to-Peak Waviness	The total vertical distance between the highest peak and the lowest trough	Large fluctuations, pronounced oscillations	Smaller fluctuations, smoother signal
Average Wave Height	The mean vertical distance between consecutive peaks and troughs	Larger average vertical oscillations	Smaller average vertical oscillations
Max Peak Height	The greatest upward deviation (peak) from the best-fit line	Large positive deviations (spikes)	Smaller positive deviations (gentler oscillations)
Max Trough Height	The greatest downward deviation (trough) from the best-fit line	Large negative deviations (deep troughs)	Smaller negative deviations (milder dips)
Peak Spacing	The average distance between consecutive peaks in the signal	Longer distance between oscillations (low frequency)	Shorter distance between oscillations (high frequency)
Trough Spacing	The average distance between consecutive troughs in the signal	Fewer troughs, slower variations	More frequent troughs, quicker variations

scanned region. Since the defects run along the length of the scanned region, the waviness characteristics are consistent across each B-scan.

4.3.4.1 Defective

Figure 4.28 and Figure 4.29 present representative scans of the defective specimens showing higher and lower levels of waviness. Specimen D1_1 (Figure 4.28) exhibits the least out-of-plane waviness among the defective specimens, whereas specimen D2_3 (Figure 4.29) demonstrates the greatest waviness. Both specimens display significantly high levels of out-of-plane waviness compared to the benchmark pristine specimens, as will be discussed. These results align with expectations, given the presence of un-reworked defects in the defective specimens.

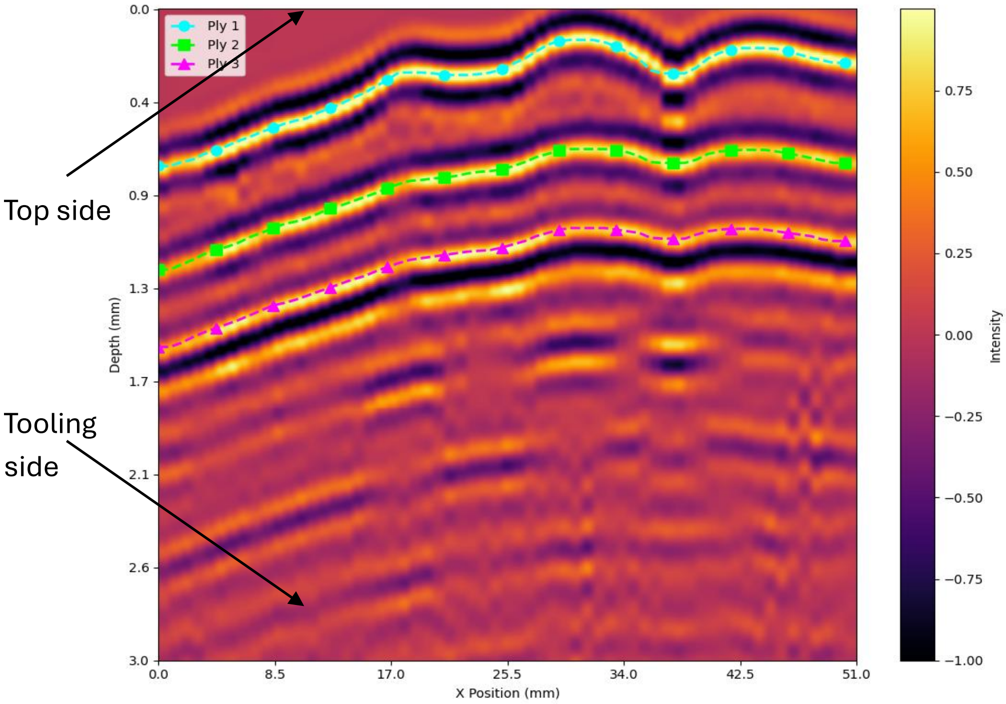

Figure 4.28. B-scan of defective specimens D1_slice 71, with ply middle lines (coloured – dashed) and indication of tooling and top side directions

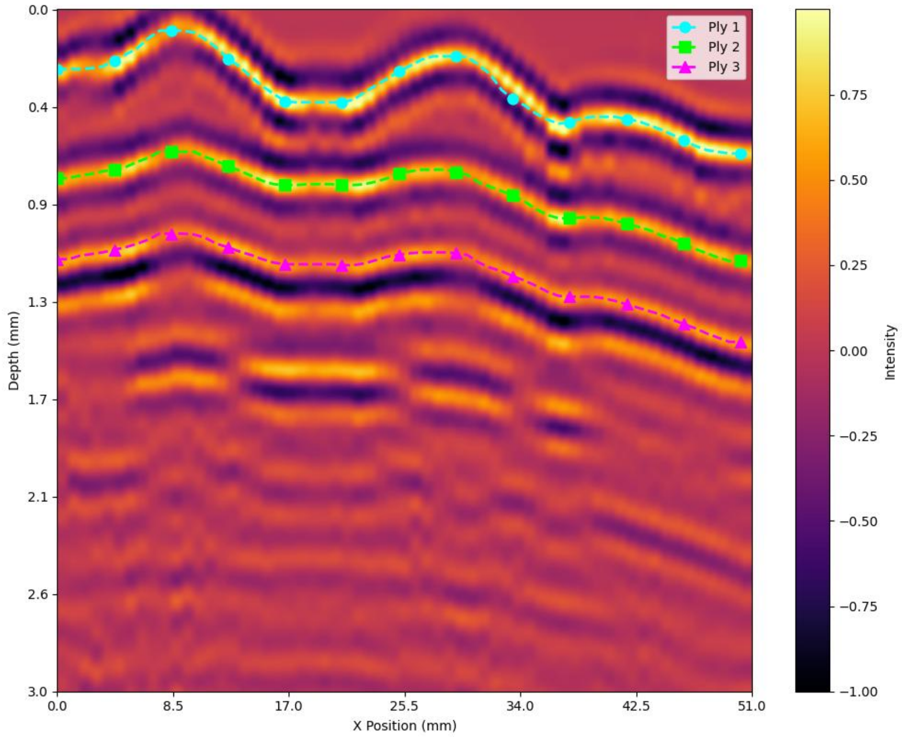

Figure 4.29. B-scans of defective specimens D2_33 with ply middle lines (coloured – dashed)

Table 4.15 shows the median waviness metrics recorded for the defective specimens broken down by ply with each specimen. Plies are numbered sequentially with ply_1 positioned one layer below the laminate's top surface, continuing inward to ply_3 nearest the tooling surface. This consistent numbering convention is maintained throughout all specimen scans and waviness measurements in this study. Across all waviness metrics, there is a trend of decreasing waviness and hence increasing planarity from ply 1 (upper most 0° ply) to ply 3 (lowest 0° ply). This trend is pronounced in all specimens, regardless of class. This can be accounted for by looking to the layup process itself, where the layup of subsequent plies on top of those already laid involves the application of a consolidation force, effectively smoothing out the waviness in the lower plies, this process is again compounded by curing, where the application of pressure consolidates the plies in the downwards direction further still. Additionally, during curing, the elevated temperature decreases the viscosity of the resin and encourages resin flow. This resin flow will follow the gradient of the topology of the plies and fill in voids progressively from the bottom up, leading to reduced waviness in the lower plies.

Table 4.15. Waviness Metrics for Defective Specimens

		Specimen							
Metric	**Ply**	**D1_1**	**D1_2**	**D1_3**	**D2_1**	**D2_2**	**D2_3**	**Median**	**Std Dev**
RMS waviness (mm)	**1**	0.09	0.07	0.05	0.07	0.08	0.16	0.08	0.03
	2	0.04	0.04	0.06	0.05	0.04	0.08	0.05	0.01
	3	0.03	0.03	0.05	0.03	0.03	0.07	0.04	0.02
Peak to peak waviness (mm)	**1**	0.36	0.26	0.17	0.34	0.42	0.61	0.33	0.14
	2	0.20	0.14	0.22	0.22	0.22	0.29	0.21	0.04
	3	0.16	0.11	0.20	0.18	0.18	0.27	0.18	0.05
Average wave height (mm)	**1**	0.08	0.06	0.04	0.04	0.04	0.17	0.06	0.05
	2	0.03	0.03	0.03	0.02	0.02	0.07	0.03	0.02
	3	0.03	0.02	0.02	0.02	0.01	0.05	0.02	0.01
Max peak height (mm)	**1**	0.22	0.17	0.09	0.18	0.22	0.31	0.18	0.07
	2	0.12	0.09	0.10	0.12	0.12	0.14	0.11	0.02
	3	0.09	0.07	0.10	0.09	0.09	0.13	0.09	0.02
Max trough height (mm)	**1**	0.15	0.08	0.08	0.16	0.09	0.29	0.13	0.07
	2	0.08	0.05	0.11	0.11	0.04	0.15	0.08	0.04
	3	0.07	0.04	0.10	0.10	0.03	0.14	0.07	0.04
Peak spacing (mm)	**1**	10.07	7.09	6.70	6.62	5.85	13.52	7.94	2.68
	2	8.53	6.75	5.84	5.11	5.85	10.70	6.89	1.92
	3	7.45	5.96	5.37	5.08	4.74	8.81	6.08	1.44
Trough spacing (mm)	**1**	11.20	7.55	7.95	7.17	5.47	13.60	8.43	2.73
	2	9.09	6.69	5.92	5.06	4.98	10.44	6.75	2.05
	3	8.11	6.15	5.49	5.01	4.39	8.59	6.10	1.56

Conversely, in outer plies a more pronounced effect of planarity deviation is seen as a compounding effect through the thickness of the laminate.

The RMS waviness across all plies and all specimens ranges between a minimum of 0.03 mm for ply 3 of several of the specimens, to a maximum of 0.16 mm for D2_3. Given that the nominal thickness of Hexply M91 Prepreg is 0.184 mm [180], this extent of waviness is a serious undulation in the ply topology. Peak-to-peak waviness is similarly large, with median values for plies 1, 2 and 3 of 0.33, 0.21, and 0.18 mm respectively. The maximum value for peak-to-peak waviness was 0.61 mm for D2_3. Since this value represents the maximum distance from trough to peak it is sufficient in capturing the waviness at the defect location itself, where the waviness is expected to be the highest.

The average wave height across the entire specimen was lower than the peak-to-peak waviness, with median values across the specimens for plies 1, 2 and 3 of 0.06, 0.03 and 0.02 mm respectively.

Reviewing the distribution of waviness over the middle line, a max peak height range from 0.07 – 0.31 mm is observed with a median value of 0.12 mm, while max trough heights range from 0.03 – 0.29 mm with a median value of 0.09 mm. Across all specimens and plies, the max peak heigh is equal or greater than the max trough height. This trend can be attributed to the topological characteristics of the gap/overlap effect of the defect inserted in the middle 0° ply. Since the gap portion of the defect causes local reductions in ply thickness and the overlap causes local increase in ply thickness. The additive nature of AFP manufacturing, will tend to reduce thickness variations in the downwards direction, as undulations in lower plies are systematically flattened downwards in the thickness direction, through consolidation force of subsequent plies during deposition, and through resin flow and consolidation force during curing.

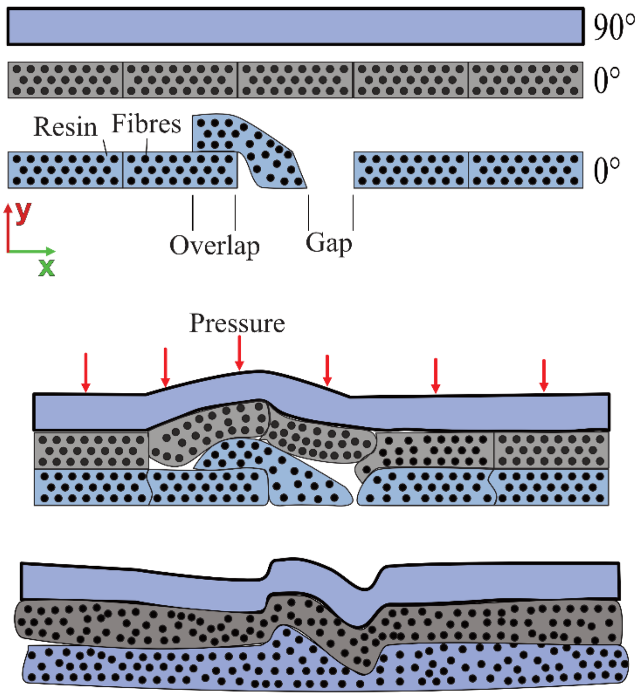

Figure 4.30. Diagram of process leading to double bump waviness caused by Gap/Overlap defect. Pre-curing (top), during curing (middle), post-curing (bottom)

Peak and trough spacing mirror one another in distribution and scale, however in the defective specimens, these values are typically larger than the width of one tow, indicating the effect of the defect is not isolated to its location within the laminate, but also effects the surrounding tows.

A characteristic of the out-of-plane waviness caused by internal gap/overlap defects identified throughout the defective specimens is the "double bump" effect seen in the topography of the defective scans. An explanation for this could be resin flow from the overlapping tow flowing in both directions, on one side onto the surface of the overlapped tow, and on the other into the gap. The results of this would be a gradient of resin from expected tow height, up to the surface of the overlapped tow, down into the gap to the surface of the underlying ply, and up once more onto the surface of the properly laid tow adjacent to the gap. A diagram showing how this process might take place is shown in Figure 4.30.

4.3.4.2 Pristine

Figure 4.31 shows an indicative scan for the pristine specimens. These show a relatively high level of planarity with respect to the curvature of the specimens, and little to no undulations. This is the expected results given the absence of defects in these specimens. Some low amplitude undulations can be seen occurring at regular intervals across the width of the sample, with decreasing amplitude from ply 1 to ply 3. Table 4.16, overpage, shows the waviness metrics for the pristine specimens.

Specimen P1_1 stands out significantly from other pristine specimens, with a substantially higher RMS waviness (0.10 mm in Ply 1 vs. 0.02 - 0.03 mm in other specimens) and much larger peak-to-peak waviness (0.41 mm in Ply 1 vs. 0.08 - 0.13 mm in others). Given the inconsistency of these results with the other pristine specimens, the characteristics of P1_1 warrant further examination.

Figure 4.32 overpage shows a B-scans of P1_1. Readers are directed to the clear and distinct undulation in the topology of the plies, in particular in ply 1. The lack of evidence of the double bump in the waviness shown in Figure 8 for specimen P1_1 supports the claim made that this is in fact not an effect of the type of defect considered in this study, but instead a defect induced by layup error in one of the 0° plies. It should be noted importantly the distinction between a gap/overlap defect where some but not all of the material across the width of the misaligned tow overlaps with a second tow, rather than two tows being laid directly in alignment with each other, as seen in P1_1, producing a waviness in the scanned profile in a single rather than double bump.

Given the layup defect included in specimen P1_1, the results of this specimen shall not be included when examining the pristine specimen class as a whole, hence the waviness metrics for this specimen are not included in the following table and discussion of results.

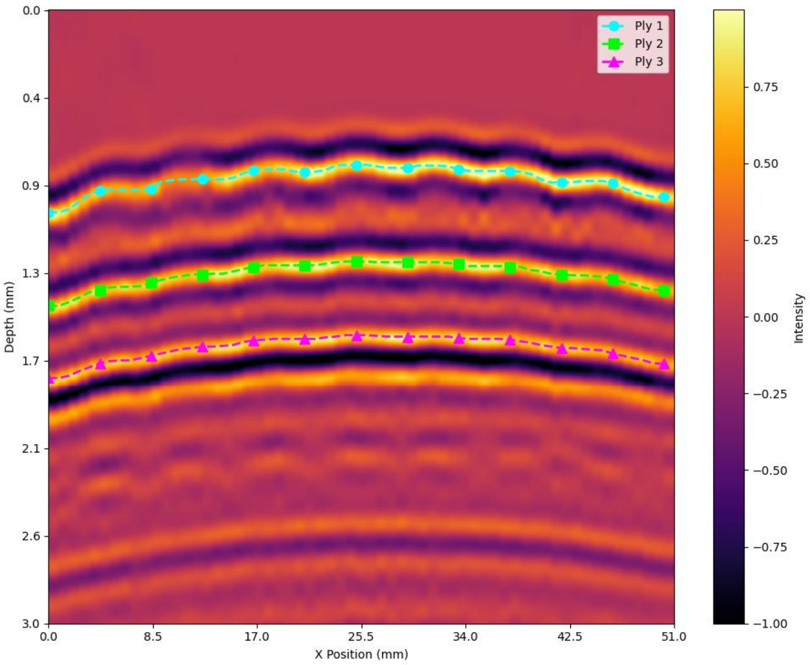

Figure 4.31. B-scan of P1_2 slice 28 with ply middle lines (cyan – dashed)

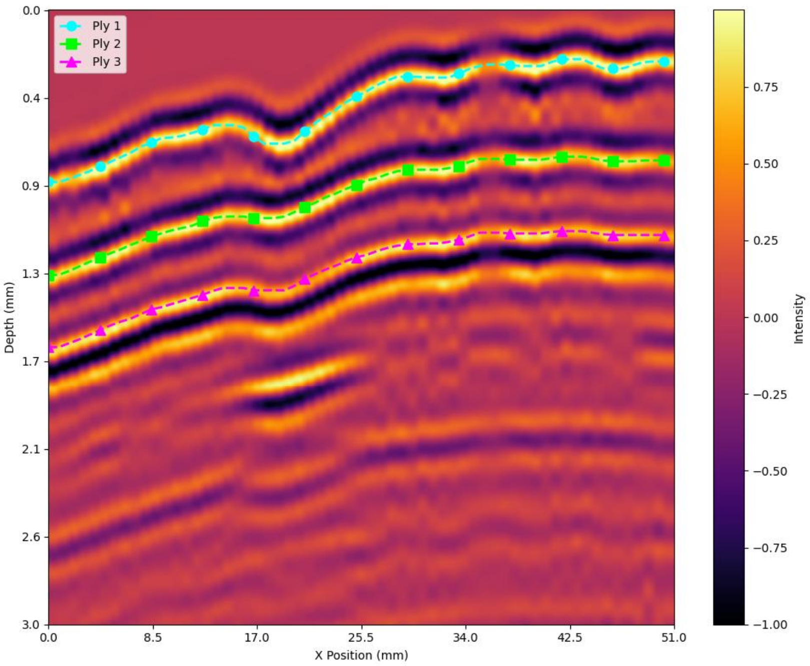

Figure 4.32. B-scan of P1_1 at slice 27 with ply middle lines (cyan – dashed)

Table 4.16. Waviness Metrics for Pristine Specimens

Metric	Ply	Specimen							
		P1_1	P1_2	P1_3	P2_1	P2_2	P2_3	Median	Std Dev
RMS waviness (mm)	**1**	0.10	0.03	0.03	0.02	0.03	0.02	0.02	0.03
	2	0.05	0.01	0.02	0.01	0.01	0.01	0.01	0.01
	3	0.04	0.01	0.01	0.01	0.01	0.01	0.01	0.01
Peak to peak waviness (mm)	**1**	0.41	0.11	0.12	0.12	0.13	0.08	0.11	0.11
	2	0.20	0.07	0.08	0.06	0.07	0.05	0.07	0.05
	3	0.20	0.05	0.07	0.06	0.06	0.05	0.06	0.05
Average wave height (mm)	**1**	0.05	0.03	0.03	0.01	0.03	0.01	0.02	0.01
	2	0.02	0.01	0.01	0.01	0.01	0.01	0.01	0.00
	3	0.02	0.01	0.01	0.01	0.01	0.01	0.01	0.00
Max peak height (mm)	**1**	0.28	0.05	0.06	0.07	0.06	0.05	0.06	0.08
	2	0.14	0.03	0.03	0.04	0.04	0.03	0.03	0.04
	3	0.14	0.03	0.03	0.03	0.04	0.03	0.03	0.04
Max trough height (mm)	**1**	0.14	0.06	0.06	0.05	0.07	0.04	0.05	0.03
	2	0.07	0.03	0.04	0.02	0.03	0.03	0.03	0.02
	3	0.06	0.02	0.03	0.02	0.03	0.02	0.02	0.01
Peak spacing (mm)	**1**	8.25	6.81	6.26	5.17	6.49	5.99	6.12	0.93
	2	7.11	6.06	4.98	3.99	4.89	4.99	4.94	0.99
	3	5.57	4.59	4.51	3.44	4.85	4.55	4.36	0.63
Trough spacing (mm)	**1**	7.86	6.76	6.64	4.69	6.40	5.82	6.01	0.96
	2	6.94	5.91	5.23	3.72	4.81	4.63	4.80	1.02
	3	5.64	4.36	4.54	3.37	4.59	4.19	4.19	0.67

As seen in the defective specimens, the trend of decreasing waviness, and increasing planarity through plies 1-3 is replicated in the pristine specimens. Across all metrics, a trend of decreased waviness was observed when compared to the defective specimens. This aligns with expectations, since these laminates featured no significant artificial defects. What waviness is seen is minimally impactful on the general planarity of the specimens and tends to be located with a spacing which indicates its source as small “micro-gaps” between the tows.

The RMS waviness consistently ranges between 0.01-0.03 mm across specimens and plies. Peak-to-peak waviness is relatively small, spanning from 0.05 mm to 0.13 mm.

The average wave height is minimal, not exceeding 0.03 mm in most specimens. Additionally, there is a symmetry between peak heights and trough heights not seen in the defective specimens. Max peak heights across the pristine specimens ranges between 0.03 – 0.07 mm, while max trough height range from 0.02 – 0.07 mm.

Peak and trough spacing metrics provide insights into the manufacturing process. Both metrics range between 3.44 mm and 6.81 mm, with a median of 4.94 mm. Notably, the largest peak spacings align closely with individual tow widths. This suggests that the observed surface variations are inherent to the manufacturing process rather than indicative of significant defects.

4.3.4.3 Reworked

With the context of the dual benchmarks of the pristine and defective specimens, analysis of the reworked specimens was performed, in order to evaluate the process in terms of its effect on the waviness plies post-reworking. Table 4.17 shows the waviness metrics recorded for the reworked specimens.

Firstly, the trend seen in both the pristine and defective specimens of a decreasing waviness through plies 1-3 is replicated in the reworked specimens. This is result is consistent with the conclusion that this is caused by the layup and subsequent curing processes which are consistent between the specimen classes.

Across the reworked specimens' waviness metrics, a clear resemblance to the pristine specimens was seen. There are however clear variations in outcomes within the reworked specimens with a general trend across all metrics between specimens R1_1, R1_2 and R1_3, which feature reduced planarity and increased waviness, and specimens R2_1, R2_2 and R2_3 which more closely resemble pristine specimens and feature improved planarity and reduced waviness. This difference between specimens is most pronounced in the RMS waviness and peak-to-peak waviness values. Figure 4.33 and Figure 4.34, show B-scans for R2_1 and R1_2, representing the lower and upper bounds of out-of-plane waviness seen in the reworked specimens, respectively.

Table 4.17. Waviness metrics for all reworked specimens.

		Specimen							
Metric	**Ply**	**R1_1**	**R1_2**	**R1_3**	**R2_1**	**R2_2**	**R2_3**	**Median**	**Std Dev**
RMS waviness (mm)	**1**	0.03	0.09	0.04	0.02	0.02	0.03	0.03	0.02
	2	0.02	0.05	0.03	0.02	0.01	0.02	0.02	0.01
	3	0.02	0.04	0.02	0.02	0.01	0.01	0.02	0.01
Peak to peak waviness (mm)	**1**	0.16	0.35	0.17	0.11	0.09	0.13	0.15	0.09
	2	0.09	0.18	0.15	0.09	0.05	0.06	0.09	0.05
	3	0.07	0.16	0.12	0.10	0.04	0.06	0.08	0.04
Average wave height (mm)	**1**	0.02	0.05	0.03	0.01	0.02	0.02	0.02	0.01
	2	0.01	0.02	0.02	0.01	0.01	0.01	0.01	0.00
	3	0.01	0.02	0.01	0.00	0.01	0.01	0.01	0.01
Max peak height (mm)	**1**	0.08	0.23	0.08	0.05	0.05	0.07	0.08	0.06
	2	0.04	0.12	0.09	0.04	0.03	0.03	0.05	0.03
	3	0.03	0.11	0.07	0.04	0.02	0.03	0.04	0.03
Max trough height (mm)	**1**	0.08	0.12	0.09	0.05	0.04	0.05	0.07	0.03
	2	0.05	0.06	0.06	0.03	0.02	0.03	0.04	0.02
	3	0.04	0.05	0.05	0.03	0.02	0.02	0.03	0.01
Peak spacing (mm)	**1**	5.44	7.43	5.22	5.30	7.95	8.99	6.56	1.48
	2	5.18	6.01	5.67	3.82	5.73	7.43	5.53	1.07
	3	4.83	6.06	5.17	3.63	5.66	6.38	5.20	0.90
Trough spacing (mm)	**1**	5.65	7.11	5.37	5.38	7.75	9.73	6.66	1.58
	2	5.25	5.91	5.63	3.67	5.80	7.65	5.53	1.17
	3	4.40	5.50	5.12	3.48	5.78	6.49	5.03	0.97

In terms of RMS waviness, a range between 0.01 – 0.09 mm is observed, with a median for plies 1, 2 and 3 of 0.03, 0.02 and 0.02 mm respectively. Specimens R1_N all exhibit RMS waviness values on or above the median value, while R2_N specimens exhibit values on or below the medain. This variance is particularly interesting as it highlights variations in the result of the reworking activity, rather than the uniform restoration of near-pristine ply topology. The implications of this are discussed further in this chapter.

For peak-to-peak waviness a relatively large difference of was seen between the pristine and reworked specimens with the median value for reworked specimens. Median values for plies 1-3 for the pristine sample were 0.06, 0.07, and 0.11 mm respectively, whereas reworked specimen median values were 0.08, 0.09, and 0.15 mm respectively. A maximum value of 0.35 mm was recorded for R1_2. Given the nominal thickness of a tow is 0. 184 mm, a peak-to-peak waviness of 0.35 mm represents a large deviation from the plane of the ply and falls within the characteristics of defective laminates.

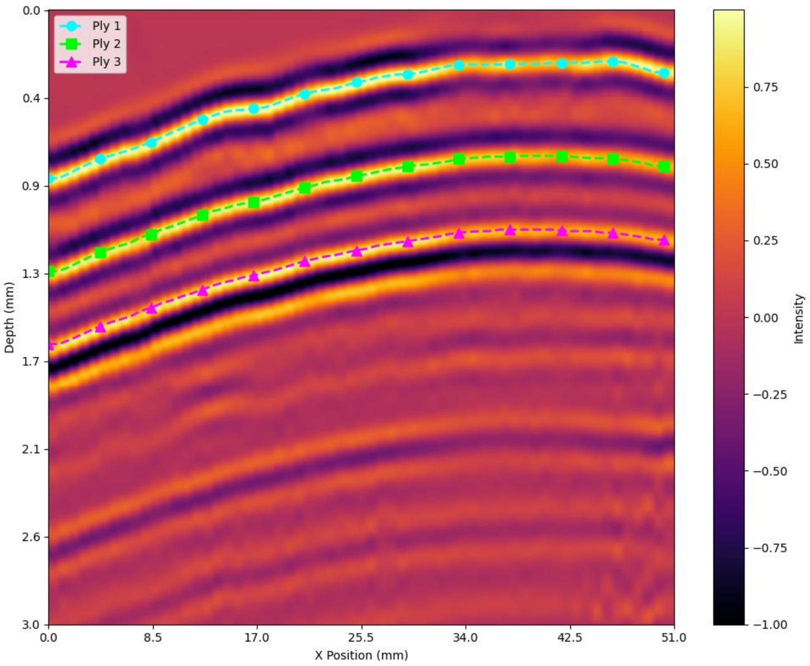

Figure 4.33. B-scans for reworked specimen R2_1 slice 49 with ply middle lines

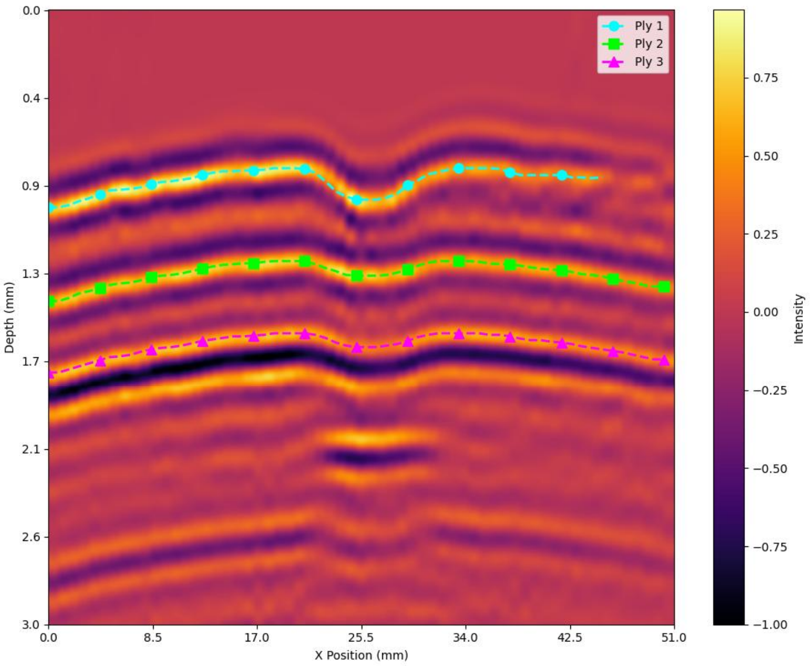

Figure 4.34. B-scans for reworked specimen R1_2 slice 26 with ply middle lines

Average wave height across the reworked specimens ranges from 0.00 to 0.05 with a median value across plies 1, 2 and 3 of 0.02, 0.01 and 0.01 mm respectively. These values are very consistent with the values for the pristine specimens.

Max wave height and max trough height are consistent with each other, showing even distribution of waviness in both directions, and again replicating the observed trend from the pristine samples. The values for max wave height range from 0.02 – 0.23 mm with median of 0.18, 0.11 and 0.09 for plies 1, 2, and 3 respectively. These are mirrored in max trough height by a range of 0.02 – 0.12 mm and medians of 0.13, 0.08 and 0.07 mm for plies 1, 2, and 3 respectively.

Peak and trough spacing mirror each other and align generally with the width of 1 tow. The median values across plies 1, 2, and 3 for peak spacing are 6.56, 5.53, and 5.20 mm respectively, and for trough spacing these values are 6.66, 5.53 and 5.03 mm respectively.

4.3.5 Discussion

The ultrasonic scanning method used in this study effectively captured the internal ply topography of composite laminates, revealing clear distinctions between pristine, reworked, and defective specimens. The ability of ultrasonic scanning to detect and quantify subtle defects, such as resin-rich zones and voids, highlights its value for quality control and structural optimisation in industries relying on composite materials. This sensitivity is critical for early defect detection, reducing the likelihood of premature failure and enhancing the reliability and safety of composite-based applications.

In this study, pristine specimens consistently exhibit the lowest waviness across all metrics, serving as a benchmark for evaluating both defective and reworked specimens. The waviness metrics for pristine specimens indicate superior laminate uniformity and structural integrity, validating their use as a standard for assessing defect severity and rework success.

Conversely, defective specimens display significantly higher waviness metrics, particularly in peak-to-peak waviness, max peak height, and trough spacing. These elevated values align with the expected structural disturbances caused by defects such as gaps and overlaps, which induce pronounced out-of-plane irregularities. Notably, the outermost ply (Ply 1) consistently shows the highest waviness metrics, further confirming that surface and near-surface layers are more susceptible to defect propagation. This fact is true of both other specimen classes, indicating that even small irregularities in ply topology, such as the micro gaps between tows in the pristine specimens, propagate through the laminate and cause waviness in the surface or near-surface plies.

The reworked specimens exhibit a wide range of waviness metrics, highlighting both the potential and limitations of rework processes. While rework generally results in waviness values closer to those of pristine laminates, significant variability remains, especially in the outermost ply. For example, the median peak-to-peak waviness for reworked specimens (Median Reworked = 0.15mm) shows notable improvement compared to defective specimens (Median Defective = 0.33 mm), but it still exceeds that of pristine specimens (Median Pristine = 0.11 mm). This trend indicates that the rework process is successful in mitigating some of the out-of-plane waviness seen in the defective specimens, however, not entirely to the extent of restoring the laminates to a near-pristine state. Figure 4.35 shows a side-by-side comparison of the specimen classes in terms of RMS waviness and peak-to-peak waviness.

Inner plies (e.g., Ply 2 and Ply 3) in reworked specimens demonstrate the most substantial improvements, with waviness metrics approaching pristine benchmarks. This indicates that disturbances to the topology of the inner plies caused by rework are suppressed by later plies consolidating on top of the internal plies, and at the outer layers the absence of this leads to the observation of residual waviness

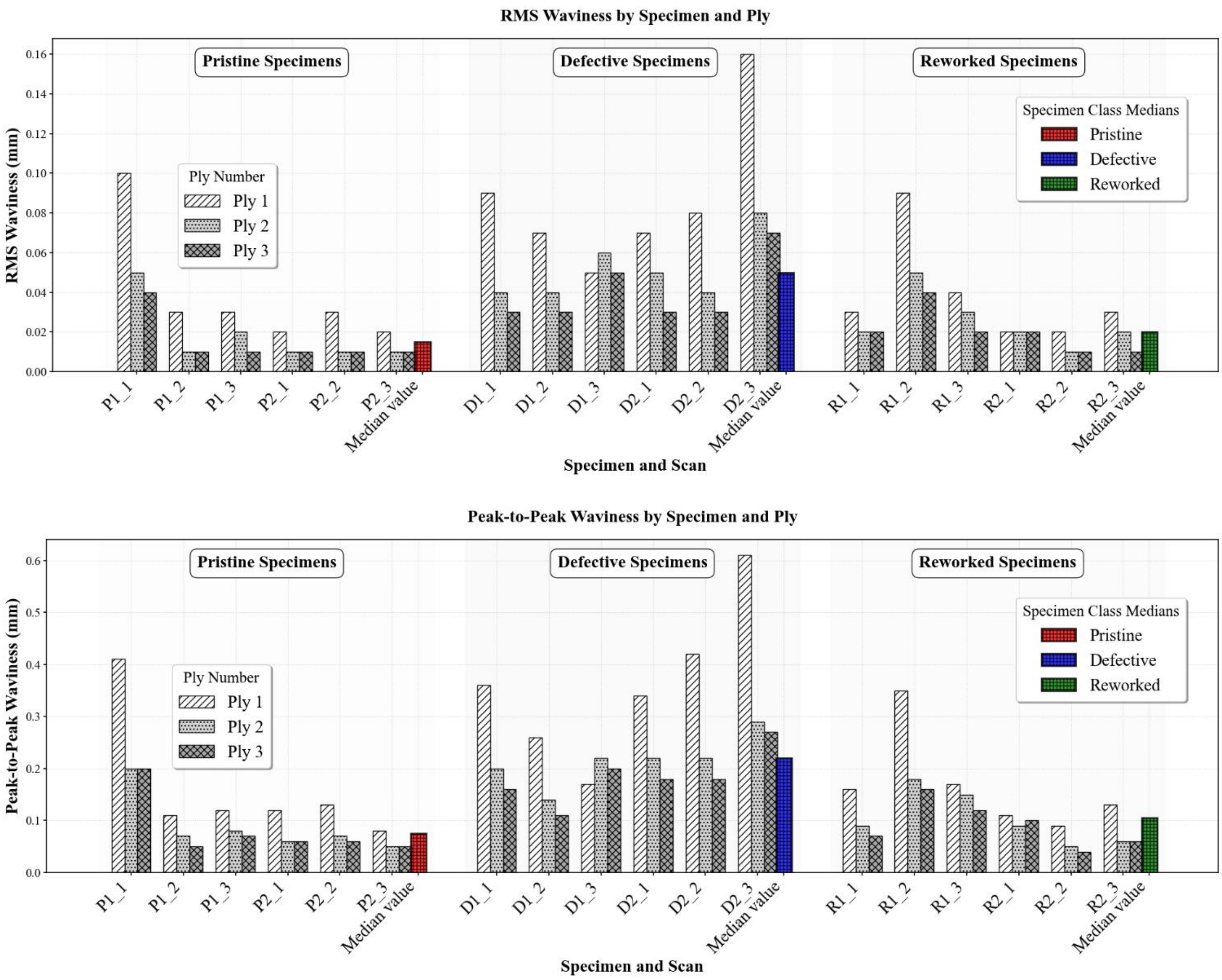

Figure 4.35. Median RMS waviness (top) and peak-to-peak waviness (bottom) across all scans by specimens' class, split by ply number within specimen. Median values for each specimen class are shown right of each classes data (coloured)

The variability among reworked specimens demonstrates the need for process optimisation. Metrics such as trough spacing and peak spacing reveal higher consistency in pristine specimens compared to reworked ones, where values remain scattered. This variability indicates that while rework enhances the laminate structure, inconsistencies in the process can leave residual defects, particularly in regions directly exposed to manufacturing stresses. Additionally, this variability in results of reworking highlights the need for further research into rework techniques to achieve uniform improvements across all plies, bringing the quality of reworked laminates closer to pristine standards. The findings emphasise the importance of quantitative metrics like waviness metrics for establishing acceptance criteria for defect reworking in composite manufacturing. By defining thresholds for acceptable waviness values, manufacturers can implement consistent quality control standards, ensuring the reliability of laminates used in critical applications.

The below best practices are given for the reworking of defects following this study:

- Tool dominated reworking resulted in the least damage to the underlying tows, removed tow and gapped tow.
- Both in-plane and out-of-plane peel angles should be kept as close to 0° with respect to the fibre angle of the current ply.
- The application of additional heat is essential in minimising the damage to surrounding material, and in ensuring even tow removal with minimal tow breakage.
- Where defect sizes span the entire width of one tow, rework can be performed with less damage than is the case for smaller defects.

These best practices, derived from experimental observations, provide practical recommendations for technicians and engineers involved in gap and overlap defect reworking. Implementing these best practices can lead to improved efficiency, reduced damage, and enhanced overall quality in the AFP manufacturing process. A more comprehensive body of research concerning the rework process can be developed as the best practices presented by Sacco et al. [31] for addressing wrinkle-type defects are integrated.

4.3.6 Limitations

It is critical to acknowledge the limitations of this study for its generalisation. Firstly, the study focused on specimens that underwent manual rework procedures. This approach may not fully represent the challenges and variability encountered in industrial-scale AFP processes, limiting the generalisability of the results to larger-scale production environments. Secondly, due to the Benchtop-AFP setup used in this study, the specimen size was limited. A larger specimen size encompassing a wider range of defect types and severities could provide more comprehensive insights and improve the statistical significance of the findings. Next, the ultrasonic scanning method was designed for larger thickness parts (> 10 mm), which may have resulted in a loss of resolution when applied to the relatively thin composite laminates (1.25 mm) used in this study. Higher resolution imaging techniques could potentially reveal finer details and defect characteristics that were not captured in the current analysis.

Additionally, manual rework processes are inherently variable, as the defect characteristics and the skill level of the operator can introduce inconsistencies from one rework to another. This variability may contribute to the observed differences in the waviness metrics among the specimens, potentially limiting the generalisability of the results to more controlled and automated rework processes.

Finally, the results in this study are comprehensive in understanding the process of reworking gap and overlap defects for the material type used. Different thermoset prepregs may have radically different tackiness levels, and hence the same recommendations for the use of RM1 may not apply. Further testing should establish this basis.

4.4 Conclusions

This chapter examines the rework activity and studies a range of mechanistically defined reworking methods. The methods were evaluated based on the extent of damage imparted on the surrounding material during the reworking process. Empirical analysis was undertaken to assess the effects of the tension and tool components, and the resultant variance in geometry from the emergent peel front. The need for additional heat during the peeling process to minimise negative effects on underlying tows underscores the significance of temperature control in achieving successful rework outcomes. Furthermore, the effect of both in-plane and out-of-plane peel angles in the removal of defective tows with minimal damage highlights the importance of careful mechanical process control. These insights contribute to a deeper understanding of the complexities involved in defect reworking and pave the way for further research and development.

Additional developments in this study, alongside conclusions drawn by Sacco et al., [31], on wrinkle defect rework, provide valuable demystification of this activity and can lead to further novel research. Such research would yield useful insight into, firstly, improvement in reworking techniques, and secondly, opportunities for automation. Automation would be valuable both in part, to aid manual reworking, and in full to eliminate this task and reduce the manufacturing time required.

In conclusion, this research offers insights and practical recommendations for industry professionals and contributes to the demystification of the rework activity in academia. The best practices presented offer a significant step towards a full set of guidelines and standardisation of the rework activity. This chapter forms the basis for the reworking methods used throughout this Thesis. In the next chapter, the effect of the reworking process is examined, through non-destructive and destructive methods and in terms of laminate topology and mechanical performance.

The ultrasonic scanning method employed in section 4.3 of this chapter has demonstrated its effectiveness in detecting and quantifying defects in composite laminates. By extracting the internal ply topography and calculating a quantitative waviness metrics, this approach enabled the identification and out-of-plane waviness as a result of embedded gap/overlap defects. The results clearly distinguished pristine specimens from defective ones, with the latter exhibiting higher waviness metrics and pronounced undulations in the internal ply structure. The observation of the waviness metrics for pristine and defective specimens served as effective opposing benchmarks with which to evaluate the effect the process of reworking defects on the out-of-plane waviness. Study of specimens of this class revealed considerable improvements on the defective benchmark after reworking, however, a measurable residual out-of-plane waviness in the reworked specimens remained, indicating the presence of residual defects even after reworking has been performed. Thus informed, it can be said that reworking of defects under current practices can improve but not necessarily fully mitigate the effect of defects and return a laminate to pristine-like quality. Additionally, the variation in results within the rework specimens highlight the inherent variability of the current practice and underlines the need for process improvement and optimisation.

The ability to quantify defect levels through the waviness coefficient offers valuable insights for quality control and performance optimisation in the composite industry. By establishing acceptance criteria based on this metric, manufacturers can implement objective and consistent quality standards to the reworking process. Furthermore, the detailed mapping of internal ply topography opens opportunities for advanced computational modelling and simulation, allowing researchers and engineers to incorporate actual ply geometry and defect distributions into numerical models for more accurate predictions of material behaviour under various loading conditions.

Finally, the Benchtop-AFP approach used in this work demonstrated effective manufacture of test specimens, enabling examination of the effect of some of the conventional AFP process at a fraction of the cost. This approach yields some promise in ensuring that AFP manufacturing research may be advanced in a more democratic fashion as it relates to the capital access.

Chapter 5. Analysis of the Effect of Defect Rework

The previous chapter outlined best practices based on a cosmetic pass/fail basis and the extent of damage to surrounding material, and in terms of the internal out-of-plane waviness in the plies and shown by the Ultrasonic NDT. A discernible difference in waviness indicated that, first, a discrepancy between the goals and outcomes of reworking. The primary goal of reworking is to achieve near-pristine quality by modifying defective plies or tows to mitigate scrap waste [27]. However, if measurable differences in quality are observed between reworked specimens and pristine ones, the effectiveness of reworking techniques comes into question. Moreover, such differences in waviness may also point to mechanical performance knockdowns that are often overlooked in quality analyses, which typically assume that reworked defects are as good as pristine. This chapter provides a detailed investigation of the impact of defect rework on the quality of the part.

To further evaluate the effect of reworking on part quality, flexural strength testing of coupons from each of the three classes, following the ISO 14125 method, provides a quantitative assessment of how reworking influences composite laminate performance under constrained loading conditions. Variations both between and within classes not only reflect the consistency of the reworking process but also reveal the broader structural consequences of defect remediation.

Finally, subsequent analysis was performed on laminates using the same dual-benchmark approach. Firstly, Scanning Electron Microscopy (SEM) was conducted in order to examine the microstructure of cross sections of cured laminates. This enabled a comparison between the macro- and microstructure of pristine and defective laminates, and a comparison of both against reworked laminates. This analysis serves as a further basis for understanding the impact of reworking.

The findings presented in this chapter highlight the need to refine and optimise reworking practices, emphasising their significance not only from an economic standpoint but also from a structural performance perspective.

5.1 Mechanical Testing Analysis

With the above non-destructive analysis in mind, it remains to study the implications of reworking on the mechanical performance parts. It has been extensively reported in Chapter 2 the extent to which gap and overlap defects result in knockdowns in mechanical performance, however no study has been performed to confirm that reworking these defects necessarily restores the mechanical performance of the laminates to near-pristine quality. This section shall address this through investigation of the response of pristine, defective and reworked laminate manufactured using conventional AFP under ISO 14215 bending test conditions.

5.1.1 Experimental Setup

To investigate the quality implications of reworking, coupons were generated in one of three classes, these were 1) pristine, where no defects were included; 2) defective, where artificial Gap-Overlap defects were included; and 3) reworked, where artificial defects were initially included, then reworked in accordance with the best practices outlined in Chapter 4.

The test coupons were manufactured using an AFP cell consisting of a 6-axis Kuka KR120-r3100 industrial robot, bespoke Accudyne AcuFP1000+ AFP head [71] with integrated material feeding and compaction set at 100 mm/s and 150 N respectively, heated tooling plate set at 55°C. The material used was Hexcel® M91/34%/UD194/T700GC 6.35 mm width prepreg tows [180].

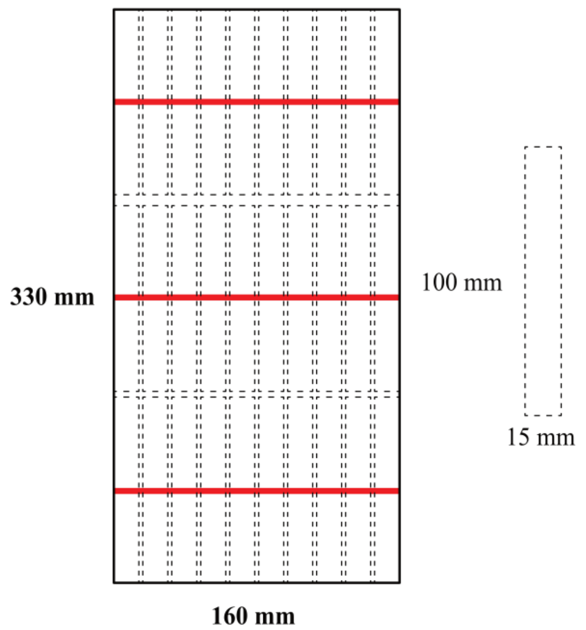

Figure 5.1. Laminate diagram (left) showing defect locations (red) and specimen locations (dashed); and specimen dimensions (right)

Several 330 x 160 mm laminates were manufactured with a $[0/90]_{3s}$ structure. Figure 5.1 shows the laminate configuration for the bending test specimens. Each zone (1-3) contains one embedded defect running horizontally through the laminate in the 90° plies. Each zone yielded ten test specimens. In each case where defects were included in the initial layup, the defects were a 2 mm gap defect in a single tow, followed by an overlap in the subsequent tow, which is deposited in alignment with the baseline patterns and hence overlapped by the gapped tow (Figure 5.2). The panels were cured as per manufacturer's instructions, before being cut into coupon sizes as specified in the ISO 14125 standard documentation, shown in Figure 5.1 (right).

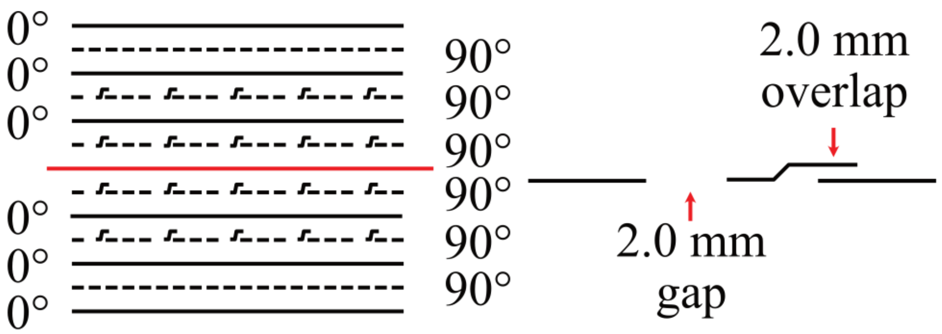

Figure 5.2. Ply-level diagram with gap and overlap defects (left) and diagram of defect (right)

In the case of the reworked coupons, each ply was deposited, then the defective tows were removed followed by the depositing of new properly aligned tows in the locations of the now removed defective tows. Reworking was performed using hand picking tools as specified in the literature [31], [174], [181]. The best practice for the reworking process described in Chapter 4 was followed. Care was taken to reduce disturbance of neighbouring tows and the avoid fibre breakage during reworking which would leave behind fibres upon which subsequent tows would be deposited. Figure 5.3 shows a still of video recordings of the reworking process including the first acquisition of the end of the tows using a pick to separate the defective tow from the substrate, then the removal of the tow by applying tension through the tow length and using the thinnest part of the hand-tool to separate the tow from the substrate along its length.

5.1.2 ISO 14125 Methods

Results from the ISO 14125 3-point bending tests were as follows. The tests were carried out on a Zwick Z250 testing machine, using the test speed of 5 mm/min as specified in the standard documentation. The test machines recorded the load in Newtons (N), distance travelled by the bending former (mm), deformation as a percentage (%), for each test time step. The flexural stress and strain in the coupon at each stage of the test can be calculated using the following:

The flexural stress at a given load is given by:

$$\sigma_f = \frac{3FL}{2bh^3} \tag{5.1}$$

Where F is the force at a given point in newtons (N), L is the gauge length in mm, b is the specimen width in mm, and h is the specimen thickness in mm.

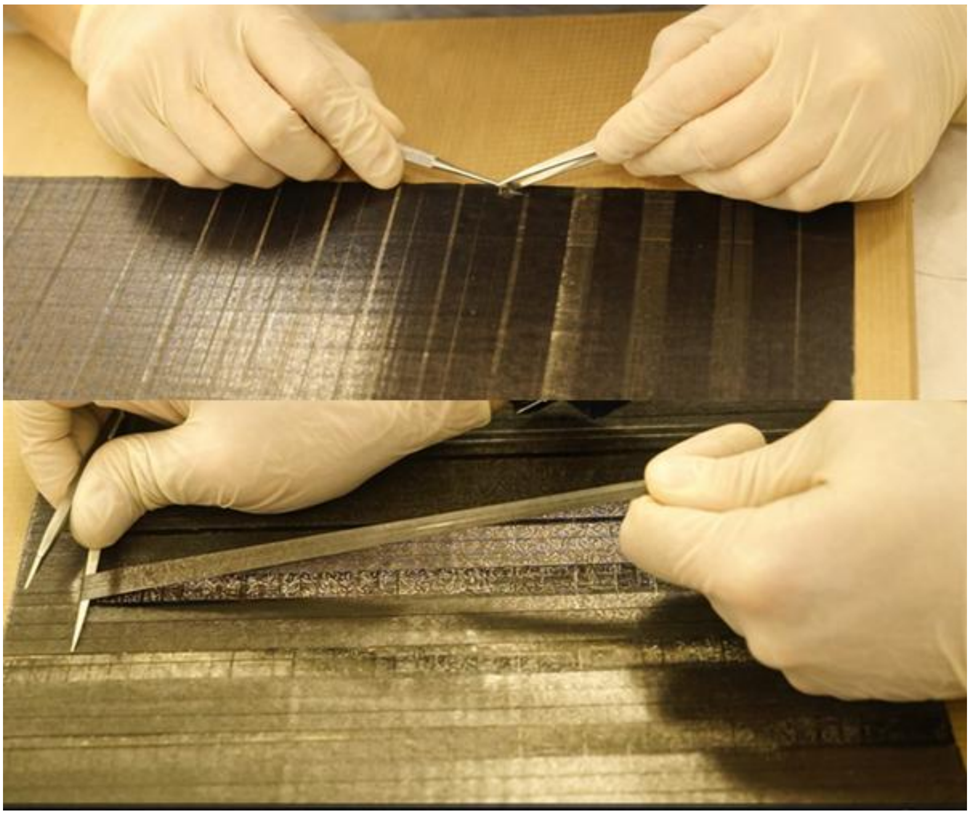

Figure 5.3. Video stills from reworking showing; initial acquisition of end tab of defective tow (top) and tool dominated reworking through length of tow (bottom)

The flexural strain on the outer surface at a given load is given by:

$$\varepsilon_f = \frac{6sh}{L^2} \tag{5.2}$$

Where s is the deflection of the centreline at the load point in mm.

The flexural modulus for a specimen was calculated between the beam mid-point deflection points s' and s'' derived from:

$$s' = \frac{\varepsilon_f{}' L^2}{6\,h} \quad and \quad s'' = \frac{\varepsilon_f'' L^2}{6\,h} \qquad (5.3) \text{ and } (5.4)$$

Where $\varepsilon_f{}'$ and $\varepsilon_f{}''$ are the given strain values at 0.0005 and 0.0025 deformation respectively, for material of this type as specified in the standard documentation.

The flexural modulus, E_f, is calculated, as per ISO 14125, using:

$$E_f = \frac{L^3}{4bh}\left(\frac{\Delta F}{\Delta s}\right) \tag{5.5}$$

Where ΔF is the change in force recorded at s' and s'', and Δs is the difference in deflection between the two points.

For comparison between the specimen types both the stress and strain at the break point were recorded, and the stress at standard deflection, defined as:

$$\sigma_s = 1.5 \times h \tag{5.6}$$

This allows for comparison between all specimens including those which did not break as well as the analysis of the break point stress and strains.

5.1.3 Testing Results

Testing of 66 specimens (15 pristine, 17 defective, 34 reworked) revealed distinct performance characteristics across the three specimen types. Table 5.1 shows the recorded results from the testing, Values are presented as median (interquartile range, IQR), where IQR = Q3 − Q1. Figure 5.5 and Figure 5.6 show the median flexural properties determined according to ISO 14125. Bars represent median values, and error bars indicate the interquartile range (Q1–Q3). Break-related values (σ_{fB}, ε_B) are based on failed specimens only. 0Appendix 5A ISO 14125 full results contains the results for every specimen tested.

The defective specimens show a pronounced reduction in flexural modulus, 32.00 % below pristine from 67.8 to 46.1 GPa, alongside a more moderate reduction in strength 20.40 % from 1196 to 952 MPa. These disproportionate knockdowns highlight that stiffness is more sensitive to defects than relative strength. The modulus of the specimens is governed by the load transfer capability of the fibres and is highly affected by the out-of-plane waviness of the fibres. From the SEM micrographs, extremely high degrees of waviness are seen in the defective specimens. In bending, fracture and catastrophic failure is predominantly governed by management of peak stress concentrations in the outermost

Table 5.1. Flexural properties of specimen types

Property/Specimen	Pristine	Defective	Reworked
Flexural Modulus, E_f, (GPa)	67.75 (4.71)	46.11 (10.88)	62.15 (7.33)
Stress at standard deflection, σ_{fC}, (MPa)	512.00 (13.88)	420.95 (32.09)	478.89 (23.94)
Stress at break, σ_{fB}, (MPa)	1196.83 (108.72)	952.70 (133.21)	1114.36 (362.07)
Strain at break, ε_B, (%)	1.97 (0.22)	2.23 (0.17)	1.97 (0.58)

plies. Since in these samples the fibres in the outermost plies are continuous through the length of the specimen, continuous load transfer is expected. Sub-surface defects however disrupt the fibre alignment in the outermost ply and reduce the efficiency of this load transfer. The stress-strain curves in Figure 5.4 reinforce this, the noticeably shallower slope of the median defective curve confirms that the defect degrades the global stiffness of the specimens rather than resulting in a locally weaker part at the defect site and defect-induced fracture initiation.

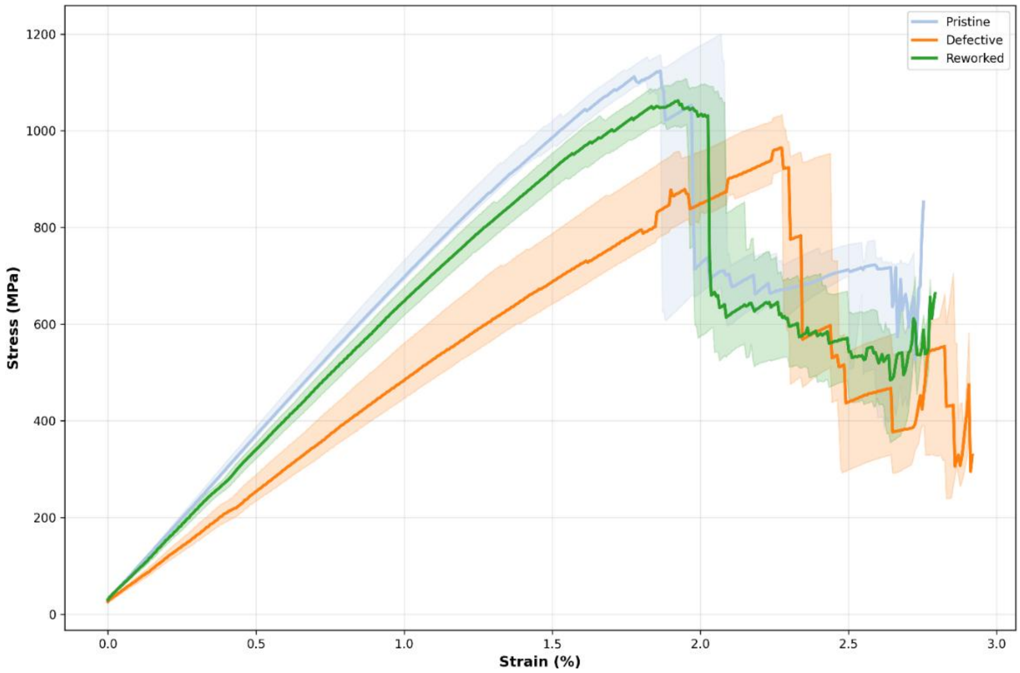

Figure 5.4. Median stress-strain curves for all samples, grouped by sample type showing 25^{th}-75^{th} percentile envelopes (shaded)

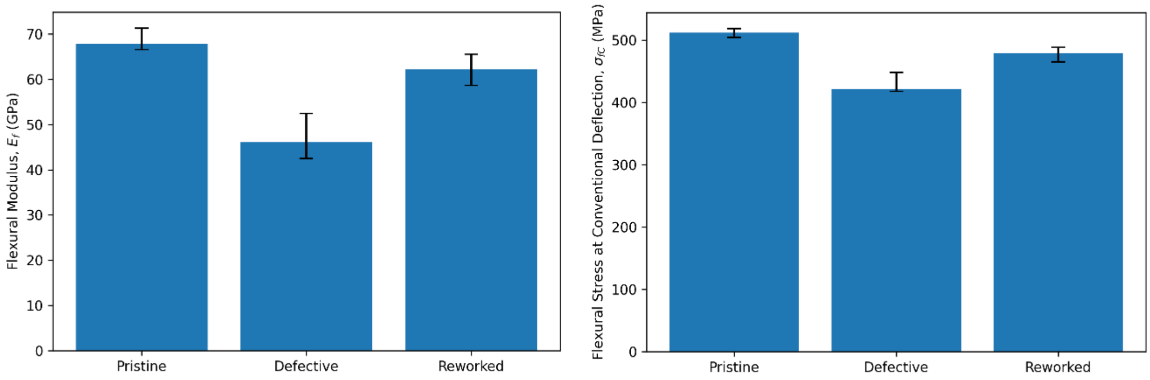

Figure 5.5. Median Flexural Modulus (left) and Flexural stress at standard deflection (right) by specimen type.

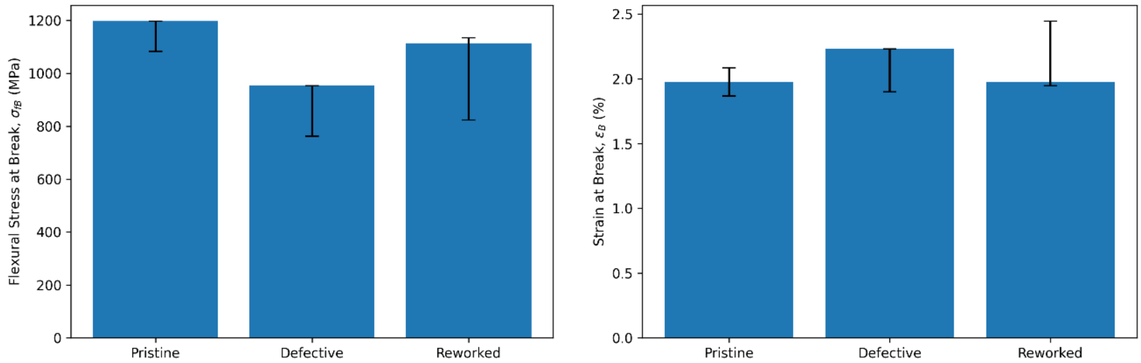

Figure 5.6. Median Flexural stress (left) and strain (right) at break by specimen type

The difference in strain at break between the defective and pristine specimens (2.23 % vs 1.97 %) is informative. The defects result in a more compliant material where the reaching of peak stresses is delayed, compared to pristine samples. Reworked samples have a marginally lower Young's modulus than the pristine samples, and as such reach peak stresses at similar strain levels.

The reworked specimens recover a substantial portion of the lost properties. Modulus recovery is partial, but significant. The reworked E_f of 62.15 GPa represent 92 % of the pristine values, recovering approximately two-thirds of the modulus lost to the defect. This partial recovery suggest that the rework process successfully restores continuity of the load path but does not fully replicate the original fibre architecture. Residual misalignment, as seen in the SEM results would be consistent with this 8.33 % stiffness deficit. Even well performed rework may leave heterogeneity at ply-ply interfaces which impacts the modulus through reduced continuous load transfer through the entirety of the specimen.

Strength recovery is similarly partial. The median stress at break, σ_{f_B}, of 1114 MPa is 93.14 % of pristine, a substantial recovery. Critically, the reworked samples recover more of their strength relative to the modulus. Since the critical failure region is located in the outermost ply and is not directly affected by rework, the recovery in strength is more pronounced than the recovery in stiffness. Even if the internal fibre architecture is not perfectly pristine, strength restoration is more effective because it depends less on the global elastic architecture of the laminate than the modulus does.

Table 5.2 describes the failure modes as defined in the ISO 14125 standard, broken down by sample types. The specimens which experienced the primary tensile fracture of the outermost layer failure mode also exhibited secondary compressive failure on the topside. Figure 5.7 - Figure 5.12 show microscopic images of failed specimens. It is notable that in the defective specimens the location of both the compressive and tensile fracture does not align with the tooling contact point. Instead, it is centred over the local thickness decrease in the laminate aligned with the location of the gap. In both the pristine and reworked specimens, the failure location was aligned with the tooling contact point.

Table 5.2. Failure modes by specimen type

Failure mode/Specimen	Pristine	Defective	Reworked
Tensile fracture of fibre	0	0	0
Tensile fracture of outermost layer	5	16	17
Compressive Failure	10	12	15
Tensile fracture (including interlaminar shear)	0	0	2
Compressive fracture (including interlaminar shear)	0	0	0
Interlaminar shear fracture	0	0	0

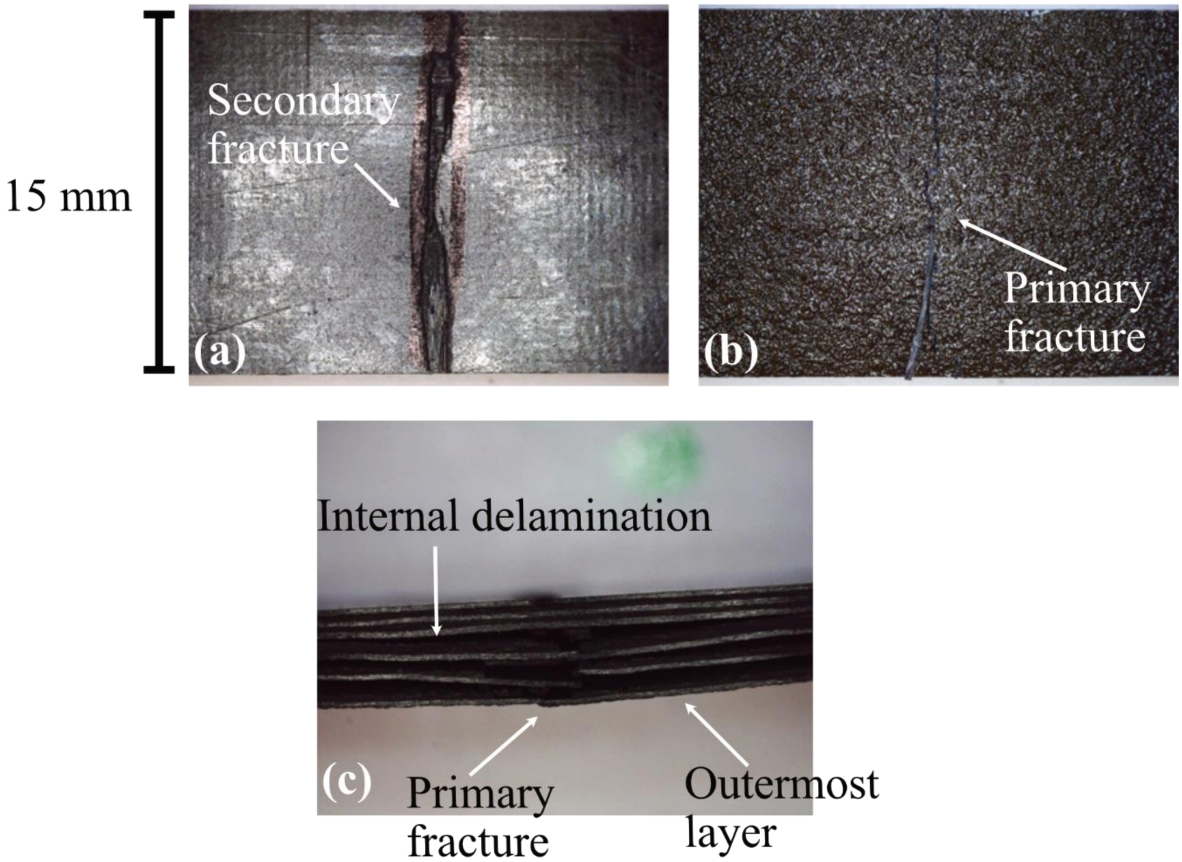

Figure 5.7. Pristine samples with Mode 2 failure: tensile failure in outermost layer

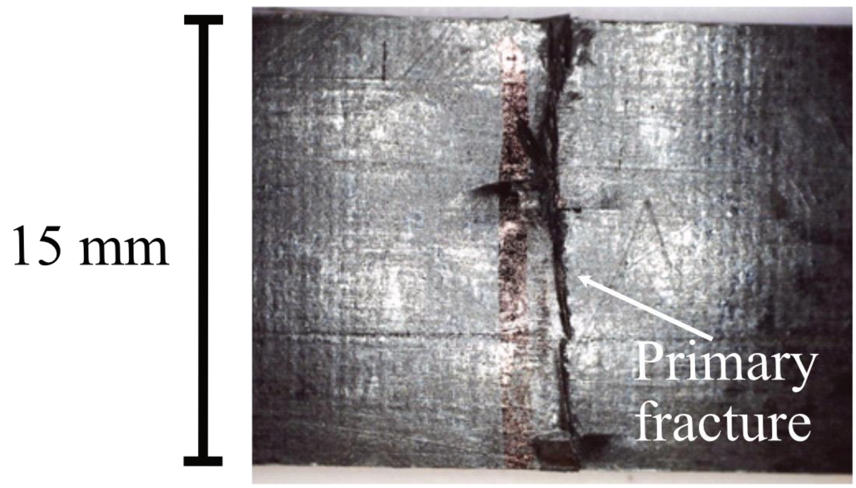

Figure 5.8. Pristine samples with Mode 3 failure: compressive failure

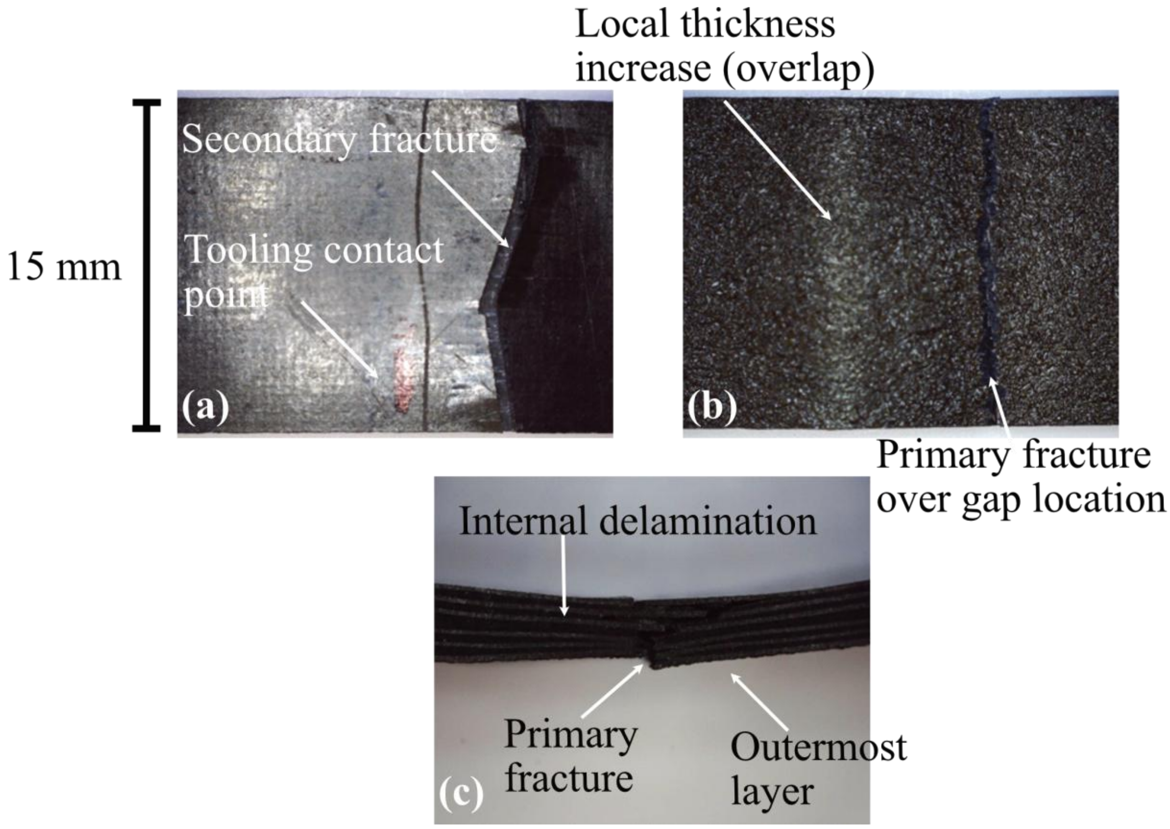

Figure 5.9. Defective samples with Mode 2 failure: tensile failure in outermost layer.

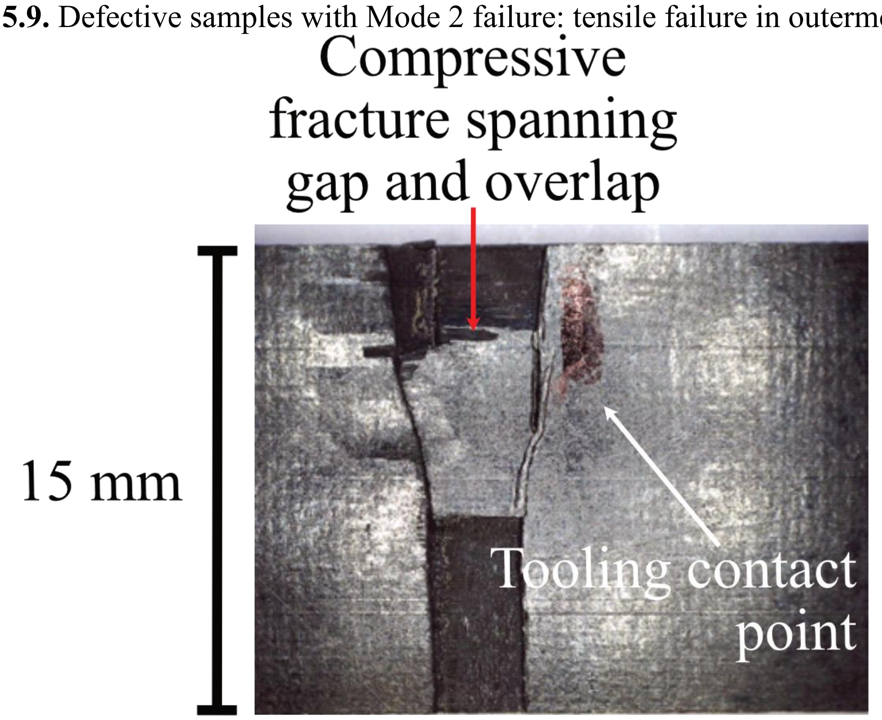

Figure 5.10. Defective samples with Mode 3 failure: compressive failure

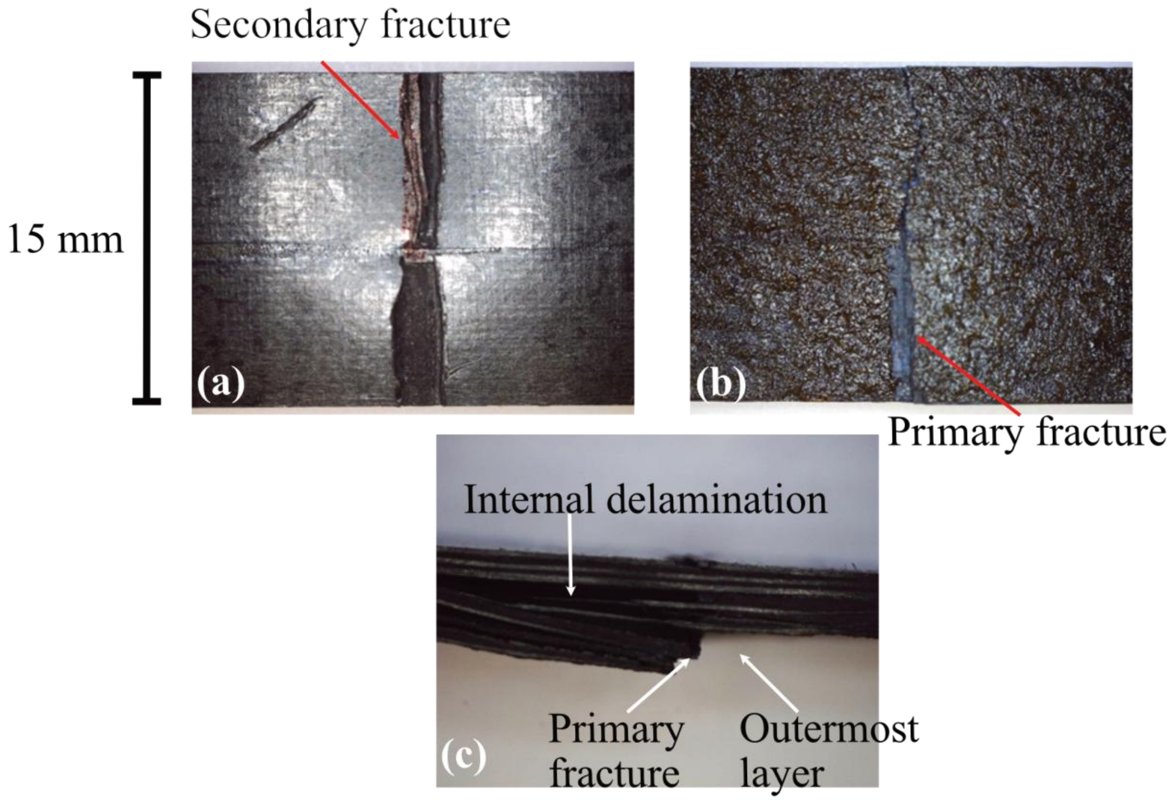

Figure 5.11. Reworked samples with Mode 2 failure: tensile failure in outermost layer.

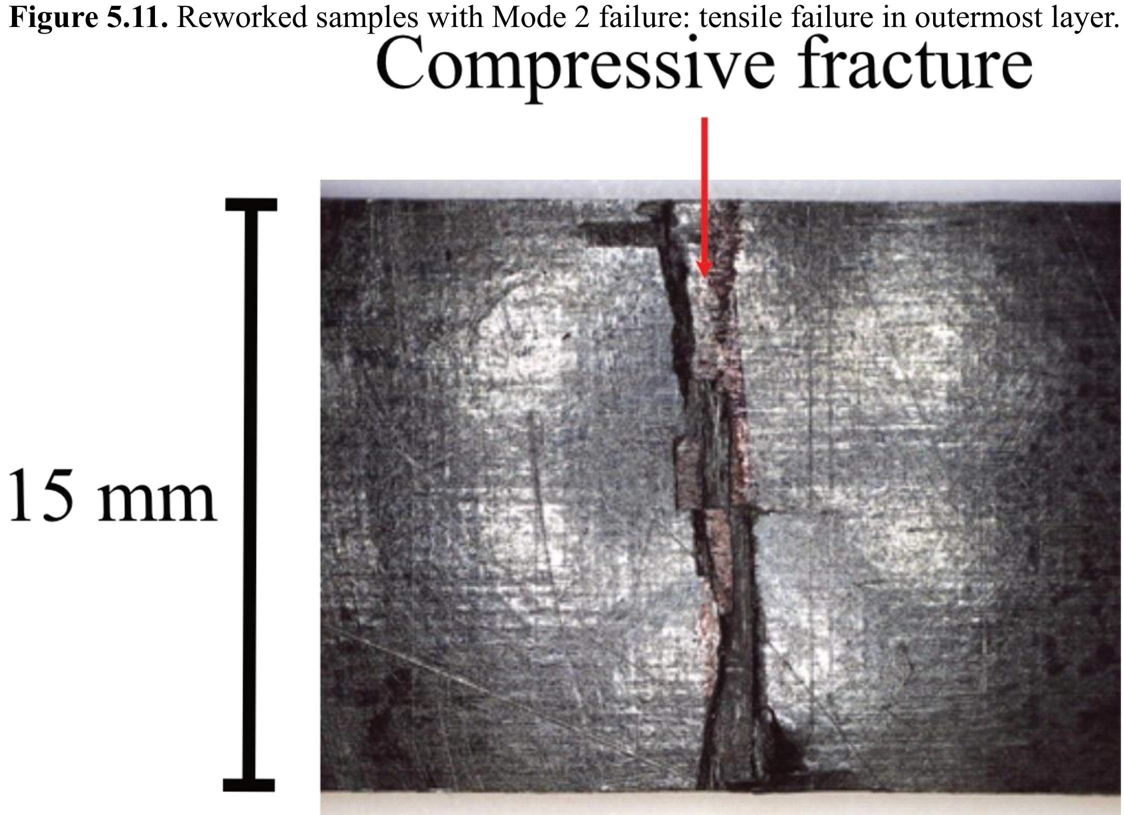

Figure 5.12. Reworked samples with Mode 3 failure: compressive failure

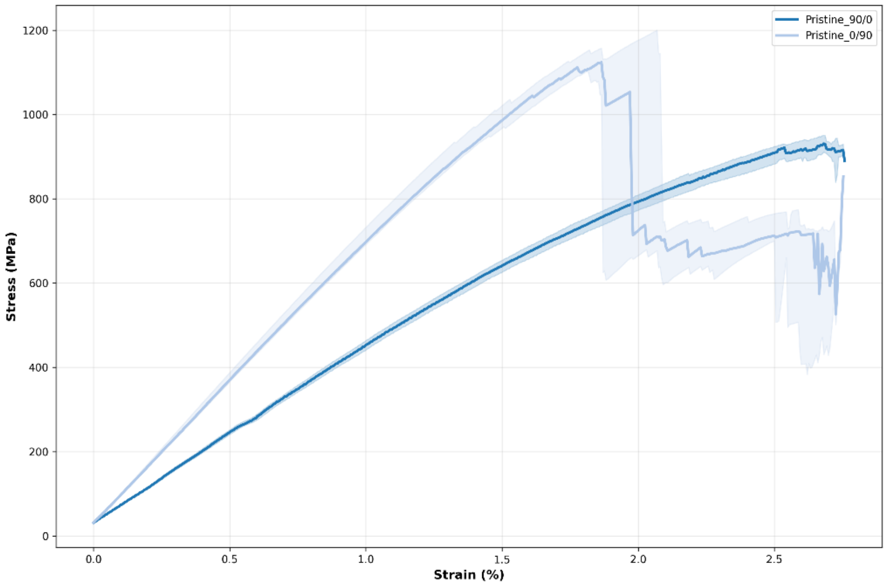

Figure 5.13. Median stress-strain curves for two pristine specimen types, grouped by sample type showing 25th-75th percentile envelopes (shaded)

Additional insight is provided by the behaviour of pristine specimens tested after being cut at 90° to the original orientation, effectively changing the stacking sequence from [0/90]3s to [90/0]3s relative to the bending axis. The results for these specimens are shown in Table 5.3 and Figure 5.13 below. These specimens show a markedly lower flexural modulus (41.8 GPa) and reduced strength (934.35 MPa), together with an increased strain at break (2.69 %). This behaviour reflects the strong dependence of flexural stiffness on the orientation of the outer plies relative to the loading direction. When the outer plies are aligned with the bending axis, the high longitudinal modulus of the fibres dominates the response, conversely, when they are oriented transverse to the loading direction, bending stiffness is governed more by the lower transverse and matrix-dominated properties, resulting in a substantial reduction in effective modulus. The accompanying increase in strain at break indicates more progressive damage accumulation.

Table 5.3. Flexural properties by pristine sample type

Property/Specimen	Pristine $[0/90]_{3s}$	Pristine $[90/0]_{3s}$
Flexural Modulus, E_f, (GPa)	67.75 (4.71)	41.84 (2.22)
Stress at standard deflection, σ_{fC}, (MPa)	512.00 (13.88)	336.44 (12.23)
Stress at break, σ_{fB}, (MPa)	1196.83 (108.72)	934.35 (76.58)

Strain at break, ε_B, (%)	1.97 (0.22)	2.69 (0.13)

5.2 Microstructure analysis

In order to further understand the effect of reworking on the resultant laminates, SEM was used to obtain micrographs of cross sections of laminates of the three classes: pristine, defective and reworked. The sample specimens were cut from the same $[0/90]_{3s}$ laminates manufactured using identical experimental setup to the section above. The cross-sections varied in width; a scale has been included in the micrographs images to allow for comparison across the specimens. In the case of defective and reworked specimens, the defect or rework site are included in the centre of the cross sections. The section below displays and describes these micrographs.

The SEM results for specimen type each specimen type are in Figure 5.14 - Figure 5.19 below. Multiple micrographs of reworked specimens are shown to highlight the consistency in microstructure across the specimen class.

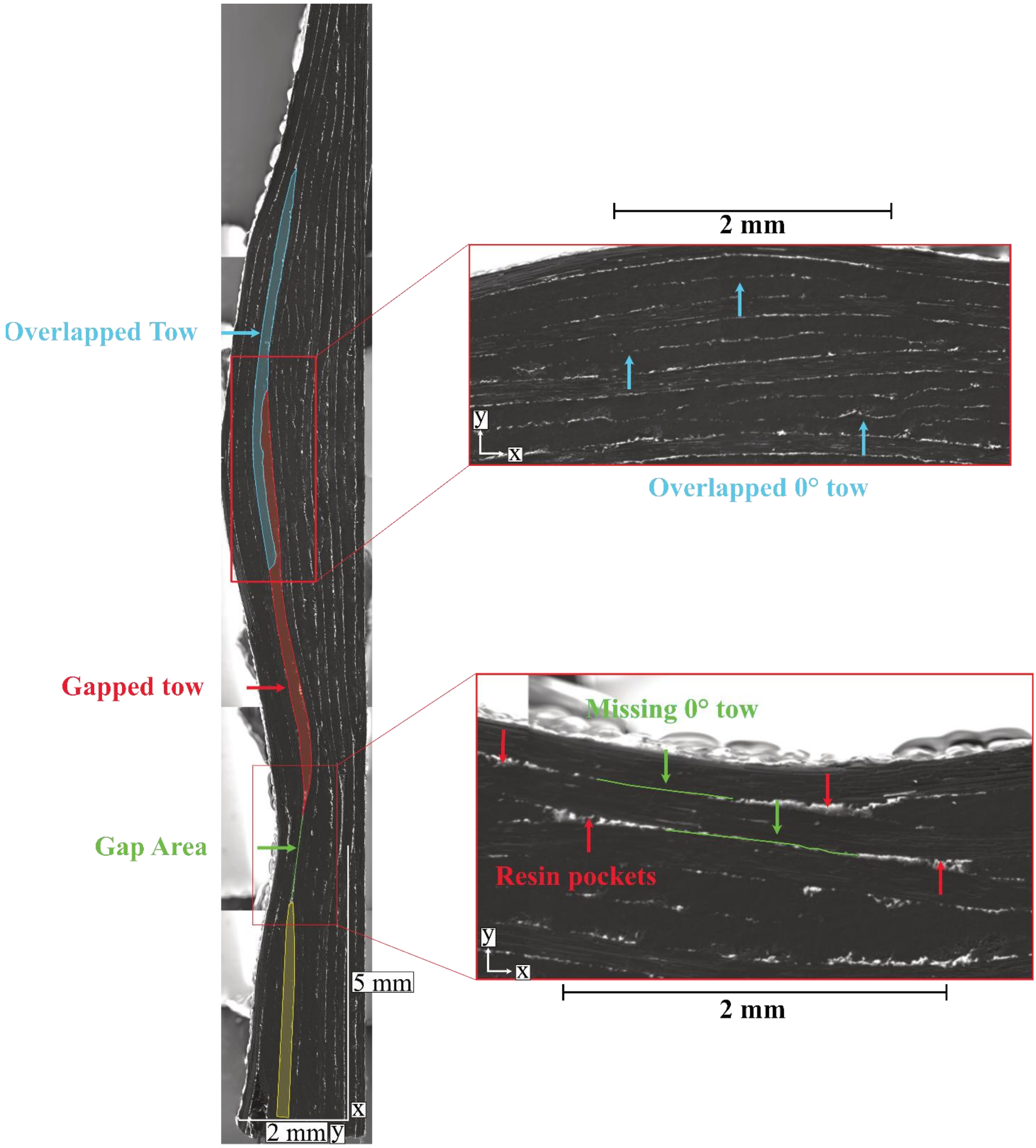

Figure 5.14. Defective specimen SEM (magnification: x45, HV: 15.00kV, dwell: 45μs)

The local thickness changes can be clearly seen in the defective specimen SEM, aligning with the region of the gap (local thickness decrease) and overlap (local thickness increase) regions. The combined effect of this is a pronounced out of plane waviness in these regions at both the macro-scale in terms of the thickness distribution across the entire specimens, and at the micro-scale in term of the individual plies.

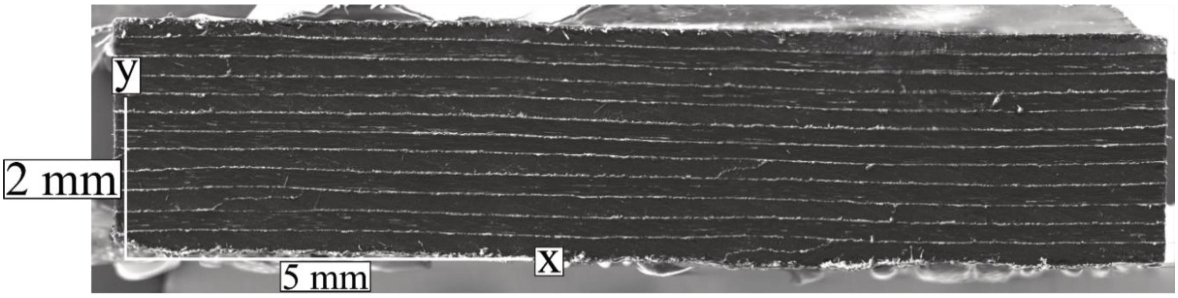

Figure 5.15. Pristine Specimen SEM (magnification: x45, HV: 15.00kV, dwell: 45µs)

In contrast to the defective specimens a relatively uniform thickness distribution is seen across the pristine specimen with limited waviness at either the micro or macro scales. Additionally, clear alignment and separation of the individual plies can be seen.

For the reworked specimens, a more complex pattern can be seen at the formally defective sites where the rework has taken place. A local thickness increase is observed, though these are not at the scale of those seen in the defective specimens. This increase in the thickness of the plies at these sites is likely caused by additional resin or fibres left behind by the defective tows which were removed during the reworking process. Additionally, the clear alignment and separation of consecutive plies seen in the pristine specimens is not replicated in the reworked specimens. Instead, the individual plies appear, in particular in the internal two consecutive 0° plies, disturbance of the tows inside the rework area is observed. This appears to be a dislocation of the plies in the through thickness direction where the rework took place.

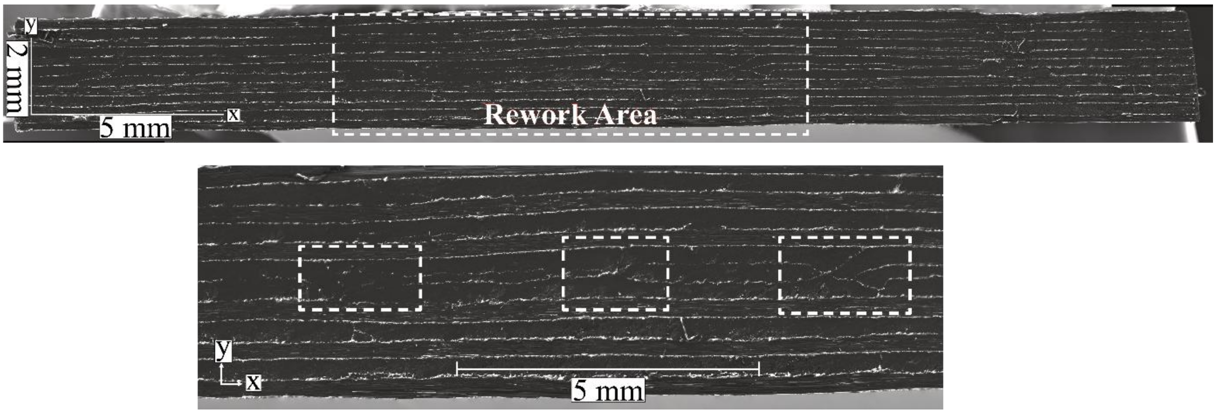

Figure 5.16. 2-Reworked SEM (magnification: x45, HV: 15.00kV, dwell: 45μs) full view (top) and magnified view of reworked area (bottom) showing areas of distortion of tows over ply-ply boundaries caused by rework

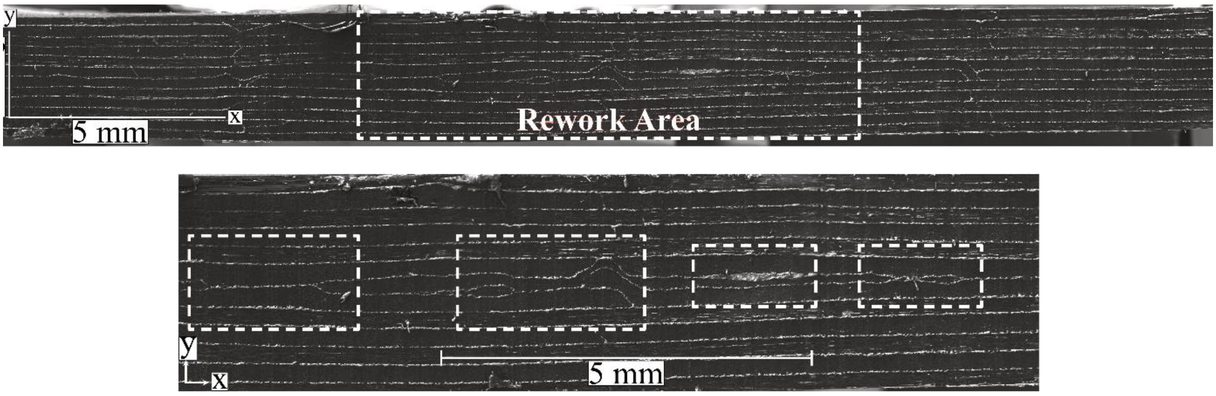

Figure 5.17. 5-Reworked SEM (magnification: x50, HV: 15.00kV, dwell: 45μs) full view (top) and magnified view of reworked area (bottom) showing areas of distortion of tows over ply-ply boundaries caused by rework

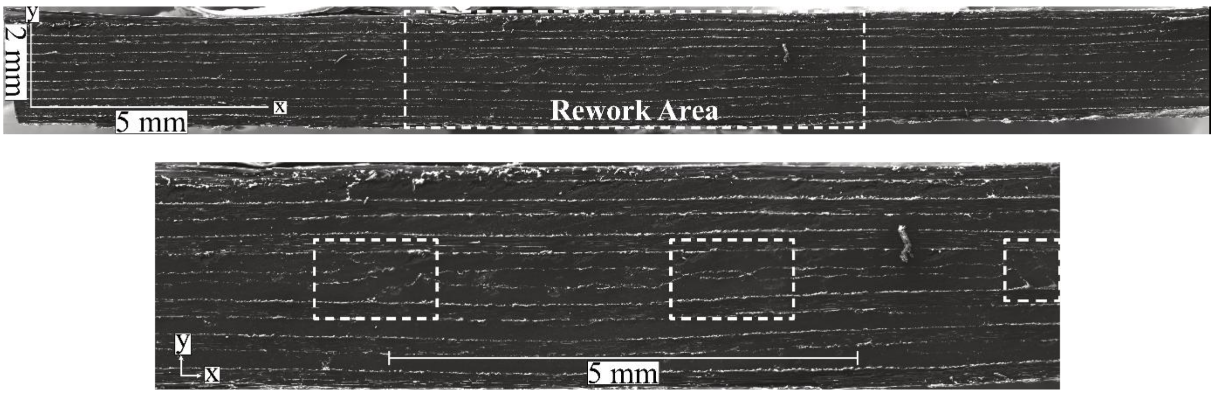

Figure 5.18. 6-Reworked SEM (magnification: x45, HV: 15.00kV, dwell: 45μs) full view (top) and magnified view of reworked area (bottom) showing areas of distortion of tows over ply-ply boundaries caused by rework

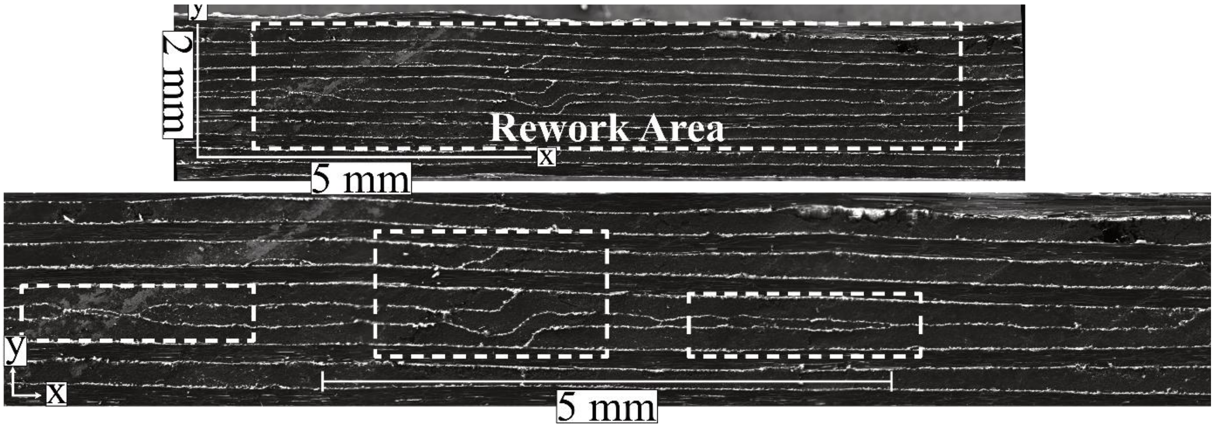

Figure 5.19. 16-Reworked SEM (magnification: x90, HV: 15.00kV, dwell: 45μs) full view (top) and magnified view of reworked area (bottom) showing areas of distortion of tows over ply-ply boundaries caused by rework

It is notable that the micrographs of the reworked specimens do not entirely align with those of the pristine specimens, since, from the macro scale of the operator performing the rework, they appear cosmetically similar and hence are considered to be successfully reworked by the current standards in industry. The following section shall show that this discrepancy between macro scale similarity and micro scale differences transfers on to different responses under identical loading conditions.

The micrographs display a similar pattern to the ultrasonic NDT results from section 4.3.4.3, where the reworked specimens closely resemble the pristine specimens, but retain a prominent residual waviness. In this way, the findings validate further the use of the ultrasonic NDT methods described for very thin laminates. Additionally, the agreement between the samples manufactured through conventional AFP, and those in Chapter 4 manufactured through Benchtop-AFP serves to validate the Benchtop-AFP approach as a reasonable substitute for conventional AFP for examining sub-processes.

5.3 Discussions

Taken together, the results indicate that defects primarily act to reduce the efficiency of load transfer and the effective bending stiffness of the laminate through disruption to the fibre alignment caused by out-of-plane waviness. Reworking largely restores stiffness to near-pristine levels, however residual out-of-plane waviness and ply-ply disturbance marginally reduces the global stiffness and leads to variations in the management of stresses. This microstructure is highlighted through SEM micrographs which show both the extreme out-of-plane waviness resultant from the embedded defects in the defective specimens, and the residual misalignment of the ply-ply interfaces in the reworked specimens. The orientation-dependent behaviour of the 90°-cut pristine specimens further reinforces the conclusion that flexural response in these laminates is governed predominantly by structural architecture and load-path integrity, both of which are strongly influenced by defects and only partially recoverable through reworking.

The implications of these findings for the wider Thesis are firstly, that reworking, through the methods discussed in the previous chapter, mostly restores the stiffness and strength of the laminates to pristine like qualities. However, marginal knockdowns are seen, most likely caused by residual misalignment of fibres at the rework location, as seen through the micrographs of similar specimens. Such misalignment is seen to be most pronounced where the reworked ply and the underlying ply share the same fibre orientation, as effective load transfer across this interface is highly sensitive to even small residual fibre waviness.

Secondly, the reworked specimens exhibit greater variability in stress and strain at break compared to pristine specimens, as reflected in the larger interquartile ranges measured for these properties. This increased scatter indicates that the reworking process introduces a degree of outcome variability associated with manual execution and local geometric differences at the repair site. While the average mechanical performance approaches pristine behaviour, the reproducibility of that performance is reduced. This observation reinforces the need for continued research aimed at optimising and standardising rework procedures to improve consistency and reliability of repaired laminates.

Collectively, these findings indicate that while current reworking techniques are capable of restoring near-pristine mechanical performance, they remain sensitive to the execution of the manual reworking process and therefore introduce measurable variability. The combination of high recoverability and process-dependent scatter highlights a clear opportunity for the development of automated reworking approaches capable of delivering improved repeatability, tighter control of fibre alignment, and more consistent consolidation at the repair interface. The following chapter therefore builds on these observations by examining how automation may be employed to standardise rework procedures.

Chapter 6. Recompaction-based automated rework

Following the previous chapter assessing the effect of manual rework, methods for the automation of gap reworking in AFP were developed and tested. This chapter investigates transverse tow deformation in thermoset AFP, focusing on tow width change and transverse displacement under recompaction. This study assessed whether compaction-induced width change could mitigate AFP gap defects in-process.

A full factorial experimental design evaluated the effects of process parameters on width change, and transverse dislocation as responses to the process parameter variations. Separate regression models and Analysis of Variance (ANOVA) were used to identify significant factors and interactions for each response.

Distinct governing mechanisms were identified. Tow width change showed viscosity-dominated behaviour, with tooling temperature as the primary factor and compaction force significant through interaction effects. Strong multi-parameter coupling demonstrated that meaningful width expansion requires coordinated thermal, mechanical, and temporal control rather than single-factor optimisation. In contrast, transverse displacement was governed solely by compaction force, indicating a shear-driven mechanical mechanism.

A focused follow-up experiment isolating compaction force at moderate temperature confirmed this asymmetry. Width change decreased even at maximum compaction, demonstrating the requirement for thermal activation, while transverse displacement remained fully active, confirming its purely mechanical nature.

Compaction-induced width change is deemed ineffective for gap mitigation in thermoset AFP. Achievable width changes are far below gap tolerances and are accompanied by displacement that degrades placement accuracy, representing a fundamental material limitation rather than a parametric optimisation issue.

6.1 Introduction

A potential mechanism for reworking gap defects lies in the thermally driven flow of resin during consolidation. Thermoset matrix systems undergo distinct flow regimes based on their thermal-viscosity profile. The viscosity of uncured thermoset resin decreases with increasing temperature, facilitating fibre realignment and resin migration. As temperature increases further, approaching the gel point, the resin begins to crosslink and progresses from the fusible A-stage to the thermoplastic-like B-stage, leading to a rapid increase in viscosity. Beyond the gel point, the resin reaches the C-stage and becomes semi-solid and loses the ability to flow, even at elevated temperatures [192], [193].

In AFP manufacturing, resin flow is possible, since the typical temperature ranges during the process should be above the prepreg glass transition points but below the gel point. Lukaszewicz and Potter [194] demonstrated experimentally that thermoset prepreg systems exhibit variant viscoelastic and plastic behaviour under compaction depending on the temperature and resin state. It was observed by Simacek et al. [184] that the primary flow mechanisms under post-deposition consolidation were squeeze flow; where the resin moves together with the fibres transversely in-plane, followed by bleeding flow, which is the directionally independent movement of the resin around the fibres. Other works indicate that the onset of bleeding flow occurs when the resin viscosity drops below ~10 mPa.s [195]. Examining resin flow around the sites of embedded gap defects, Simacek et al. [184] further observed that both shear flow, where the entire composite system deforms together driven by shear deformation of the matrix, and bleeding flow mechanisms act from the edge of gaps inward in the transverse direction allowing resin to fill voids.

Squeeze flow induced transverse resin deformation has been observed to significantly mitigate voids and fill gaps embedded within a laminate during the post-deposition consolidation phase, especially during autoclave curing [184], [195]. Minakuchi et al. [195]

and Nixon-Pearson et al. [170] demonstrated that the extent of transverse in-plane resin deformation increased with an increase in temperature of the system up to a threshold (~60-70°C), beyond which the flow mechanism shifts from squeeze flow to bleed flow. At temperatures above this threshold, the lower resin viscosity causes resin migration away from regions of already high fibre volume fraction, as the resin bleeds out along the fibre direction along channels between the fibres and interfaces between the plies. This phenomenon creates temporary healing of the gap area with resin rich regions where the resin has bled out at the interfaces to fill gaps, without allowing fibre migration into the gap area [195].

Previous work by Engelhardt et al. [196] investigated the influence of several AFP process parameters such as compaction force, layup velocity, and IR lamp power on the extent of laminate compaction measured as resultant laminate thickness. Their results showed that compaction force alone varied between 100 – 500 N did not produce statistically significant changes in laminate thickness. Layup velocity has a negative correlation with the magnitude of compaction of the laminate, likely due to reduced dwell time at higher layup speeds. IR lamp power, on the other hand, was reported to have significant positive correlation with compaction extent. Since the IR lamp power directly correlates to increased temperature of the material when deposited, and by extension decreased resin viscosity, resin could more freely flow between layers and lead to a greater deformation of the laminate in the through-thickness direction.

While Engelhardt et al.'s work addressed the through-thickness deformation at a laminate level, their findings are nevertheless instructive of the coupled mechanical relationships between processing parameters and their role in deformation behaviour of thermoset prepregs under AFP processing conditions. The identified dependencies on thermal input and dwell time can also be expected to influence deformation at the tow-level, such as in width expansion which plays a critical role in gap defect rework.

Earlier studies by Ivanov et al. [197] examined the increase of tow width during initial compaction during deposition, where increase of up to 40 % in tow width was observed at elevated temperatures. This suggests that there lies potential for transverse deformation of tow widths during the deposition stage, particularly in conjunction with thermal softening of the resin.

Yadav et al. [198] developed a prototype ATL head for thermoplastic systems equipped with inline force and width monitoring. Their study systematically varied compaction force (50–750 N) while holding layup speed and heat input constant and found that tape width increased nonlinearly with force, reaching up to 50 % expansion in tapes with narrow initial widths. For 25.4 mm tapes used in ATL, the width increased by up to 8.8 % at 350 N, with even greater expansions achieved for narrower tapes at higher forces (e.g., 50.7 % increase for 6.3 mm tape at 750 N). Importantly, the study established a quadratic correlation between applied force and width spread and demonstrated the feasibility of real-time width control using pre-programmed and inline compaction force variation.

However, these findings are limited to thermoplastic materials, where in-situ consolidation and matrix flow mechanisms differ significantly from those in thermoset prepregs. It remains unclear whether comparable tow width expansion can be achieved in thermoset AFP systems, where resin viscosity, cross-linking behaviour, and consolidation dynamics impose stricter process constraints. Understanding whether such deformation can be reliably induced, especially within processing limits of temperature, force, and speed, is critical to evaluating this technique's potential for gap rework in industrial AFP applications.

Valverde et al., [199], examined the impact of moderate processing conditions on first ply deposition behaviour in thermoset AFP using 12.7 mm IM7/M91 prepreg. Their experimental approach employed a novel heated glass tool that enabled direct observation of material behaviour beneath the compaction roller during layup, a region typically inaccessible due to the opacity of conventional tooling. Four test conditions were evaluated: room temperature baseline, tool heating alone (35 °C), IR lamp heating alone (50 °C), and combined heating (35 °C tool + 50 °C lamp). The study employed a deposition speed of 1200 mm/min and compaction force of 50 N, representative of typical AFP parameters. Using machine vision analysis, they quantified tape width changes during and after compaction across all temperature conditions.

The results demonstrated that elevated temperature during layup induced measurable transverse tape spreading, with width increases ranging from 0.5 mm (3.9 %) at room temperature to 0.75 mm (5.9 %) under combined heating conditions, relative to the nominal as-supplied width of 12.7 mm. Interestingly, tool heating proved more effective than IR lamp heating at inducing width expansion, despite the lower absolute temperature, which the authors attributed to more stable and uniform heat transfer from the tool's large thermal mass. Critically, the material exhibited dimensional stability after initial width changes from compaction pressure, with minimal width reduction (0.07 – 0.18 mm) observed 32 mm after the compaction zone, indicating that the deformation induced during consolidation was largely preserved. The study confirmed that thermoset prepregs undergo controlled lateral flow under temperature-assisted compaction, though the magnitude of expansion (≈6 % maximum) was considerably lower than that reported for thermoplastics under comparable force conditions.

Jamora et al. [200] studied the effects of laminate thickness on transverse deformation of thermoset AFP tows. The authors examined the extent of width change under the compaction roller during the initial deposition of a tow, varying compaction force (10, 30 and 50 N) and the number of underlying plies (1-10). Their results showed that increasing the number of underlying plies decreased tow width change under initial compaction conditions. The width change mechanism transitioned from a maximum spreading effect of 6 % under 50 N of force on a single ply to contraction of -0.5 % width under 50 N of force on top of 10 plies.

Mechanistically this reversal occurs because of, firstly, increased heat retention in thicker composite substrates maintaining prolonged resin softness, and secondly, increased substrate compliance causing elastic recovery after roller passage that contracts rather than expands tow width. As such, it can be said that the width change observed for the first ply deposited represents the maximum possible width change.

From a material-conservation perspective, tow width change during compaction must be accompanied by either through-thickness reduction, lengthwise extension, or transverse material displacement. In a fully consolidated tow without voids, width expansion implies material redistribution from other directions. However, void reduction during compaction can enable apparent width expansion without equivalent dimensional change elsewhere, as entrapped air is expelled and the fibre network densifies. Distinguishing between true material flow and void-collapse-driven dimensional change therefore requires consideration of the initial consolidation state. In the present study, the coupling between width change and transverse displacement likely reflects both mechanisms: viscosity-driven squeeze flow causing genuine material redistribution, and mechanical shear forces causing rigid-body translation of partially consolidated tows. The relative contribution of each depends on initial consolidation and resin viscosity at the processing temperature.

These findings establish that width modification in thermoset AFP is feasible but more constrained than in thermoplastic systems, supporting the need for optimised process parameters, particularly elevated temperatures that reduce resin viscosity, to maximise achievable tow deformation for gap mitigation strategies.

Several studies, therefore, have shown that width change is possible during the initial deposition step, in both thermoplastic [198] and thermoset [197], [199], [200] materials. What remains to be studied is the extent to which it is possible to achieve further width changes in a subsequent recompaction pass, in this instance framed as a mechanism for achieving process-controlled gap defect mitigation. Furthermore, the previous studies on tow width modulation have not addressed the coupling of additional deformation mechanisms with the width change mechanism, particularly the transverse displacement of tows incurred by the elevated process parameters. This study addresses these gaps by, firstly, systematically investigating compaction-induced width change across multiple parameters; secondly, simultaneously evaluating transverse displacement to identify detrimental side effects; and finally, evaluating whether optimisation can decouple these competing mechanisms to enable effective gap defect mitigation.

6.2 Experimental Methods

The influence of compaction force, layup speed, tooling temperature, external heating, and lie time on the extent of tow deformation during recompaction are investigated first in a generalised screening study. While this study explored the role of these parameters in detail, it does so only within the context of first ply layups of material onto the tooling surface. This limitation reflects findings in the literature, [200], which report that width change effects diminish with increasing number of underlying plies; hence first ply deposition represents the maximum achievable width change.

Through a factorial [201] and focused statistical analysis, the individual and interactive effects of the parameters was modelled. Following this, a focused study on compaction force in isolation was conducted, with this parameter identified as the most readily controllable parameter for developing a potential reworking method.

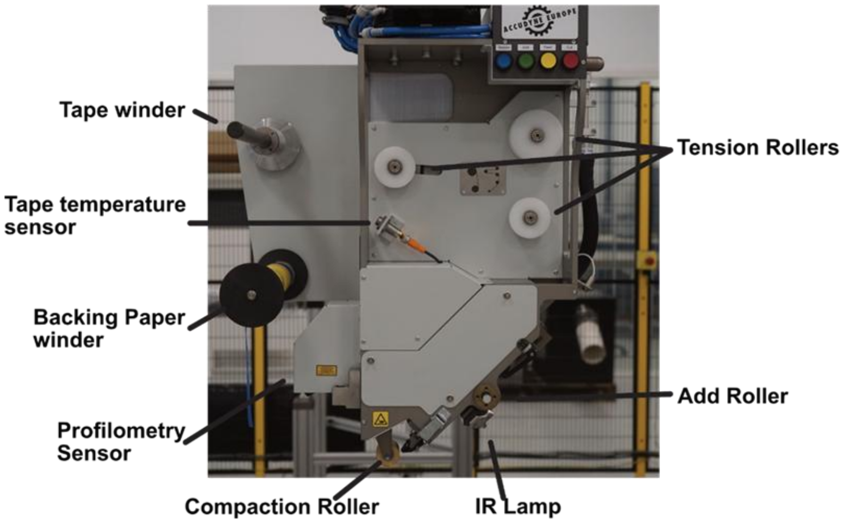

Figure 6.1. Single tow Accudyne 1000+ end-effector [71].

The AFP system used comprised a KUKA KR120 R3100 6-axis industrial robot, and a bespoke single tow Accudyne 1000+ end-effector. Figure 6.1 shows an annotated image of this end-effector. Featured in the head is a Borflex FIBERROLL 101 silicone compaction roller with a rated Shore A hardness value of 40 ShA, covered with a layer of PTFE tape. Compaction roller compliance plays a critical role in load distribution and material deformation during AFP. Softer rollers distribute compaction forces over a larger contact area, while harder rollers concentrate forces over smaller contact areas. Distributed compaction forces potentially reduce peak contact stresses and can promote more uniform pressure application; however, excessive compliance may reduce the effectiveness of force transmissions for inducing material flow. Smaller contact areas may concentrate force transmission but can also induce fibre distortion [202]. The silicone compaction roller used in this study represents a medium compliance design typical of AFP systems. Compaction force is supplied to the roller through an air cylinder. The air pressure within the cylinder is held at constant value, ensuring constant compaction force during layup. The compaction force applied by the roller can be programmatically varied between 50-750 N. Hexcel M91/34%/UD194/T700GC 6.35 mm thermoset prepreg slit tape was used.

A heated tooling plate was used as the substrate onto which the material was laid. The temperature of the tooling plate was monitored constantly using four thermocouples connected to the AFP system Human-Machine Interface (HMI). Heat was also supplied through an IR heat lamp located in the end-effector. This heat lamp is used to apply external heating to the layup surface ahead of the tow. The power of this heater is varied within the HMI as a function of the layup speed, within a range of 0-400W. When on, the maximum power relative to the layup speed is outputted.

A Micro-Epsilon scanCONTROL 3012-50 2D/3D profilometry sensor [203] was employed to record the surface profile of the tow after the end-effector has passed over it. The sensor returns profile data at a sampling rate of 50 Hz as an array of 2048 height values arranged in their position in the x-direction (perpendicular to the direction of the tow).

6.2.1 Placement process

During the experiments, trials were performed with parameter settings defined by the factorial experimental design. In each trial, first a single 200 mm length tow was placed using baseline values of 150 N compaction force, 100 mm/s layup speed, tooling temperature at the level set for that specific trial, and external heating on. Here experimental temperature refers to the level (High or Low) in the experimental design for a given experimental trial. The heated tooling plate takes a considerable time to change its temperature from its current value to a new set value. Hence, it was not feasible to maintain a baseline value for the initial tow layup across all experimental trials followed by heating or cooling to the experimental trial temperature. Thus, the temperature during initial deposition was the same as the temperature used during the subsequent recompaction trial, as defined by the experimental design.

Following initial deposition, a second pass with the AFP end-effector was conducted in "dry-run" mode. Here, the AFP end-effector followed the same coordinates used when depositing the material without depositing any new material. In this second pass, the values for the parameters under investigation were set to the levels defined for that given run, as set by the factorial experimental design.

Figure **6.2** shows a graphical demonstration of this two-stage process in both end and plan view.

The mean change in tow width pre- and post-recompaction value, and the root mean squared transverse displacement (RMSTD) of the tow centre lines were used as the response variables in the following analyses.

To investigate the relationship between processing parameters and compaction-induced transverse material flow for deformation-driven tessellation, two sequential experiments were conducted. The first experiment provided a comprehensive analysis of the effects of all process parameters to identify statistically significant factors and their interactions. The second experiment focused specifically on compaction force effects to evaluate its potential for practical application in automated gap defect reworking through controlled tow-width variation.

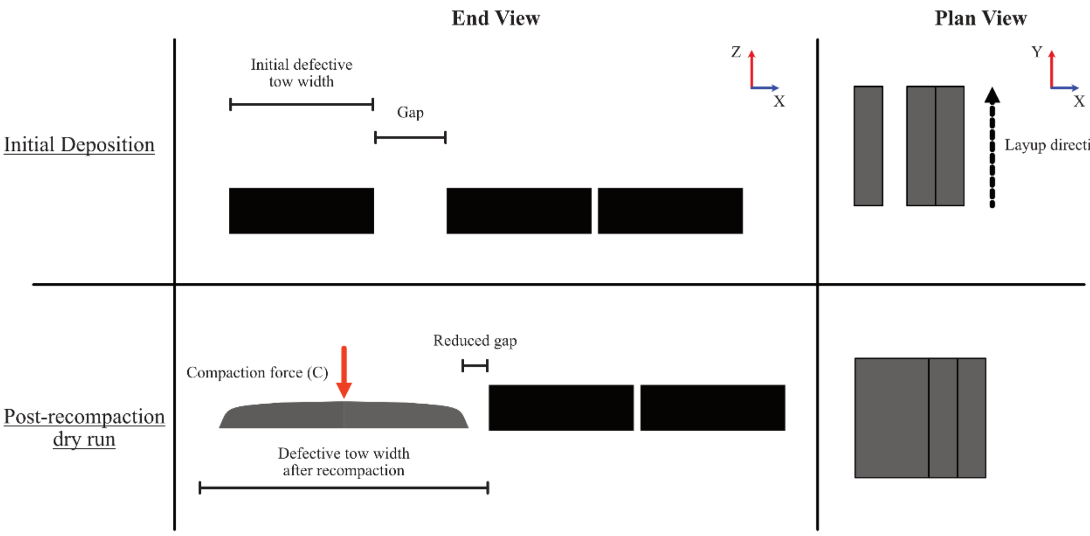

Figure 6.2 Proposed compaction driven width change based automated gap reworking method, end view (left) and top view along layup direction (right) of tows pre- and post-recompaction.

6.2.2 Data Processing

The raw data from the profilometer was processed with a Savitsky-Golay filter [204] to reduce noise in the signal. The method fits successive subsets of data points to a low-degree polynomial curve using a least squares regression. The window length of each subset was set to 11 points, and the polynomial degree was set to 3. These parameters were selected to effectively reduce measurement noise while preserving the genuine edge features of the tow, enabling more reliable edge detection in subsequent processing steps.

For each profile, the edge locations were calculated by first applying Otsu's thresholding method [205], which generates dynamic threshold values across a range of data. This allowed for simple threshold based rising and falling edge detection at the indices where the signal crossed over the threshold. From this the width of the material for a single profile could be determined from the distance between rising and falling edges.

Figure **6.3**. (A) shows a representation of one profile scan with the detected edges shown with red and blue vertical lines.

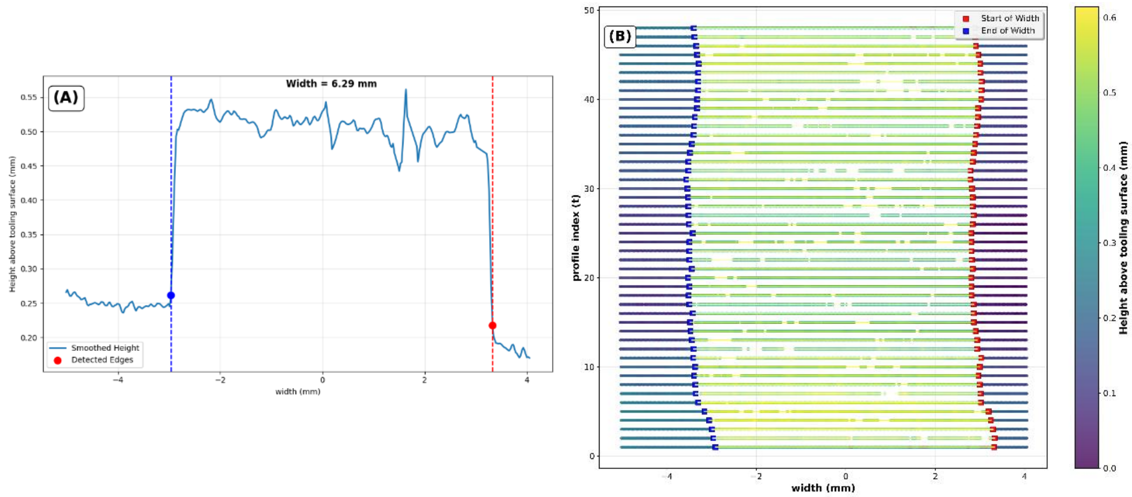

Figure 6.3. A: Profile 2 of experiment 1, R_3_1 with detected tow edges; B: Trial R_3_1 over full 200 mm length showing detected edges (red and blue markers)

Figure **6.3** (B) shows a 2D representation of an entire tow over its full length of 200 mm, with red and blue markers for the detected edges. The colour scale for each pixel shows the height of the signal at that point in x for that profile.

The baseline width, W_o for a given trial, R, following initial material deposition was recorded using the mean of recorded widths across all measurement profiles:

$$\mathrm{W_o} = \overline{W_i} \tag{6.1}$$

where W_i is the recorded width for a single profile, *i*. The measurement uncertainty was quantified using the mean absolute deviation (MAD), which provides robust estimation less sensitive to outliers than standard deviation:

$$MAD_o = \overline{|W_i - W_0|} \tag{6.2}$$

Following the recompaction process, the material width was similarly analysed using the same statistical approach.

The combined measurement uncertainty, σ_{MAD}, for a given trial across the original width, W_0, and recompacted width, W_r, was calculated using standard error propagation principles. This approach accounts for uncertainties from both measurement phases and provides the total uncertainty in the width change calculation.

$$\sigma_{MAD} = \sqrt{MAD_o^2 + MAD_r^2} \tag{6.3}$$

The net width change, with uncertainty, ΔW, was determined as:

$$\Delta W = (W_r - W_o) \pm \sigma_{MAD} \tag{6.4}$$

The profiles were compared both pre- and post-recompaction to measure the absolute position of the tows under the end-effector. Given that the end-effector travelled the same path during both compaction trials, this gives an accurate measurement of the shifting of the material in the transverse direction even if the absolute width of the material does not change. This was performed by comparing the position of theoretical centre line of each tow in pre- and post-recompaction, calculated as the mathematical mean between the edges for each position profile along the length of the scan. With this information, it is possible to calculate the transverse displacement of the tows.

From the displacement profile, several statistical metrics are calculated to characterise the transverse movement behaviour. The mean displacement provides the overall direction and magnitude of lateral drift, indicating whether the specimen moved predominantly in one direction. The root mean squared transverse displacement (RMSTD) quantifies the typical magnitude of movement regardless of direction, while the standard deviation measures the variability in displacement along the specimen length. The RMSTD is calculated using the change in location of the centreline of the tow, x_c, in the y-axis direction between initial deposition and recompaction using:

$$x_c(p_i) = \frac{x_{e_1}(p_\mathrm{i}) + x_{e_2}(p_i)}{2} \tag{6.5}$$

where $x_{e_1}(p_\mathrm{i})$ and $x_{e_2}(p_i)$ are the positions of the edges along the x-axis for each profile, p_i. The centreline displacement between initial deposition, x_{c_o}, and recompaction, x_{c_r}, for a given profile, p_i, is calculated using:

$$\Delta x_c(p_i) = x_{c_o}(p_i) - x_{c_r}(p_i) \tag{6.6}$$

The RMSTD, y_{rms}, is calculated as:

$$y_{rms} = \sqrt{\frac{1}{n}\sum_{i=1}^{n}[\Delta x_c(p_i)]^2} \tag{6.7}$$

Where n = the number of profiles taken over the length of the tows, and $\Delta x_c(p_i)$ is the transverse displacement of the centrelines for each profile, p_i, in the y-direction.

Figure 6.4 and Figure 6.5 show comparative displacement plots for two example trials (Trials 10 and 15) showing high displacement (Figure 6.4) and low displacement (Figure 6.5).

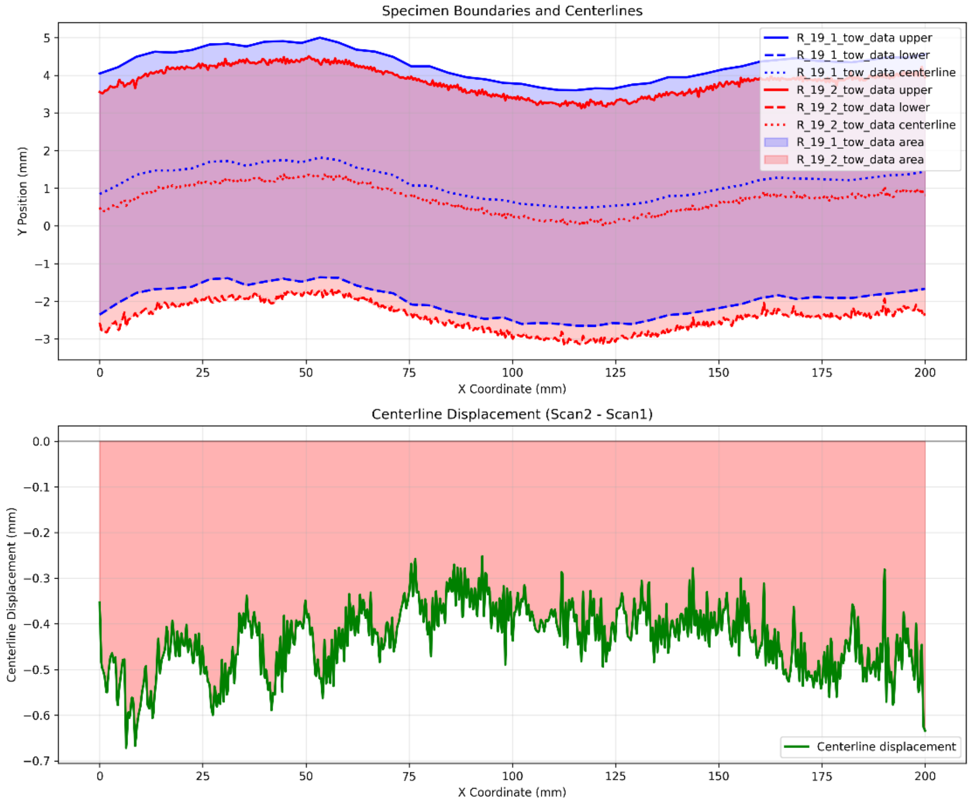

Figure 6.4. Displacement comparison for Experiment 1: Trial 10

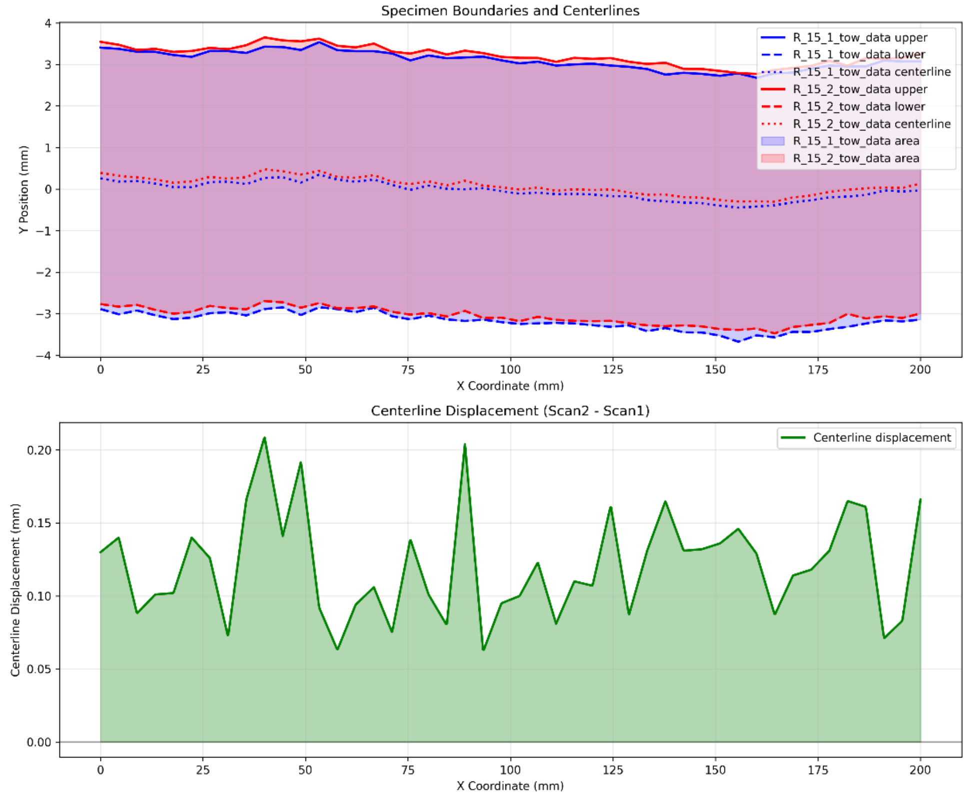

Figure 6.5. Displacement comparison for experiment 1: Trial 15

6.3 Model and Factor Analysis

The results were analysed using the Minitab statistical analysis software [206], using mean width change and transverse displacement across each tow as the response variables in separate analyses. The method allows for the derivation of a model for the response variables, using a linear factorial regression model including main effects and selected interaction terms taking the form:

$$y = \beta_o + \sum_{i} \beta_i x_i + \sum_{i<j} \beta_{ij} x_i x_j + \sum_{i<j<k} \beta_{ijk} x_i x_j x_k + \varepsilon \qquad (6.8)$$

Where, y is the response variable, x_i are the coded factor levels, β are the regression coefficients, and ε represents the residual error.

Weighted least squares regression was performed using measurement uncertainty (MAD) to calculate weighting for each trial as:

$$w_i = \frac{1}{\sigma_{MAD}{}_i^2} \qquad (6.9)$$

Where, σ_{MAD} is the mean average deviation calculated from Eq. 6.3.

The fitted model from $Eq.$ 6.8 was then analysed using ANOVA [207] to partition the total response variability into contributions from individual factors and their interactions. Sequential (Type I) sums of squares were used, such that the sum of squares for each term represents the additional variability explained by that term, conditional on the terms preceding it in the model. The total, SS_T, and residual, SS_E, sum of squares were defined as:

$$SS_T = \sum (y_i - \bar{y})^2 \qquad (6.10)$$

$$SS_E = SS_T - \sum SS_K \qquad (6.11)$$

Where, SS_k denotes the sequential sum of squares associated with a given model term, k. y_i is the recorded response variable for a given trial, i. $\bar{y}$ is the grand mean of all the recorded response variables across all trials.

The Mean Squared Error (MSE) was used to provide an estimate of the residual variance of the model and was calculated as:

$$MS_E = \frac{SS_E}{df_E} \tag{6.12}$$

Where, df_E is the residual degrees of freedom calculated as:

$$df_E = N - df_{model} - 1 \tag{6.13}$$

Where N is the total number of observations made. The degrees of freedom for each model term were determined by the number of independent contrasts associated with that effect, and the total degrees of freedom of the model, df_{model}, is the sum of the degrees of freedom of all the model terms.

For comparative purposes, the model goodness fit, R^2, and a percentage relative contribution, C_k, for each factor were used and are both dependant on the use of the sequential sum of squares as:

$$R^2 = 1 - \frac{SS_E}{SS_T} \tag{6.14}$$

And

$$C_k = \frac{SS_k}{SS_T} \times 100 \tag{6.15}$$

The strength of each factor was recorded in the F-value assessed against the MSE of the model, and the p-value reports the statistical significance of a given factor. Statistical significance was assessed at a confidence level of 95% ($p < 0.05$).

It should be noted that the model is near-saturated, with only four degrees of freedom available for error estimation. Consequently, the estimated residual variance and associated F- and p-values are sensitive to individual observations. While the consistency between ANOVA and regression coefficient confidence intervals supports the identified trends, confirmation

Table 6.1. Factors and levels in Experiment 1

Factor	Description	Level 1	Level 2
Compaction force (C)	Normal force applied by compaction roller	50 N (Low)	750N (High)
Tooling Temperature (T)	Set temperature of tooling surface below deposited tows	40° (Low)	100° (High)
Layup Speed (S)	Velocity of the end-effector across the layup surface	10 mm/s (Low)	100 mm/s (High)
External Heating (H)	External heat from the IR lamp on the end-effector	On	Off
Lie Time (L)	Time elapsed between initial material deposition and recompaction	< 1 min (Short)	> 5 min (Long)

experiments with increased replication are required to robustly validate higher-order interaction effects.

6.4 Results and Discussion

6.4.1 Experiment 1 – Multi Parameter Screening Study

A generalised 2^5 full factorial Design of Experiments (DOE) [201] study was conducted across all processing parameters to quantify their statistical significance and interaction effects on tow deformation behaviour. This analysis focused on two deformation mechanisms: squeeze-flow-induced width change driven by the resin viscosity and consolidation force, and transverse displacement, driven by shear forces at the roller-tow interface. By analysing both mechanisms simultaneously, the influence of the chosen processing parameters on each can be better understood, with the objective of maximising width change while minimising transverse displacement. This is critical to enabling automated reworking of gap-type defects through width-change-induced tessellation across the tooling surface.

This study investigated the main effects of each factor as well as the two- and three-way interactions between factors on the response variables of width change and transverse displacement. The absolute mean change in width and the RMSTD were used as response

Table 6.2. Response variables in Experiment 1

Response Variable	Description	Abbreviation	Units
Width Change	Absolute mean change in tow width	W_{Δ}	mm
Transverse Displacement	Root mean square displacement of the tow centreline along the entire length of the tow	RMSTD	mm

variables, see Table 6.2. The trial running order was randomised across the experimental design. No blocking was applied, because all experiments were performed under the same external conditions by the same operator. All factors were assigned two levels, high/low for incremental factors and on/off for binary factors, as shown in Table 6.1. The factor level settings for Experiment 1 are shown in full for all trials in Appendix 6A Experimental settings for experiment 1.

Compaction force (C) was set between the minimum and maximum levels available which are 50 and 750 N. Tooling temperature was set between 40 and 100°C. The Hexcel M91 prepreg used in this study has a glass transition temperature (T_g) of 185-190°C and a cure temperature of 180°C. While Valverde et al. [199] investigated maximum heat lamp temperatures of 50°C, the elevated maximum of 100°C in this study was selected to induce significantly greater resin flow and viscosity reductions, which is critical for achieving measurable tow deformation during recompaction, while maintaining a substantial safety margin below the prepreg cure onset temperature of 180°C [180].

The Layup Speed (S) was varied between 10% and 100% of the maximum layup speed of the AFP machine which was 100 mm/s.

Lie time was varied between 1 to 5 minutes. This was to simulate the time between deposition and performing the reworking task after a full ply has been deposited for a small and large layup respectively. The full results from Experiment 1 are shown in Appendix 6B Width change results for experiment 1 showing the recorded initial width (W_o), recompacted width (W_r), and the change in width (W_{Δ}).

Trials 12 and 21 failed to reconsolidate the tow without dislocating fully. The tows were physically distorted to the extent that adhesion to the tooling surface was lost. As such these trials were excluded from the analysis.

Figure 6.6 - Figure 6.8 show the effect on width change of each parameter as a main effect and in key two-way interactions. The dashed line on the figures is the predicted response when from $Eq.\,6.8$ when all factor levels are set to 0 hence the only remaining term is, β_o, computed as 0.06245. The figures should not be viewed as indicative of statistical significance unless supported by the results of the ANOVA. The effect of changing a parameter from a lower setting to a higher setting, as defined by the model is shown in the figures. The larger the effect of changing the parameter, the steeper the slope. Changes that increase the response variable, i.e., the induce a larger width change, show a steep positive slope between low and high settings for a given parameter. Smaller effects result in a less steep slope, and effects which are negatively associated with width change, i.e., changing the parameter from low to high leads to a reduction in width change, and shown by a negative slope. In this way a visual representation of the modelled effect of each parameter (in Figure 6.6), or interactions between parameters (in Figure 6.7 and Figure 6.8), can be obtained.

Table 6.3. ANOVA table for Experiment 1 showing main effects and key interactions only

Source	DF	F-Value	P-Value	Contribution
Model	25	14.22	0.010	98.89%
Main Effects				
C	1	22.36	0.009	8.87%
T	1	60.76	0.001	50.59%
S	1	5.11	0.087	0.44%
H	1	1.24	0.327	0.12%
L	1	1.55	0.281	0.85%
Key Interactions				
C×T	1	7.19	0.055	14.31%
C×S	1	12.24	0.025	0.75%
C×L	1	5.09	0.087	0.78%
T×S	1	7.96	0.048	1.82%
H×L	1	6.5	0.063	0.05%
C×T×S	1	22.25	0.009	7.11%
C×S×H	1	10.44	0.032	3.91%
T×S×L	1	10.26	0.033	2.03%
Error	4			1.11%

Table 6.3 presents the findings of the analysis of variance for width change.

Width change in thermoset AFP recompaction is primarily governed by thermal activation, with tooling temperature (T) contributing 50.59 % of the total experimental variation ($F = 60.76$, $p = 0.001$). Compaction force (C), by comparison contributed only 8.87 % ($F=22.36$, $p=0.009$). This disparity reveals the underlying mechanism, where elevated temperatures allow the Hexcel M91 system to transition through the low-viscosity B-stage, enabling material flow under mechanical loading. Temperature exhibited the strongest main effect (Figure 6.6), with width change increasing by 0.116 mm between 40 °C and 100 °C. The statistical model itself ($R^2 = 98.89$ %, $F = 14.22$, $p = 0.010$) confirms these effects are systematic rather than random variation.

Critically, compaction force effectiveness depends on thermal activation. The compaction force and tooling temperature interaction (C×T) approached significance ($F = 7.19$, $p = 0.055$) but notably accounts for a large portion of experimental variation (14.31 %) relative to other interactions, suggesting this relationship warrants further investigation. Figure 6.7b demonstrates this dependency. At low temperatures, increasing force produces minimal width change, whereas at high temperature, the same force increase generates substantial width change through material flow. Mechanistically, compaction force can only drive flow when resin viscosity has been sufficiently reduced through thermal input. Mechanical pressure alone cannot mobilise the material at low temperatures.

Layup speed (S), external heating (H), and lie time (L) showed negligible individual effects (contributions < 1.5 %, $p > 0.08$) but participated in significant higher-order interactions. The interaction between compaction force and layup speed (C×S) was significant ($F = 12.24$, $p = 0.025$), revealing that the force effects are amplified at higher speeds, Figure 6.7a highlights this effect. Similarly, the tooling temperature and layup speed interaction (T×S) ($F = 7.96$, $p = 0.048$), shows that temperature effects are more pronounced at lower speeds, likely due to increased dwell time allowing thermal penetration and viscosity reduction through the tow cross-section.

One highly significant three-way interaction exists between compaction force, temperature and layup speed (C×T×S) ($F = 22.25$, $p = 0.009$). This interaction is between the three most individually significant factors and is itself significant, contributing 7.11 % of the total experimental variation. This interaction reveals that width change requires coordinated multi-parameter control rather than single-factor optimisation. Figure 6.8 visualises this coupling, optimal width change occurs only when high temperature, high force and high-speed act in concert. Mechanistically, this coupling reflects the need for simultaneous thermal softening, mechanical loading, and sufficient mechanical work rate to mobilise the material. Two additional three-way interactions, C×S×H ($F = 10.44$, $p = 0.032$, 3.91 % contribution) and T×S×L ($F = 10.26$, $p = 0.033$, 2.03 % contribution), further demonstrate that even factors with negligible main effects participate in governing width change through complex interactions.

The following equation represents the explicit regression model for width change in uncoded units, with all insignificant terms omitted, derived from Eq. 6.8. This expression captures the key linear and interaction effects of the processing parameters that significantly influence the response.

$$\Delta W = 0.06245 + 0.03192\, C + 0.05800\, T$$
$$+0.02701\, \mathrm{C} \times S + 0.02340\, T \times \mathrm{S} + 0.03779\, \mathrm{C} \times \mathrm{T} \times \mathrm{S} +$$
$$0.01695\, \mathrm{C} \times \mathrm{S} \times \mathrm{H} + 0.018772\, \mathrm{T} \times \mathrm{S} \times \mathrm{L} \quad (6.16)$$

This multi-parameter coupling has critical practical implications. Optimal layup speed depends on both temperature and force settings, meanwhile temperature effectiveness depends on speed and force, and force effectiveness depends on temperature and speed. Independent optimisation of individual parameters with the aim of maximising width change is not possible. Any automated reworking strategy must control all three primary parameters (C, T, S) simultaneously. This requirement creates a conflict between the rapid, localised response required for on-demand defect reworking, where tooling temperature exhibits slow thermal response incompatible with localised adjustments.

Despite robust statistical significance and clear mechanistic understanding, the absolute magnitude of achievable width limits the practicality of the technique for gap rework. The maximum observed width change (0.28 mm) represents only 14 % of the 2.0 mm gap threshold typically requiring rework [27]. Even under optimal multi-parameter combinations, width expansion falls below practical requirements.

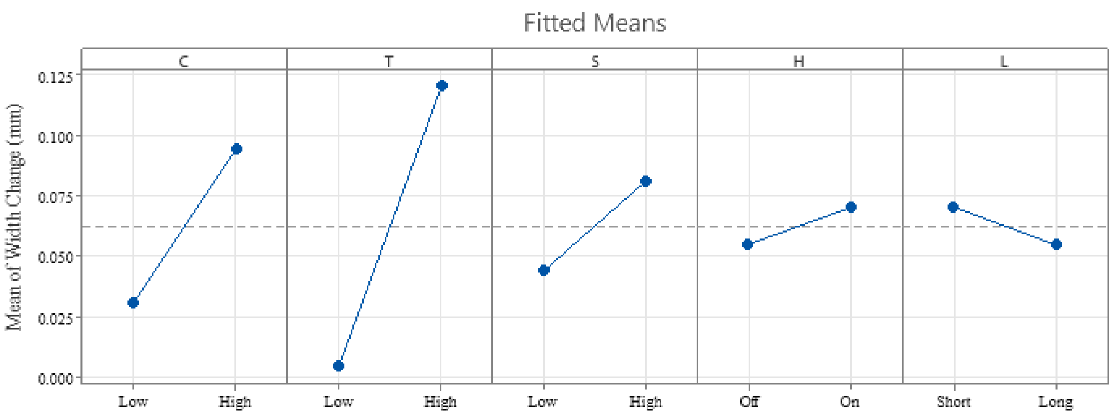

Figure 6.6. Main isolated effects of factors on width change

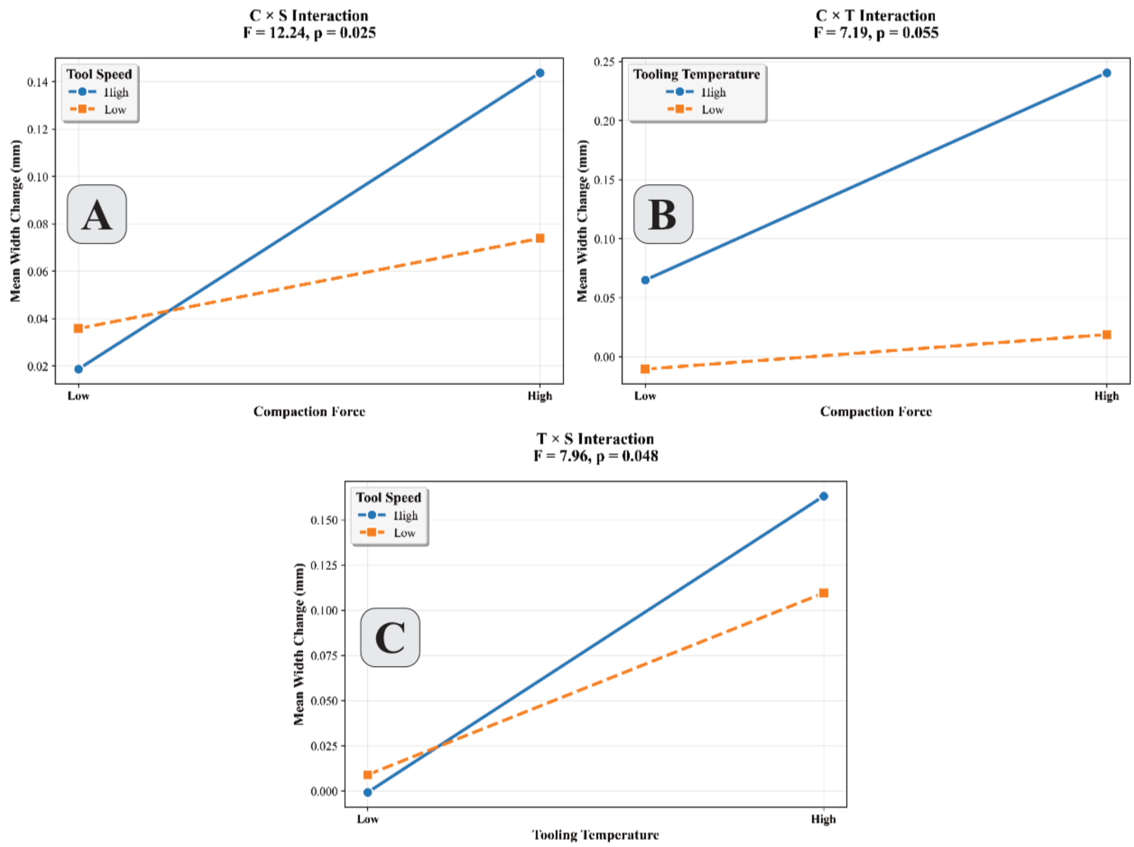

Figure 6.7. Matrix of key two-way interactions of factors on width change in Experiment 1

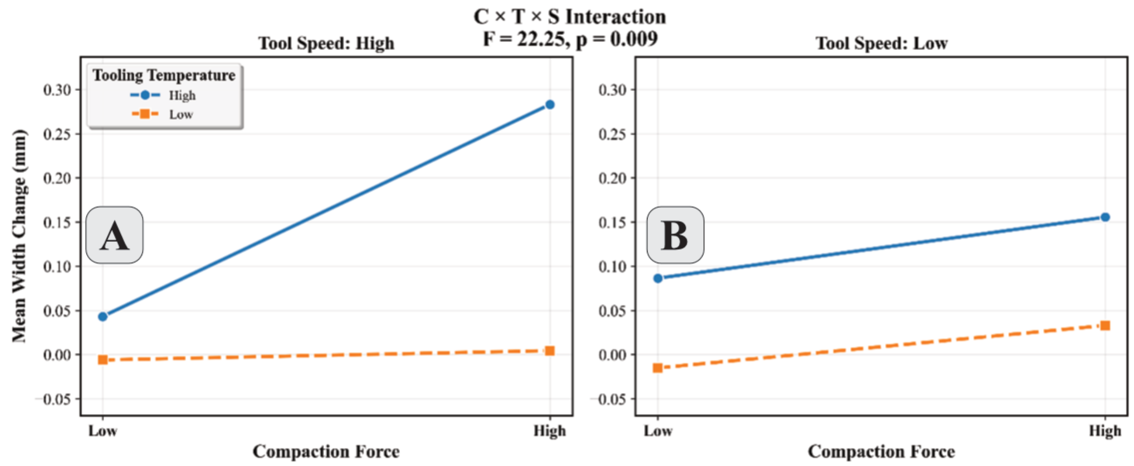

Figure 6.8. Matrix of key three-way interactions of factors on width change in Experiment 1

6.4.1.1 Transverse displacement

The same factorial design was analysed through ANOVA, using RMSTD as the response variable. The results are detailed in Table 6.4 and Table 6.5 and

Figure **6.9.** Main isolated effects of factors on transverse displacement

Table 6.4. Comparison between factor settings for displacement groupings

Level	Compaction force (C)	Tooling temperature (T)	Layup speed (S)	External heating (H)	Lie time (L)
			RMSTD ≤ 0.12 mm – sample size: 10		
Low	90.00%	50.00%	50.00%	30.00%	40.00%
High	10.00%	50.00%	50.00%	70.00%	60.00%
			0.12 ≤ RMSTD ≤ 0.45 mm – sample size: 10		
Low	50.00%	75.00%	62.50%	50.00%	50.00%
High	50.00%	25.00%	37.50%	50.00%	50.00%
			RMSTD ≥ 0.45 mm – sample size: 10		
Low	10.00%	50.00%	20.00%	50.00%	60.00%
High	90.00%	50.00%	80.00%	50.00%	40.00%

. By contrast to width change, transverse displacement was found to be entirely governed by compaction force (F = 24.56, p = 0.006) which contributed 71.88 % of experimental variance. All other factors in isolation and all other interaction effects, both two-way and three-way, were statistically insignificant. The main effect plots in Figure 6.9

show this clearly, where a steep increase in mean displacement of the tows is seen for elevated compaction force level, whereas other parameters show a negligible or negative effect on the tow displacement.

The regression equation for transverse displacement with insignificant terms omitted is:

$$y_{rms} = 0.2700 + 0.1229\,C \qquad (6.17)$$

Comparing all factors in terms of RMSTD of the samples, the trials stratified based on the magnitude of their response: those with low level displacement (RMSTD ≤ 0.12 mm), medium displacement (0.12 ≤ RMSTD ≤ 0.45 mm), and those with high displacement (RMSTD > 0.45 mm). Table 6.4 shows these groupings and the distribution of high/low values for each of the process parameters.

Table 6.5. ANOVA table for Experiment 1 showing main effects and Key interactions only

Source	DF	F-Value	P-Value	Contribution	95 % confidence interval
Model	25	5.48	0.055	97.17 %	(0.1967, 0.3434)
Main Effects					
C	1	24.56	0.008	71.88 %	(0.0541, 0.1918)
T	1	0.30	0.616	0.19 %	(-0.0908, 0.0610)
S	1	2.04	0.226	1.37 %	(-0.0406, 0.1267)
H	1	0.11	0.753	1.58 %	(-0.0786, 0.0615)
L	1	1.11	0.352	1.45 %	(-0.0889, 0.0400)
Error	4			2.83 %	

The dominance of compaction force is evident across these groupings. Low-displacement trials were strongly associated with low compaction settings (90 %), whereas high displacement trials were predominantly associated with high compaction force (90 %). Medium displacement trials showed an even distribution between force levels, consistent with a transitional regime in which force magnitude determines the onset of displacement. By contrast, tooling temperature, layup speed, external heating, and lie time exhibited broadly balanced distributions across all displacement groupings, indicating minimal association with the response. Although some apparent tendencies can be observed in the grouped data, these are not supported by the ANOVA results and should therefore be interpreted with caution.

Layup speed shows no consistent trend across the low- and medium-displacement groups, although a higher proportion of high-speed settings appears in the high-displacement group. Similarly, external heating displays broadly balanced distributions in the medium-

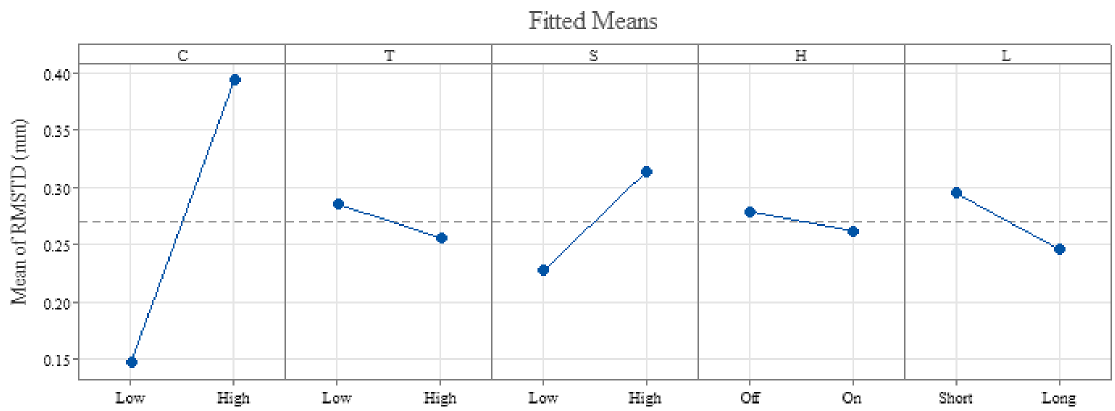

Figure 6.9. Main isolated effects of factors on transverse displacement

and high-displacement groups, with only resulting from experimental scatter rather than a systematic process effect. Lie-time values remain relatively uniform across all displacement groupings, reinforcing the conclusion that temporal effects have limited influence on transverse displacement.

The dominance of compaction force in governing transverse displacement, coupled with the absence of tooling-temperature effect in contrast to the width change behaviour, suggest that the underlying mechanism is not governed by viscosity dominated material flow. Instead, transverse displacement appears to arise from a shear-driven mechanism dominated by frictional forces. At higher compaction settings these forces overcome the adhesion force between the tow and the substrate, resulting in lateral tow movement rather than the squeeze flow required for effective gap reworking. This distinction highlights a fundamental conflict between the mechanical conditions required to induce width change and those that promote undesirable transverse displacement.

6.4.1.2 Process Limitations and Failure Mechanisms

The failure of trials 12 and 21 of experiment 1 illustrates the dominance of the transverse displacement mechanism over the squeeze flow mechanism under specific parameter constraints. In these trials, high Compaction force (750 N) and high tooling temperature (100 °C) were combined with low layup speed (10 mm/s) and no external IR heating. The combination of high compaction force with extended dwell time (low speed) generated substantial delaminating forces on the tow. However, without the localised surface softening provided by the external IR heater, which was present in other high-force, high-temperature trials, the transverse displacement forces exceeded the adhesive forces between the tow and the tooling surface, leading to delamination and tow failure. This demonstrates two findings: (1) while both mechanisms activate simultaneously under high force conditions, the transverse displacement mechanism can produce failure modes (delamination) that prevent the beneficial squeeze flow mechanism from completing successfully, and (2) the external heater, while statistically insignificant as a main effect in both width change and transverse displacement, plays a critical role in preventing failure modes by locally softening the tow surface and enabling it to accommodate the substantial mechanical loads without loss of adhesion.

Analysis of the two deformation responses revealed distinct governing mechanisms despite being measured on the same experimental trials. Width change is governed by complex thermo-mechanical behaviour requiring coordinated parameter control. In contrast, transverse displacement was governed almost entirely by compaction force with all other factors and interactions being statistically insignificant.

6.4.2 Experiment 2 - Focused Study on Compaction Force

Building upon the findings from Experiment 1, this focused investigation examined whether compaction force alone could produce meaningful width changes for practical defect mitigation, or whether the multi-parameter combinations identified in Experiment 1 are required for rework. This question is critical for implementation: compaction force can be rapidly adjusted during AFP operations, whereas tooling temperature exhibits slow thermal response incompatible with localised, on-demand defect correction.

Experiment 1 revealed that width change was governed by effects of compaction force, tooling temperature, and their interaction. However, it remained unclear the extent to which the compaction force effect could be decoupled from the thermal effects of elevated tooling temperature. To address this question, compaction force was systematically varied across three levels (50, 375, and 750 N) while maintaining other parameters at moderate, practically achievable values: tooling temperature at 70 °C, layup speed at 55 mm/s (55 % of maximum), with external heating and lie time retained as two-level factors with the same settings in Table 6.1.

The three-level compaction force design enables detection of non-linear relationships and provides enhanced statistical power compared to traditional two-level factorial designs. Both width change (ΔW) and transverse displacement (RMSTD) were measured for all trials following the same method as experiment 1, to characterise both deformation mechanisms under these moderate-temperature conditions. Appendix 6E Experimental Settings for Experiment 2 display the level settings (Table 6D.1) and results (Table 6D.2) for width change and transverse displacement for experiment 2.

6.4.2.1 Width Change

While a numerical trend toward increased width change with compaction force was observable (from -0.034 mm at 50 N to +0.075 mm at 750 N), these changes are much smaller than those seen in experiment 1. The maximum observed width change of 0.075 mm (Trial 3: 750 N, H = OFF, L = 60 s) represents only 3.75 % of the 2.0 mm gap threshold [27] requiring rework and occurred at the maximum force level tested. By comparison, Experiment 1 achieved 0.28 mm width change (14 % of gap threshold) only under extreme conditions (100 °C, 750 N, 100 mm/s) which, although still inadequate for practical rework, is nearly four times greater than the maximum observed in Experiment 2.

External heating showed no statistically detectable effect on width change, with numerical variations between ON and OFF conditions remaining below 0.04 mm. Similarly, lie time variations (60 s vs 300 s) produced no systematic effect on width change magnitude. The findings support the conclusions from experiment 1, that tooling temperature is required to enable the effectiveness of consolidation force in inducing width change. Without sufficient thermal activation to reduce resin viscosity, mechanical loading alone cannot mobilise material flow in the tow.

6.4.2.2 Transverse Displacement

In contrast to width change, transverse displacement demonstrated a sustained relationship with compaction force at moderate temperature (Figure 6.10). The trend of increased displacement with increased force observed in experiment 1 persisted under these conditions. All trials at maximum compaction force (750 N) exhibited substantial transverse displacement regardless of external heating or lie time settings:

- Trial 3 (C = 750 N, H = OFF, L = 60 s): RMSTD = 0.432 mm
- Trial 6 (C = 750 N, H = OFF, L = 300 s): RMSTD = 0.462 mm
- Trial 9 (C = 750 N, H = ON, L = 60 s): RMSTD = 0.410 mm
- Trial 12 (C = 750 N, H = ON, L = 300 s): RMSTD = 0.442 mm

These displacement magnitudes (mean RMSTD = 0.437 mm at C = 750 N) are comparable to the high-displacement regime observed in Experiment 1 (RMSTD ≥ 0.45 mm), despite the 30 °C lower tooling temperature. This confirms the mechanistic finding from Experiment 1: transverse displacement is driven purely by mechanical forces and operates independently of thermal effects.

Lower compaction forces produced correspondingly lower displacements: intermediate force (375 N) yielded RMSTD = 0.136 - 0.176 mm, while low force (50 N) produced RMSTD = 0.089 - 0.117 mm. This force-displacement relationship persisted across all combinations of external heating and lie time, demonstrating that thermal parameters cannot decoupled from the mechanically driven displacement response from compaction force.

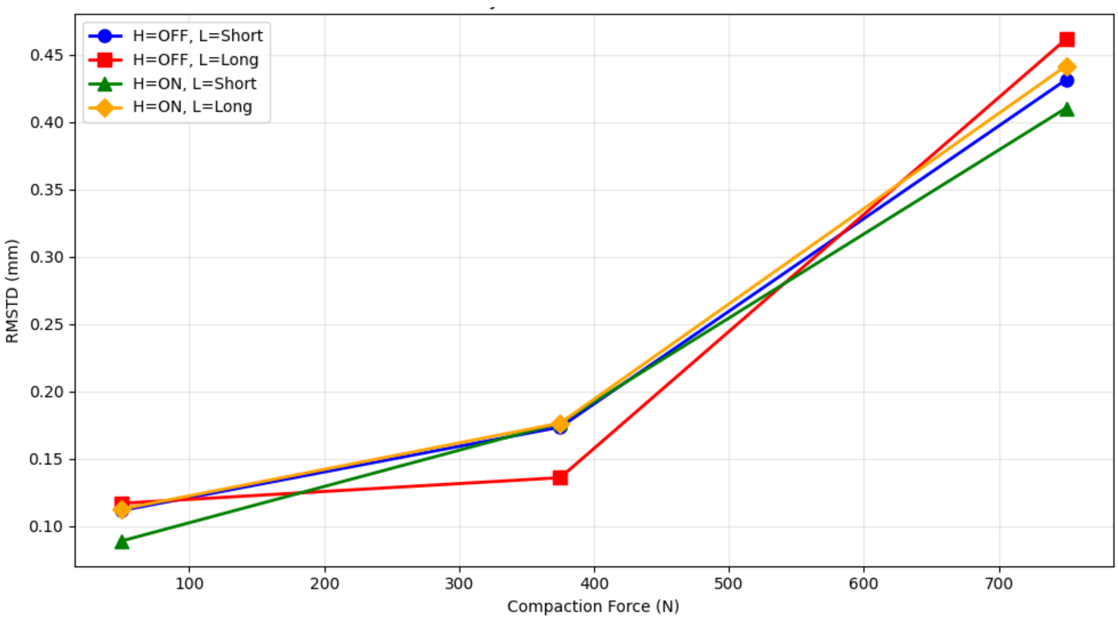

Figure 6.10. Interaction plot: transverse displacement vs Compaction Force (by H and L combinations)

These results further demonstrate that compaction force in isolation cannot produce meaningful width changes at moderate processing temperatures, even at maximum force levels. Width change requires the combined influence of compaction force and elevated temperature, identified in the generalised factorial study. The focused compaction force study therefore highlights a fundamental distinction between the activation conditions of the two deformation mechanisms. At moderate temperatures, the width change mechanism remains inactive due to insufficient viscosity reduction, whereas transverse displacement is activated solely by mechanical loading and occurs even at lower thermal conditions. Figure 6.10 illustrates this behaviour, showing the consistent increase in transverse displacement with compaction force across all combinations of external heating and lie time.

6.5 Summary

The combined results of the factorial parameter study and the focused compaction force investigation demonstrate that compaction-induced width change faces fundamental limitations as a gap-defect mitigation strategy. Most critically, the achievable magnitude of width expansion remains substantially below practical requirements. In the generalised study, the maximum width change achieved under extreme parameter settings was 0.28 mm, representing only 14 % of the 2 mm gap-threshold typically requiring rework. In the focused study, compaction force up to 750 N at moderate tooling temperature produced no statistically significant width change distinguishable from measurement noise. Consistent with the findings of Jamora et al. [200], these results indicate that width change during first-ply deposition represents the upper bound for achievable transverse flow for parameter ranges investigated, and that recompaction over additional plies would yield further reduced effectiveness.

Beyond the limited magnitude of width change, a fundamental coupling exists between the two deformation mechanisms examined. The experimental conditions required to maximise width change simultaneously activate transverse displacement. This occurs because compaction force, the primary driver of width expansion under thermally softened conditions, is also the dominant driver of shear-induced lateral tow movement. The focus study confirms that temperature control cannot decouple these responses. Moderate temperatures suppress width change through insufficient viscosity reduction but do not eliminate transverse displacement, which remains fully active under mechanical loading alone. As a result, no processing window was identified in which beneficial width change can be achieved without inducing detrimental tow displacement that compromises layup accuracy and laminate quality.

These findings reveal an asymmetry in the activation of the two mechanisms. Width change requires combined thermal–mechanical activation and becomes inactive at moderate temperatures, whereas transverse displacement is driven solely by compaction force and persists across all thermal conditions examined. This divergence imposes a fundamental constraint on the effectiveness of recompaction-based gap reworking: parameter combinations that promote useful transverse flow inevitably produce unacceptable tow displacement, while combinations that suppress displacement eliminate meaningful width-change capability.

Ultimately, alternative rework or defect-mitigation strategies must be considered. More broadly, the results demonstrate that any compaction-based defect-mitigation approach must address width expansion and transverse displacement simultaneously, as their shared dependence on compaction force creates an unavoidable coupling that represents a mechanistic, rather than parametric, limitation of the process.

6.6 Limitations

While the experimental design utilised in this study successfully measured the effects of the parameters on width change, the single replicate per experimental condition increases measurement uncertainty and reduces the statistical power for detecting smaller effects. Although the 2^5 factorial design in Experiment 1 provides systematic coverage of the parameter space, additional replicates would improve the precision of effect estimates and enable more robust statistical inference.

An additional limitation is that tow tack was not directly measured in this study. While thermal parameters were systematically varied, and their effects on material deformation quantified, the role of tack in governing adhesion and displacement behaviour was inferred qualitatively rather than measured directly. The relationship between thermal conditions, resin tackiness, and the transverse displacement mechanism represents an area requiring further investigation with dedicated tack measurement techniques.

The mechanistic explanations for width change and transverse displacement presented in this study are supported by empirically derived statistical correlation but lack validation through frictional or viscoelastic modelling. The observed parameter dependencies are consistent with established composites processing theory. Additionally, cure kinetics were not explicitly monitored or modelled, meaning it is difficult to account for the influence of any early-stage cure-induced stiffening which may have occurred, particularly for interpreting the influence of lie time. Further work should incorporate rheological characterisation, cure kinetics monitoring, and physics-based modelling to provide mechanistic validation for the empirically observed trends.

While width change has been shown in the literature to diminish with quantity of underlying tows, the same relationship has not been studied in terms of the transverse displacement mechanisms. The experimental design in this study reflects the finding in terms of diminishing effect of width change, as studying only the first-ply deposition represents the maximum achievable width change, however the same may not be said of transverse displacement, where underlying substrate layer quantity and composition may play an important role in modulating the transverse displacement mechanism.

Chapter 7. Real-time trajectory control for defect mitigation

In this chapter an online control method for AFP deposition and trajectory execution is proposed and tested. The new method enables real-time monitoring and correction of deposition paths based on a laser line scanner (LLS) profilometry method. The new method utilises KUKA's Robot Sensor Interface (RSI) software add-on, and a novel version of the Interfacing Toolkit for Robotic Arms (ITRA), upgraded to support a 12-degrees-of-freedom system. The integration of the profilometry system for the detection of placement effects and the on-the-fly correction method through ITRA and RSI is managed and enabled through a custom architecture supported by the Robotic Operating System (ROS) middleware. Previous research focused on online detection rarely translates to corrective actions, instead focusing on locating and characterising defects for further processing and logging. The approach documented in this Chapter enables low-latency on-the-fly correction of deposition paths within the robot's standard six degrees of freedom and also across six external axes including the material deposition axis, informed by the defect detection in real-time. AFP programming uniquely links deposition control with external axis control, requiring integration into path planning. By linking the detection of defects with reactive deposition path corrections, this method enables the mitigation of placement induced defects and a reduction in their size in a controlled manner, respecting the non-holonomic constraints of tow deposition in AFP.

7.1 Existing work in real-time control within AFP

Various technologies have been explored and developed for real-time detection of defects within AFP. For a more detailed review readers are directed to [208]. Some of the key methods explored include machine vision and digital image processing, thermographic monitoring, optical methods including Optical Fibre-Bragg (OFB) sensor, optical coherence tomography, fibre edge detection sensors, and LLSs, stress wave analysis, and integrated systems involving multimodal methods.

Real-time control of AFP processing parameters with a relatively low latency has been demonstrated. An online path correction method has been demonstrated, using scanned data from a previously laid tow's edge location to alter the subsequent tow's placement trajectory. The data was scanned from the material 1100 mm ahead of the layup point by a forerunner LLS mounted on a Computer Numerical Control (CNC) controlled robot. This correction was performed after the tow was laid and does not account for misalignment in the tow being laid, only relative position of the tows planned centre line with respect to the previous tow [154].

In [209], the authors use a wide array of sensors in pre-deposition (LLS for tow width, Laser Profile Scanner (LPS) for tow thickness), deposition (Infrared pyrometers monitoring temperature, and load cells adjusting compaction levels) and post-deposition (LLSs measure the width and thickness of the entire laminate). Experimentally, the authors used the system to detect wrinkle-type defects in the materials, and programmatically controlled deposition force and temperature locally over the defect in order to mitigate the through-thickness propagation of the defect. The work is instructive in indicating the complexity of process parameters involved within AFP manufacturing and indicates that non-homogeneity may be a desirable characteristic of process parameter control to avoid or mitigate defects.

Online path corrections using visual sensing to indicate positional defects in the layup were achieved more recently by Cao et al., [210]. An intermediate path planning action was performed between the point where the deviation was detected and a look forward point where the correct path could be rejoined, such that the nonholonomic constraints of the deposition path were maintained during the correction. The roller remains in contact with the layup surface and always rolls toward the path's tangent, avoiding the roller's transverse shift. These transverse shifts are undesirable as they can result in early contact of tows with the layup surface, or in the exertion of transverse friction forces on the material, as well as limiting the effects of tow steering – where there is a deviation between the direction of travel of the incoming tow and the direction of deposition. The authors design and experimentally test the system with a cycle time of 50ms for image processing and running of an external control loop and limited the deposition speed in their experiments to 1000 mm/min [210].

To the best knowledge of the author of this Thesis, on-the-fly low latency path corrections, and multi-degree-of-freedom control techniques have not been previously explored within AFP research. This chapter addresses this gap.

7.2 ITRA

A cornerstone of the proposed method is the ITRA toolkit [211]. This is a C++ toolbox designed to integrate industrial robotic arms with server computers, sensors, and actuators, initially developed within the University of Strathclyde. ITRA offers real-time positional control in cartesian and joint spaces. The toolkit is designed for use with KUKA robots controlled using the fourth generation KUKA robot controller (KRC4) which is divided into three main systems: a Graphic User Interface (GUI) for writing and executing robot programs, an embedded version of Windows XP running the GUI, and a separate operating system called VxWorks, which controls all robot drives. The Windows XP and VxWorks operating systems are entirely separate, and any information that is passed between them is sent over a virtual Transmission Control Protocol/Internet Protocol (TCP/IP) connection within the KRC4 architecture. ITRA is compatible with all KRC4 robots with the KUKA software add-on RSI [212]. The Robot Sensor Interface (RSI) add-on runs under the VxWorks operating system in real-time, enabling communication between the robot controller and an external system. Cyclical data transmission from the robot controller to the external system takes place parallel to the execution of the KUKA Robot Language (KRL) program. The robot controller

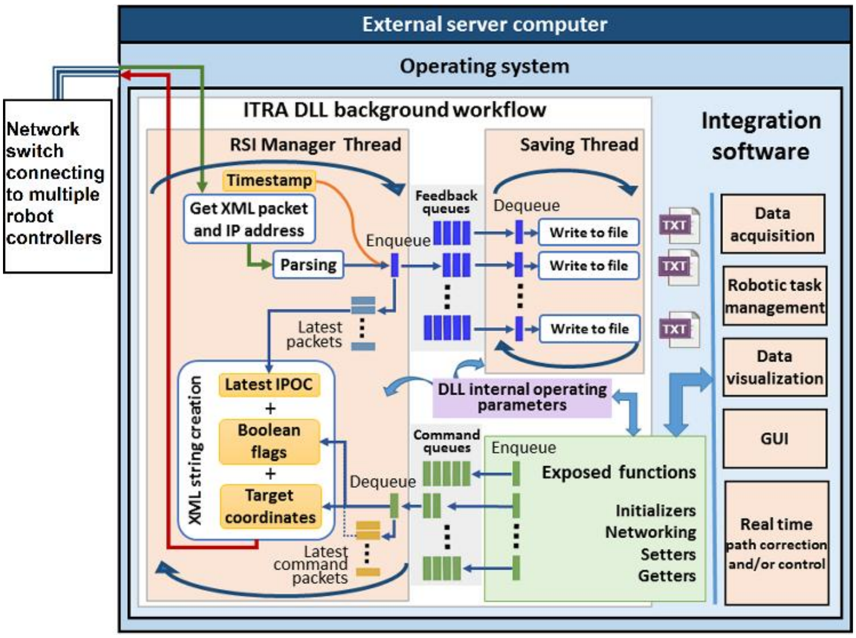

Figure 7.1. Workflow of the ITRA toolkit architecture, after [211]

communicates with the external system via the Ethernet User Datagram Protocol (UDP/IP) protocol. Figure 7.1, from [211], illustrates the workflow of the ITRA toolkit architecture. Once ITRA is loaded into a hosting programming environment, the constructor initialises fundamental variables to support UDP/IP connection with the robots. ITRA has been used extensively across a range of robotic applications, for example in 3D surface reconstruction in unplanned environments [213], autonomous and optimised trajectories for NDT inspection [214], and battery disassembly operations [215].

7.2.1 Expanded ITRA

The ITRA toolkit was developed for real-time control of a six-axis industrial robot. This however was problematic for an AFP system which relies on additional degrees of freedom for control of external axes, including the add roller inside the end-effector, responsible for material deposition, the linear axis upon which the KR120 is mounted, and the external rotating mandrel onto which material can be deposited. As such, collaborative work was undertaken to upgrade the existing ITRA package to support an expanded number of degrees of freedom.

The primary difference between the original and the expanded version of ITRA is the addition of external axis position, velocity and acceleration values to the XML data template which controls the structure of both the ASCII packets sent by RSI to the server computer, and the packets received by RSI from the server computer. The expanded XML template includes up to 6 additional degrees of freedom beyond the conventional 6-axes included in the robot system. This supports the external carriage, (E1), rotating mandrel, (E2), and tow add roller, (E3), within this AFP system included in these chapters, while having an additional three free external degrees of freedom which may be used for parameter control, or the introduction of further controllable elements in the end-effector, effectively future proofing the system.

It should be made clear here, the contributions of the author of this Thesis lie in the conceptualisation and testing of the expanded ITRA toolkit and in the development of and testing of the ROS-based real-time control method for sensor integration with the developed ITRA toolkit, and not in the toolkit design itself, which is the contribution of the original designer of the system, C. Mineo. As such, descriptions of the expansion to the system included below are included in this Thesis to the degree that they support the subsequent contribution by this Thesis' author but are not presented as an individual contribution to knowledge from this Thesis in their own right.

7.2.2 Validation of Robot Control

To demonstrate the effectiveness of the upgraded ITRA toolkit, initial trials were conducted using the AFP systems and controlling the trajectory from the server computer running the ITRA toolkit through a MATLAB interface. Movement commands were sent as offsets from the current Tool Centre Point (TCP) position of the robot. Firstly, an offset in the X and Z axes was sent, then a second offset in the Y and Z axis. The E3 external axis controlling the material deposition is programmed to move the distance of the sum of the squares of movement in the X, Y, and Z axis during the movement. Between move commands, the position

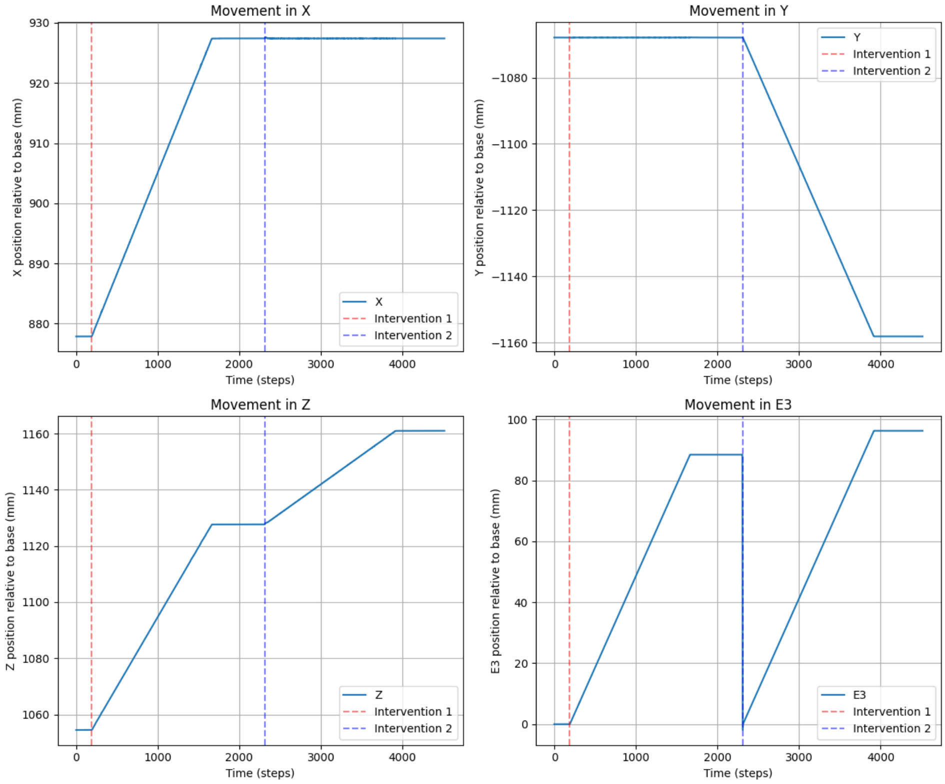

Figure 7.2. Relative movement in axes X, Y, Z, and E3

of the E3 axis is reset to 0 virtually within the KRC controller but does not actually drive the add roller back to 0. Figure 7.2 illustrates the feedback positions in the X, Y, Z, and E3 axes over discrete timesteps as received from the robot controller during operation. The vertical dashed lines indicate the moments when positional updates were sent via the server computer. As shown, interventions in the X-Z axis (Intervention 1) and the Y-Z axis (Intervention 2) resulted in corresponding movements in each axis.

7.3 ROS-Based Online Defect Detection and Correction System

The main contribution of this chapter is detailed below. Here a novel ROS based system was developed, enabling closed-loop, low latency defect mitigation strategy which leverages the trajectory control of the upgraded ITRA system with advanced defect detection methods using the LLS integrated into the AFP head. The section below details the design philosophy behind the ROS based system, describes the architecture of the ROS nodes, integration of the LLS, and describes both the defect detection and correction algorithms developed to mitigate the extent of placement inaccuracy induced gaps. In the subsequent section testing and evaluation of the method is discussed.

7.3.1 System Design Philosophy

ROS [216] is an open-source set of software libraries and tools developed to allow for building of robotic applications. ROS enables integration of communication between the different hardware aspects of a robotic system through a unified communication network. ROS runs on a server computer running Ubuntu Linux. The system described in this chapter was developed in the ROS1 system. Since the development of the system, ROS2 has been released. This architecture of this differs in noticeable ways to ROS1. The Real-time trajectory control method described here is described in terms of its construction using ROS1 terminology. For future work the method should be updated to make use of ROS2, however this extends beyond the scope of this chapter.

The ROS structure defines nodes, services, topics, and messages. These performs different tasks and communicate in different ways. Nodes can be thought of as agents. Each node performs a specific action and can both publish data to or receive data from specific topics. Topics are thus the main mode of communication between nodes. A topic is similar to a messaging board. Each topic has a specific name, and nodes can publish data to a specific topic. Other nodes can subscribe to a specific topic to receive the data being published to it. Topics publish messages, which are the specific instances of data published to a topic. These can contain various data types defined at once or a single data type. Services are a method for nodes to request a specific action or receive a specific piece of data from another node. The format of the request-response is defined in the service definition file.

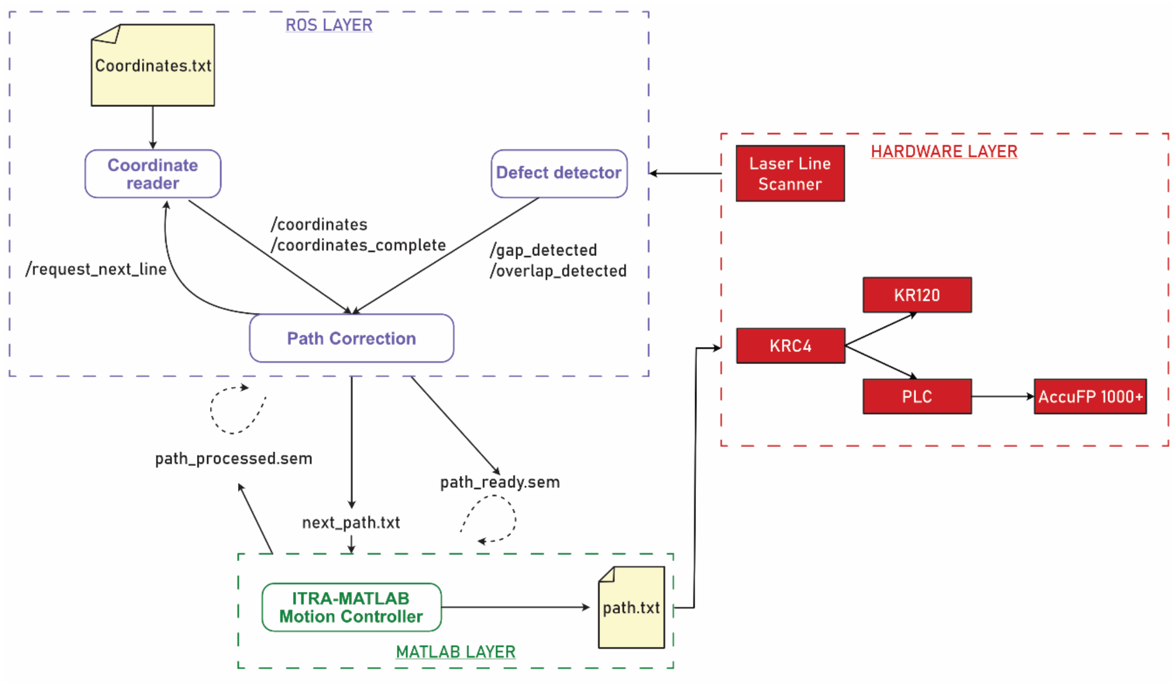

Figure 7.3. System architecture diagram showing three computational layers (ROS, MATLAB, Hardware), the data flows between them, and the physical AFP cell components. Dashed circular arrows between ROS and MATLAB layers represent the filesystem semaphore handshake.

7.3.2 System Architecture

As illustrated in Figure 7.3, the architecture is organised into three distinct computational layers: a ROS layer that handles sensing, decision making, and waypoint management, a MATLAB layer hosting the ITRA motion control programs handling interpolation and packaging of coordinates in the XML format appropriate for execution on the robot hardware, and a hardware layer comprising of the laser line scanner, KRC4 controller, KR120 Robot and AccuFP 1000+ end-effector connected through a Programmable Logic Controller (PLC). Each layer communicates with the next through a mechanism suited to the components within it. ROS publishers and subscribers are used in the ROS layer, a filesystem semaphore protocol was used at the ROS-MATLAB interface, and the KUKA RSI hard real-time UDP protocol is used at the MATLAB-Hardware interface.

7.3.3 ROS Layer

The ROS layer runs on a Ubuntu-Linux workstation and contains three nodes. Together they implement a demand-driven pipeline in which no waypoint is dispatched to the robot until the previous one has been fully executed and confirmed. The nodes communicate via ROS topics and their interface to the MATLAB layer uses the filesystem semaphore protocol described in section 7.3.3.3.

7.3.3.1 Coordinate Reader

The coordinate reader is the upstream entry point of the AFP path execution pipeline. It functions as a text file-based waypoint sequencer. It loads the full set of pre-planned robot waypoints from disk at startup, then releases them one at a time to the path correction node in response to explicit requests and coordinated by a filesystem semaphore protocol. It does not perform any geometric computation or sequence alterations; its sole function is orderly, request-driven despatch of waypoints into the file system.

On startup the reader loads coordinates from a specified file path, reads the file line by line, skipping blank lines, splits each line and converts the line to a float data type, validates at least nine values are present (X, Y, Z, A, B, C, E1, E2, E3), and appends the first nine values as a list. The complete coordinate set is stored in memory as $self.coordinates$.

The reader then advertises two latched publishers */coordinate_reader/coordinates* and */coordinates_complete*. The reader also subscribes to the topic */request_next_line*.

The node then connects to processing semaphores and subscribers and only sets *system_initialised* once at least one subscriber is detected. The coordinate reader does not send any waypoints initially, instead the first dispatch is only triggered when an explicit request arrives on */request_next_line*.

The coordinate dispatch mechanism uses two state-flags to enforce strict one-at-a-time sequencing:

- *Coordinate_sent*: true from the moment a waypoint is published until the processed semaphore confirms it has been consumed by the MATLAB layer.
- *next_line_requested*: true when a */request_next_line* message has been received but not yet fulfilled.

The semaphore timer (*check_semaphore_status*) drives the state machine: if *coordinate_sent* is True and *path_processed.sem* exists, *coordinate_sent* is reset to False. If *coordinate_sent* is False and *next_line_requested* is True and neither semaphore file exists, *send_next_coordinate()* is called. Unexpected semaphore files trigger *cleanup_semaphores().* When *current_line* reaches *total_lines*, True is published on */coordinates_complete* instead of a waypoint, signalling the end of a sequence.

7.3.3.2 Defect detection node

The defect detection node interfaces directly with the Micro-Epsilon laser line scanner via the ScanControl Linux SDK [217] including the Aravis-based libmscan C library, and liblinllt C++ wrapper. The node receives raw cross-sectional height profiles of the layup surface at 50 Hz through an interrupt-driven callback.

The defect detection node creates four ROS publishers at module scope: */gap_detected, /overlap_detected, /gap_widths*, and */overlap_widths. /gap_detected* and */overlap_detected* are subscribed to by the path correction node and inform the sliding window validation of defects within the correction algorithm. */gap_widths* and */overlap_widths* contain richer data on the detected defects in a deposition sequence but are not consumed by any node, instead they are available for external logging, visualisation, and debugging.

7.3.3.3 Path Correction node

The path correction node is the decision-making core. It subscribes to both the waypoint stream from the Coordinate reader and the scalar defect measurements from the defect detection node. Before applying any correction, it requires confirmation through a sliding consensus window of five consecutive non-zero defect readings, preventing single-scan artefacts from causing unnecessary trajectory modifications. When a defect is confirmed, a non-holonomic path correction algorithm based on the method described by Cao et al., [210], computes incremental lateral and heading adjustments that progressively close the measured error across subsequent segments rather than attempting a single abrupt correction. This algorithm is described in Section 7.3.7 and displayed in pseudo code in Appendix 7C: Path correction algorithm.

Three programs exchange waypoint data in a strictly ordered sequence: the coordinate reader dispatches pre-planned waypoints, the path correction node applies defect-based correction and writes the corrected waypoints to the disk, and the IRTA-MATLAB motion control layer reads the corrected waypoints and executes it on the robot. Since the ITRA-MATLAB motion control layer exists outside of the ROS system, coordination of the exchange of waypoint data is controlled via a filesystem semaphore protocol.

path_ready.sem is created by the path correction node and confirms that the corrected waypoints have been written to *next_path.txt* and is ready for the ITRA-MATLAB motion controller to consume.

path_processed.sem is created by the ITRA-MATLAB motion controller and confirms that the layer has read *next_path.txt* and that the python layers may proceed to the next waypoint.

The full handshake protocol for a single waypoint cycle is shown in Appendix 7B: Full handshake protocol, in pseudo code.

7.3.4 MATLAB Layer

The MATLAB layer contains the ITRA-MATLAB motion controller, which translates corrected waypoints into kinematically smooth, time-discretised trajectories and executes them on the KUKA robot in 12 ms real-time. It is isolated from ROS firstly because the KUKA RSI protocol imposes a hard 12 ms cycle deadline incompatible with ROS's non-deterministic scheduling, and secondly due to version incompatibility with the ROS topic system and the MATLAB version required for the ITRA-MATLAB motion controller.

At each cycle the ITRA-MATLAB controller polls for *path_ready.sem*, reads *next_path.txt*, and immediately creates *path_processed.sem* to release the ROS layer. It then generates a trapezoidal velocity profile and re-samples the path at 12 ms intervals using interpolation. The resulting N-step trajectory is then serialised and by the compiled MEX function *write_12DoFs_coordinates()* into path.txt in KUKA RSI XML [212] attribute format and streamed to the robot controller. The MATLAB layer communicates with the rest of the system exclusively through the two semaphore files and path files on the shared filesystem.

7.3.5 Startup Sequencing

The programs have a dependency ordering at start-up. The correct launch sequence is:

1. Defect Detection Node: the scanner hardware is initialised at import time before the ROS node starts. If launched after the path correction node, early scan measurement will be missed, but the 5-reading consensus window prevents any correction being triggered until a complete window has accumulated.
2. Coordinate Reader: this node is launched before the path correction node, and the latched publishers ensure that a late-connecting path correction node subscriber immediately receives the most recent coordinate value, but the */request_next_line* handshake will not begin until the path correction node is active.

3. Path correction node: this node waits one second before issuing the first */request_next_line*, providing time for subscriber detection in coordinate reader to complete.
4. ITRA-MATLAB motion controller: establishes the connection to the KUKA KRC4 controller, then immediately begins polling for *path_ready.sem.* This file only appears after the path correction node has received and corrected a waypoint from the coordinate reader node, enforcing the correct ordering implicitly.

The semaphore protocol enforces the full four-way dependency without any explicit synchronisation barrier; the MATLAB layer cannot process without *path_ready.sem*; the path correction node cannot create it without a coordinate from Coordinate Reader; Coordinate Reader will not dispatch it without */request_next_line* from the path correction node. The defect detection node is the only node that runs independently throughout, publishing measurements whether the robot is moving, stationary, or mid-correction.

7.3.6 Defect Detection Algorithm

The defect detection was handled by a new custom algorithm as described below. The system processes 1-dimensional cross sectional height profiles captured by the LLS mounted on the AFP head. The method is purely geometric and does not rely on material properties or learned models and is therefore transferable to any layup configuration. The defect detection node is not involved in the filesystem semaphore protocol. It does not read or write *path_ready.sem* or *path_processed.sem*, nor does it access *next_path.txt*, and has no knowledge of the waypoint sequencing state. This separation means that defect detection runs continuously and independently of the robot's motion state. On every cycle, functions *publish_gap_data()* and *publish_overlap_data()* are called regardless of whether defects are detected. When no defects are present, a fload32 value of 0.0 is published on */gap_detected* or */overlap_detected*. This unconditional publishing means the path correction nodes sliding window validation of defect continues even when no defect is present without stalling waiting for defect data that never arrives. In the case of no defects the processed paths are “corrected” with no impact from defects, i.e., they are passed to the motion control node without alteration.

Each one-dimensional profile acquisition returns a discrete set of measurement pairs of the form:

$$P = ((x_i, z_i))_{i=1}^{N} \quad (7.1)$$

Where $x_i \in \mathbb{R}$ is the lateral position in mm along the scanner baseline, $z_i \in \mathbb{R}$ is the measured surface height in mm, and N is the number of valid measurements after sensor-level filtering up to a maximum of 2048 x-z pairs. The profile is acquired at a fixed frame rate via a hardware interrupt callback, and each frame is treated as an independent observation.

Only points that fall between the physical detection window and within valid depth bounds are retained. This acceptance criteria can be expressed, as:

$$P_f = \{ (x_i, z_i) \in P \mid \; X_{min} \le x_i \le X_{max} \wedge Z_{low} \le z_i \le Z_{high} \} \quad (7.2)$$

Where $X_{min} = -7.0\ mm$, $X_{max} = 7.0\ mm$. $Z_{low} = 50\ mm$, $Z_{high} = 300\ mm$. The values of ±7.0 mm were chosen as these allowed for focusing of a region of interest in the signal covering the full width of the tow currently being deposited, and the edges of the previous tow. The values for Z_{low} and Z_{high} were established empirically and operate on the raw numerical output of the laser profilometer. Under the configured sensor parameter, out-of-range or invalid returns are encoded as exactly 0.0 mm, while ROS timestamp values appended to the profile data produce erroneous numerical outputs of the order 10^3 mm. The thresholds therefore serve to exclude both null returns and timestamp artefacts, while retaining the valid surface height measurements, which are scaled in the sensor output to a range between the two thresholds. The filtered profile is re-indexed so that the lateral coordinates per profile are strictly ascending:

$$x_1 < x_2 < x_3 < \cdots < x_n \tag{7.3}$$

The ordering is required for the finite difference gradient scheme used in the edge detection method.

Measurement noise is attenuated by using a three-point moving average filter, where the z values in x-coordinate order are convolved by the kernel:

$$h = \frac{1}{3}[1, 1, 1] \tag{7.4}$$

The kernel replaces each z_i value with the mean of itself and its two neighbours. The weights of each element are equal, hence the filter is mean preserving and will filter out high-frequency noise without shifting the baseline height.

$$\tilde{z}_i = \frac{1}{3}(z_{i-1} + z_i, +Z_{i+1}), i = 2, \ldots, N - 1 \tag{7.5}$$

Boundary values are preserved unmodified ($\tilde{z}_1 = z_1, \tilde{z}_n = z_n$) to avoid edge artefacts from zero-padding. This box filtering acts as a discrete low-pass element, suppressing high-frequency noise while preserving the large amplitude step discontinuities that characterise material edges.

A thresholded discrete first-order derivative operation is employed to detect discontinuities in the smoothed height profile. The local gradient is computed at each point in the profile, using three different schemes depending on the ordered x-position. The gradient is estimated using a central finite-difference scheme for interior points, and a forward/backward differences at the boundaries where $i = 1 \; or \; N$. The discrete gradient is computed as:

$$g_i = \{ \begin{array}{ll} \tilde{z}_2 - \tilde{z}_1 & i = 1 \\ \dfrac{\tilde{z}_{i+1} - \tilde{z}_{\,i-1}}{2} & 1 < i < N \\ \tilde{z}_N - \tilde{z}_{N-1} & i - N \end{array} \tag{7.6}$$

Edge classification is computed by thresholding the gradient against the threshold parameter τ_e:

$$e_i = \; +1 \; if \; g_i > \; +\tau_e \tag{7.7}$$

$$e_i = -1 \; if \; g_i < -\tau_e \tag{7.8}$$

$$else: e_i = 0 \tag{7.9}$$

A *rising edge* ($e_i = +1$) corresponds to a positive height step meaning a transition from a lower to a higher surface, for example from a gap or the substrate onto a deposited tow. A *falling edge* ($e_i = -1$) marks the reverse transition, for example from a tow to the substrate, or from an overlapped tow to the underlying tow. The threshold $\tau_e = 0.05 \, mm$ was selected empirically to reject noise-induced gradient spikes while remaining sensitive to genuine material boundaries. The ordered set of edges is defined as:

$$E = \{ \, i \mid e_i \neq 0\} \tag{7.10}$$

Defect classification requires a scalar reference representing the nominal, fully deposited tow surface height. The nominal surface height is estimated using a robust order-statistics estimator in the 70th sample percentile, mitigating bias introduced by negative outliers corresponding to material gaps:

$$z_{base} = Q_{0.70}(\{\tilde{z}_i\}_{i=1}^{N}) \tag{7.11}$$

A percentile-based estimator is preferred over the arithmetic mean, which would be systematically biased downward in the presence of large gaps, and over the mode, which is less stable for continuous height distributions. The estimator remains unbiased provided that the gaps covered no more than 30 % of the filtered profile width, corresponding to a gap size of 4.2 mm.

Between each pair of consecutive detected edge x coordinate indices $E_i, E_j \in E$ with i < j, a candidate plateau segment is defined as:

$$S_{ij} = \{ \, \tilde{z}_l \mid i < k < j\} \tag{7.12}$$

Three statistical descriptors are computed for each candidate segment:

$$\mu_S = mean \left(S_{ij}\right) \tag{7.13}$$

$$\sigma_S = std\left(S_{ij}\right) \tag{7.14}$$

$$w_S = x_j - x_i \tag{7.15}$$

A segment is accepted as a stable plateau only if it satisfies both of the following conditions simultaneously:

$$\sigma_S < \tau_\sigma \tag{7.16}$$

$$w_S > w_{min} \tag{7.17}$$

The stability condition ($Eq. 7.16$) ensures that the segment represents a genuinely flat surface rather than a noisy transition or ramp. The minimum width condition (Eq. 7.17) suppresses short lived artefacts below the spatial resolution of practical defect significance. Figure 7.4 displays a graphical description of the plateau evaluation for a signal representing a single tow with gaps on either side.

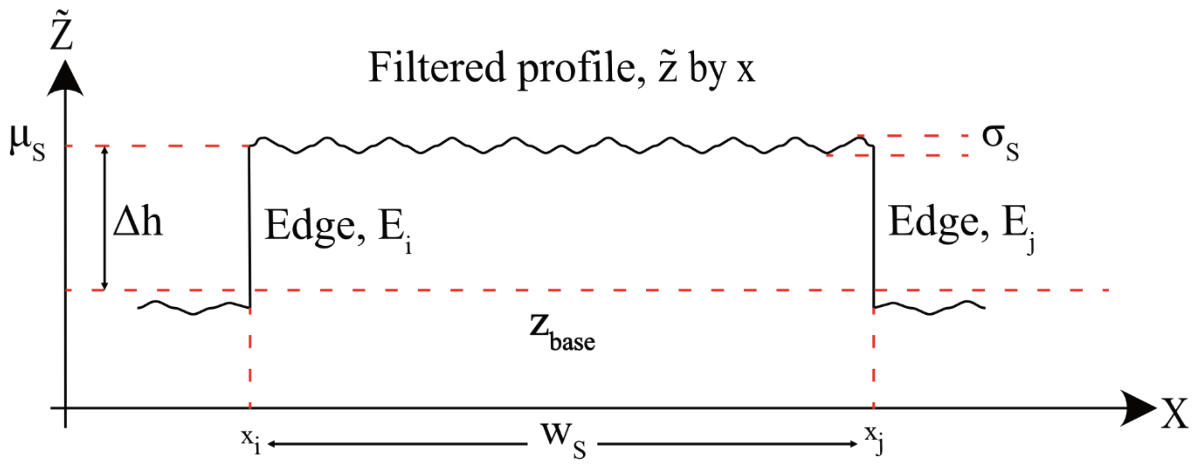

Figure 7.4. Graphical representation of plateau evaluation metrics

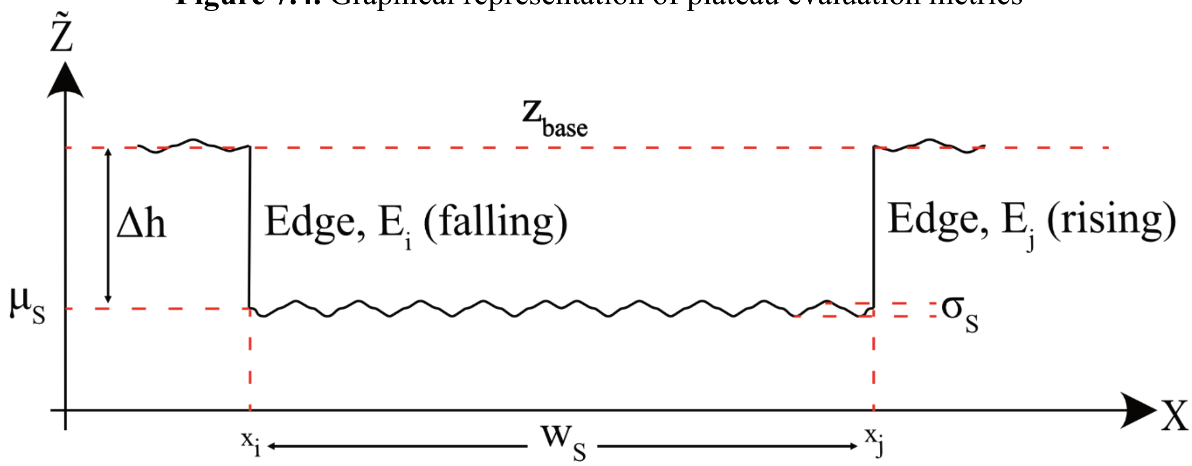

Figure 7.5. Graphical representation of a gap signal

Through the above methods, defects were classified as gaps or overlaps accordingly. A stable plateau that is significantly below the baseline, and whose bounding edges represent a falling edge followed by a rising edge, was classified as a gap:

$$e_i = -1, e_j = +1, w_S > w_{min}, \sigma_S < \tau_\sigma, z_{base} - \mu_S > \Delta h_{min} \qquad \text{Eq. 7.18}$$

The quantity $z_{base} - \mu_S$ represents the depth of the gap below the nominal tow surface. This pattern corresponds to a region where the tow is absent, exposing the underlying substrate or tooling surface. Figure 7.5 displays a representation of a gap signal with the evaluation metrics.

A stable plateau that is significantly over the baseline, flanked by a rising edge then a falling edge was classified as an overlap:

$$e_i = +1, e_j = -1, w_S > w_{min}, \sigma_S < \tau_\sigma, \mu_S - z_{base} > \Delta h_{min} \qquad \text{Eq. 7.19}$$

The quantity $\mu_S - z_{base}$ represents the height excess above the nominal surface. This pattern corresponds to a region where the incoming tow is deposited on top of the previous tow, creating a local thickness buildup. Figure 7.6 displays a representation of a gap signal with the evaluation metrics. For each confirmed defect, the */gap_detected* or */overlap_detected* topics are populated with a message containing the defect width and flag.

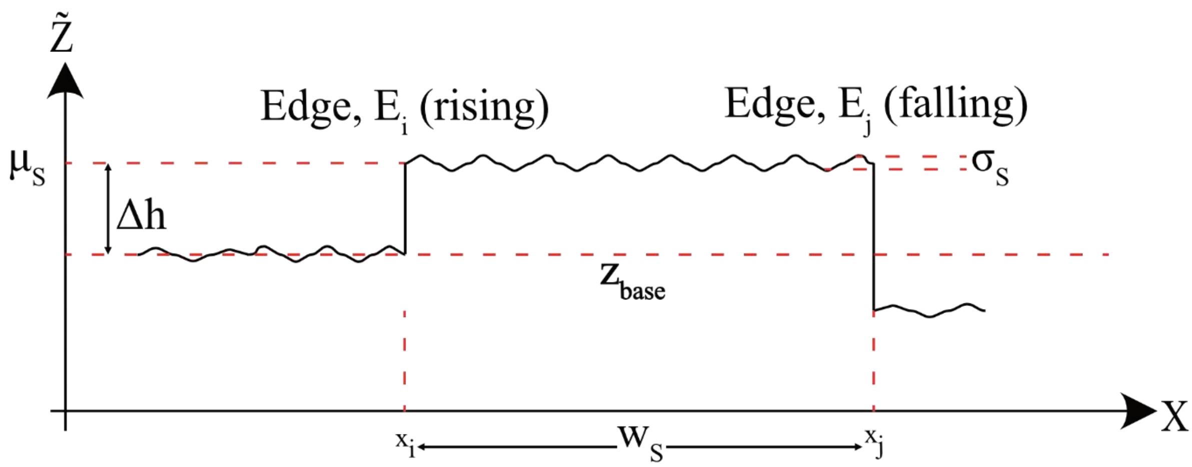

Figure 7.6. Graphical representation of an overlap signal

Table 7.1. Defect characterisation record fields output per detected defect

Field	Definition	Symbol
Start position	x-coordinate of the leading edge, x_i	x_{start}
End position	x-coordinate of the trailing edge, x_j	x_{end}
Centre position	$\frac{x_{start} + x_{end}}{2}$	x_c
Width	$w_S = x_j - x_i$	w
Depth (gaps only)	$z_{base} - \mu_S$	d
Height (overlaps only)	$\mu_S - z_{base}$	h

A flow diagram of the defect detection process is shown in Figure 7.7. The complete algorithm is shown in Appendix 7A: Defect detection algorithm, structured in pseudo-code. The algorithm was executed once per acquired profile frame at the callback rate of the laser profilometer of 25 Hz.

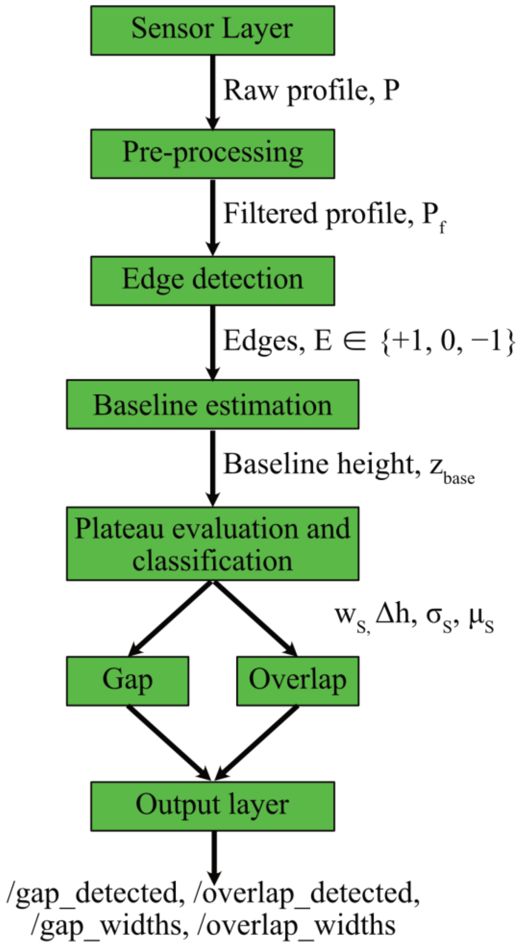

Figure 7.7. Flow diagram of defect detection process

7.3.7 Correction Algorithm

With the defect characteristics being broadcast through the */gap_detected* or */overlap_detected* topics. The path correction node computes corrections to the deposition trajectory in order to mitigate the extent of the defects. The corrections algorithm is based on work by Cao et al., [210], who introduced non-holonomic constraint-based corrections. In this Thesis the correction method is applied within the real-time enabled system within the deposition of the current tow, rather than the subsequent tow. The pursuit geometry (look-ahead point, arc radius, angular velocity) follows Cao et al. [210]; the proportional control law, stability constraints, defect validation scheme, and system integration are original contributions of this work.

The system architecture consists of two coupled classes. The outer class *PathCorrection* manages the defect validation, target computation, coordinate I/O, and ROS communication. The inner class, *NonHolonomicPathCorrector,* implements the per-segment geometric correction low.

The first step in correction is the validation of the defect detection. A single profile measurement reporting a defect is insufficient to trigger a path correction, as isolated false positives from sensor noise or transient surface irregularities must be rejected. Therefore, a consensus-based validation scheme was employed. Specifically, a defect is confirmed only if it is observed consistently across a window of minimum consecutive profile frames, n_{req}. The defect measurement history is considered a sliding window of the most recent measurements, as:

$$H_k = \left\{d_{\{k-n_{req}+1\}}, d_{\{k-n_{req}+2\}}, \ldots, d_k\right\} \subset \mathbb{R} \tag{7.20}$$

Where $d_k \geq 0$ is the reported defect width in mm, at profile frame k with $d_k = 0$ indicating no defect detected. A defect is validated when all the measurements in the window exceed the minimum detection threshold d_{thr}:

$$Validated \Leftrightarrow \forall\, d_i \in H_k : \; d_i > \; d_{thr} \tag{7.21}$$

Upon validation, the correction target is computed as the median of the window, providing a robust estimate of the true defect magnitude that is insensitive to outlying measurements within the window:

$$\bar{d} = \widetilde{H_k} \tag{7.22}$$

The median is preferred over the arithmetic mean as an estimator of central tendency because it is insensitive to the boundary measurements at index $k - n_{req} + 1$ and k, which may capture partial defect transition. In the implementation, $n_{req} = 5$ and $d_{thr} = 0.0\,mm$ (any non-zero measurement qualifies), with corrections inhibited once the correction_applied flag is set.

The sign convention for the correction target δ^* is defined by the defect type and the required physical response. A gap indicates that the current tow is being placed too far from the previous tow, so the next tow must be shifted laterally towards the previous one (negative x-direction). An overlap, conversely, indicates that the tow is being placed too close, requiring a shift away (positive x-direction).

The remaining lateral error during a correction step is evaluated using:

$$e_k = \; \delta^* - \delta_k \tag{7.23}$$

Where δ_k is the cumulative lateral correction applied up to step *k*. The correction sequence terminates when $|e_k| \; \leq 0.1\,mm$, i.e., when the defect is no longer present as the tows have become contiguous.

The AFP end-effector in motion is modelled as a non-holonomic vehicle subject to a no-lateral-slip constraint; at any instant, the robot can only move in the direction it is pointing. The state of the corrector at segment step *k* is described by tow cumulative qualities:

$$\delta_k \; \in \; \mathbb{R} \tag{7.24}$$

$$\varepsilon_k \; \in \; \mathbb{R} \tag{7.25}$$

δ_k is the cumulative lateral position correction, in mm, and ε_k is the cumulative orientation correction, in radians. Both states are initialised to zero at the start of each correction sequence and accumulate across successive path segments. The path segment length ℓ_{seg} is computed from the Euclidean distance between consecutive waypoint coordinates p_{k-1} and p_k.

$$\ell_{seg} = \|p_k - p_{k-1}\|_2 = \sqrt{\Delta x^2 + \Delta y^2 + \Delta z^2} \quad (7.26)$$

The time elapsed during traversal of segment k at nominal linear layup speed velocity v_{layup} is:

$$\Delta t_k = \frac{\ell_{seg}}{v_{layup}} \quad (7.27)$$

The orientation of the steering correction is computed using a modified vector pursuit formulation [210]. A look-ahead target point is defined in the local frame of the corrector at lateral deviation y_{tar} and longitudinal distance x_{tar} from the current position:

$$y_{tar} = e_k = \delta^* - \delta_k \quad (7.28)$$

$$x_{tar} = \min(L, 5 \cdot \ell_{seg}) \quad (7.29)$$

Where L is a configurable maximum look-ahead distance. The adaptive term $5 \cdot \ell_{seg}$ prevents the look-ahead from extending beyond the local path geometry. The desired steering angle to the look-ahead point is:

$$\theta = 2 \cdot \arctan\left(\frac{y_{tar}}{x_{tar}}\right) \quad (7.30)$$

This form of the pursuit angle is derived from the inscribed angle theorem applied to a circular arc passing through the current position and the look-ahead point. The radius of the curvature of that arc is:

$$r_t = \frac{x_{tar}^2 + y_{tar}^2}{2 \cdot y_{tar}} \quad (7.31)$$

The corresponding angular velocity required to follow the arc at speed v_x is:

$$\omega_t = \frac{v_x}{|r_t|} \cdot sgn(r_t) \tag{7.32}$$

Where the sign of r_t , $sgn(r_t)$, encodes the direction of the curvature. Positive values indicate a left-hand correction, and negative values a right-hand correction.

At each path segment step, incremental correction to the lateral position and heading are computed using a proportional law with a scalar gain, g:

$$\Delta\delta_k = g \cdot e_k \cdot \Delta t_k \tag{7.33}$$

$$\Delta\varepsilon_k = g \cdot \omega_t \cdot \Delta t_k \tag{7.34}$$

The increments are independently clamped to prevent abrupt actuator commands that could violate mechanical constraints or destabilise the deposition process:

$$\Delta\delta_k \leftarrow sat_{[-lim,+lim]}(\Delta\delta_k) \tag{7.35}$$

$$\Delta\varepsilon_k \leftarrow sat_{[-0.1,+0.1]}\,(\Delta\varepsilon_k) \tag{7.36}$$

Where $sat_{[a,b]}(x) = \max(a, \min(x, b))$ denotes the saturation function that restricts the control input updates to lie within the specified lower bound a and upper bound b. The cumulative states are then updated:

$$\delta_{\{k1+\}} = \delta_k + \Delta\delta_k \tag{7.37}$$

$$\varepsilon_{(k+1\}} = \varepsilon_k + \Delta\varepsilon_k \tag{7.38}$$

An additional anti-windup limit is applied to the cumulative position correction to prevent runaway in the event of a sustained residual error:

$$\delta_{\{k+1\}} \leftarrow sat_I\left(\delta_{\{k+1\}}\right)\ where\ I = [\,-5|\delta^*|, +5|\delta^*|\,\})\tag{7.39}$$

$$\varepsilon_{\{k+1\}} \leftarrow sat_{[-0.3,+0.3]}(\varepsilon_{\{k+1\}}) \tag{7.40}$$

At each segment step, the nominal six-dimensional robot waypoint, $p\ = (x, y, z, A, B, C)$, where (x, y, z) are Cartesian coordinates, and (A, B, C) are Euler angles (yaw, pitch, roll) in degrees, is modified by applying the cumulative corrections:

$$x' = x + \delta_k \tag{7.41}$$

$$A' = A + \varepsilon_k \cdot \left(\frac{180}{\pi}\right) \tag{7.42}$$

The y and z coordinate, and the pitch and roll angles, are left unchanged. This is suitable for the test set explored here, where material is laid up onto a flat tooling plate, requiring correction only in the x-direction relative to the layup direction, and about the yaw axis. The corrected waypoint $p' = (x', y, z, A', B, C)$ is written to the semaphore-synchronised output file for immediate consumption by the robot executor.

Each defect validation event triggers at most one correction sequence. The correction sequence terminates, and no further corrections are issued or the current defect, when either of the following conditions is satisfied:

$$|e_k| = |\delta^* - \delta_k| \leq \varepsilon_{tol} = 0.1\ mm \tag{7.43}$$

or when the defect is no longer reported in the sliding window signalling that the defect sequence has ended. In either case, the *correction_applied* flag is set to True, inhibiting further adjustments. This single fire design prevents cumulative overcorrection.

The complete protocol is displayed in Appendix 7C: Path correction algorithm in structured pseudo-code. The algorithm has two concurrent execution contexts: the defect validation loop, which runs at the ROS subscriber callback rate, and the correction application loop which s synchronistical with each incoming path waypoint.

Figure 7.8 shows a representation of the path correction algorithm as a flow chart.

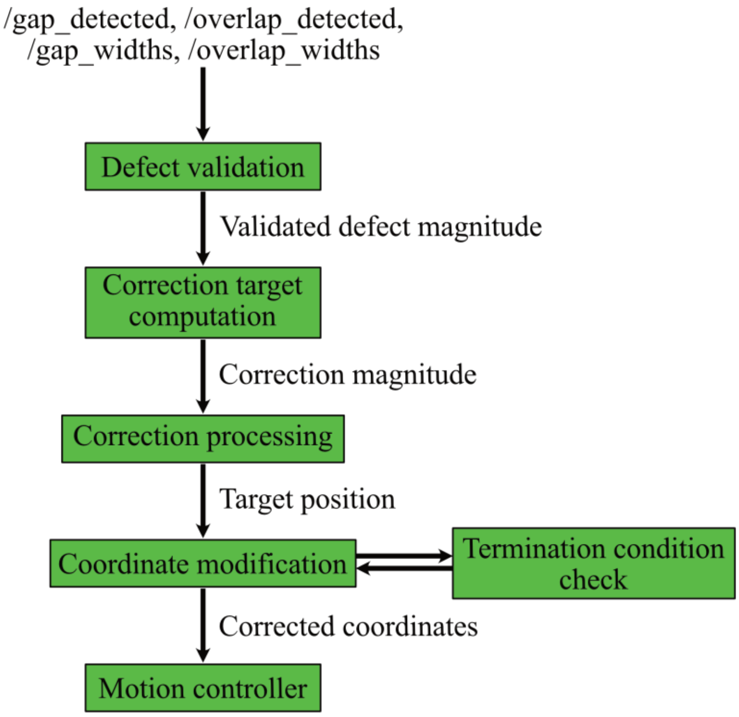

Figure 7.8. Flow diagram of defect correction process

The correction law (Eqs. 7.33 – 7.40) is a discrete-time first-order proportional controller with anti-windup. Convergence of the cumulative correction δ_k to the target δ^* is guaranteed providing effective loop gain $g \cdot \Delta t_k$ remains below 2 for all segments, a condition ensured in practice by the per-step clamp and anti-windup limit equation (Eqs. 7.35 and 7.39).

The single-fire design ensures that the correction sequence does not interact with subsequent defects until the *correction_applied* flag is explicitly reset. This prevents compounding corrections across multiple defect windows from accumulating unbounded lateral drift.

The clamping of the orientation increments to $|\Delta\varepsilon_k| \leq 0.1\, rad \approx 5.7°$ per segment ensures that the heading correction remains within the mechanical joint-rate limits of the KUKA robot throughout the correction sequence. This is a vital safeguard, as the RSI add-on functions below the safety level of the KRC4 controller, and thus unsafe motions will be attempted even if they exceed joint torque limits or configuration boundaries.

Table 7.2. ITRA-MATLAB motion control system parameters and default values

Symbol	Default	Units	Physical Interpretation
$\mathbf{v_{max}}$	25	mm/s	Maximum TCP speed along path segment
$\mathbf{a_{max}}$	100	mm/s^2	Maximum TCP acceleration/deceleration
$\mathbf{\Delta t}$	0.012	mm	RSI hard real-time cycle period
$\mathbf{d_{min}}$	1	-	Dead-band displacement threshold for motion trigger
$\mathbf{n_{req}}$	9	-	Expected number of coordinate values per waypoint
computerIP	192.168.3.200	-	IP address of the control computer (UDP socket)
robotIP	192.168.3.1	-	IP address of the KUKA robot controller (KRC4)
port	59152	-	RSI UDP communication port number

7.3.8 ITRA-MATLAB Motion Controller

The MATLAB layer operates as a closed-loop real-time motion controller. Formal presentation of the ITRA method is included at [211]. For an in depth understanding of the mathematical basis of the method, readers are directed to the original work, rather than presenting the fundamental work here. The layer ingests target waypoints produced by the path correction node, applies kinematically consistent speed-constrained trajectory interpolation, transmits the resulting path to the robot via a KUKA RSI UDP link at a real-time cycle of 12 ms, and reads back actual end-effector pose feedback from the robot. Appendix 7D: ITRA-MATLAB motion control presents the complete motion control procedure in structured pseudo-code. Table 7.2 summarises all the configurable parameters in the ITRA-MATLAB motion control system and their roles in the algorithm.

7.4 Experimental Evaluation

With the system developed, validation tests were performed to, firstly, optimise the tuneable parameters in the path correction node, and examine the defect mitigation performance for a range of defect sizes.

7.4.1 Experimental Setup

The primary contribution of this chapter is the design and implementation of the system described in the above sections. The experimental results that follow are intended to demonstrate that this system operates as designed under real manufacturing conditions, with real material and live robotic placement. They are not presented as comprehensive characterisation of the correction performance envelope which would require hardware modifications beyond the scope of the current work. Within these constraints, the results establish proof-of-concept for real-time reactive gap mitigation across a range of industrially relevant defect sizes and provide a meaningful step forward towards automated defect mitigation and rework.

The AFP system comprised of a KR120-R3100 industrial robot, mounted on a linear track and controller through a KRC4 controller. Mounted on the end of the KR120 is the AccuFP1000+ [71] AFP end-effector detailed in previous chapters, and displayed in Figure 7.9. The system featured a heated tooling plate as the deposition substrate. The material was Hexcel® M91/34%/UD194/T700GC 6.35 mm width prepreg tows [180]. The laser line scanner was a Micro-Epsilon ScanControl 3012-50 2D/3D profilometry sensor [203]. The sensor returns profile data at a sampling rate of 50 Hz as an array of 2048 height values arranged in their position in the x-direction (perpendicular to the direction of the tow).

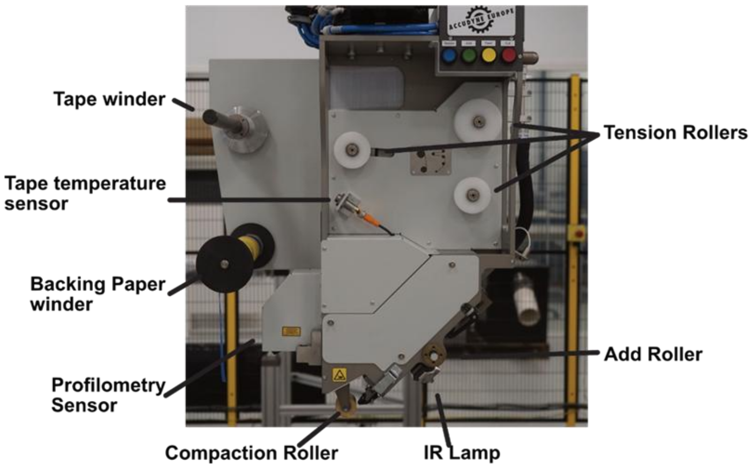

Figure 7.9. Single tow Accudyne 1000+ end-effector [71].

7.4.2 Hardware limitations

Several key limitations should be addressed with respect to the system. Firstly, the location of the LLS in the system used is sub-optimal for this method. Since the LLS is positioned behind the robot TCP, the defect detection is being performed on data from behind the point at which the correction is being applied. This lag is seen in the correction results.

Secondly, tow slippage on the roller is not accounted for. Research [218] has shown that this accounts for a large percentage of the cause of defect misplacements. As such, though corrections can be made with the defect size in mind, the translation of the correction to the placement path is not fully realised.

Finally, the current version of the ITRA 12DoF upgrade functions in a way such that a full path segment must be completed before the next path segment can be sent, including any applied corrections to the next path segment. In the original version of ITRA, the system could receive on-the-fly updates to target positions and function in 4 ms real-time. If this were enabled for the real-time trajectory control system, corrections could be initiated instantaneously, rather than after each path segment completes.

7.4.3 Correction Algorithm Parameter Study

The experimental results presented here serve to validate the operational capability of the system under real manufacturing conditions, rather than to characterise an optimised control law. Given the hardware constraints described above clean parametric relationships between control parameters and correction performance were not expected and are not observed. The parameter study is therefore presented as an empirical search for a workable operating point, rather than a systematic optimisation. An initial tow was laid, followed by the deposition of a tow using the proposed system with a 2.5 mm gap between the two tows. The parameters lookahead distance (L) and gain (g) were varied between four levels of (L) and three levels of (g). The final gap size was measured using vernier callipers, and the settling distance along the tow path was measured using a steel rule. For settling distance, the value was recorded at the point where the gap width stabilised to the final gap size. Smoothness was scored between 1-3 (low to high) qualitatively. Figure 7.10 shows a schematic of the physical parameters and evaluation metrics for the parameter study. Figure 7.11 - Figure 7.14 display the correction results for the varying parameter settings.

The correction results across the look-ahead distance and gain combinations tested are shown in Table 7.3. No monotonic relationship between either parameter and final gap size, settling distance, or smoothness is evident across the range tested, reflecting the confounding influence of the hardware constraints on the system response. Despite this, the parameter sweep identifies several configurations capable of substantially reducing the 2.5 mm gap within the correction distance, with full closure achieved at multiple settings.

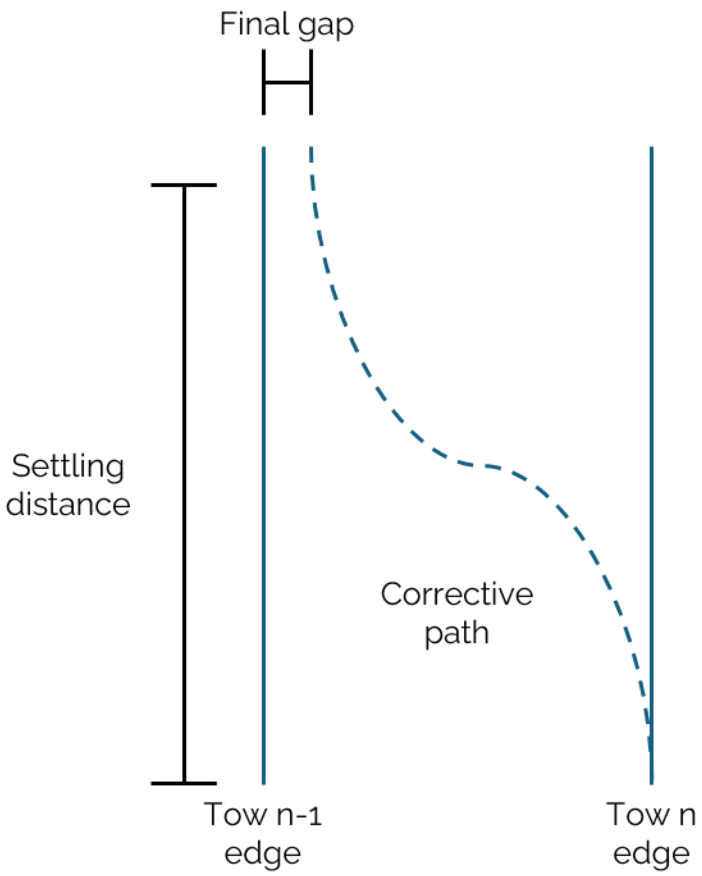

Figure 7.10. Schematic of physical parameters and evaluation metrics for correction algorithm parameter study

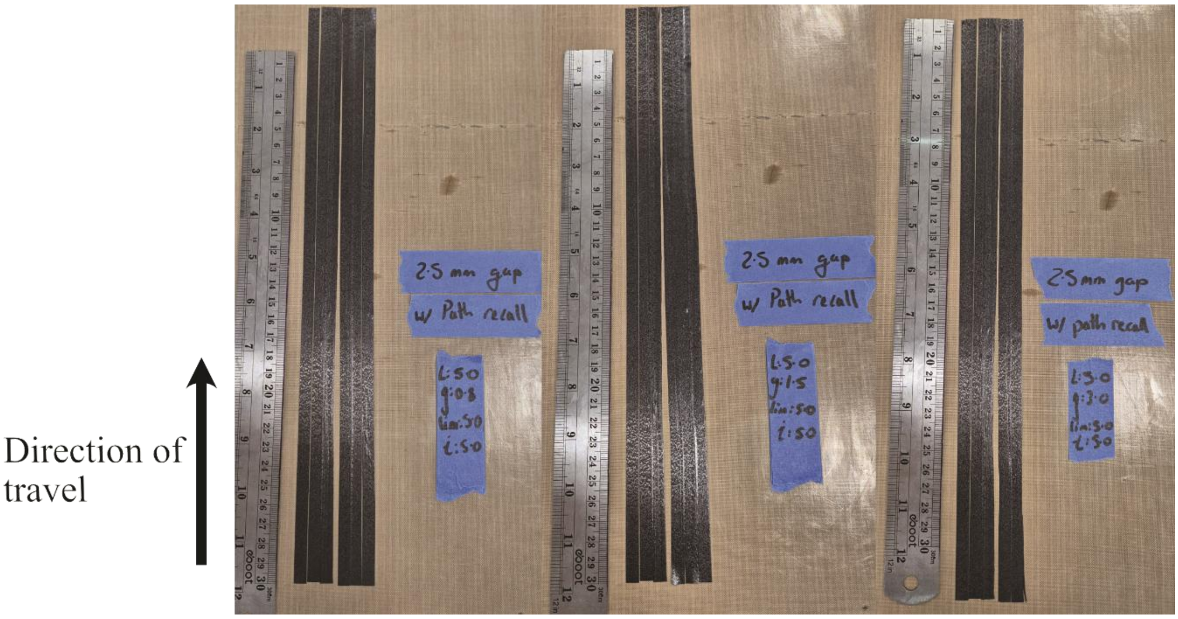

Figure 7.11. 2.5 mm gap mitigation for L = 5.0 mm with varying gain values (0.8, 1.5, 3.0)

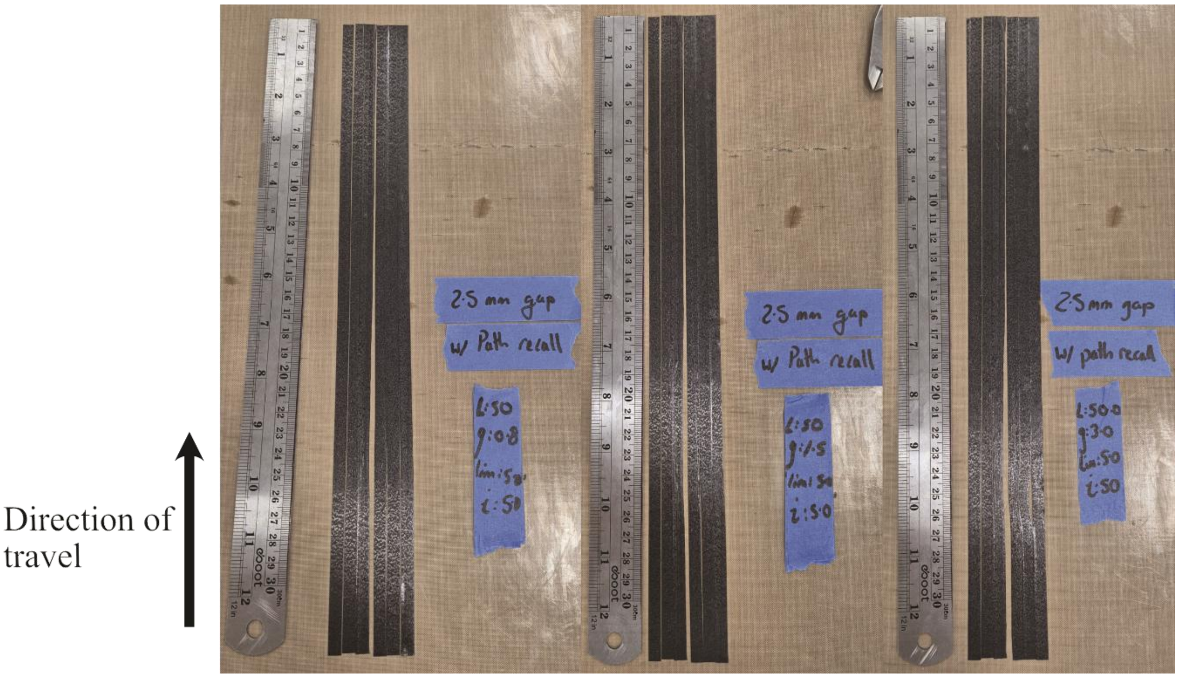

Figure 7.12. 2.5 mm gap mitigation for L = 50.0 mm with varying gain values (0.8, 1.5, 3.0)

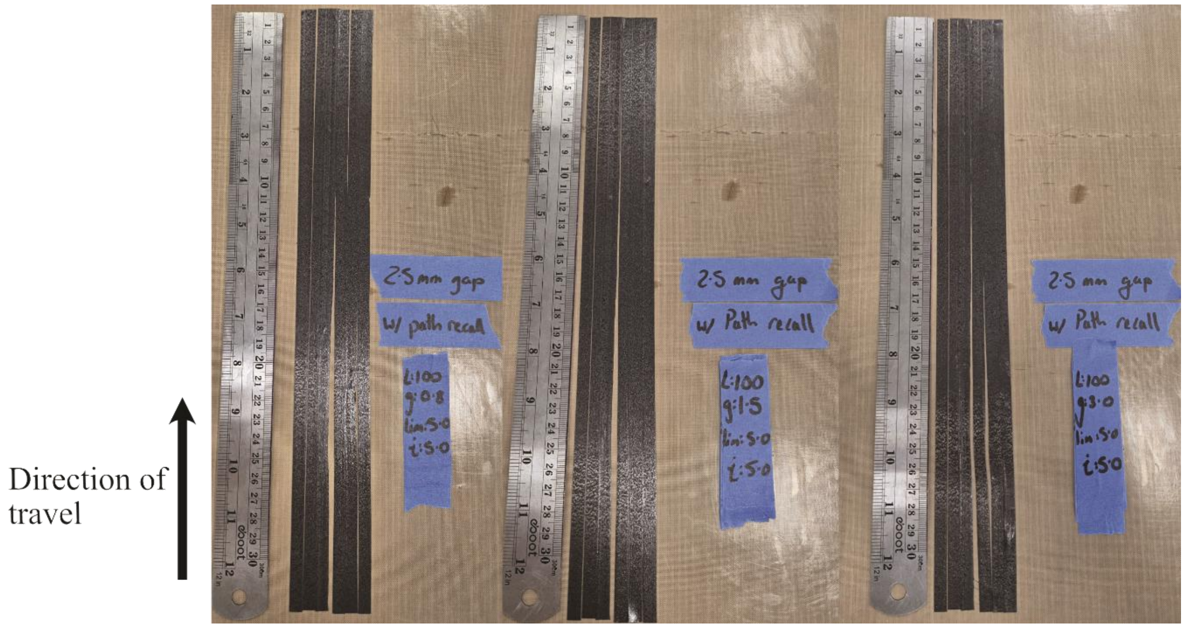

Figure 7.13. 2.5 mm gap mitigation for L = 100.0 mm with varying gain values (0.8, 1.5, 3.0)

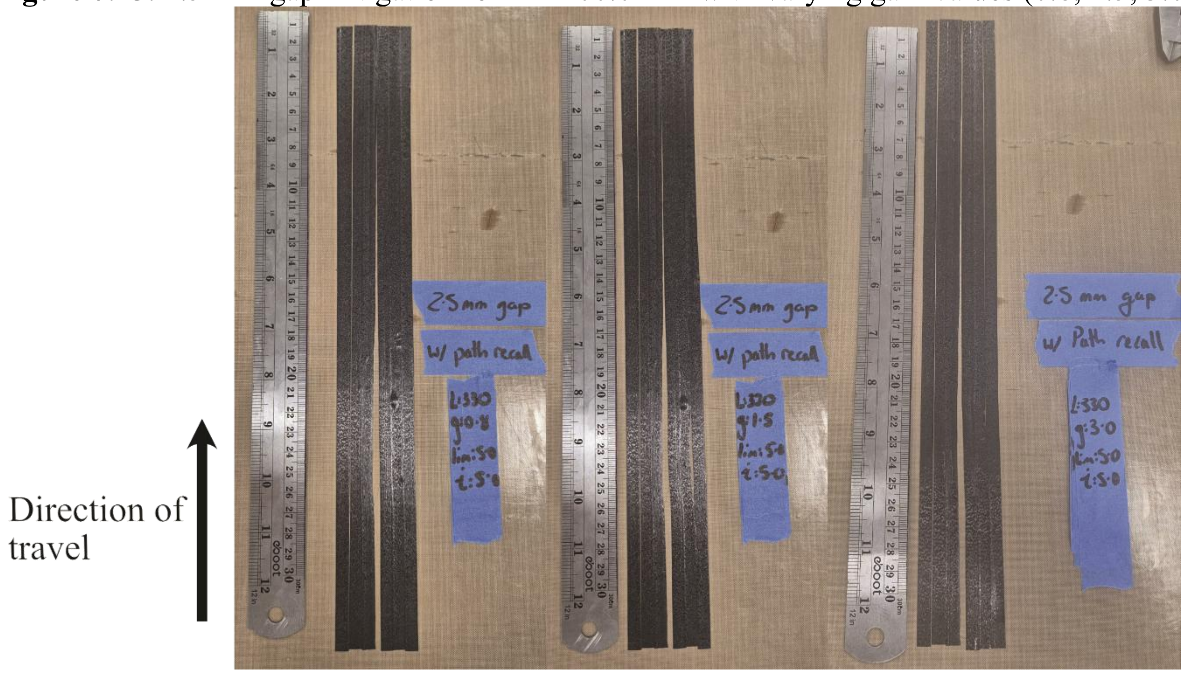

Figure 7.14. 2.5 mm gap mitigation for L = 330.0 mm with varying gain values (0.8, 1.5, 3.0)

Table 7.3. correction results for varied levels of look-ahead distance, and gain

Look-ahead distance (mm)	Gain	Final gap size (mm)	Settling distance (mm)	Smoothness (1-3)
5	0.8	0.00	300	3
5	1.5	0.25	150	3
5	3.0	0.25	200	2
50	0.8	0.45	200	3
50	1.5	0.25	330	3
50	3.0	0.25	150	1
100	0.8	0.75	200	2
100	1.5	0.00	250	3
100	3.0	0.00	200	1
330	0.8	0.00	250	3
330	1.5	0.00	250	3
330	3.0	0.25	150	3

Table 7.4. Optimised parameter settings for smoothness, settling distance, and final gap magnitude, and composite desirability score

Solution	L	gain	Smoothness Fit	Settling Distance Fit	Final Gap Fit	Composite Desirability
1	330	3	3	150	0.25	0.873580
2	5	1.5	3	150	0.25	0.873580
3	330	1.5	3	250	0.00	0.763143

A formal optimisation minimising final gap and settling distance, while maximising smoothness, summarised in Table 7.4 selects L=330 mm and g=3.0 as the primary operating point on the basis of composite desirability across all three metrics, and this configuration is carried forward for generalisation testing.

The central experimental finding of this chapter is presented in Figure 7.15, which shows the correction performance of the system at the selected operating points across initial gap sizes ranging from 0.0 mm to 4.5 mm.

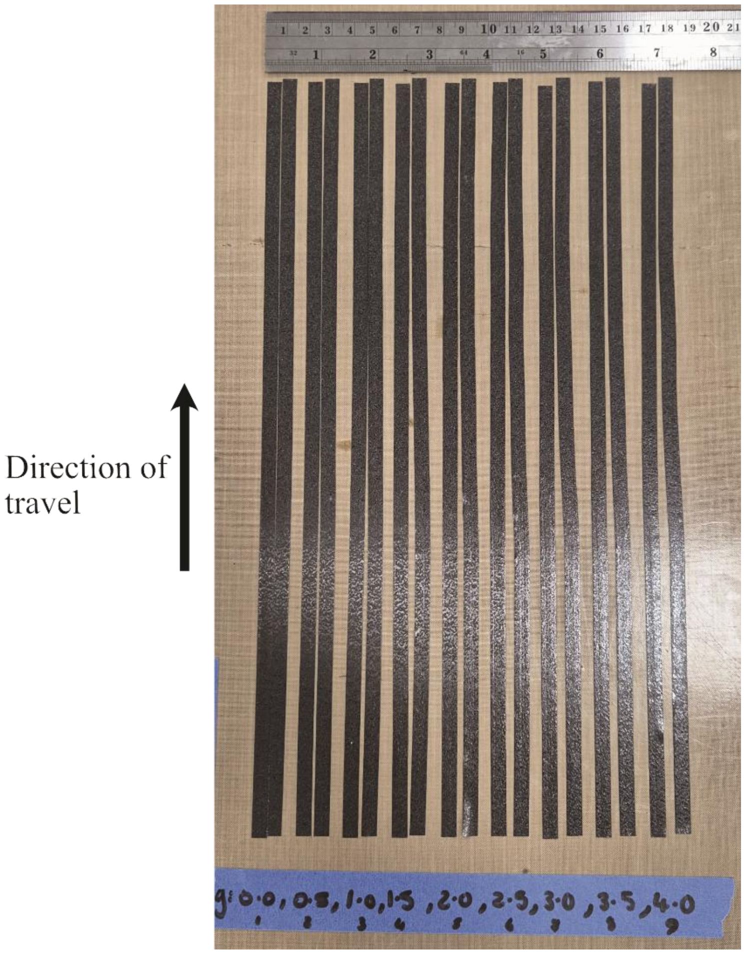

Figure 7.15. Defect mitigation at optimal correction algorithm settings for various gap sizes

For small initial gap sizes, the system performs well, with corrections driving residual gaps toward zero. However, a progressive increase in final gap size is observed with increasing initial gap width, indicating that the correction algorithm does not scale linearly with defect magnitude. This is consistent with the fundamental operating principle of the vector pursuit controller: the correction magnitude applied per path segment is constrained by the look-ahead distance and gain settings, imposing an effective ceiling on the rate at which gap error can be reduced. For larger initial gaps, this ceiling is reached before full closure is achieved within the available correction distance. Critically, even or the largest gaps tested, a meaningful reduction in defect magnitude is achieved.

It is worth noting that more aggressive parameter settings where higher gain or shorter look-ahead distance could in principle reduce the residual gap for larger defects by increasing the per-segment correction magnitude.

7.5 Conclusions

In this chapter, a real-time reactive defect mitigation system is proposed and tested. The system utilises the enabling technologies of an upgraded ITRA robot motion control system for a 12 degree of freedom robotic cell, a custom built defect detection method using Laser profilometry, correction through a modified vector pursuit algorithm taking into account non-holonomic constraints, all joined together in a custom architecture using the ROS middleware, and a semaphore based communication layer.

The system successfully mitigates the gap defects tested by performing corrections to the placement gap to close the size of the gap without abrupt changes that may result in tow wrinkling. Within the constraints of the hardware limitations of the AFP system the system was tested for a variety of gap sizes between 0.0 mm to 4.5 mm and showed mitigation of gap defects even for the largest size of gaps. There was however a progressive increase in the size of the final gap between tows, as the size of the initial gap increased, showing a limitation of the method for large gap size. More abrupt corrections may have allowed for the closing of larger gaps over shorter distances but pose the risk of introducing tow wrinkling through excessive tow steering.

7.6 Discussion

This chapter introduces a novel automated method of mitigation of defects that, while still reactive, brings this reaction much closer temporally to the onset of defects. As such the extent of the defects can be mitigated in the first instance, limiting the required time and labour for rework as a subsequent step in the AFP process. The system presented here sits in-between design-led defect avoidance, such as the work of Matveev et al., [166] combining dry fibre layup with RTM, or strategic design of the outer plies to ensure defect free outer surfaces as in [167], [168], and the remediation of defects through rework as has been discussed and analysed throughout this Thesis. The capability for on-the-fly corrections allowed for effective mitigation, rather than rework, potentially removing the need for, or reducing the effort involved in manual rework as a subsequent step.

The modularity of the ROS middleware enables future development of bolt-on additions to the system. For instance, in the method displayed in this chapter used static initial path coordinates previously generated using an offline path planning software. An online path generation module could be added on in future developments, which could enable a more fully end-to-end automated material deposition system. Additionally, integration of data from additional defect detection modalities could enrich the detection capabilities. For instance, research from Pantoji et al., [218], highlight that lateral slippage of tows on a roller cause a large proportion of placement errors in AFP. Real-time trajectory control based on the lateral position of the tow on the roller could allow for correction closer to the source of the defect and reduce the need for lateral correction whilst a tow is being deposited.

Additionally, the work presented by Nguyen et al., [209], showcased effective real-time control of compaction pressure in response to defect detection both before and after the nip point in the end-effector. Joining this control lever together with trajectory control could yield impressive results in defect mitigation and rework across a wider range of defects.

Further, the work of Burke et al., [150], and Koptolev et al., [149], shows great promise in the ability to use advanced machine learning techniques for the prediction of defects prior to their occurrence during placement. Effective mitigation strategies informed by the predictive powers of these methods could eliminate rather than mitigate or rework some defects.

Chapter 8. Conclusions and Further Work

Defects in AFP require significant attention to increase the market acceptance of the method and streamline the technique [14], [23]. Untreated defects have been repeatedly revealed to lead to detrimental knockdowns in mechanical performance in finished parts. The inspection and reworking of defects accounts for a disproportionately high amount of the cycle time of the entire manufacturing cycle [28], [29], [30]. While significant work has been done in developing mature inspection techniques [13], [208], little to no research has been conducted into the subsequent reworking step itself [31], [174]. The rework process currently resembles a craft of sorts, undocumented in literature and unrecorded by those who implement it [31]. Where any account of the procedure is made, it is generally understood to be a time- and labour-intensive manually performed exercise. This stands in direct opposition to the objective of AFP in automating the composite manufacturing operation. Furthermore, the effect of the reworking activity is not widely known and has not been extensively studied; quality assessments are primarily visually cosmetic assessment. While this may give an approximation of the quality recovery from defective to reworked laminates, the extent and reliability of this recovery is not known.

To address the significant gap in knowledge in this area, a fully end-to-end body of research was required. This begins with analysis of industry best practices and research relating to defect rework in AFP. This is followed by a detailed analysis of the method and its effects, culminating with the development and testing of novel methods of reworking. These novel methods may address the issues surrounding automation, reduce cycle time and optimise quality and financial outputs.

8.1 Summary of Work

Through the review of the existing literature, most previous research effort was directed towards understanding defects and/or developing mature intelligent inspection systems, whereas very little research has been directed towards the reworking step. While the understanding of the impact of defects and improving the inspection methods are of critical importance, there is merit in exploring the subsequent reworking step in more detail, especially given the total absence of either standard procedures or automation for this activity.

Interviews with leading experts from industry yielded broad validation to the conclusions drawn from the literature review and the aims of this Thesis. There was unanimous agreement amongst the experts regarding the high capital costs linked to AFP research and manufacturing, the lack of standardisation in rework and the need for further automation. The majority of experts agreed that inspection and rework are the primary bottlenecks to more efficient AFP, and that visual inspection is still the primary method for defect detection and rework evaluation. The expert outreach activity served to both validate the conclusions drawn from the literature review and the objectives of the Thesis. Importantly, the diversity of viewpoints represented by the different experts, being leading figures in academic research, manufacturing, and aerospace consultancy respectively, showcases the universality of the viewpoints, rather than being application specific opinions.

Through the experimental work performed in Chapter 4, a first formal analysis of the reworking methods was presented. Principally this analysed the effect in terms of damage to the surrounding material through various reworking methods. The output of this is a first of its kind set of best practices for performing the reworking activity. These best practices set a benchmark from which further work within the Thesis and by researchers can be undertaken to optimise the activity. Additionally, the output of the exploratory stage, comprised of the literature review, expert outreach, and rework process analysis, confirmed the need for further investigation of the effect of reworking, as this has not been previously presented in the literature, and is only loosely implied to be understood by the experts in purely cosmetic terms.

The effect of rework was analysed through various methods. Firstly, a novel benchtop-AFP cell was developed and utilised, which itself forms a basis for a test bed for the further democratisation of the AFP process.

Ultrasonic NDT of the three classes of manufactured coupons revealed that a residual out-of-plane waviness existed for reworked samples, which resembled more closely the defective samples tested than those pristine. This implied that while surface-level improvements to the laminate were secured through reworking, a gap in quality existed between reworked and fully pristine samples. This was confirmed by SEM of the microstructure of samples manufactured through conventional AFP, which showed elevated levels of ply-ply disturbance in the reworked samples compared with the pristine samples, though not to the same extent as the defective samples. Further analysis of the mechanical performance of the three classes of samples under ISO 14125 bending conditions revealed that the stiffness of the reworked coupons was marginally lower than the pristine samples, and a corresponding marginal knockdown in stress transfer capability was seen. Taking the evidence from Ultrasonic NDT, SEM micrographs and the mechanical testing together, it can be said that reworking under the best practices presented in Chapter 4 on the whole restores the quality of the parts to near-pristine levels, but with an elevated level of sensitivity to the execution of the manual process which may introduce tow disturbances which degrade the load carrying capacity of the coupons.

The work in Chapters Chapter 4 and Chapter 5 describing the analysis of the reworking process and effect of the process respectively are important in two ways. Firstly, since neither of these studies are present in the literature, their analysis serves to deepen the understanding of the process across industry and academia. Secondly, the analysis provides assurance for manual reworking that following the proposed best practices can allow for effective quality assurance in the final structures and reduce the need for concessions on the part of manufacturers.

With the implications of the effect of manual reworking in mind, investigation into automated methods was undertaken under two streams of work. Firstly, controlled variation of compaction force was explored as a potential method for the reworking of gap type defects in chapter 6. This was analysed in terms of the effect of the variance of the main processing parameters on the deformation mechanisms involved. It was revealed that an undesirable coupling exists between the transverse displacement of the tow and width change. At process parameter tunings where width change is achieved, unacceptable levels of transverse displacement were also seen.

The second stream of research into automated reworking and defect mitigation methods took the form of the development and testing of the real-time positional control method for defect mitigation, described in Chapter 7. Here existing motion control systems were upgraded and developed into a ROS-based end-to-end defect detection and mitigation system. The system was trialled and was shown to successfully mitigate the extent of gaps of ranging initial width.

8.2 Reflection on Aims and Objectives

The primary motivation for this research is the inefficiencies cited in the AFP process in the inspection and rework stage of the process. The aim and objectives of this Thesis, as laid out in Chapter 1 were as follows. The two research questions were defined as:

(Q1) What is the impact of reworking defects on part quality?

The impact in question is cosmetic, mechanical, and in terms of impact of reworking for machine time and operator labour. By determining the impact of rework as a practice, the case for process improvements, innovations or optimisation is made evident.

(Q2) How can reworking be improved?

Given the assessment from question (Q1), the reworking process may be improved to yield minimal negative impact to the laminate, or to the cycle time of typical AFP production, or improvements may made to efficiency approaching fully autonomous AFP.

Objectives were defined within each of the research questions as:

(Q1.O1) Examine the manual reworking process in line with the current state of the art practices.

(Q1.O2) Suggest guidelines for manual reworking, to inform further study of the activity with reduced variability.

(Q1.O3) Examine the effect of reworking in terms of geometric consistency in the laminate and part performance and determine the effective reduction in the mechanical performance knockdown induced by defects.

(Q2.O1) Investigate viable methods for increasing the effectiveness of reworking and reducing the process efficiency reductions incurred by manual rework.

(Q2.O2) Develop automated methods of reworking that do not incur the process efficiency reductions associated with manual reworking, while maintaining the defect mitigation and quality control in the parts.

(Q2.O3) Validate the developed methods of automated reworking for their effectiveness in addressing defects.

(Q1.O1) was addressed through the review of the literature and experts outreach contained in Chapters 2 and 3, respectively. Through these activities the conclusions were, firstly, the lack of reported knowledge relating to the reworking activity, contrasted with the reality that the activity is well practiced within AFP manufacturing. From the experts outreach an initial understanding of the manual process was detailed and analysed, including some variance in techniques and tools depending on the defect type were identified.

(Q1.O2) was addressed through the rework process analysis study enclosed in Chapter 4. Here the manual methods defined in the previous two chapters were examined with varying tool and tension components in terms of the effect on the damage to surrounding materials. Through this study and compiled next to the guidelines for wrinkle defect rework presented by Sacco et al., [31], a more comprehensive set of guidelines for manual rework was produced. These guidelines helped to define and constrain all the analysis of the results of reworking in subsequent Chapters. The findings of this chapter were published in preliminary form in [174].

(Q1.O3) was addressed extensively through Chapter 5. Here three methods were employed. Firstly, ultrasonic NDT was used to analyse the internal ply topography of pristine, defective and reworked laminates, the main findings were published in [181]. Description of the development and use of the Bencthop-AFP system was published in [219]. Secondly, the microstructure of cross sections of the three laminate types were examined using SEM. Finally, the effect of reworking on mechanical performance was analysed using the ISO 14125 flexural strength tests for the three laminate types.

Collectively, these objectives serve to address research question (Q1), primarily through the findings in Chapter 5, with the previous chapters serving as the basis for the scientific rigour underpinning the findings in Chapter 5.

(Q2.O1), (Q2.O2), (Q2.O3), and as a whole, research question (Q2), were addressed collectively through the description of the automated reworking methods discussed in Chapters 6 and 7. The findings from Chapter 6 focused on recompaction as the main lever for gap defect reworking, but found that the method was ineffectual to serve as the basis for automated defect reworking. Nevertheless, the findings were illustrative of the mechanical complexity of the material and its sensitivity to processing parameter variation. The main findings of this chapter were published in [220]. Through Chapter 7 a viable method for defect reworking was developed and tested. This proof-of-concept for on-the-fly defect mitigation was shown to effectively mitigate even very large gap defects, despite the ceiling on the correction behaviour imposed by the material constraints. Additionally, the end-to-end nature of the ROS-based system, directly contributes to a more efficient quality assurance method for AFP manufacturing. Both the defect detection and mitigation are synchronised with the initial material deposition step. Descriptions of the system development and testing were published in [221] and Publication 7 (presented April 2026), respectively.

8.3 Discussion

The central finding of this Thesis is that AFP rework, despite being a routine industrial activity, had no formal empirical basis prior to this work. The consequences of this absence extend beyond academic considerations into industries where AFP is prevalent, where safety, quality, and performance are paramount. The reliance on tacit practitioner knowledge and cosmetic assessment that characterised rework practice prior to this work is inconsistent with those requirements. The research presented here begins to address that incompatibility directly.

The convergence of opinion from expert outreach, across the academic, industrial, and consultancy perspectives, that rework lacks standardisation and that automation remains an unmet need is significant beyond its role in validating the Thesis objectives. The consistency of this view across such diverse respondents suggest that the problem is structural to AFP manufacturing as a discipline, rather than a limitation of particular organisations or applications. This raises questions for the research priorities in AFP. Considerable investment is directed towards inspection system development which has not been matched by equivalent effort on the rework side, despite rework being the downstream consequence of inspection findings.

The most significant finding in terms of practical consequence is the disconnect between cosmetic recovery and real, structural recovery in reworked laminates. The prevailing basis for rework acceptance in industry is surface appearance. The multi-method assessment presented in Chapter 5 demonstrates that this basis is insufficient. Residual out-of-plane waviness and elevated ply-ply disturbance persisted in reworked laminates even where surface appearance was acceptable, and these features manifested as elevated mechanical variability under flexural loading. For safety critical structural applications, variability of this kind is undesirable, since it undermines the statistical confidence underpinning design allowables. The implication is that current industry acceptance practice may be systematically underestimating the structural risk associated with reworked components.

The negative result in developing an automated reworking strategy from the recompaction based automated rework method in Chapter 6 is instructive in a broader sense. The coupling between transverse tow displacement and width change at effective parameter ranges reflects the well-established sensitivity of thermoset tow materials to process parameters interactions, a theme consistent with the wider literature on resin flow mechanics and tow deformation in AFP. That this coupling renders recompaction alone ineffective as a rework strategy narrows the solution space in a useful way, and points towards positional correction, rather than material redistribution, as the more promising basis for automation.

The real-time correction system developed in Chapter 7 is significant not only for its demonstrated effectiveness in gap mitigation, but for what its architecture enables. The alignment of defect detection and correction with the deposition step itself represent a reconceptualisation of where in the manufacturing cycle the quality problem is addressed. The broader trajectory of AFP research towards inline sensing, closed-loop control and intelligent manufacturing, highlighted in Section 2.3.5, suggest that this method is in the direction which the field is heading. The ROS-based architecture positions the system to evolve alongside that trajectory.

The primary contributions of this Thesis are as follows. Firstly, this Thesis provides the first systematic empirical investigation of rework of gap and overlap defects in AFP, establishing an evidence base for an activity within AFP that had previously predominantly relied on practitioner experience and cosmetic evaluation. Secondly, the findings demonstrate that cosmetic success of the reworking process does not necessarily respond to full structural recovery, showing that a residual out-of-plane waviness can persist despite acceptable surface appearance. Thirdly, the Thesis quantifies, for the first time, the effect of manual gap and overlap rework on laminate mechanical performance under flexural loading, documenting both the measurable stiffness knockdown and increases variability in flexural response, thereby providing data relevant to design allowable and manufacturing concessions. Fourthly, it identifies a previously undocumented coupling between transverse tow displacement and tow width change during recompaction-based automated rework, revealing a fundamental limitation of material redistribution approaches for defect correction and demonstrating the limits of process parameter control. Finally, it develops and validates a novel real-time defect mitigation methodology based on a closed-loop positional correction within a ROS-enabled control architecture, demonstrating the feasibility of integrating defect detection and correction directly into the deposition process.

8.3.1 Limitations

Important limitations to the findings in this Thesis should be addressed. Firstly, all testing for the effect of reworking was done at a coupon level, not at a structural level. While this serves as a meaningful assessment of the quality impact of rework, propagation of the findings onto the performance of larger composite structures cannot be stated with any certainty. The limited absolute knockdowns in performance may be mitigated by the loading response of the wider rework and defect free structure.

Secondly, analysis of the effect of manually performed rework presented in Chapters Chapter 4 and Chapter 5 is intrinsically variable precisely because of the manual nature of the process. While this is mitigated to an extent by the replication of experiments within these Chapters, replication of the experiments by other researcher may result in differences in the scale of results though the relationships between the different classes of samples manufactured can be expected to be maintained.

Further, the findings here are limited to the material and AFP cell used in the course of this Thesis. Larger AFP machines are capable of depositing multiple tows at one time, and may not be suitable for the trajectory control method described in Chapter 7. Further the limitations of the hardware used in this Thesis limit the impact of the findings in Chapter 7. Further work testing the system with alternative sensor positions, and indeed sensors, are vital in improving the methods.

While gap and overlap defects are the most commonly seen defect within AFP, they are far from the only type. Further work on wrinkle defects, fuzzballs, and defects resulting from tow steering is vital in advancing the field with the aim of a zero-defect manufacturing process.

The Benchtop-AFP method is narrow in its focus and, while useful in creating a low-cost test bed for some parts of AFP research, cannot fully approach simulate the full conventional AFP approach. As a very early iteration of a novel method of AFP-like manufacturing it warrants further development, but in its current state cannot be used for large scale research efforts.

8.4 Further work

The process of reworking defects in AFP is costly in terms of machine downtime and remains one of the few tasks to be conducted manually by technicians. Further work in this field should aim at developing automated rework processes. Doing so would allow for near or full automation of the AFP process. To achieve this end, further work is required in analysing the effect of the rework process.

No recognised industrial standard has been found for assessing the success of the process, emphasising the necessity to develop a robust framework for evaluating automated solutions. The establishment of such a standard practice would prove highly advantageous to both academia and industry, as it would provide a shared benchmark for assessing and comparing various methodologies, promoting innovation, ensuring quality control, and facilitating meaningful research and development within the field.

Further, the use of tooling across manual rework must be accounted for in any attempts at automated rework. As such, custom end-effectors or end-effector modules may be developed and evaluated for their success at performing the rework task. Future research efforts could address the limitations of the work in Chapter 4 by exploring larger specimen sizes, incorporating automated rework processes, employing higher-resolution imaging techniques, and expanding the data set to include a wider range of composite materials and defect types. Further work examining alternative NDT methods, complemented by destructive testing for physical examination, will be critical to validate the ultrasonic method described in this Thesis against ground truth measurements. This validation pathway will establish confidence in the method while providing quantitative assessment of its detection accuracy and limitations

Critically, further destructive mechanical testing, beyond the work enclosed in Chapter 5, into the correlation between residual out-of-plane waviness and mechanical properties could enhance the qualitative study of the process, ultimately leading to increased efficiency, and cost-effectiveness in various applications of composite materials.

The automated methods presented in Chapters 6 and 7 serve as the jumping off points for the development of a more mature automated defect reworking system. The real-time correction method presented in Chapter 7 has the potential for bolt-on additions thanks to the ROS-based architecture design, future-proofing the method and allowing for a higher degree of flexibility for alternative AFP manufacturing cells. Additionally, the 12 degrees of freedom available in the expanded ITRA motion control system can be further utilised. At present, 9 of the 12 degrees have been incorporated in the analysis within this Thesis, leaving three available. These may be used for real-time control of digitally operated process parameters such as compaction force, tow tension or an infrared heat lamp.

References

[1] A. K. Kaw, *Mechanics of composite materials*. CRC Press, 1999.

[2] T. W. Clyne, *An introduction to composite materials*, Third edition. Cambridge, United Kingdom ; New York: Cambridge University Press, 2019.

[3] F. L. Matthews, *Composite materials : engineering and science*. Boca Raton : Cambridge, England: CRC Press ; Woodhead Publishing, 1999.

[4] A. Kelly and S. T. Mileĭko, *Fabrication of composites*. North-Holland ; Sole distributors for the U.S.A. and Canada, Elsevier Science Pub. Co., 1983.

[5] R. M. Jones, *Mechanics Of Composite Materials*. CRC Press, 2014.

[6] R. Harik and A. Brasington, *Automated Fiber Placement: Status, Challenges, and Evolution*. SAE International, 2025. doi: 10.4271/9781468603064.

[7] R. Slayton and G. Spinardi, "Radical innovation in scaling up: Boeing's Dreamliner and the challenge of socio-technical transitions," *Technovation*, vol. 47, pp. 47–58, Jan. 2016, doi: 10.1016/j.technovation.2015.08.004.

[8] T.-D. Ngo, "Introduction to Composite Materials," in *Composite and Nanocomposite Materials - From Knowledge to Industrial Applications*, IntechOpen, 2020. doi: 10.5772/intechopen.91285.

[9] T. G. P. Gutowski, *Advanced composites manufacturing*. New York: Wiley, 1997.

[10] G. Marsh, "Composites help improve wind turbine breed," *Reinforced Plastics*, vol. 49, no. 4, pp. 18–22, Apr. 2005, doi: 10.1016/S0034-3617(05)70609-3.

[11] E. Poodts, R. Panciroli, and G. Minak, "Design rules for composite sandwich wakeboards," *Compos. B Eng.*, vol. 44, no. 1, pp. 628–638, Jan. 2013, doi: 10.1016/j.compositesb.2012.02.014.

[12] C. L. Davis and S. N. Kukureka, “Effect of materials and manufacturing on the bending stiffness of vaulting poles,” *Phys. Educ.*, vol. 47, no. 5, pp. 524–529, Sep. 2012, doi: 10.1088/0031-9120/47/5/524.

[13] E. Oromiehie, B. G. Prusty, P. Compston, and G. Rajan, “Automated fibre placement based composite structures: Review on the defects, impacts and inspections techniques,” *Compos. Struct.*, vol. 224, p. 110987, Sep. 2019, doi: 10.1016/j.compstruct.2019.110987.

[14] D. H.-J. A. Lukaszewicz, C. Ward, and K. D. Potter, “The engineering aspects of automated prepreg layup: History, present and future,” *Compos. B Eng.*, vol. 43, no. 3, pp. 997–1009, Apr. 2012, doi: 10.1016/j.compositesb.2011.12.003.

[15] R. J. H. Wanhill, “Carbon Fibre Polymer Matrix Structural Composites,” in *Aerospace Materials and Material Technologies*, vol. Volume 1, 2017, pp. 309–341. doi: 10.1007/978-981-10-2134-3_14.

[16] S. Carosella, S. Hügle, F. Helber, and P. Middendorf, “A short review on recent advances in automated fiber placement and filament winding technologies,” *Compos. B Eng.*, vol. 287, p. 111843, Dec. 2024, doi: 10.1016/j.compositesb.2024.111843.

[17] H. Parmar, T. Khan, F. Tucci, R. Umer, and P. Carlone, “Advanced robotics and additive manufacturing of composites: towards a new era in Industry 4.0,” *Materials and Manufacturing Processes*, vol. 37, no. 5, pp. 483–517, Apr. 2022, doi: 10.1080/10426914.2020.1866195.

[18] W. Goldsworth and E. Hardesty, “ Geodesic path length compensator for composite-tape placement head,” US3810805A, 1974

[19] R. L. Anderson, C. G. Grant, and NASA, “Advanced Fiber Placement of Composite Fuselage Structures,” in *First NASA Advanced Composites Technology Conference, Part 2*, Seattle, USA, 1991.

[20] M. Enders and P. Hopkins, “Developments in the Fibre Placement Process,” in *36th International SAMPE Symposium*, San Diego, USA, 1991.

[21] R. Measom and K. Sewell, “Fiber Placement Low-Cost Production for Complex Composite Structures,” in *American Helicopter Society 52nd Forum*, Washington DC, USA, Jun. 1996.

[22] M. Pasanen, J. Martin, R. Langone, and J. Mondo, “Advanced Composite Fibre Placement Process to Application,” 1997.

[23] D. Lukaszewicz, “Considerations for automated layup of carbon-fibre thermoset preimpregnates,” *Aerospace Engineering, University of Bristol*, 2011.

[24] K. Croft, L. Lessard, D. Pasini, M. Hojjati, J. Chen, and A. Yousefpour, “Experimental study of the effect of automated fiber placement induced defects on performance of composite laminates,” *Compos. Part A Appl. Sci. Manuf.*, vol. 42, no. 5, pp. 484–491, May 2011, doi: 10.1016/j.compositesa.2011.01.007.

[25] D. O. Evans, “Fiber Placement,” in *Handbook of Composites*, S. T. Peters, Ed., Boston, MA: Springer US, 1998, pp. 476–487. doi: 10.1007/978-1-4615-6389-1_23.

[26] R. J. Grone, L. R. Schnell, and W. L. Vearil, “Composite tape laying machine and method,” US4557783A, 1983

[27] D. Hughes, “Materials waste reduction,” in *Design and Manufacture of Structural Composites*, Elsevier, 2023, pp. 475–497. doi: 10.1016/B978-0-12-819160-6.00016-0.

[28] T. Rudberg, J. Nielson, M. Henscheid, and J. Cemenska, “Improving AFP Cell Performance,” *SAE International Journal of Aerospace*, vol. 7, no. 2, pp. 317–321, Sep. 2014, doi: 10.4271/2014-01-2272.

[29] A. Halbritter and R. Harper, “Big parts demand big changes to the fiber placement status quo,” *SME composites manufacturing*, vol. 2012, 2012.

[30] T. Rudberg, J. Cemenska, and E. Sherrard, “A Process for Delivering Extreme AFP Head Reliability,” in *SAE Technical Paper Series*, in AEROTECH. SAE International, Mar. 2019. doi: 10.4271/2019-01-1349.

[31] C. Sacco *et al.*, “On the effect of manual rework in AFP quality control for a doubly-curved part,” *Compos. B Eng.*, vol. 227, Dec. 2021, doi: 10.1016/j.compositesb.2021.109432.

[32] M. Saunders, P. Lewis, and A. Thornhill, *Research Methods for Business Students*, 8th ed. Pearson, 2019.

[33] N. Saba, M. Jawaid, and M. T. H. Sultan, “Thermal properties of oil palm biomass based composites,” in *Lignocellulosic Fibre and Biomass-Based Composite Materials*, Elsevier, 2017, pp. 95–122. doi: 10.1016/b978-0-08-100959-8.00006-8.

[34] P. K. Mallick, *Composites engineering handbook*. CRC Press, 1997.

[35] J. C. . Halpin, *Primer on composite materials: analysis*, 2nd Edition. Technomic Publishing, 1969.

[36] M. A. Albazzan, R. Harik, B. F. Tatting, and Z. Gürdal, “Efficient design optimization of nonconventional laminated composites using lamination parameters: A state of the art,” *Compos. Struct.*, vol. 209, pp. 362–374, Feb. 2019, doi: 10.1016/j.compstruct.2018.10.095.

[37] Grand View Research, “Composites Market (2023 - 2030),” 2023.

[38] Markets and Markets, “Composites Market by Fibre Type, Resin Type, Manufacturing Process, End-use Industry, and Region - Global Forecast to 2028,” 2024.

[39] Precedence Research, “Composites Market Size, Share, and Trends 2026 to 2035,” 2025.

[40] M. Jawaid and M. Thariq, *Sustainable composites for aerospace applications*. Woodhead publishing, 2018.

[41] J. Müssig and K. Haag, “The use of flax fibres as reinforcements in composites,” in *Biofiber Reinforcements in Composite Materials*, Elsevier, 2015, pp. 35–85. doi: 10.1533/9781782421276.1.35.

[42] L. Mishnaevsky, K. Branner, H. Petersen, J. Beauson, M. McGugan, and B. Sørensen, “Materials for Wind Turbine Blades: An Overview,” *Materials*, vol. 10, no. 11, p. 1285, Nov. 2017, doi: 10.3390/ma10111285.

[43] M. Elkington, D. Bloom, C. Ward, A. Chatzimichali, and K. Potter, “Hand layup: understanding the manual process,” *Advanced Manufacturing: Polymer and Composites Science*, vol. 1, no. 3, pp. 138–151, Jul. 2015, doi: 10.1080/20550340.2015.1114801.

[44] E. Paul. DeGarmo, J. Temple. Black, and R. A. . Kohser, *Materials and processes in manufacturing*. Prentice Hall, 1997.

[45] D. M. Crowley, M. P. Elkington, C. Ward, and K. D. Potter, “Hand lay-up of complex geometries-prediction, capture and feedback,” in *International SAMPE Technical Conference*, United States: Society for the Advancement of Material and Process Engineering, May 2016.

[46] E. Shehab, W. Ma, and A. Wasim, “Manufacturing cost modelling for aerospace composite applications,” in *Advanced Concurrent Engineering*, 2013, pp. 425 – 433. doi: 10.1007/978-1-4471-4426-7_37.

[47] K. Schwab, “The Fourth Industrial Revolution: what it means, how to respond1,” in *Handbook of Research on Strategic Leadership in the Fourth Industrial Revolution*, Edward Elgar Publishing, 2024, pp. 29–34. doi: 10.4337/9781802208818.00008.

[48] V. Varriale, A. Cammarano, F. Michelino, and M. Caputo, “Interconnected Industry 4.0 technologies: Identifying current network value and integration opportunities,” *J. Ind. Inf. Integr.*, vol. 45, p. 100838, May 2025, doi: 10.1016/j.jii.2025.100838.

[49] A. K. Gupta, S. K. Arora, and J. Riescher. Westcott, *Industrial automation and robotics*. Mercury Learning and Information, 2017.

[50] M. P. Groover, *Industrial Automation and Robotics*. McGraw-Hill, 1998.

[51] C. Taesi, F. Aggogeri, and N. Pellegrini, “COBOT Applications—Recent Advances and Challenges,” *Robotics*, vol. 12, no. 3, p. 79, Jun. 2023, doi: 10.3390/robotics12030079.

[52] A. Correia Simões, A. Lucas Soares, and A. C. Barros, “Factors influencing the intention of managers to adopt collaborative robots (cobots) in manufacturing organizations,” *Journal of Engineering and Technology Management*, vol. 57, p. 101574, Jul. 2020, doi: 10.1016/j.jengtecman.2020.101574.

[53] S. Micheler, Y. Goh, and N. Lohse, “Influencing factors for implementing automation in manufacturing businesses–a literature review,” in *Proceedings of the 14th International Conference on ManufacturingResearch (ICMR)*, Loughborough, UK: Loughborough University, 2016, p. 7.

[54] G. Rajan and B. G. Prusty, Eds., *Structural Health Monitoring of Composite Structures Using Fiber Optic Methods*. CRC Press, 2016. doi: 10.1201/9781315369815.

[55] S. Mazumdar, *Composites Manufacturing*. CRC Press, 2001. doi: 10.1201/9781420041989.

[56] X. Li, J. Dufty, and G. M. Pearce, “Automation of tow wise modelling for automated fibre placement and filament wound composites,” *Compos. Part A Appl. Sci. Manuf.*, vol. 147, p. 106449, Aug. 2021, doi: 10.1016/j.compositesa.2021.106449.

[57] L. Zhang, X. Wang, J. Pei, and Y. Zhou, “Review of automated fibre placement and its prospects for advanced composites,” Jun. 01, 2020, *Springer*. doi: 10.1007/s10853-019-04090-7.

[58] T. Kukwi, C. Shan, L. Pengfei, B. Zhang, G. Leiyang, and Z. Wang, “Continuous Improvement in Composite Manufacturing: A Review of Automated Fiber Placement

Process Evolution and Future Research Prospects," *Applied Composite Materials*, vol. 32, no. 4, pp. 1267–1314, Aug. 2025, doi: 10.1007/s10443-025-10325-5.

[59] M. Szcesny, F. Heieck, S. Carosella, P. Middendorf, H. Sehrschön, and M. Schneiderbauer, "The advanced ply placement process – an innovative direct 3D placement technology for plies and tapes," *Advanced Manufacturing: Polymer & Composites Science*, vol. 3, no. 1, pp. 2–9, Jan. 2017, doi: 10.1080/20550340.2017.1291398.

[60] N. Bakhshi and M. Hojjati, "Effect of compaction roller on layup quality and defects formation in automated fiber placement," *Journal of Reinforced Plastics and Composites*, vol. 39, no. 1–2, pp. 3–20, Jan. 2020, doi: 10.1177/0731684419868845.

[61] SAE. International, *Composite Materials Handbook, Volume 3*. SAE International, 2025.

[62] M. Barile, L. Lecce, G. D'Amato, M. Esposito, and A. Sportelli, "Advanced AFP Applications on Multifunctional Composites," in *The 2nd International Symposium on Automated Composites Manufacturing (ACM2)*, Montreal, Canada, Mar. 2015.

[63] M. Jonsson, D. Eklund, A. Järneteg, M. Åkermo, and J. Sjölander, "Automated manufacturing of an integrated pre-preg structure," in *The Second International Symposium on Automated Composites Manufacturing*, 2015, pp. 23–24.

[64] A. Björnsson, J.-E. Lindback, and K. Johansen, "Automated Removal of Prepreg Backing Paper - A Sticky Problem," Sep. 2013. doi: 10.4271/2013-01-2289.

[65] S. V. Hoa, *Principles of the manufacturing of composite materials*, 2nd Edition. DEStech Publications, Inc., 2018.

[66] C. Ward, S. Hancock, and K. Potter, "Forming Complex Shaped Components Using Drape Simulation Software: Informing Manual and Automated Production Needs,"

SAE International Journal of Aerospace, vol. 01, no. 1, pp. 2008-01–2316, Sep. 2008, doi: 10.4271/2008-01-2316.

[67] C. G. Grant, “Fiber placement process utilization within the worldwide aerospace industry,” *Sampe Journal*, vol. 36, pp. 7–12, Jan. 2000.

[68] A. Brasington, C. Sacco, J. Halbritter, R. Wehbe, and R. Harik, “Automated fiber placement: A review of history, current technologies, and future paths forward,” Oct. 01, 2021, *Elsevier B.V.* doi: 10.1016/j.jcomc.2021.100182.

[69] T. S. Angell and T. Rudberg, “Manufacture of substructure by automated fiber placement,” Wichita, Kansas, 2013.

[70] F. Kochoski, V. Dukovski, S. Samak, D. Vajdeska, and B. Petkoska, “Manufacturing Thermoplastic Composites by Laser Automatic Tape Placement Toolless Technology with Dual Robot System,” *International Journal of Engineering and Technical Research*, vol. 11, p. 238, Jan. 2022.

[71] Accudyne Systems, “AccuFP 1000+ fibre placement head [Apparatus],” 2022, *https://www.accudyne.com/*.

[72] K. Wu, B. Stewart, and R. Martin, “ISAAC Advanced Composites Research Capability,” Oct. 2015.

[73] C. Schmidt, B. Denkena, T. Hocke, and K. Völtzer, “Influence of AFP Process Parameters on the Temperature Distribution Used for Thermal in-process Monitoring,” *Procedia CIRP*, vol. 66, pp. 68–73, 2017, doi: 10.1016/j.procir.2017.03.220.

[74] M. Belhaj *et al.*, “Dry fiber automated placement of carbon fibrous preforms,” *Compos. B Eng.*, vol. 50, pp. 107–111, Jul. 2013, doi: 10.1016/j.compositesb.2013.01.014.

[75] M. A. Khan, P. Mitschang, and R. Schledjewski, “Identification of some optimal parameters to achieve higher laminate quality through tape placement process,”

Advances in Polymer Technology, vol. 29, no. 2, pp. 98–111, Jun. 2010, doi: 10.1002/adv.20177.

[76] J. Chen, T. Chen-Keat, M. Hojjati, A. Vallee, M.-A. Octeau, and A. Yousefpour, “Impact of layup rate on the quality of fiber steering/cut-restart in automated fiber placement processes,” *Science and Engineering of Composite Materials*, vol. 22, no. 2, pp. 165–173, Mar. 2015, doi: 10.1515/secm-2013-0257.

[77] R. Engelhardt, R. Irmanputra, K. Brath, N. Aufenanger, and K. Drechsler, “Thermoset Prepreg Compaction during Automated Fiber Placement and Vacuum Debulking,” *Procedia CIRP*, vol. 85, pp. 153–158, 2019, doi: 10.1016/j.procir.2019.09.025.

[78] T. T. Zacchia, F. Shadmehri, Jeffrey Fortin-Simpson, and S. Van Hoa, “Design of Hard Compaction Rollers for Automated Fiber Placement on Complex Mandrel Geometries,” *Journal of Mechanics Engineering and Automation*, vol. 8, no. 6, Jun. 2018, doi: 10.17265/2159-5275/2018.06.003.

[79] B. Denkena, C. Schmidt, and P. Weber, “Automated Fiber Placement Head for Manufacturing of Innovative Aerospace Stiffening Structures,” *Procedia Manuf.*, vol. 6, pp. 96–104, 2016, doi: 10.1016/j.promfg.2016.11.013.

[80] M. A. Lamontia, M. B. Gruber, B. J. Waibel, R. D. Cope, and A. B. Hulcher, “Conformable compaction system used in automated fiber placement of large composite aerospace structures,” 2002. [Online]. Available: https://api.semanticscholar.org/CorpusID:113987482

[81] F. W. Billmeyer, *Textbook of polymer science*. John Wiley & Sons, 1984.

[82] S. C. Mantell and G. S. Springer, “Manufacturing Process Models for Thermoplastic Composites,” *J. Compos. Mater.*, vol. 26, no. 16, pp. 2348 – 2377, 1992, doi: 10.1177/002199839202601602.

[83] Z. Qureshi, T. Swait, R. Scaife, and H. M. El-Dessouky, “In situ consolidation of thermoplastic prepreg tape using automated tape placement technology: Potential and possibilities,” *Compos. B Eng.*, vol. 66, pp. 255–267, Nov. 2014, doi: 10.1016/j.compositesb.2014.05.025.

[84] N. Bakhshi and M. Hojjati, “Time-dependent wrinkle formation during tow steering in automated fiber placement,” *Compos. B Eng.*, vol. 165, pp. 586–593, May 2019, doi: 10.1016/j.compositesb.2019.02.034.

[85] E. Oromiehie, B. Gangadhara Prusty, P. Compston, and G. Rajan, “In-situ simultaneous measurement of strain and temperature in automated fiber placement (AFP) using optical fiber Bragg grating (FBG) sensors,” *Advanced Manufacturing: Polymer & Composites Science*, vol. 3, no. 2, pp. 52–61, Apr. 2017, doi: 10.1080/20550340.2017.1317447.

[86] O. Aghababaei Tafreshi, S. Van Hoa, F. Shadmehri, D. M. Hoang, and D. Rosca, “Determination of convective heat transfer coefficient for automated fiber placement (AFP) for thermoplastic composites using hot gas torch,” *Advanced Manufacturing: Polymer & Composites Science*, vol. 6, no. 2, pp. 86–100, Apr. 2020, doi: 10.1080/20550340.2020.1764236.

[87] L. Zacherl, F. Shadmehri, and K. Rother, “Determination of convective heat transfer coefficient for hot gas torch (HGT)-assisted automated fiber placement (AFP) for thermoplastic composites,” *Journal of Thermoplastic Composite Materials*, vol. 36, no. 1, pp. 73–95, Jan. 2023, doi: 10.1177/0892705720982363.

[88] R. H. Rizzolo and D. F. Walczyk, “Ultrasonic consolidation of thermoplastic composite prepreg for automated fiber placement,” *Journal of Thermoplastic Composite Materials*, vol. 29, no. 11, pp. 1480–1497, Nov. 2016, doi: 10.1177/0892705714565705.

[89] R. Calawa and J. Nancarrow, "Medium Wave Infrared Heater for High-Speed Fiber Placement," Sep. 2007. doi: 10.4271/2007-01-3842.

[90] B. L. C. Greenberg, "Design and Control of an Arrayed Infrared (MAT-IR) Heater for Accurate Heating Control During Automated Fiber Placement," Doctoral Dissertation, 2020.

[91] E. Beyeler, W. Phillips, and S. I. Güçeri, "Experimental Investigation of Laser-Assisted Thermoplastic Tape Consolidation," *Journal of Thermoplastic Composite Materials*, vol. 1, no. 1, pp. 107–121, Jan. 1988, doi: 10.1177/089270578800100109.

[92] C. M. Stokes-Griffin and P. Compston, "The effect of processing temperature and placement rate on the short beam strength of carbon fibre–PEEK manufactured using a laser tape placement process," *Compos. Part A Appl. Sci. Manuf.*, vol. 78, pp. 274–283, Nov. 2015, doi: 10.1016/j.compositesa.2015.08.008.

[93] W. Zhang, F. Liu, Y. Lv, and X. Ding, "Modelling and layout design for an automated fibre placement mechanism," *Mech. Mach. Theory*, vol. 144, p. 103651, Feb. 2020, doi: 10.1016/j.mechmachtheory.2019.103651.

[94] M. Razavi Setvati, Z. Mustaffa, N. Shafiq, and Z. I. Syed, "A Review on Composite Materials for Offshore Structures," in *Volume 5: Materials Technology; Petroleum Technology*, in OMAE2014. American Society of Mechanical Engineers, Jun. 2014. doi: 10.1115/omae2014-23542.

[95] S. Van Hoa, "Automated composites manufacturing," *Science and Engineering of Composite Materials*, vol. 22, no. 2, p. 113, Mar. 2015, doi: 10.1515/secm-2015-0060.

[96] Mtorres, "Digitization," https://mtorres.es/en/digitization.

[97] Broetje-Automation, "SOUL RMOS Digital Twin & Machine Simulation," https://broetje-automation.de/products/smart-process/digital-solutions/product/soul-rmos/.

[98] MTorres, “TorresFactory 4.0, solution for your digitalization needs,” https://mtorres.es/en/news/other-projects/torresFactory-4-solution-digitalization.

[99] Coriolis, “CoDa,” https://www.coriolis-composites.com/software-solutions/coda/.

[100] Coriolis, “CADFibre,” https://www.coriolis-composites.com/software-solutions/cadfiber/.

[101] Coriolis Composites, “CATFiber,” https://www.coriolis-composites.com/software-solutions/catfiber/.

[102] Addcomposites, “AddPath,” https://www.addcomposites.com/all-products/addpath.

[103] Coriolis Composites, “Human Machine Interfaces (HMI),” https://www.coriolis-composites.com/machines/human-machine-interfaces-hmi/.

[104] Electroimpact, “Electroimpact’s Catalog of Advanced Composite Manufacturing Products,” https://www.electroimpact.com/Products/composites-manufacturing/technology.

[105] Ingersoll Machine Tools, “Automated Composite Structure Inspection System,” https://en.machinetools.camozzi.com/products/composite-manufacturing/all-products/acsis-.kl.

[106] Fives, “Composite Optical Automated Surface Tracking,” https://www.fivesgroup.com/high-precision-machines/composites-automated-solutions/forming-inspection/composite-optical-automated-surface-tracking.

[107] W. T. Freeman Jr and B. A. Stein, “Filament winding-Waking the sleeping giant,” *Aerosp. Am.*, vol. 24, no. ISSN: 0740-722X, 1985.

[108] S. Krolewski and T. Gutowski, “Economic comparison of advanced composite fabrication technologies,” in *International SAMPE Symposium and Exhibition, 34 th, Reno, NV, Proceedings. Book 1*, 1989.

[109] American Composites Manufacturing Association (ACMA), *Basic Composites Study guide*. Arlington: ACMA 2017, 2017.

[110] S. Krolewski and T. Gutowski, “Effect of the automation of advanced composite fabrication process on part cost,” *SAMPE Q.;(United States)*, vol. 18, no. 1, 1986.

[111] M. N. Grimshaw, C. G. Grant, and J. M. L. Diaz, “Advanced technology tape laying for affordable manufacturing of large composite structures,” *International SAMPE Symposium and Exhibition (Proceedings)*, vol. 46, pp. 2484–2494, Mar. 2001.

[112] C. M. H.-17 (CMH-17), *Composite Materials Handbook, Volume 3 - Polymer Matrix Composites - Materials Usage, Design, and Analysis (CMH-17)*. SAE International on behalf of CMH-17, a division of Wichita State University, 2012. [Online]. Available: https://app.knovel.com/hotlink/toc/id:kpCMHVPM1E/composite-materials-handbook/composite-materials-handbook

[113] B. A. R. Soares, E. Henriques, I. Ribeiro, and M. Freitas, “Cost analysis of alternative automated technologies for composite parts production,” *Int. J. Prod. Res.*, vol. 57, no. 6, pp. 1797–1810, Mar. 2019, doi: 10.1080/00207543.2018.1508903.

[114] Y. Bauswein, L. Veldenz, and C. Ward, “Developing a cost comparison technique for hand lay-up versus automated fibre placement and infusion versus out-of-autoclave,” Nov. 2017. [Online]. Available: https://www.sampe-europe.org/conferences/conference-2017-stuttgart

[115] C. Houchins, B. James, Y. Acevedo, and Z. Watts, “Hydrogen Storage System Cost Analysis (2017-2021) (Final Report),” Golden, CO (United States), Sep. 2022. doi: 10.2172/1975554.

[116] A. Air and B. G. Prusty, “A cost comparison of automated fibre placement and filament winding for composite pressure vessel manufacturing,” *J. Manuf. Process.*, vol. 156, pp. 447–458, Dec. 2025, doi: 10.1016/j.jmapro.2025.11.044.

[117] R. Harik, Z. Gurdal, C. Saidy, S. J. Williams, and B. Grimsley, "Automated fiber placement defect identity cards: cause, anticipation, existence, significance and progression," Long Beach, CA: SAMPE Conference and Exhibition, May 2018.

[118] W. E. Guin, J. R. Jackson, and C. M. Bosley, "Effects of tow-to-tow gaps in composite laminates fabricated via automated fiber placement," *Compos. Part A Appl. Sci. Manuf.*, vol. 115, pp. 66–75, Dec. 2018, doi: 10.1016/j.compositesa.2018.09.014.

[119] R. Lichtinger, J. Lacalle, R. Hinterhölzl, U. Beier, and K. Drechsler, "Simulation and experimental validation of gaps and bridging in the automated fiber placement process," *Science and Engineering of Composite Materials*, vol. 22, no. 2, pp. 131–148, Mar. 2015, doi: 10.1515/secm-2013-0158.

[120] A. W. Blom, "Structural performance of fiber-placed, variable-stiffness composite conical and cylindrical shells," 2010.

[121] L. Raps, F. Atzler, A. Chadwick, and H. Voggenreiter, "In-situ automated fiber placement gap defects filled by fused granular fabrication," *Manuf. Lett.*, Apr. 2024, doi: 10.1016/j.mfglet.2024.03.007.

[122] A. Sawicki and P. Minguett, "The effect of intraply overlaps and gaps upon the compression strength of composite laminates," in *39th AIAA/ASME/ASCE/AHS/ASC Structures, Structural Dynamics, and Materials Conference and Exhibit*, Reston, Virigina: American Institute of Aeronautics and Astronautics, Apr. 1998. doi: 10.2514/6.1998-1786.

[123] M. Lan, D. Cartié, P. Davies, and C. Baley, "Microstructure and tensile properties of carbon–epoxy laminates produced by automated fibre placement: Influence of a caul plate on the effects of gap and overlap embedded defects," *Compos. Part A Appl. Sci. Manuf.*, vol. 78, pp. 124–134, Nov. 2015, doi: 10.1016/j.compositesa.2015.07.023.

[124] M. Lan, D. Cartié, P. Davies, and C. Baley, "Influence of embedded gap and overlap fiber placement defects on the microstructure and shear and compression properties of carbon–epoxy laminates," *Compos. Part A Appl. Sci. Manuf.*, vol. 82, pp. 198–207, Mar. 2016, doi: 10.1016/j.compositesa.2015.12.007.

[125] Y. M. Elsherbini and S. V Hoa, "Experimental and numerical investigation of the effect of gaps on fatigue behavior of unidirectional carbon/epoxy automated fiber placement laminates," *J. Compos. Mater.*, vol. 51, no. 6, pp. 759–772, Mar. 2017, doi: 10.1177/0021998316655393.

[126] W. Woigk, S. R. Hallett, M. I. Jones, M. Kuhtz, A. Hornig, and M. Gude, "Experimental investigation of the effect of defects in Automated Fibre Placement produced composite laminates," *Compos. Struct.*, vol. 201, pp. 1004–1017, Oct. 2018, doi: 10.1016/j.compstruct.2018.06.078.

[127] M. H. Nguyen, A. A. Vijayachandran, P. Davidson, D. Call, D. Lee, and A. M. Waas, "Effect of automated fiber placement (AFP) manufacturing signature on mechanical performance of composite structures," *Compos. Struct.*, vol. 228, p. 111335, Nov. 2019, doi: 10.1016/j.compstruct.2019.111335.

[128] M. H. Nguyen, P. Davidson, and A. M. Waas, "Experimental and numerical study on the tensile failure behavior of toughened-interlayer composite laminates with automated fiber placement (AFP) induced gap and overlap defects," *International Journal of Material Forming*, vol. 14, no. 1, pp. 105–119, Jan. 2021, doi: 10.1007/s12289-020-01581-w.

[129] M. Nartey *et al.*, "Understanding the impact of fibre wrinkle architectures on composite laminates through tailored gaps and overlaps," *Compos. B Eng.*, vol. 196, p. 108097, Sep. 2020, doi: 10.1016/j.compositesb.2020.108097.

[130] M. Ghayour, R. Ganesan, and M. Hojjati, “Flexural response of composite beams made by Automated Fiber Placement process: Effect of fiber tow gaps,” *Compos. B Eng.*, vol. 201, p. 108368, Nov. 2020, doi: 10.1016/j.compositesb.2020.108368.

[131] M. Ghayour, M. Hojjati, and R. Ganesan, “Effect of tow gaps on impact strength of thin composite laminates made by Automated Fiber Placement: Experimental and semi-analytical approaches,” *Compos. Struct.*, vol. 248, p. 112536, Sep. 2020, doi: 10.1016/j.compstruct.2020.112536.

[132] B. Böckl, A. Wedel, A. Misik, and K. Drechsler, “Effects of defects in automated fiber placement laminates and its correlation to automated optical inspection results,” *Journal of Reinforced Plastics and Composites*, vol. 42, no. 1–2, pp. 3–16, Jan. 2023, doi: 10.1177/07316844221093273.

[133] D. Del Rossi, V. Cadran, P. Thakur, M. Palardy-Sim, M. Lapalme, and L. Lessard, “Experimental investigation of the effect of half gap/half overlap defects on the strength of composite structures fabricated using automated fibre placement (AFP),” *Compos. Part A Appl. Sci. Manuf.*, vol. 150, Nov. 2021, doi: 10.1016/j.compositesa.2021.106610.

[134] S. S. Nimbal, M. M. Banker, A. Roopa, B. Varughese, and R. Sundaram, “Effect of Gap Induced Waviness on Compressive Strength of Laminated Composites,” *Mater. Today Proc.*, vol. 4, no. 8, pp. 8355–8369, 2017, doi: 10.1016/j.matpr.2017.07.179.

[135] H. Suemasu, Y. Aoki, S. Sugimoto, and T. Nakamura, “Effect of gap on strengths of automated fiber placement manufactured laminates,” *Compos. Struct.*, vol. 263, p. 113677, May 2021, doi: 10.1016/j.compstruct.2021.113677.

[136] H. Suemasu, Y. Aoki, S. Sugimoto, and T. Nakamura, “Effect of interaction of gaps on compressive strength of automated-fiber-placement-manufactured laminates,”

Compos. Struct., vol. 306, p. 116607, Feb. 2023, doi: 10.1016/j.compstruct.2022.116607.

[137] H. Suemasu, Y. Aoki, Y. Tateishi, S. Sugimoto, and T. Nakamura, “Effect of a gap on the open hole tension strength of carbon fiber reinforced plastic laminates,” *J. Compos. Mater.*, vol. 57, no. 21, pp. 3377–3391, Sep. 2023, doi: 10.1177/00219983231184590.

[138] D. Cartié, M. Lan, P. Davies, and C. Baley, “Influence of Embedded Gap and Overlap Fiber Placement Defects on Interlaminar Properties of High Performance Composites,” *Materials*, vol. 14, no. 18, p. 5332, Sep. 2021, doi: 10.3390/ma14185332.

[139] S. Qian, X. Liu, Y. Ye, Q. Xu, T. Zhang, and X. Li, “Effect of gap and overlap fiber placement defects on the delamination behavior of L-shaped composite laminates,” *Compos. Struct.*, vol. 268, p. 113963, Jul. 2021, doi: 10.1016/j.compstruct.2021.113963.

[140] J. Brüning, B. Denkena, M.-A. Dittrich, and T. Hocke, “Machine Learning Approach for Optimization of Automated Fiber Placement Processes,” *Procedia CIRP*, vol. 66, pp. 74–78, 2017, doi: 10.1016/j.procir.2017.03.295.

[141] E. D. Gregory and P. D. Juarez, “In-situ thermography of automated fiber placement parts,” 2018, p. 060005. doi: 10.1063/1.5031551.

[142] B. Denkena, C. Schmidt, K. Völtzer, and T. Hocke, “Thermographic online monitoring system for Automated Fiber Placement processes,” Jul. 15, 2016, *Elsevier Ltd*. doi: 10.1016/j.compositesb.2016.04.076.

[143] P. D. Juarez and E. D. Gregory, “In Situ Thermal Inspection of Automated Fiber Placement for manufacturing induced defects,” *Compos. B Eng.*, vol. 220, Sep. 2021, doi: 10.1016/j.compositesb.2021.109002.

[144] C. Schmidt, B. Denkena, K. Völtzer, and T. Hocke, “Thermal Image-based Monitoring for the Automated Fiber Placement Process,” in *Procedia CIRP*, Elsevier B.V., 2017, pp. 27–32. doi: 10.1016/j.procir.2016.06.058.

[145] C. Schmidt, T. Hocke, and B. Denkena, “Artificial intelligence for non-destructive testing of CFRP prepreg materials,” *Production Engineering*, vol. 13, no. 5, pp. 617–626, Oct. 2019, doi: 10.1007/s11740-019-00913-3.

[146] E. Hu and Y. He, “Surface profile measurement of moving objects by using an improved π phase-shifting Fourier transform profilometry,” *Opt. Lasers Eng.*, vol. 47, no. 1, pp. 57–61, Jan. 2009, doi: 10.1016/j.optlaseng.2008.08.003.

[147] C. Sacco, “Machine Learning Methods for Rapid Inspection of Automated Fiber Placement Manufactured Composite Structures,” 2019.

[148] J. Cemenska, T. Rudberg, and M. Henscheid, “Automated In-Process Inspection System for AFP Machines,” *SAE International Journal of Aerospace*, vol. 08, no. 2, pp. 2015-01–2608, Sep. 2015, doi: 10.4271/2015-01-2608.

[149] A. Koptelov, B. El Said, and I. Tretiak, “Enhancing AFP manufacturing with AI: Defects forecasting and classification,” *Compos. B Eng.*, vol. 304, p. 112655, Sep. 2025, doi: 10.1016/j.compositesb.2025.112655.

[150] G. Burke, D. Nguyen, and I. Tretiak, “Artificial intelligence for process monitoring of automated fibre placement: Real-time defect detection and classification,” *Proceedings of the 21st European Conference on Composite Materials: Manufacturing*, vol. 5, no. 445451, 2024.

[151] Y. Tang, Q. Wang, L. Cheng, J. Li, and Y. Ke, “An in-process inspection method integrating deep learning and classical algorithm for automated fiber placement,” *Compos. Struct.*, vol. 300, p. 116051, Nov. 2022, doi: 10.1016/j.compstruct.2022.116051.

[152] Y. Tang, Q. Wang, H. Wang, J. Li, and Y. Ke, “A novel 3D laser scanning defect detection and measurement approach for automated fibre placement,” *Meas. Sci. Technol.*, vol. 32, no. 7, p. 075201, Jul. 2021, doi: 10.1088/1361-6501/abda95.

[153] N. Yadav and R. Schledjewski, “Review of in-process defect monitoring for automated tape laying,” *Compos. Part A Appl. Sci. Manuf.*, vol. 173, p. 107654, Oct. 2023, doi: 10.1016/j.compositesa.2023.107654.

[154] C. Krombholz, M. Perner, D. Delisle, and D. Roestermundt, “Improving the production quality of the advanced automated fiber placement process by means of online path correction,” in *Proceedings of the 28th Congress of the International Council of the Aeronautical Sciences*, Brisbane, Australia, Sep. 2012, pp. 3922–3931.

[155] C. Sacco, A. Baz Radwan, A. Anderson, R. Harik, and E. Gregory, “Machine learning in composites manufacturing: A case study of Automated Fiber Placement inspection,” *Compos. Struct.*, vol. 250, Oct. 2020, doi: 10.1016/j.compstruct.2020.112514.

[156] G. Gardiner, “InFactory Solutions with Airbus,” https://www.compositesworld.com/articles/infactory-solutions-qualifies-afp-sensor-on-mtorres-equipment.

[157] C. Weimer, A. Friedberger, A. Helwig, S. Heckner, C. Buchmann, and F. Engel, “Increasing the productivity of CFRP production processes by robustness and reliability enhancement,” in *CAMX 2016—The composites and advanced materials expo and conference. Airbus Group Innovations, 81663 Munich, Germany; AirbusInfactory Solutions GmbH, 81663 Munich, Germany*, 2016.

[158] Testia, “AF Inspect,” https://www.testia.com/product/af-inspect/.

[159] G. Gardiner, “Zero-defect manufacturing of composite parts,” https://www.compositesworld.com/articles/zero-defect-manufacturing-of-composite-parts.

[160] G. Gardiner, "ZAero project update," https://www.compositesworld.com/articles/zaero-project-update.

[161] D. Maass, "Progress in automated ply inspection of AFP layups," *Reinforced Plastics*, vol. 59, no. 5, pp. 242–245, Sep. 2015, doi: 10.1016/j.repl.2015.05.002.

[162] Loop Technology Limited, "FibreEYE," https://looptechnology.com/products/fibreeye/.

[163] M. Mussatayev, Q. Yi, M. Fitzgerald, V. K. Maes, P. Wilcox, and R. Hughes, "Directional eddy current probe configuration for in-line detection of out-of-plane wrinkles," *Compos. B Eng.*, vol. 268, p. 111048, Jan. 2024, doi: 10.1016/j.compositesb.2023.111048.

[164] R. R. Hughes, B. W. Drinkwater, and R. A. Smith, "Characterisation of carbon fibre-reinforced polymer composites through radon-transform analysis of complex eddy-current data," *Compos. B Eng.*, vol. 148, pp. 252–259, Sep. 2018, doi: 10.1016/j.compositesb.2018.05.007.

[165] M. Mussatayev, Q. Yi, P. D. Wilcox, and R. R. Hughes, "Design and comparison of directional transmit to differential receiver eddy-current probe for in-line monitoring of automated fibre placement," *Compos. B Eng.*, vol. 307, p. 112883, Nov. 2025, doi: 10.1016/j.compositesb.2025.112883.

[166] M. Y. Matveev, F. G. Ball, I. A. Jones, A. C. Long, P. J. Schubel, and M. V. Tretyakov, "Uncertainty in geometry of fibre preforms manufactured with Automated Dry Fibre Placement and its effects on permeability," *J. Compos. Mater.*, vol. 52, no. 16, pp. 2255–2269, Jul. 2018, doi: 10.1177/0021998317741951.

[167] B. F. Tatting, Z. Gürdal, and D. Jegley, "Design and manufacture of elastically tailored tow placed plates," 2002.

[168] E. V. Iarve and R. Kim, "Strength Prediction and Measurement in Model Multilayered Discontinuous Tow Reinforced Composites," *J. Compos. Mater.*, vol. 38, no. 1, pp. 5–18, Jan. 2004, doi: 10.1177/0021998304038215.

[169] M. Derakhshani Dastjerdi, M. Carboni, and M. Hojjati, "Mechanical Properties of Uncured Thermoset Tow Prepreg: Experiment and Finite Element Analysis," *Journal of Composites Science*, vol. 7, no. 8, p. 312, Jul. 2023, doi: 10.3390/jcs7080312.

[170] O. Nixon-Pearson, J.-H. Belnoue, D. Ivanov, K. Potter, and S. Hallett, "An experimental investigation of the consolidation behaviour of uncured prepregs under processing conditions," *J. Compos. Mater.*, vol. 51, no. 13, pp. 1911–1924, Jun. 2017, doi: 10.1177/0021998316665681.

[171] B. C. Kim, K. Potter, and P. M. Weaver, "Continuous tow shearing for manufacturing variable angle tow composites," *Compos. Part A Appl. Sci. Manuf.*, vol. 43, no. 8, pp. 1347–1356, Aug. 2012, doi: 10.1016/j.compositesa.2012.02.024.

[172] B. C. Kim, P. M. Weaver, and K. Potter, "Manufacturing characteristics of the continuous tow shearing method for manufacturing of variable angle tow composites," *Compos. Part A Appl. Sci. Manuf.*, vol. 61, pp. 141–151, Jun. 2014, doi: 10.1016/j.compositesa.2014.02.019.

[173] E. R. Gabriel, M. Rautmann, and B. C. Kim, "Continuous tow shearing for the automated manufacture of defect-free complex 3D geometry composite parts," *Compos. Part A Appl. Sci. Manuf.*, vol. 183, p. 108212, Aug. 2024, doi: 10.1016/j.compositesa.2024.108212.

[174] S. McArthur, J. Mehnen, C. Yokan, and I. Bomphray, "An overview of current research in automated fibre placement defect rework," *Procedia Comput. Sci.*, vol. 232, pp. 2167–2180, 2024, doi: 10.1016/j.procs.2024.02.036.

[175] J. W. Creswell and J. D. Creswell, *Research design: Qualitative, quantitative, and mixed methods approaches*. Sage publications, 2017.

[176] L. A. Palinkas, S. M. Horwitz, C. A. Green, J. P. Wisdom, N. Duan, and K. Hoagwood, "Purposeful Sampling for Qualitative Data Collection and Analysis in Mixed Method Implementation Research," *Administration and Policy in Mental Health and Mental Health Services Research*, vol. 42, no. 5, pp. 533–544, Sep. 2015, doi: 10.1007/s10488-013-0528-y.

[177] G. Guest, A. Bunce, and L. Johnson, "How Many Interviews Are Enough?," *Field methods*, vol. 18, no. 1, pp. 59–82, Feb. 2006, doi: 10.1177/1525822X05279903.

[178] S. Kvale and S. Nrinkmann, *Interviews: Learning the Craft of Qualitative Research Interviewing*, 3rd ed. Sage Publishing, 2026.

[179] J. Ritchie and L. Spencer, "Qualitative data analysis for applied policy research," in *Analyzing qualitative data*, Abingdon, UK: Taylor & Francis, 1994, ch. 9, pp. 173–194. doi: 10.4324/9780203413081_chapter_9.

[180] Hexcel Corporation, "HexPly ® M91 180ºC (350ºF) curing epoxy matrix," 2020.

[181] S. McArthur, S. McKnight, I. Bomphray, and J. Mehnen, "Assessing the effectiveness of rework in automated fibre placement-produced composite laminates: A quantitative approach using out-of-plane waviness," *Compos. Part A Appl. Sci. Manuf.*, p. 109081, Jun. 2025, doi: 10.1016/j.compositesa.2025.109081.

[182] Olympus-ims, "RollerFORM: Phased Array Wheel Probe," https://www.olympus-ims.com. https://www.olympus-ims.com/en/rollerform/ (accessed April 26, 2024).

[183] S. McKnight *et al.*, "A comparison of methods for generating synthetic training data for domain adaption of deep learning models in ultrasonic non-destructive evaluation," *NDT & E International*, vol. 141, p. 102978, Jan. 2024, doi: 10.1016/j.ndteint.2023.102978.

[184] P. Simacek, N. Niknafs Kermani, V. Gargitter, and S. G. Advani, "Role of resin percolation in gap filling mechanisms during the thin ply thermosetting automated tape placement process," *Compos. Part A Appl. Sci. Manuf.*, vol. 152, p. 106677, Jan. 2022, doi: 10.1016/j.compositesa.2021.106677.

[185] R. E. Cohen, D. Lide, and G. Trigg, *AIP Physics Desk Reference*, 3rd Edition. Springer New York, 2014. [Online]. Available: https://books.google.co.uk/books?id=h5a3QgAACAAJ

[186] M. Rueda Ruiz, "Experimental and computational micromechanics of fibre-reinforced polymer composites at high strain rates," PhD Thesis, Caminos, 2021. doi: 10.20868/UPM.thesis.67638.

[187] Shining 3D, "EinScan HX - EinScan," Sep. 2023. [Online]. Available: https://www.einscan.com/einscan-hx/

[188] P. Virtanen *et al.*, "SciPy 1.0: Fundamental Algorithms for Scientific Computing in Python," *Nat. Methods*, vol. 17, pp. 261–272, 2020, doi: 10.1038/s41592-019-0686-2.

[189] J. Sauvola and M. Pietikäinen, "Adaptive document image binarization," *Pattern Recognit.*, vol. 33, no. 2, pp. 225–236, 2000, doi: https://doi.org/10.1016/S0031-3203(99)00055-2.

[190] ISO 4287:1997 , "Geometrical Product Specifications (GPS) — Surface texture: Profile method — Terms, definitions and surface texture parameters," Geneva, Switzerland, Apr. 1997.

[191] C. S. Alexander, "Dynamic response of a carbon fiber -epoxy composite subject to planar impact," *ECCM 2012 - Composites at Venice, Proceedings of the 15th European Conference on Composite Materials*, Jan. 2012.

[192] A. J. Franck, *Understanding Rheology of Thermosets*. New Castle, DE, USA: TA Instruments, 2004.

[193] K. J. Ahn, L. Peterson, J. C. Seferis, D. Nowacki, and H. G. Zachmann, “Prepreg aging in relation to tack,” *J. Appl. Polym. Sci.*, vol. 45, no. 3, pp. 399–406, May 1992, doi: 10.1002/app.1992.070450304.

[194] D. H.-J. A. Lukaszewicz and K. Potter, “Through-thickness compression response of uncured prepreg during manufacture by automated layup,” *Proc. Inst. Mech. Eng. B J. Eng. Manuf.*, vol. 226, no. 2, pp. 193–202, Feb. 2012, doi: 10.1177/0954405411411817.

[195] S. Minakuchi, P. Simacek, and S. G. Advani, “In-situ consolidation deformation of composite laminate with gaps of various widths,” *Compos. Part A Appl. Sci. Manuf.*, vol. 180, p. 108054, May 2024, doi: 10.1016/j.compositesa.2024.108054.

[196] R. Engelhardt, K. Brath, C. Ebel, and K. Drechsler, “Experimental analysis of the compaction behavior of thermoset prepreg tapes during automated fiber placement,” in *ECCM 2018 - 18th European Conference on Composite Materials*, 2019. [Online]. Available: https://www.scopus.com/inward/record.uri?eid=2-s2.0-85084163319&partnerID=40&md5=1c521938714ae59d0afb6f67c2e12bb1

[197] D. Ivanov, Y. Li, and K. Potter, “Transitional behaviour of prepregs in automated fibre deposition processes,” in *Proceedings of International Conference on Composite Materials. ICCM-19.*, Montreal, Canada, 2013.

[198] N. Yadav and R. Schledjewski, “Inline tape width control for thermoplastic automated tape layup,” *Compos. Part A Appl. Sci. Manuf.*, vol. 163, p. 107267, Dec. 2022, doi: 10.1016/j.compositesa.2022.107267.

[199] M. Valverde, R. Sun, I. Tretiak, D. H. Nguyen, and J. Kratz, “The Effect of Process Parameters on First Ply Deposition in Automated Fibre Placement,” in *American Society for Composites 2022*, Destech Publications, Inc., Sep. 2022. doi: 10.12783/asc37/36424.

[200] V. C. Jamora, C. M. Sherin, S. Dong, B. Bhattacharjee, K. Kaipa, and O. G. Kravchenko, “The effect of prepreg laminate thickness on transverse fiber tow deformation during the deposition of AFP composites,” *Compos. Part A Appl. Sci. Manuf.*, vol. 201, p. 109443, 2026, doi: https://doi.org/10.1016/j.compositesa.2025.109443.

[201] D. C. Montgomery, *Design and analysis of experiments*. John Wiley & Sons, Inc., 2013.

[202] J. Jiang, Y. He, and Y. Ke, “Pressure distribution for automated fiber placement and design optimization of compaction rollers,” *Journal of Reinforced Plastics and Composites*, vol. 38, no. 18, pp. 860–870, Sep. 2019, doi: 10.1177/0731684419850896.

[203] Micro-Epsilon, “scanCONTROL 30x0 Laser Profile Scanner – Specifications,” 2025.

[204] Abraham. Savitzky and M. J. E. Golay, “Smoothing and Differentiation of Data by Simplified Least Squares Procedures.,” *Anal. Chem.*, vol. 36, no. 8, pp. 1627–1639, Jul. 1964, doi: 10.1021/ac60214a047.

[205] N. Otsu, “A Threshold Selection Method from Gray-Level Histograms,” *IEEE Trans. Syst. Man Cybern.*, vol. 9, no. 1, pp. 62–66, Jan. 1979, doi: 10.1109/TSMC.1979.4310076.

[206] Minitab LLC, “Minitab Statistical Software,” 2021. [Online]. Available: https://www.minitab.com

[207] L. Ståhle and S. Wold, “Analysis of variance (ANOVA),” *Chemometrics and Intelligent Laboratory Systems*, vol. 6, no. 4, pp. 259–272, Nov. 1989, doi: 10.1016/0169-7439(89)80095-4.

[208] S. Sun, Z. Han, H. Fu, H. Jin, J. S. Dhupia, and Y. Wang, “Defect Characteristics and Online Detection Techniques During Manufacturing of FRPs Using Automated Fiber Placement: A Review,” *Polymers (Basel).*, vol. 12, 2020, [Online]. Available: https://api.semanticscholar.org/CorpusID:219726536

[209] D. H. Nguyen, X. Sun, I. Tretiak, M. Adrian Valverde, and J. Kratz, “Automatic process control of an automated fibre placement machine,” *Compos. Part A Appl. Sci. Manuf.*, p. 107465, Feb. 2023, doi: 10.1016/j.compositesa.2023.107465.

[210] S. Cao, Y. Guo, W. Zhu, H. Wang, Q. Huang, and Y. Ke, “Online path correction under end point nonholonomic constraints – Implementation with visual sensing in robotic fiber placement,” *CIRP J. Manuf. Sci. Technol.*, vol. 45, pp. 138–150, 2023, doi: https://doi.org/10.1016/j.cirpj.2023.06.009.

[211] C. Mineo, C. Wong, M. Vasilev, B. Cowan, C. MacLeod, G. Pierce, E. Yang., “Interfacing Toolbox for Robotic Arms with Real-Time adaptive Behavior Capabilities,” 2019.

[212] KUKA Deutschland GmbH, “KUKA.RobotSensorInterface 4.1,” Sep. 2023, *Augsburg, Germany*.

[213] C. Mineo, D. Cerniglia, V. Ricotta, and B. Reitinger, “Autonomous 3D geometry reconstruction through robot-manipulated optical sensors,” *The International Journal of Advanced Manufacturing Technology*, vol. 116, no. 5, pp. 1895–1911, 2021, doi: 10.1007/s00170-021-07432-5.

[214] C. Mineo, D. Cerniglia, and A. Poole, “Autonomous Robotic Sensing for Simultaneous Geometric and Volumetric Inspection of Free-Form Parts,” *J. Intell. Robot. Syst.*, vol. 105, no. 3, p. 54, 2022, doi: 10.1007/s10846-022-01673-6.

[215] A. Rastegarpanah, C. Mineo, C. A. Contreras, A. Aflakian, G. Paragliola, and R. Stolkin, “Electric Vehicle Battery Disassembly Using Interfacing Toolbox for Robotic Arms,” *Batteries*, vol. 10, no. 5, 2024, doi: 10.3390/batteries10050147.

[216] M. Quigley *et al.*, “ROS: an open-source Robot Operating System,” in *ICRA workshop on open source software*, 2009, p. 5.

[217] Micro-Epsilon Messtechnik GmbH & Co. KG, “Interface Documentation linLLT: C/C++ Linux,” Jul. 2022.

[218] S. Pantoji, C. Kassapoglou, and D. Peeters, “Predicting gaps and overlaps in Automated Fiber Placement composites by measuring sources of manufacturing process variations,” *Compos. B Eng.*, vol. 291, p. 111891, 2025, doi: https://doi.org/10.1016/j.compositesb.2024.111891.

[219] S. McArthur, J. Mehnen, and I. Bomphray, “Benchtop-AFP: an Exploration of Democratised Automated Fibre Placement ,” in *Proceedings of the 21st International Conference on Manufacturing Research*, Glasgow, UK, Aug. 2024, pp. 1–6.

[220] S. McArthur, C. Yokan, and J. Mehnen, “Coupled deformation responses during thermoset AFP recompaction: Process parameter analysis and defect mitigation viability,” *Compos. Part A Appl. Sci. Manuf.*, vol. 205, p. 109691, Jun. 2026, doi: 10.1016/j.compositesa.2026.109691.

[221] S. McArthur, C. Mineo, A. Poole, I. Bomphray, and J. Mehnen, “Future-Proof Adaptive Path Correction in Automated Fibre Placement: A Concept Demonstration,” in *2025 IEEE International Conference on Simulation, Modeling, and Programming for Autonomous Robots (SIMPAR)*, 2025, pp. 1–6. doi: 10.1109/SIMPAR62925.2025.10978996.

Appendices

Appendix 3A: full Questionnaire Transcript

Expert	Q1. Can you describe your experience with automated fibre placement technology?
A	I've led most of AMRC's AFP projects since 2015, laying many complex thermoset, dry fibre and thermoplastic laminates, optimising machine setups, maintenance and our approaches to program creation and data collection
B	We were acquired by Trelleborg about 5 years ago. The company was known at the time as Automated Dynamics. Automated Dynamics was an early pioneer of AFP, and got its start out of an incubator program in 1984 at RPI – local engineering school. We have roughly 100 work cells, primarily in academic and government locations, globally. Our recent focus has been in production of composite parts, i.e.. CF/PEEK, for our customers versus the actual selling of work cells.
C	Numerous projects with equipment OEMs (incl. Coriolis, MTorres, Electro Impact), on AFP/DFP processing, including in-process inspection technologies. Knowledge of Hexcel & Solvay material processing: deposition, infusion & cure. Hybrid material solutions e.g. AFP/DFP tows in combination with other material formats
Q2. In your opinion, what are the main advantages of using automated fibre placement technology compared to traditional methods?	
A	It's currently the primary, proven industrial technology for manufacturing mid-complexity, mid-volume, components that benefit most from the extensive lightweighting it can deliver, e.g. for aircraft fuselages, wing skins and spars. AFP therefore contributes to reduced aircraft fuel consumption and emissions, for example, for performance and sustainability benefits. AFP production processes also waste very little material.
B	Flexibility in designing composite solutions (parts); with the inherent advantages of composites – lightweight, stiffness, chemical resistivity, etc. Additionally with our manufacturing there is no post process required (no auto-clave step). The part is produced on a mandrel, cooled and ready for use. By eliminating the post process, we save time and money. As well, our AFP process starts with uni-directional pre-preg. In other words all the fibers, carbon or otherwise, are lined up in the same direction. This results in superior strengthen in that direction. When combined with a resin like PEEK, you get a part that can carry and sustain incredible loads across the part.
C	Repeatability, labour / Recurring Cost reductions, Operator H&S when considering scale or access issues
Q3. What are the main challenges facing the implementation of automated fibre placement technology?	
A	High costs for accurately slitting material to work well with the equipment. High cost of equipment. Time consuming and labour intensive inspection requirements. Challenges for quality in-situ consolidation (ISC) of thermoplastic composites at economically viable deposition rates. Current composites design software isn't yet mature enough to automatically design composite structures that fully exploit the physical abilities of AFP machines, e.g. through automated design of optimised curvilinear variable stiffness laminates.

B	The cost of these work cells can be expensive. The latest technology uses lasers as the heat source – sometimes multiple lasers. This equipment is quite often beyond the budget of most academic institutions.
C	Capital costs, Deposition rates for medium to complex components, Tow defect inspection & rework, stoppages or breakdowns are harder/longer to resolve vs manual. Very difficult to adopt / make business case on legacy products which are typically manufactured within low-cost supply chain. Non-recurring Engineering costs to change models / drawsets. New process or material qualifications
Q4. How does automated fibre placement technology compare to other advanced composite manufacturing techniques?	
A	High accuracy and repeatability Often enables components to be lighter than when made by other methods Relatively slow Expensive
B	The principles of AFP rely on time, temperature, and compaction in order to produce complex composite parts. Although vastly superior to metals in many applications, the raw materials used in manufacturing can be expensive as well – i.e.. CF/PEEK can exceed $120/lb. If strengthen to weight is a key ratio in evaluating applicability of AFP, there aren't many manufacturing methods that are superior.
C	Provide overall good design space (fibre orientations), limited tow steering abilities (vs tow-shearing), typically slower depo rates vs P&P or manual (on small – med components)
Q5. Can you discuss any recent advancements or innovations in the field of automated fibre placement technology?	
A	AMRC have been working on a numerical design tool for automatically designing optimised curvilinear variable stiffness laminates, e.g. for AFP, accounting for minimum tow lengths. The numerical design tool is also being developed for other manufacturing methods, e.g. TFP and RTS.
B	We have just built the first dual laser AFP machine. One laser controls the heat of the substrate, and the other laser can control the heat of the incoming pre-preg material. This creates more efficient heating and can result in faster production.
C	Tow-shearing looks to show promise for optimised component architecture but lacks analysis toolsets. Substantial improvements in in-process inspection with numerous systems now being deployed. Multiple material formats (tow widths) in development or use, offering bespoke advantages for specific components Low cost / Single tow end effectors for R&D & other bespoke applications
Q6. Are there any current research or development efforts in the field of automated fibre placement that you find particularly exciting or promising?	
A	For high quality ISC of thermoplastic composites, having independently controlled lasers for heating the substrate and the incoming tape looks like a good idea.
B	Better software integration between robot and processing head. Flaw detection capabilities. Speed of manufacturing.
C	In-process inspection, Tow-shearing,

Q7. Are there any specific challenges you have encountered when working with automated fibre placement in certain industries or applications?	
A	High quality ISC of high temperature thermoplastic composites is very challenging for many geometries. Due to large data processing requirements, some automated inspection systems struggle to flag defects in real-time.
B	Automotive and aerospace markets can have demanding production timelines. Need to increase manufacturing processes to achieve further market acceptance for advanced composites.
C	Inspection – each ply requires 100% inspection within Aero Ind. Time to rework
Q8. What are the common defects that occur in automated fibre placement technology and how do they affect the final product?	
A	Gaps, overlaps, inaccurate adds or cuts, tape folding, fibre waviness on the inside edge of steered tapes. If not detected and reworked, they contribute to stress concentrations and performance reductions, e.g. strength.
B	Our process is a combination of time, temperature and compaction. If any of these process parameters are not accurate, or the incoming pre-preg material does not meet our quality standards, you could end up with inconsistent bond quality and ultimately a failed part. I'm over simplifying on the process parameters, but there's lots of room for error based on polymers processed. (Polymers have different fiber volume and melt temperature, etc.)
C	Gaps, overlaps, missing tows, fuzzballs – if not detected can affect component performance or scrappage. Detected defects incur costs to rework and create concession documentation (if rework acceptable)
Q9. How does the prevalence and severity of defects in automated fibre placement technology compare to traditional composite manufacturing methods?	
A	AFP is often used for critical and very lightweight structures, where costs to closely inspect each ply can be justified, and selected tapes removed and relayed if necessary, so designs can expect zones or sometimes even full laminates to be essentially free of defects when cured. It often isn't viable for non-AFP parts to be similarly inspected, so their designs must be more defect tolerant, and therefore heavier.
B	Hand layup methods are subject to inconsistencies and not scalable.
C	AFP defects may be more difficult to visually observe. If missed, has greater impact on infusion, cure tooling, performance
Q10. How do you typically identify and classify defects in automated fibre placement processes?	
A	This is commonly done with visual inspection. AMRC has collaborated on some means for automated defect detection, through processing of laser line scanning and imagery, for example.
B	Material (pre-preg) may not bond as expected. Further testing of material may be needed
C	Defects are detected either visually or through use of laser/optical systems (in-process), or by using NDT post cure. Defects are classified according to specifications provided by customers. Effect of defect assessed through FE analysis.
Q11. How does the method of defect detection affect the reworking process?	
A	Automated defect detection can point to areas of interest and reduce efforts to locate defects and remove and readd material as necessary.

B	Depending on the defect will affect processing conditions – i.e.. Raise/lower temperature, increase or decrease compaction.
C	Digital data stream-lines defect recording, offering improvements in defect location & severity (less effort in concessions). Rework methods are consistent regardless of detection methods. Obviously if defect detection can be translated to rework at time of identification, reduces down-stream inspection, rework, concessions.
Q12. How do the effects of defects in automated fibre placement technology compare to other types of defects in advanced composites manufacturing?	
A	
B	Can't answer this one due to our trade secrets.
C	Any deposition process which feeds / deposits fibre or tow has similar defect ranges (gaps, overlaps, missing, fuzz) e.g Filament Winding. Less variation on fibre angles perhaps.
Q13. Have you encountered any particularly challenging defects in your work with automated fibre placement, and if so, how did you address them?	
A	Addressing defects in high temperature thermoplastic composite AFP layups is particularly challenging. It is necessary to heat tapes, e.g. with a heat gun, to remove them, though it can still be challenging to do this neatly without breaking fibres and leaving some behind. Pulling tapes straight, i.e. not bending them back on themselves, helps remove tapes neatly, though this is often only practical if there is a tab (free end) to start with.
B	All material issues. Challenge is getting consistent grade of material from pre-preg manufacturers – i.e.. Solvay, Toray, Victrex, etc..
C	
Q14. Are there any specific testing methods that are used to evaluate the effects of defects in automated fibre placement technology?	
A	ASTM D2344M ASTM D3518 ASTM D3039M ASTM D6641M
B	Every batch of material we receive is NOL processed. Once passed we know the materials have made our specifications for manufacturing.
C	
Q15. Are there any best practices or guidelines for minimizing defects in automated fibre placement technology?	
A	For thermoset materials, keeping head components, such as feed rollers and cutters, cool, to reduce how tacky the material is will reduce fibres sticking to these components and contributing to defects and downtime.
B	Material testing (NOL's) prior to product manufacturing.
C	
Q16. Can you describe your reworking process for defects in automated fibre placement, including any specific tools or techniques you use?	
A	To generally use "hook and pick set" style tools to remove tapes as necessary. Then use the machine to relay tapes where they've been removed.
B	Hot irons and other methods to batch gaps, or other inconsistencies. Compaction afterwards to ensure consolidation.
C	

Q17. How do you evaluate the effectiveness of your reworking process for defects in automated fibre placement?	
A	Inspect the rework
B	Peel test to ensure bonding.
C	
Q18. Are there any industry-specific standards or guidelines that you follow for reworking defects in automated fibre placement?	
A	Please share any you know of?
B	None
C	
Q19. Are there any opportunities for improvement in the reworking process for defects in automated fibre placement technology?	
A	Automated inspection to point to defect areas and reduce efforts to locate defects and automating the process for instructing the AFP machine to relaying only the tapes that were removed.
B	Can always be improved. Early Detection would be most helpful.
C	
Q20. Can you discuss any future developments or advancements you anticipate in the field of automated fibre placement, particularly with regards to defect reworking?	
A	
B	On the fly flaw detection.
C	

Appendix 3D: Coded responses by question and expert

Q	Expert	TECH-ADV	TECH-CHAL	TECH-REC	TECH-FUT	DEF-TYPE	DEF-IMP	DEF-INSP	DEF-DET	RW-PROC	RW-TOOL	RW-EVAL	RW-STD	RW-IMP	TIME-CRIT	INTEGR	COST	PREV
Q1	E1	-	-	-	-	-	-	-	-	-	-	-	-	-	-	-	-	-
	E2	-	-	-	-	-	-	-	-	-	-	-	-	-	-	-	-	-
	E3	-	-	-	-	-	-	-	-	-	-	-	-	-	-	-	-	-
Q2	E1	✓	-	-	-	-	-	-	-	-	-	-	-	-	-	-	✓	-
	E2	✓	-	-	-	-	-	-	-	-	-	-	-	-	-	-	✓	-
	E3	✓	-	-	-	-	-	-	-	-	-	-	-	-	-	-	✓	-
Q3	E1	-	✓	-	-	-	-	✓	-	✓	-	-	-	-	✓	✓	✓	-
	E2	-	✓	-	-	-	-	-	-	-	-	-	-	-	-	-	✓	-
	E3	-	✓	-	-	-	-	✓	-	✓	-	-	-	-	-	-	✓	-
Q4	E1	✓	✓	-	-	-	-	-	-	-	-	-	-	-	-	-	✓	-
	E2	✓	-	-	-	-	-	-	-	-	-	-	-	-	-	-	✓	-
	E3	✓	✓	-	-	-	-	-	-	-	-	-	-	-	-	-	-	-
Q5	E1	-	-	✓	-	-	-	-	-	-	-	-	-	-	-	✓	-	-
	E2	-	-	✓	-	-	-	-	-	-	-	-	-	-	-	✓	-	-
	E3	-	-	✓	-	-	-	✓	-	-	-	-	-	-	-	-	✓	-
Q6	E1	-	-	-	✓	-	-	-	-	-	-	-	-	-	-	-	-	-
	E2	-	-	-	✓	-	-	✓	-	-	-	-	-	-	-	✓	-	-
	E3	-	-	-	✓	-	-	✓	-	-	-	-	-	-	-	-	-	-
Q7	E1	-	✓	-	-	-	-	✓	-	-	-	-	-	-	✓	-	-	-
	E2	-	✓	-	-	-	-	-	-	-	-	-	-	-	✓	-	-	-

	E3	-	✓	-	-	-	-	✓	-	✓	-	-	-	-	-	-	-	-
Q8	E1	-	-	-	-	✓	✓	-	-	-	-	-	-	-	-	-	-	-
	E2	-	-	-	-	✓	✓	-	-	-	-	-	-	-	-	-	✓	-
	E3	-	-	-	-	✓	✓	-	-	✓	-	-	-	-	-	-	-	-
Q9	E1	-	-	-	-	-	✓	✓	-	✓	-	-	-	-	-	-	-	-
	E2	-	-	-	-	-	✓	✓	-	-	-	-	-	-	-	-	✓	-
	E3	-	-	-	-	-	-	-	-	-	-	-	-	-	-	-	-	-
Q10	E1	-	-	-	-	-	-	✓	✓	-	-	-	-	-	-	-	-	-
	E2	-	-	-	-	-	✓	✓	-	-	-	-	-	-	-	-	-	-
	E3	-	-	-	-	-	-	✓	-	-	-	-	✓	-	-	-	-	-
Q11	E1	-	-	-	-	-	-	✓	✓	✓	-	-	-	-	-	✓	-	-
	E2	-	-	-	-	-	-	-	-	✓	-	-	-	-	-	-	-	-
	E3	-	-	-	-	-	-	-	-	✓	-	-	-	-	✓	✓	-	-
Q12	E1	-	-	-	-	-	-	-	-	-	-	-	-	-	-	-	-	-
	E2	-	-	-	-	-	-	-	-	-	-	-	-	-	-	-	-	-
	E3	-	-	-	-	✓	-	-	-	-	-	-	-	-	-	-	-	-
Q13	E1	-	-	-	-	✓	-	-	-	✓	✓	-	-	-	✓	-	-	-
	E2	-	-	-	-	-	-	-	-	-	-	-	-	-	-	-	-	-
	E3	-	-	-	-	-	-	-	-	-	-	-	-	-	-	-	-	-
Q14	E1	-	-	-	-	-	-	-	-	-	-	✓	✓	-	-	-	-	-
	E2	-	-	-	-	-	-	-	-	-	-	-	-	-	-	-	-	-
	E3	-	-	-	-	-	-	-	-	-	-	-	-	-	-	-	-	-
Q15	E1	-	-	-	-	-	-	-	-	-	-	-	-	-	-	-	-	✓
	E2	-	-	-	-	-	-	-	-	-	-	-	-	-	-	-	-	✓

	E3	-	-	-	-	-	-	-	-	-	-	-	-	-	-	-	-	-
Q16	E1	-	-	-	-	-	-	-	-	✓	✓	-	-	-	-	-	-	-
	E2	-	-	-	-	-	-	-	-	✓	✓	-	-	-	-	-	-	-
	E3	-	-	-	-	-	-	-	-	-	-	-	-	-	-	-	-	-
Q17	E1	-	-	-	-	-	-	-	-	-	-	✓	-	-	-	-	-	-
	E2	-	-	-	-	-	-	-	-	-	-	✓	-	-	-	-	-	-
	E3	-	-	-	-	-	-	-	-	-	-	-	-	-	-	-	-	-
Q18	E1	-	-	-	-	-	-	-	-	-	-	-	✓	-	-	-	-	-
	E2	-	-	-	-	-	-	-	-	-	-	-	✓	-	-	-	-	-
	E3	-	-	-	-	-	-	-	-	-	-	-	-	-	-	-	-	-
Q19	E1	-	-	-	-	-	-	-	✓	-	-	-	-	✓	-	✓	-	-
	E2	-	-	-	-	-	-	-	✓	-	-	-	-	✓	-	-	-	-
	E3	-	-	-	-	-	-	-	-	-	-	-	-	-	-	-	-	-
Q20	E1	-	-	-	-	-	-	-	-	-	-	-	-	-	-	-	-	-
	E2	-	-	-	✓	-	-	-	✓	-	-	-	-	✓	-	-	-	-
	E3	-	-	-	-	-	-	-	-	-	-	-	-	-	-	-	-	-
Sum		6	8	3	4	5	6	13	5	11	3	3	4	3	5	7	11	2

Appendix 5A ISO 14125 full results

Specimen class	No.	E_f (GPa)	σ_{fC} (MPa)	ε_C (%)	σ_{fB} (MPa)	ε_B (%)
Defective	D-1	46.11747	442.1185	0.008987	877.9556	1.902216
	D-2	40.33597	420.952	0.0095795	833.1443	2.08761
	D-3	41.05392	419.0841	0.0093823	841.8753	2.030538
	D-4	50.97079	456.0102	0.0083723		
	D-5	52.409	460.8097	0.0081676	1040.924	2.006516
	D-6	38.13082	404.2698	0.0100701	714.3383	1.898371
	D-7	40.59741	402.7855	0.0094551	722.8743	1.845981
	D-8	42.46944	417.8833	0.0093026	836.8293	2.231362
	D-9	43.52477	415.8961	0.0090583	774.2596	1.988584
	D-10	51.30898	438.6561	0.008127	969.8577	2.296713
	D-11	52.86659	450.0496	0.0079054	1034.023	2.27504
	D-12	45.74676	419.988	0.0086699	963.5183	2.475414
	D-13	54.59641	453.6531	0.0078323	1045.52	2.33704
	D-14	56.28901	447.9099	0.0075299	976.8251	1.958183
	D-15	45.40432	412.5444	0.0086211	885.0433	2.236937
	D-16	55.38954	446.6925	0.0076738	1034.639	2.441337
	D-17	46.63709	419.7518	0.0085516	952.7001	2.462312
Pristine : [90/0]3s	P90-1	42.14098	336.4194	0.0070875	886.5343	2.180525
	P90-2	41.4737	336.7109	0.0072654	935.3097	2.554086
	P90-3	41.19808	341.2368	0.0071508	957.937	2.591333
	P90-4	39.48191	320.527	0.0072782	914.5967	2.724529
	P90-5	39.84407	326.4194	0.007452	860.745	2.511913
	P90-6	45.89964	357.6877	0.0069743	967.906	2.597892
	P90-7	42.72254	341.8206	0.0071826		
	P90-8	40.7002	327.1589	0.0071572		
	P90-9	42.33317	340.9693	0.0070875		
	P90-10	43.0227	341.663	0.0070623	956.8525	2.684851
	P90-11	40.63898	326.821	0.0071889		
	P90-12	42.09062	338.9713	0.0072527		
	P90-13	38.13898	320.1918	0.0074909		
	P90-14	41.33139	332.425	0.0072974		
	P90-15	41.8802	330.3994	0.0071762		
	P90-16	43.65032	331.2788	0.0068372	958.114	2.528082
	P90-17	40.4077	329.3525	0.0072654		
	P90-18	43.23025	340.9647	0.0071826	969.0149	2.688776
	P90-19	41.79635	336.4699	0.0071889		
	P90-20	39.76532	338.2937	0.0074197		
	P90-21	42.69934	335.2548	0.0069618	947.3638	2.602066
	P90-22	43.43151	347.334	0.0072271	894.0782	2.385079
Reworked	R-1	69.52146	495.5947	0.0067692	1230.168	1.934865
	R-2	65.62631	485.1077	0.0069806	1131.008	1.844783
	R-3	62.95606	478.143	0.0071572	1141.514	2.150164
	R-4	64.29926	480.4921	0.0069994	1175.507	2.024385
	R-5	65.39837	490.4514	0.0070939	1175.549	1.97417
	R-6	68.46808	496.8738	0.0068683	1150.346	1.833921

	R-7	73.25917	515.3182	0.0066463	1229.29	1.833087
	R-8	67.14109	487.4702	0.0068869	1211.581	2.027535
	R-9	66.41645	487.8209	0.0069181	1166.841	1.95694
	R-10	66.47676	488.7321	0.0069243	1188.984	1.910421
	R-11	68.25088	489.1556	0.0066892	1225.04	1.980204
	R-12	59.94617	470.4836	0.0073423	1019.009	1.793505
	R-13	66.40941	485.0037	0.0068994	1201.977	2.059376
	R-14	64.78886	497.1205	0.0073038	1155.115	2.077508
	R-15	64.19312	487.0228	0.0071445	1135.479	1.894571
	R-16	63.94357	489.0275	0.007208	1197.981	2.083314
	R-17	62.97034	498.5496	0.0074391	1151.687	2.0231
	R-18	60.18518	488.309	0.0076541	1116.384	1.93376
	R-19	58.95788	462.9387	0.0074391	1092.278	2.175532
	R-20	58.85339	473.0365	0.0075886	1141.525	2.355251
	R-21	58.64703	456.7526	0.0073038	1130.296	2.327416
	R-22	63.28142	478.4006	0.0071953	1152.769	2.083141
	R-23	57.42158	448.4932	0.0071255	1078.673	1.910785
	R-24	57.67481	456.6154	0.0070939	1068.984	1.923978
	R-25	60.45216	467.0962	0.0071572	1142.997	1.950012
	R-26	57.68804	464.7804	0.0074326	1014.467	1.765442
	R-27	59.20403	474.6166	0.0073874	1094.663	2.044374
	R-28	61.3481	458.2027	0.0069306	1170.338	2.251546
	R-29	51.20261	438.6535	0.0078455	953.4768	1.940219
	R-30	57.99037	472.9813	0.0074909	1146.673	2.076606
	R-31	57.82369	465.7553	0.0074326	1066.049	1.900628
	R-32	51.8993	426.0908	0.0073552	991.4482	1.909362
	R-33	58.65183	479.3805	0.007556	1143.384	2.245905
	R-34	57.10728	464.8923	0.0074909	1138.5	2.220791
Pristine : [0/90]3s	P0-1	72.27898	522.3728	0.681974	1184.3	1.879303
	P0-2	68.49186	523.4604	0.729423	1170.315	2.072258
	P0-3	66.33957	512.0038	0.717566	1195.425	2.080484
	P0-4	62.81125	502.2368	0.735106	1085.943	2.183423
	P0-5	67.56727	510.7058	0.713424	1159.025	1.974523
	P0-6	72.93608	513.7863	0.656258	1195.63	1.868241
	P0-7	71.70663	534.1658	0.70822	1135.453	1.867953
	P0-9	73.50695	568.3951	0.732811	1186.095	1.822457
	P0-10	66.61692	505.1412	0.714154	1057.227	1.818293
	P0-11	67.75315	503.5085	0.696952	1182.135	2.088364
	P0-12	67.01459	499.9096	0.700134	1049.756	1.874664
	P0-13	70.85465	512.637	0.676621	1233.481	2.100579
	P0-14	63.74902	495.4502	0.724792	1076.535	2.029218
	P0-15	67.78116	513.3444	0.7105	1238.91	2.255663
	P0-16	66.52375	504.8987	0.711807	1078.126	1.854616

Appendix 6A Experimental settings for experiment 1

Run	C	T	S	H	L
1	High	Low	High	On	Short
2	Low	High	Low	Off	Short
3	High	Low	Low	Off	Short
4	High	Low	High	Off	Long
5	High	High	High	Off	Long
6	Low	Low	Low	Off	Short
7	Low	Low	High	On	Long
8	Low	High	Low	On	Short
9	Low	High	High	Off	Short
10	High	High	High	On	Long
11	High	Low	High	On	Long
12	Low	High	High	Off	Short
13	Low	Low	Low	Off	Long
14	High	Low	Low	On	Short
15	Low	Low	High	Off	Short
16	High	Low	Low	On	Long
17	Low	High	High	On	Long
18	High	Low	High	Off	Short
19	High	Low	Low	Off	Long
20	Low	High	High	On	Short
21	High	Low	High	On	Long
22	Low	Low	High	Off	Long
23	High	High	High	On	Short
24	Low	Low	Low	On	Long
25	High	High	High	Off	Short
26	High	High	Low	On	Long
27	Low	High	High	Off	Long
28	Low	Low	High	On	Short
29	Low	High	Low	On	Long
30	Low	High	Low	Off	Long
31	Low	Low	Low	On	Short
32	High	High	Low	On	Short

Appendix 6B Width change results for experiment 1

Trial No.	W(o) ± MAD (mm)	W(r) ± MAD (mm)	ΔW ± σ_MAD (mm)	RMSTD (mm)
1	6.399 ± 0.037	6.388 ± 0.035	-0.011 ± 0.051	0.466
2	6.324 ± 0.044	6.516 ± 0.062	0.192 ± 0.076	0.120
3	6.292 ± 0.02	6.284 ± 0.022	-0.008 ± 0.03	0.451
4	6.242 ± 0.02	6.256 ± 0.024	0.014 ± 0.031	0.444
5	6.343 ± 0.028	6.624 ± 0.058	0.281 ± 0.064	0.481
6	6.262 ± 0.026	6.25 ± 0.026	-0.012 ± 0.037	0.114
7	6.258 ± 0.026	6.25 ± 0.02	-0.008 ± 0.033	0.087
8	6.308 ± 0.026	6.412 ± 0.04	0.104 ± 0.048	0.281
9	6.283 ± 0.023	6.334 ± 0.024	0.051 ± 0.033	0.113
10	6.312 ± 0.024	6.66 ± 0.12	0.348 ± 0.122	0.491
11	6.286 ± 0.028	6.289 ± 0.023	0.003 ± 0.036	0.503
12	6.247 ± 0.025	-	-	
13	6.282 ± 0.026	6.258 ± 0.026	-0.024 ± 0.037	0.178
14	6.312 ± 0.028	6.318 ± 0.03	0.006 ± 0.041	0.487
15	6.288 ± 0.022	6.267 ± 0.034	-0.021 ± 0.04	0.124
16	6.26 ± 0.022	6.402 ± 0.042	0.142 ± 0.047	0.203
17	6.24 ± 0.028	6.294 ± 0.018	0.054 ± 0.033	0.087
18	6.274 ± 0.028	6.284 ± 0.028	0.010 ± 0.04	0.53
19	6.294 ± 0.024	6.292 ± 0.026	-0.002 ± 0.035	0.438
20	6.284 ± 0.032	6.338 ± 0.044	0.054 ± 0.054	0.075
21	6.282 ± 0.036	-	-	
22	6.29 ± 0.02	6.259 ± 0.025	-0.031 ± 0.032	0.110
23	6.252 ± 0.02	6.483 ± 0.038	0.231 ± 0.043	0.466
24	6.258 ± 0.026	6.242 ± 0.022	-0.016 ± 0.034	0.100
25	6.282 ± 0.026	6.56 ± 0.043	0.278 ± 0.05	0.481
26	6.27 ± 0.026	6.362 ± 0.038	0.092 ± 0.046	0.070
27	6.4 ± 0.058	6.414 ± 0.046	0.014 ± 0.074	0.541
28	6.331 ± 0.039	6.367 ± 0.056	0.036 ± 0.068	0.199
29	6.302 ± 0.016	6.324 ± 0.028	0.022 ± 0.032	0.098
30	6.284 ± 0.028	6.332 ± 0.052	0.048 ± 0.059	0.168
31	6.26 ± 0.026	6.252 ± 0.026	-0.008 ± 0.037	0.119
32	6.345 ± 0.029	6.566 ± 0.186	0.221 ± 0.188	0.393

Appendix 6C Full ANOVA table for Experiment 1

Source	DF	Seq SS	Contribution	Adj SS	Adj MS	F-Value	P-Value
Model	25	101.402	98.89%	101.402	4.0561	14.22	0.010
Linear	5	62.423	60.88%	54.152	10.8304	37.98	0.002
C	1	9.097	8.87%	6.377	6.3770	22.36	0.009
T	1	51.877	50.59%	17.327	17.3267	60.76	0.001
S	1	0.447	0.44%	1.458	1.4584	5.11	0.087
H	1	0.127	0.12%	0.355	0.3547	1.24	0.327
L	1	0.875	0.85%	0.443	0.4430	1.55	0.281
2-Way Interactions	10	21.922	21.38%	26.435	2.6435	9.27	0.023
C×T	1	14.671	14.31%	2.049	2.0495	7.19	0.055
C×S	1	0.766	0.75%	3.490	3.4896	12.24	0.025
C×H	1	0.054	0.05%	0.336	0.3356	1.18	0.339
C×L	1	0.804	0.78%	1.452	1.4516	5.09	0.087
T×S	1	1.870	1.82%	2.269	2.2692	7.96	0.048
T×H	1	1.814	1.77%	0.209	0.2089	0.73	0.440
T×L	1	1.509	1.47%	1.181	1.1808	4.14	0.112
S×H	1	0.021	0.02%	0.069	0.0695	0.24	0.647
S×L	1	0.365	0.36%	0.818	0.8181	2.87	0.166
H×L	1	0.048	0.05%	1.855	1.8550	6.50	0.063
3-Way Interactions	10	17.056	16.63%	17.056	1.7056	5.98	0.050
C×T×S	1	7.292	7.11%	6.345	6.3454	22.25	0.009
C×T×H	1	0.204	0.20%	0.234	0.2342	0.82	0.416
C×T×L	1	0.046	0.05%	0.010	0.0102	0.04	0.859
C×S×H	1	4.008	3.91%	2.977	2.9767	10.44	0.032
C×S×L	1	0.905	0.88%	0.032	0.0320	0.11	0.755
C×H×L	1	0.794	0.77%	1.240	1.2402	4.35	0.105
T×S×H	1	0.579	0.56%	0.120	0.1195	0.42	0.553
T×S×L	1	2.081	2.03%	2.927	2.9269	10.26	0.033
T×H×L	1	0.289	0.28%	0.512	0.5122	1.80	0.251
S×H×L	1	0.858	0.84%	0.858	0.8580	3.01	0.158
Error	4	1.141	1.11%	1.141	0.2852	-	-
Total	29	102.543	100.00%				

Appendix 6D Coded Coefficients Table for Experiment 1

Term	Effect (mm)	Coef	SE Coef	95% CI	T-Value
Constant		0.06245	0.00719	(0.04248, 0.08243)	8.68
C	0.06384	0.03192	0.00675	(0.01318, 0.05066)	4.73
T	0.11599	0.05800	0.00744	(0.03734, 0.07866)	7.79
S	0.03709	0.01854	0.00820	(-0.00422, 0.04131)	2.26
H	0.01532	0.00766	0.00687	(-0.01141, 0.02672)	1.12
L	-0.01575	-0.00787	0.00632	(-0.02541, 0.00966)	-1.25
C×T	0.03631	0.01815	0.00677	(-0.00065, 0.03695)	2.68
C×S	0.05402	0.02701	0.00772	(0.00557, 0.04844)	3.50
C×H	0.01407	0.00704	0.00649	(-0.01097, 0.02504)	1.08
C×L	0.02758	0.01379	0.00611	(-0.00318, 0.03076)	2.26
T×S	0.04680	0.02340	0.00830	(0.00037, 0.04643)	2.82
T×H	-0.01152	-0.00576	0.00673	(-0.02445, 0.01293)	-0.86
T×L	-0.02490	-0.01245	0.00612	(-0.02944, 0.00454)	-2.03
S×H	-0.00619	-0.00309	0.00627	(-0.02049, 0.01431)	-0.49
S×L	0.01881	0.00940	0.00555	(-0.00601, 0.02482)	1.69
H×L	0.02728	0.01364	0.00535	(-0.00121, 0.02849)	2.55
C×T×S	0.07558	0.03779	0.00801	(0.01555, 0.06004)	4.72
C×T×H	0.01235	0.00617	0.00681	(-0.01274, 0.02509)	0.91
C×T×L	-0.00239	-0.00119	0.00631	(-0.01871, 0.01632)	-0.19
C×S×H	-0.03390	-0.01695	0.00525	(-0.03152, -0.00238)	-3.23
C×S×L	-0.00333	-0.00166	0.00497	(-0.01547, 0.01214)	-0.33
C×H×L	0.02006	0.01003	0.00481	(-0.00332, 0.02339)	2.09
T×S×H	0.00811	0.00406	0.00627	(-0.01334, 0.02145)	0.65
T×S×L	0.03754	0.01877	0.00586	(0.00250, 0.03504)	3.20
T×H×L	0.01475	0.00738	0.00550	(-0.00791, 0.02266)	1.34
S×H×L	-0.01633	-0.00817	0.00471	(-0.02124, 0.00491)	-1.73

Appendix 6E Experimental Settings for Experiment 2

Trial No.	Compaction force (C)	Tooling temperature (T)	Layup speed (S)	External heating (H)	Lie time (L)
1	50	70	55	OFF	60
2	375	70	55	OFF	60
3	750	70	55	OFF	60
4	50	70	55	OFF	300
5	375	70	55	OFF	300
6	750	70	55	OFF	300
7	50	70	55	ON	60
8	375	70	55	ON	60
9	750	70	55	ON	60
10	50	70	55	ON	300
11	375	70	55	ON	300
12	750	70	55	ON	300

Trial No.	W(o) ± MAD (mm)	W(r) ± MAD (mm)	ΔW ± σ_MAD (mm)	RMSTD (mm)
1	6.332 ± 0.04	6.298 ± 0.042	-0.034 ± 0.058	0.111
2	6.352 ± 0.034	6.373 ± 0.056	0.021 ± 0.066	0.173
3	6.332 ± 0.044	6.407 ± 0.073	0.075 ± 0.085	0.432
4	6.35 ± 0.043	6.302 ± 0.036	-0.048 ± 0.056	0.117
5	6.322 ± 0.045	6.308 ± 0.038	-0.014 ± 0.059	0.136
6	6.296 ± 0.032	6.352 ± 0.063	0.056 ± 0.071	0.462
7	6.284 ± 0.036	6.278 ± 0.046	-0.006 ± 0.058	0.089
8	6.294 ± 0.038	6.332 ± 0.03	0.038 ± 0.048	0.176
9	6.336 ± 0.036	6.39 ± 0.068	0.054 ± 0.077	0.410
10	6.348 ± 0.048	6.296 ± 0.036	-0.052 ± 0.06	0.112
11	6.338 ± 0.046	6.338 ± 0.038	0 ± 0.06	0.176
12	6.332 ± 0.042	6.393 ± 0.071	0.061 ± 0.082	0.442

Appendix 7A: Defect detection algorithm

Algorithm 1. Defect detection and classification

Input: Profile $P = \{(x_i, z_i)\}$, thresholds τ_e, w_{min}, Δh_{min}
Output: Set of Gaps G, Overlaps O
1. Filter profile to detection range
2. Sort points by x-coordinate
3. Smooth z using moving average filter
4. Compute discrete gradient g_i
5. Classify edges using threshold τ_e
6. Estimate baseline height z_{base} (70th percentile)
7. For each consecutive edge pair (i, j):
    Compute plateau statistics μ_S, σ_S, width w_S
    If $w_S > w_{min}$ AND $\sigma_S < \tau_\sigma$:
        If $e_i = -1$ and $e_j = +1$ and
         $z_{base} - \mu_S \geq \Delta h_{min}$:
            classify as GAP
        If $e_i = +1$ and $e_j = -1$ and
         $\mu_S - z_{base} \geq \Delta h_{min}$:
            classify as OVERLAP
8. Return detected gaps and overlaps

Appendix 7B: Full handshake protocol

Algorithm 2. Full Handshake — One Waypoint Cycle

Step 1: [Path Correction node → Coordinate Reader via ROS]
1. monitor_processed_semaphore() detects path_processed.sem
2. cleanup_semaphores() deletes both files
3. publishes Empty on /request_next_line and /path_correction/ready_for_next
4. currently_processing set False

Step 2: [Coordinate Reader dispatches waypoint]
5. next_line_callback() sets next_line_requested = True
6. check_semaphore_status() verifies no semaphores exist
7. send_next_coordinate() publishes Float64MultiArray[9] on /coordinate_reader/coordinates
8. coordinate_sent = True
9. current_line incremented

Step 3: [Path Correction node applies correction]
10. coordinate_callback() receives waypoint
11. calculates segment_length
12. if defect validated (5 consecutive non-zero readings)*:* compute and apply increments
13. *write_coordinates_to_file()* writes corrected [X,Y,Z,A,B,C,E1,E2,E3] to *next_path.txt*
14. creates path_ready.sem
15. currently_processing = True

Step 4: [MATLAB reads corrected waypoint]
16. readNextPath() polls for path_ready.sem
17. reads next_path.txt
18. parses 9 comma-delimited values
19. creates path_processed.sem
20. returns *layupMatrix* to control loop

Step 5: [MATLAB executes trajectory]
21. *F_applySpeedPattern()* generates Interpolated N-step trajectory
22. write_12DoFs_coordinates() serialises to path.txt in KUKA RSI XML format
23. setToolPathFromFile() streams to robot
24. inner loop reads *feedbackPos* at 12 ms RSI cycle

Step 6: [Path Correction node detects completion]
25. monitor_processed_semaphore() polls every 100 ms
26. detects path_processed.sem
27. cycle restarts at Step 1 [Coordinate Reader simultaneously resets *coordinate_sent = False* via its own 200 ms timer]

Appendix 7C: Path correction algorithm

Algorithm 3: Path Correction Algorithm

Input: Stream of defect measurements $\{d_k\}$, nominal waypoints $\{p_k\}$

Parameters: $L,\ g,\ lim,\ v_x,\ n_{req},\ d_{thr},\ \varepsilon_{tol}$

Output: Corrected waypoints $\{p'_k\}$

// —— PHASE 1: DEFECT VALIDATION (runs at ROS callback rate) ————

1. Initialise: $H \leftarrow deque\left(maxlen = n_{req}\right), \delta^* \leftarrow 0, correction_{applied} \leftarrow False$
2. On each defect measurement d_k:
   3. H.append((d_k)
   4. if $|H| < n_{req}$ then return //insufficient history
   5. if all($d_i > d_{thr}, for\ d_i \in H$) and not correction_applied then
      6. $\bar{d} \leftarrow medain(H)$
      7. if defect_type == 'gap' then $\delta^* \leftarrow -\bar{d}$
      8. if defect_type == 'overlap' then $\delta^* \leftarrow +\bar{d}$
      9. $\delta_k \leftarrow 0$; $\varepsilon_k \leftarrow 0$ // reset corrector state
   10. if not all ($d_i > d_{thr}$) and $|\delta^* - \delta_k| < \varepsilon_{tol}$, then correction_applied ← True

// —— PHASE 2: CORRECTION APPLICATION (runs per incoming waypoint) ——

11. On each nominal waypoint $p = (x, y, z, A, B, C)$:
    12. $\ell_{seg} \leftarrow \left\|p - p_{prev}\right\|_2$ Euclidean distance to previous waypoint)
    13. if $|\delta^*| \leq d_{thr}$ or correction_applied then write p unchanged; return
    14. $\varepsilon_k \leftarrow \delta^* - \delta_k$ (remaining lateral error)
    15. if $|e_k| \leq 0.1\ mm$ then write p unchanged; return

    16. // Vector pursuit steering
    17. $y_{tar} \leftarrow e_k$
    18. $x - tar \leftarrow \min\left(L, 5 \cdot \ell_{seg}\right)$
    19. $\Theta \leftarrow 2 \cdot \arctan(\frac{y_{tar}}{x_{tar}})$
    20. $r_T \leftarrow \frac{x_{tar}^2 + y_{tar}^2}{2 \cdot y_{tar}}$
    21. $\omega_t \leftarrow \frac{v_x}{|r_t|} \cdot sgn(r_t)$

    22. // Incremental corrections
    23. $\Delta t_k \leftarrow \frac{\ell_{seg}}{v_x}$
    24. $\Delta\delta \leftarrow clamp(\ g \cdot e_k \cdot \Delta t_k,\ -lim,\ +lim\ )$
    25. $\Delta\varepsilon \leftarrow clamp(\ g \cdot \omega_t \cdot \Delta t_k,\ -0.1,\ +0.1\ )$

    26. // Cumulative state update with anti-windup
    27. $\delta_{\{k+1\}} \leftarrow clamp(\ \delta_k + \Delta\delta,\ -5|\delta^*|,\ +5|\delta^*|\ )$
    28. $\varepsilon_{\{k+1\}} \leftarrow clamp(\ \varepsilon_k + \Delta\varepsilon,\ -0.3,\ +0.3\ )$

    29. // Apply to waypoint
    30. $x' \leftarrow x + \delta_{\{k+1\}}$
    31. $A' \leftarrow A + \varepsilon_{\{k+1\}} \cdot (180/\pi)$
    32. $p' \leftarrow (x', y, z, A', B, C)$
    33. write p' to output; signal semaphore
    34. $p_{prev} \leftarrow p$; $\delta_k \leftarrow \delta_{\{k+1\}}$; $\varepsilon_k \leftarrow \varepsilon_{\{k+1\}}$

Appendix 7D: ITRA-MATLAB motion control algorithm

Algorithm 4. ITRA-MATLAB Motion Control

Input: y_{max} (mm/s), a_{max} (mm/s^2), $\Delta t = 0.012\ s, S.R \in \mathbb{R}\ SO(3)$

Output: Interpolated 12-DoF trajectory to be executed on KUKA robot

// —— PHASE 1: INITIALISATION ——

1. Load ITRA shared library via DLL interface
2. Configure: $setNumRob(1), setRobIP(robotIP), setOutputDir(pwd)$
3. $openConn(ComputerIP, port)$ // establish UDP socket connection
4. $startRSIManager()$; poll $isRobotTaskActive()$ until active
5. Initialise: $p_{prev} \leftarrow 0_{12}$; $n \leftarrow 1, feedbackLog \leftarrow '[]'$
6. $p_n \leftarrow readNextPath()$ // read first waypoint via semaphore

// —— PHASE 2: MAIN CONTROL LOOP (12 ms hard real-time cycle) ——

7. while $isRobotTaskActive()$ do:
   8. $p_n \leftarrow readNextPath()$ // blocks until path_ready.sem exists
   9. $targetPos \leftarrow [p_n(1{:}9), 0, 0, 0] \in \mathbb{R}^{12}$
   10. $d_1 \leftarrow \|targetPos(1{:}3) - p_{prev}(1{:}3)\|_2$
   11. $d_2 \leftarrow \|targetPos(7{:}9) - p_{prev}(7{:}9)\|_2$
   12. if $d_1 > 1$ or $d_2 > 1$ then:
      13. $F\_applySpeedPattern(L, v_{max}, a_{max}, \Delta t)$
      14. $coord_{full} \leftarrow zeros(N, 12)$;
      15. $coord_{full(:,1:3)} \leftarrow coord(:,1{:}3)$; $coord_{full}(:,7{:}9) \leftarrow coord(:,4{:}6)$
      16. $data\ to\ write = [coord_{full}, flag]^T \in \mathbb{R}^{\{13\times N\}}$
      17. $setToolPathFromFile(0,' path.txt')$ // stream to RSI executor
   22. for i ← 1 to N do: // inner feedback loop
      23. $feedbackPos \leftarrow getCurrPos() \in \mathbb{R}^{19}$
      24. $R_{total} \leftarrow R_A(feedbackPos(4)) \cdot R_B(feedbackPos(5)) \cdot R_C(feedbackPos(6))$
      25. $R \leftarrow R_{total} \cdot S.R^{-1}$
      26. $feedbackPos(5) \leftarrow atan2(-R_{31}, \sqrt{(R_{11}^2 + R_{21}^2)})$ $(B', degrees)$
      27. if $|feedbackPos(5)| \neq 90°$:
         28. $feedbackPos(4) \leftarrow atan2(R_{21}, R_{11})$; $feedbackPos(6) \leftarrow atan2(R_{32}, R_{33})$
      29. else (gimbal lock):
         30. $feedbackPos(4) \leftarrow 0$; $feedbackPos(6) \leftarrow sgn(B') \cdot atan2(R_{12}, R_{22})$
      31. $feedbackLog \leftarrow [\ feedbackLog\ ;\ feedbackPos'\ ]$ // *append row*
      32. wait until$(t_{now} - t_{old}) \geq \Delta t$; $t_{old} \leftarrow t_{now}$
   33. $p_{prev} \leftarrow targetPos$; $n \leftarrow n + 1$

// —— PHASE 3: SHUTDOW——

34. $requRealTimeEd(0)$ // request RSI_MOVECORR termination
35. poll $isRobotTaskActive()$ until inactive; $allowRobotFinish(0)$
36. poll $isRSIRunning()$ until $inactive$; $terminateRSIManager()$
37. $closeConn()$; $unloadlibrary('robotComms2')$